Abstracts of Papers

CONTENTS

Conférences générales

1. F. C. Frank. *Crystal growth.*

2. W. Kleber. *Kristallwachstum, Morphologie und Struktur.*

(1) Die Korrespondenz zwischen Morphologie und Struktur ist nach zwei Richtungen hin verfolgt worden: Die erste geht von der Kristallfläche, die zweite von der Kristallkante bzw. dem Zonenvektor als Fundamentalelement aus. Diese beiden Korrespondenzgruppen, Fläche$\longleftrightarrow$Netzebene und Zonenvektor$\longleftrightarrow$Gittervektor, sind natürlich nicht unabhängig voneinander. Trotzdem erfolgt die Entwicklung nach beiden Richtungen divergent. Sie ist nach der einen Seite hin gekennzeichnet durch die Namen: Bravais$\rightarrow$Niggli$\rightarrow$Donnay–Harker, nach der anderen durch die Namen: Niggli$\rightarrow$Kleber$\rightarrow$Hartman–Perdok. Ohne Zweifel hat das Verfahren von Donnay und Harker zu wesentlichen Ergebnissen geführt, wenn es auch in seinen Prinzipien nicht unwidersprochen geblieben ist. Die Diskussion zahlreicher Beispiele hat gezeigt, dass die rein geometrischen Bauprinzipien grundsätzlich nicht genügen, um die Korrespondenz zwischen Morphologie und Struktur vollständig zu erfassen.

(2) Zunächst ist das Korrespondenzprinzip durch Berücksichtigung des Bindungscharakters (Elektronendichteverteilung) zu ergänzen. In dieser Hinsicht liefert gerade die Methode von Hartman–Perdok neue Gesichtspunkte und Möglichkeiten. Bei isotypen Strukturen können die 'P. B. C. vectors' durch anders geartete Bindungsverhältnisse entscheidend beeinflusst werden und damit auch die Trachtentwicklung verändern.

(3) Schon mehrfach ist bei den kritischen Erörterungen des Korrespondenzprinzips auf die Bedeutung der Milieufaktoren hingewiesen worden. Durch umfangreiches statistisches Material wird versucht, die Unterschiede auszugleichen. Neuerdings haben die Experimentaluntersuchungen von Kern das Problem wesentlich unterstrichen. Die Frage der Trachtänderungen als Milieufaktor fordert intensiv ihre Berücksichtigung bei der morphologisch-strukturellen Korrespondenz.

3. I. Fankuchen & B. Post. *Low-temperature determinations.*

Until very recently low-temperature X-ray crystallographic studies, with only two or three exceptions, were limited to the use of Debye–Scherrer techniques. Since 1947, however, interest in low-temperature single-crystal investigations has been greatly stimulated by the development of techniques which facilitate the collection of the data.

Two procedures are used for studies of this type. In one, favored by French workers, the crystals are grown and oriented in cold chambers and then transferred to the X-ray equipment. In the alternative method, developed at about the same time by Lipscomb and the authors, the specimen is sealed into thin-walled glass capillary tubes and transformed into a single crystal, on the X-ray goniometer head, by controlled freezing, using a stream of cold gas as coolant.

As a result of the availability of these simplified techniques, scores of structure determinations in this field have been published within the past five or six years. These include a number of simple organic molecules, hydrocarbons, and various inorganic acids and bases. In some instances the results included descriptions of structural transformations in the solid state.

The paper will include a description of some of these results as well as work now in progress in our laboratories.

4. H. M. Powell. *Clathrate compounds.*

5. D. Hodgkin. *The X-ray crystallographic study of the structure of vitamin B_{12}.*

Vitamin B_{12} has been given an approximate formula $C_{61-63}H_{86-97}O_{13-20}N_{14}PC$. From chemical work alone it is known to contain a nucleotide-like residue and a CN group, both of which may be varied by biological or chemical agencies. Further, the crystals in their mother liquor contain water of crystallization, part of which they lose, with small changes in the lattice constants, on ex-

posure to the air. X-ray diffraction measurements have been made of both wet and dry forms of B_{12} itself and of B_{12} derivatives with the CN group changed to H_2O, CNS and CNSe and also of two compounds with modified 'nucleotide' groups. The heavy-atom positions in the crystal unit can be unambiguously found and electron-density series have been calculated, with phase constants based in the first instance on these heavy-atom contributions, for B_{12} itself and for B_{12}SeCN, both in the wet and dry state. These electron-density series are being refined and the conclusions derived from them checked and improved by the parallel investigation of a degradation product of B_{12} from which the 'nucleotide' has been removed. In all of these compounds, in spite of their molecular complexity, it is possible to find the positions of individual atoms in the crystal structures. Some of these can be correlated with atomic positions in the chemically known parts of the molecule. Others indicate the probable atomic arrangement in regions about which there is at present no chemical information.

6. H. A. Levy. *Recent progress in neutron diffraction.*

The past three or four years has seen increasing application of neutron diffraction to physical and chemical problems. Studies fall into two groups: those concerned with magnetic properties, and those concerned with crystal structures.

Magnetic studies have included several ferrite systems, the transition elements, including several oxides and alloys, and several rare earth metals and oxides. Of particular note is clarification of the role of orbital angular momentum in neutron scattering.

Crystallographic applications are distinguished by increasing use of single-crystal methods and of Fourier analysis. Specific studies to be described include ferrites, phosphates, ice, oxalic acid dihydrate, and urea.

§ 1a. Appareillage

1. R. Pepinsky & K. Drenck. *High-intensity X-ray diffraction tubes.*

Several new high-intensity X-ray diffraction tubes are described. These include a modification of the high-brilliance microbeam tube previously described; a radiation-cooled rotating anode tube with a zirconium boride disc or molybdenum disc target; a cylindrical anode tube, which will tolerate loadings of as much as 200 kW.; and a water-cooled rotating-anode tube which avoids the use of rotary high-vacuum seals by employing gallium-rich liquid alloys as a heat-conducting medium.

2. Z. Nishiyama. *A new X-ray tube with a water-cooled induction-rotating anode.*

The object of this research is to obtain a high-intensity X-ray tube adaptable for an electric apparatus of ordinary capacity (< 50 mA.). In the newly designed X-ray tube, the anode is rotated by induction from a stator outside the tube, and the target is cooled with water through a medium of mercury. The tube has the following characteristics and uses:

(1) The tube has no rotating vacuum seal.

(2) The capacity of the tube is largest when the filament is set vertical. Therefore this setting is most favorable for obtaining the vertical rectangular beam as used in Debye–Scherrer cameras. In that case the first slit is dispensable and consequently the time of exposure may be reduced to about 1/50 of that with ordinary fixed-target X-ray tubes.

(3) The position of the focal spot is variable on the surface of the target cylinder, hence the lifetime of the target cylinder is much longer than that of the non-variable.

(4) The change of target may be made easily and in a short time.

3. H. W. v. d. Voorn. *The possibilities of a new cathode in X-ray diffraction tubes.*

In almost all X-ray diffraction techniques a homogeneously loaded focal spot is desirable. It will be shown that an inhomogeneous load is not advantageous to increase the total loading.

The assumption that the permissible specific loading should be inversely proportional to the linear dimension of the focal spot is not always justified; the temperature is not the only limiting factor, as the temperature gradient becomes, especially in the smaller foci, a very important limitation.

The focal spot obtained with the present cathodes, consisting of a tungsten helix, always has a banded structure. It seems necessary to use a homogeneously emitting cathode in order to obtain a homogeneously loaded focal spot. First of all one might think of a tungsten strip, but the focus obtained with such a cathode also has some intense lines.

We have experimented with the *L*-cathode, a type of dispenser cathode. This cathode has a homogeneously emitting surface. It has however two disadvantages: (1) There is a continuous evaporation of barium from the cathode, which might give rise to contamination of the anode. It is proved that this disadvantage is not serious as the barium is not deposited on the relatively hot focal spot. (2) It is not very well possible to control the tube current by the temperature of the cathode; instead grid control has been used.

Results obtained so far will be dealt with.

4. Z. Mihailovic & A. Rimsky. *Utilisation des dispositifs à focalisation électrostatique des électrons pour la production de rayons X.*

Etude critique et expérimentale d'un système de focalisation à lentilles symétriques et à champ nul qui présente des inconvénients en cours de fonctionnement. Il s'agit de l'existence de surtension de haute fréquence dont on explique l'origine.

Etude d'un système de lentilles asymétriques à champ non nul, à potentiel croissant, qui assure l'accélération des électrons et la focalisation de ceux-ci sur l'anticathode.

Réalisation et rôle de la grille de contrôle.

5. R. Rabillon. *Nouvelle méthode de refroidissement des tubes de cristallographie.*

L'étude mathématique complète et rigoureuse de la répartition de la chaleur dans l'anticathode d'un tube à rayons X, faite par Matricon, et publiée dans le *Journal de Physique et le Radium* de janvier 1951, montre que pour un foyer de dimensions données, la charge maximum admissible augmente lorsque: (*a*) le temps de pose élémentaire diminue, (*b*) l'épaisseur de l'anticathode diminue.

On peut facilement diminuer le temps de pose élémentaire en faisant tourner l'anode, ce qui revient à répartir la charge sur une plus grande surface d'impact.

On peut difficilement réduire l'épaisseur de l'anticathode à moins de 1 mm., car la méthode classique de refroidissement par circulation d'eau provoque: (1) l'entartrage de la surface de refroidissement, (2) la caléfaction, (3) la recristallisation du cuivre, (4) le 'vieillissement' du foyer.

Nous avons surmonté ces difficultés en remplaçant l'eau par un liquide approprié, porté à l'ébullition à l'intérieur de l'anode et se condensant sur une paroi froide pour retourner dans le cycle.

Des essais effectués sur un tube démontable à foyer fin, anode tournante et anticathode mince (Cristallobloc CGR légèrement modifié) ont donné des résultats encourageants qui vérifient très exactement les calculs de Matricon et permettent un gain de puissance appréciable, même pour une anode de faible diamètre tournant à vitesse réduite.

6. R. GRIFFOUL. *Générateurs de radiocristallographie à tubes scellés.*

Les critiques qui sont formulées à l'encontre des générateurs de radiocristallographie à tubes scellés concernent sourtout le manque de brillance et d'homogénéité de leur foyer.

Dans le but de pallier ces inconvénients, les tubes scellés de la CGR possèdent une cathode polarisée automatiquement par une fraction constante de la haute tension (0,5%). Le foyer obtenu est de dimensions indépendantes de la haute tension, réduites à la moitié des dimensions habituelles et parfaitement homogène. La brillance en résultant les rend comparables aux tubes démontables à anode fixe.

Cette conception entraîne une réalisation un peu particulière de l'appareillage.

(1) *Le Dictyobloc.*—C'est un bloc compact comprenant le transformateur spécial à trois sorties et polarisation automatique, le tube à rayons X horizontal à deux fenêtres de béryllium et foyer homogène et le tableau de commande. Il est prévu pour recevoir tous les accessoires habituels sur des bancs d'optique facilitant le réglage.

(2) *La gaine indépendante.*—Il est possible d'alimenter par le Dictyobloc, une gaine contenant un tube de cristallographie identique au précédent. Cette gaine est isolée par un gaz aux propriétés remarquables: l'hexafluorure de soufre, qui lui confère les qualités diélectriques d'une gaine isolée à l'huile, sans en présenter les inconvénients.

Un support permet d'adapter cette gaine à un goniomètre à compteur de Geiger; il comporte les réglages indispensables à une mise au point rapide et précise de l'ensemble foyer–collimateur–axe du goniomètre.

7. J. DESPUJOLS. *Double focalisation des rayons X à l'aide de cristaux métalliques courbés.*

Les méthodes de préparation de cristaux métalliques par recristallisation après écrouissage critique se prêtent particulièrement bien à l'obtention de cristaux doublement courbés. Avant le dernier recuit, la lame polycristalline est courbée sous le rayon désiré; après recristallisation, le monocristal obtenu peut être: (1) courbé autour du même axe, mais avec un autre rayon, ou (2) ramené à l'état plan, puis courbé à nouveau suivant un cylindre d'axe perpendiculaire au premier.

J'ai appliqué le deuxième processus à des cristaux d'aluminium préparés suivant la méthode de Tiedema. Les cristaux obtenus, avec l'orientation désirée, ont été employés pour résoudre deux problèmes expérimentaux:

(*a*) La réalisation d'un monochromateur à foyer ponctuel, utilisant une source de rayons X ponctuelle. La focalisation n'est réalisée que pour une seule longueur d'onde.

(*b*) L'obtention d'images X vraies. En effet, quand les rayons de courbure sont égaux, les plans réticulaires prennent approximativement la forme de calottes sphériques. On peut alors utiliser ces cristaux comme des 'miroirs' sphériques, et obtenir des images agrandies d'objets réels, éclairés par un rayonnement X polychromatique.

L'étude de ces deux problèmes a été commencée il y a deux ans environ; elle a été reprise récemment en collaboration avec M. D. Lumbroso; les nouvelles expériences ont permis d'étendre le champ d'application de la méthode et d'améliorer la qualité des clichés obtenus.

8. R. RABILLON. *Montage goniometrique à rayonnement mono- ou polychromatique auto-stabilisé.*

L'analyse cristallographique quantitative, avec goniomètre à compteur de Geiger, en rayonnement mono- ou polychromatique, nécessite une émission de rayonnement X parfaitement stable.

Les procédés classiques de stabilisation par emploi d'un 'moniteur' ou d'un circuit électronique stabilisateur de la haute tension et du faisceau d'électrons, présentent de nombreux inconvénients et ne sont pas applicables à tous les cas.

Gillam & Cole ont publié en novembre 1953, dans le *Journal of Scientific Instruments*, une étude statistique détaillée de ces méthodes qui tend à prouver leur manque de précision.

Nous avons mis au point un procédé de stabilisation directe du faisceau de rayons X par l'emploi d'une cellule au sulfure de cadmium.

La cellule, solidaire du collimateur d'entrée du goniomètre, subit les fluctuations du rayonnement utile, mono ou polychromatique.

Ces fluctuations, amplifiées ou non, agissent directement sur la tension par l'intermédiaire d'un transducteur.

Il n'est plus nécessaire de stabiliser l'alimentation car toute variation du secteur ou du chauffage filament, toute baisse de rayonnement due au vieillissement du foyer ou à la pollution de l'anticathode (cas des tubes démontables) est immédiatement compensée par une variation équivalente de la tension appliquée au tube à rayons X.

Des essais effectués sur tube démontable en tension alternative (Cristallobloc, CGR) ont donné une stabilité de rayonnement comparable à celle d'une source de radium.

9. A. RIMSKY & Z. MIHAILOVIC. *Etude d'une chambre d'ionisation destinée aux mesures du rayonnement X.*

La chambre est composée de deux électrodes isolées, d'un récipient qui a pour rôle d'être le réservoir du gaz comprimé et d'assurer le blindage électrostatique.

Le caractère particulier de cet appareil est la forme donnée aux électrodes, à savoir deux hélices coaxiales et déphasées de π assurant un gradiant de potentiel homogène dans le volume effectif de travail des Rayons X mesurés suivant l'axe de l'ensemble.

Les résultats sont: (1) Polarisation optima d'une cinquantaine de Volts. (2) Un palier de réponse stable de 36 V. jusqu'à 700 V. (3) Une linéarité de réponse assurée de 1 à 10.000. (4) Un faible encombrement et un poids réduit (400 g.). (5) L'association d'une lampe préamplificatrice incorporée permet une adaptation facile à tous les usages. L'appareil peut fonctionner dans le vide.

10. G. Shinoda, T. Tomura, T. Kyo & A. Miki. *Recording mechanism of a Geiger–Müller spectrometer.*

Ordinary recording systems of a Geiger–Müller counter spectrometer, which consist of a counting rate-meter and a recorder, have the following disadvantage: suitable selections of sensitivity and time constant are necessary, and we are obliged to switch manually even during recording, when the recording spectra have many different peak values. A logarithmic recorder gives a solution of this problem, but it is not a complete one. The time constant of a logarithmic counting rate-meter is not automatically variable; then the probable error varies according to the measuring counting rates and manual switching of the time constant is also necessary. The logarithmic and automatic variable time constant counting rate-meter using a thermo-diode gives another solution, but the instability of the diode characteristics is inevitable.

To obtain an ideal accurate automatic recording apparatus, we have made an attempt to construct a logarithmic and constant probable-error recorder. This counting rate-meter consists of two servo-mechanisms and RC networks. One servo-mechanism acts as a logarithmic recorder having variable time constant and another plays a part giving higher accuracy. The principle of variable time constant is as follows: the tandem potentiometer, one part of which has exponential potential distribution and the other ordinary one, is driven by a balancing motor. The slider of the former is connected to a resistance and the other to a capacitor. The ends of these two elements are connected together to the input terminal and zero-detector. The zero-detector is a type of high impedance vibrating chopper, and its output error signal is fed into a servo-amplifier. The output of this amplifier is fed into a balancing motor and this drives the above mentioned potentiometer. When the potential characteristics of these two potentiometers are equal, the recorder acts as an ordinary current-measuring device. When the distribution of the potential of the capacitance-connected potentiometer is twice that of the other, the time constant is multiplied by two, and so on. In our counting rate-meter, this ratio is selected from 1 to 200, because, when the ratio becomes smaller than unity, the servo-system tends to become unstable. But when the ratio is chosen as 1 to 200, the discontinuity of the potentiometer has injurious effects at a longer time-constant region. To avoid this undesirable effect, we use one more balancing motor. This motor drives one linear potentiometer and this potential is fed to the capacitance potentiometer, and this motor is driven with a higher gain servo amplifier than the above mentioned motor. The reduction gear of this motor has a higher ratio, then, as soon as the action of the first motor has ceased, the second motor moves to the accurate final value. By this recording apparatus, we can record from 50 counts per sec. to 10,000 counts per sec. with the probable error of $\pm 0{\cdot}5\%$, and the time constant automatically varies from 200 sec. to 1 sec. When we wish $\pm 1\%$ probable error, the time constants are from 100 to 0·5 sec. But the recorder response is 2 sec. for full-scale travel; thus the probable error at the high counting rate region is less than 1%.

11. R. Pepinsky, A. Pavlovic & R. Keeling. *Weissenberg goniometers for X-ray diffraction observations at very low temperatures.*

Two Weissenberg cameras have been constructed, for single-crystal studies down to liquid-nitrogen and liquid-helium temperatures, respectively. Details of the first instrument have been published. The instrument for liquid-helium-temperature observations differs from the earlier design in its incorporation of a radiation shield around the helium container. The crystal is cooled by conduction through a silver goniometer head, soldered to the base of the helium container. This radiation shield is cooled by conduction from a liquid-nitrogen dewar immediately above the helium dewar. The nitrogen and helium containers, radiation shield and crystal are all enclosed in an evacuated space, the crystal being irradiated through a polystyrene vacuum cap.

X-ray single-crystal photographs at low temperatures are illustrated.

12. A. L. Patterson, C. E. Nordman, Alice S. Weldon, & C. E. Supper. *An integrating mechanism for the Buerger precession camera.*

A Buerger precession camera has been provided with an integrating mechanism of the type suggested by Wiebenga & Smits (*Acta Cryst.* (1950), **3**, 265). This permits the recording of the intensities and background for all the reflections of any row line in a single run of an automatic recording photometer. The integrating motion is of a 'saw tooth Lissajous' type of frequency ratio 7:8. It is conveyed to the film holder directly by eccentric cams geared to the precession drive of the camera. The integrating cycle is completed in 224 precession revolutions. Results obtained on the $0kl$ and $1kl$ levels of anthracene are in good agreement with the published data.

13. G. Donnay & J. D. H. Donnay. *An integrating precession technique.*

Buerger's precession method possesses the following properties. The incident beam makes a constant angle μ (precession angle) and the diffracted beams make a constant angle ν (half angle of the diffraction cone) with the normal to the reciprocal-lattice net to be photographed. A crystal plate, larger than the cross section of the beam to minimize edge effects, is cleaved or ground to uniform thickness t (cm.) parallel to the net.

The diffracting volume of crystal is constant for all layers if μ is kept constant, and since the diffracted beams strike the film at constant angle for a given layer, all spots have constant area and shape. Their central portions represent integrated intensities, which can be read on a microdensitometer. To get absolute intensities, the film is calibrated with a standard crystal plate. The constant diffracted path length, $t \sec \nu$, renders absorption correction unnecessary for any one layer. Intensities from the zero and nth layers are related as follows:

$$\ln \frac{I_0}{I_n} = t\mu_c \frac{\cos \nu_0 - \cos \nu_n}{\cos \nu_0 \cos \nu_n} - 6\mu_a n d^* \lambda ,$$

where μ_c and μ_a are the linear absorption coefficients in crystal and air, d^* (in $Å^{-1}$) is the interplanar distance of the nets under investigation, λ (in Å) is the wavelength. The crystal-to-film distance (in cm.) is $6\,(1-nd^*\lambda)$. Exposures are short, expecially with optimum thickness $t = 1/\mu_c$.

14. W. A. Wooster. *A rotation retigraph (direct-projection X-ray goniometer).*

In conjunction with Prof. W. F. de Jong the writer has designed a rotation retigraph for the production of direct projections of reciprocal-lattice planes. This instrument differs from the precession instrument of Prof. M. J. Buerger in that the crystal and the film rotate continuously in the same direction. The apparatus consists of a divided circular base on which is mounted a rectangular box supporting two parallel vertical shafts. One of these, *A*, is collinear with the axis about which the divided circle can be rotated; the other, *B*, can be set at any distance between 5 and 10 cm. from it. The former shaft carries a vertical circle on which a goniometer head may be mounted in two ways. The vertical circle always rotates about a horizontal axis and in the first mounting the goniometer head has its axis perpendicular to the horizontal axis of rotation of the vertical circle and in the second mounting the goniometer head has its axis along that of the vertical circle. The shaft *B* supports the camera and by means of worm gearing the planes of the vertical circle and of the camera are always kept parallel. A screen is mounted in front of the film and on this screen is mounted an aperture formed by lead foil on cellophane which permits only the required reflexions, lying on a cone, to reach the film. A collimator is mounted on a vertical support from the base. A microscope, which can also be used as an autocollimating telescope, is mounted concentric with the main divided circle.

The range of ξ, ζ values which may be obtained on direct projections, requiring no charts for interpretation, is considerable. In the equatorial plane the maximum value of ξ is set by the geometry of the apparatus at about 1·4 and for larger lines the possible values of ξ extend to values between 1·4 and 1·7. The maximum value of ζ which may be reached is about 1·6 and this can be studied with the same setting of the crystal as for the equatorial plane.

15. A. Rimsky. *Appareil permettant la photographie directe de l'espace réciproque.*

Cet appareil permet d'obtenir directement et sans déformation l'espace réciproque d'une substance diffractant un faisceau de rayons X monochromatique. Le rayon de la sphère de réflexion est une constante de l'appareil. L'ensemble des réglages est automatique quand on a fait le choix du plan de l'espace réciproque et l'angle d'incidence de son axe de rotation avec le faisceau de rayons X.

L'appareil permet la détermination précise des paramètres d'un réseau cristallin. La mesure des intensités des taches de diffraction est améliorée par un dispositif d'intégration photographique qui imprime au film un mouvement de balayage dont on peut régler tous les paramètres.

Sont adjoints à l'ensemble les accessoires suivants: (*a*) Un support de préparation permettant 120° de rotation de la substance suivant deux axes de cercles concentriques et perpendiculaires assurant la prise de vue suivant tous les axes possibles sans avoir à démonter la préparation. (*b*) Un chassis cylindrique pour le cristal tournant et Debye–Scherrer. (*c*) Un chassis de Laue. (*d*) Un chassis permettant d'exécuter les clichés de Sauter pour les régions voisines de l'axe de rotation de l'espace réciproque. (*e*) Une lunette de réglage.

16. A. Franks. *An optically focusing X-ray diffraction camera.*

X-rays from a micro-focus tube are totally reflected from either one glass plate or two plates at right angles to each other. The reflected beam is focused by elastically bending the plates, and forms a line image 5 microns wide in the case of the single reflector, and an image approximately 5×50 microns when both reflectors are employed.

The apparatus has been used to obtain low-angle diffraction photographs and high-resolution back-reflexion photographs from metal specimens. In the transmission photographs, the first order reflexions from spacings up to 700Å have been resolved and require comparatively short exposure times. Substances investigated include collagen, tobacco mosaic virus, coal and terylene.

17. T. C. Furnas. *A Geiger-counter apparatus for collecting complete single-crystal diffraction data.*

Three-circle goniometers based upon rotations about the three Eulerian axes will be described. An 'Eulerian cradle' (so named for its limited rotation about the horizontal axis) has been built and used for orienting single crystals in an X-ray beam so as to bring each reciprocal-lattice point into the equatorial plane for Geiger-counter measurement of the intensity. A complete hemisphere of the reciprocal lattice can be surveyed with but a single mounting of any crystal. For convenience and rapidity in making intensity measurements, the X-ray optics are arranged to achieve integration with a static crystal orientation. Data collection is further facilitated by computing appropriate angular coordinates for reciprocal-lattice points from an accurate set of lattice-parameter measurements (readily obtained with the same instrument) and setting the various circles accordingly. All angular motions are controlled by worm wheels and worms with dials for direct reading to 0·01°.

A complete set of three-dimensional data to $d = 3$ Å (2485 independent reflections each with its neighboring background intensity) from ribonuclease II (space group $P2_1$, $a = 30{\cdot}2$, $b = 38{\cdot}4$, $c = 53{\cdot}2$ Å, $\beta = 105{\cdot}85°$) was obtained in 55 hr. with less than 24 hr. total X-ray exposure to the crystal, including its initial alignment.

18. W. L. Bond. *An automatic recording X-ray diffractometer and plotting device.*

An instrument has been built for recording simultaneously the integrated intensities of X-ray reflections and the corresponding crystal orientation angles and Bragg angles. Transcription of the data on to a mechanical plotter gives an undistorted reciprocal-lattice plot. All levels may be plotted to the same scale. The intensities are determined by a Geiger counter and integrating circuit.

The single crystal and the Geiger tube are geared together and rotated at different rates about the same axis

so that, for any level, all combinations of crystal position and Bragg angle are obtained, and also a record of crystal position serves as a record of Bragg angle. While one pen is recording these, a second pen is recording the integrated intensity of each reflection in the same chart.

If θ is the Bragg angle and ω is the angle of crystal rotation from any starting position, then it can be shown that a polar plot of $r = R \sin\theta$, $\varepsilon = \theta$ is a reciprocal lattice. The plotter contains the constants of the diffractometer and lays out r and ε so that we have a reciprocal lattice. R can be adjusted in proportion to the cosine of the level angle so that all levels are plotted to the same scale.

19. E. R. EGLINGTON. *A multi-purpose recording X-ray diffractometer.*

As complement to the usual X-ray film camera, the X-ray diffractometer is now recognised as an instrument of great value to the crystallographer. The equipment to be described, besides possessing the basic, well-known features, incorporates certain refinements and additions which render it of special interest to workers both in industry and research. An attempt is made to outline the more interesting features of its construction to show the extent to which it may be applied, and to indicate the quality of result to be expected.

Short history of development.—Brief survey of the development of the fundamental instrument.

Construction of the present instrument.—Mechanics. X-ray optical system. Control rack and amplifiers.

Special features.—Monitoring system and the 'double beam' technique. Automatic 'step-by-step' mechanism and its function. Automatic scan reversal. Dual gear boxes for extra slow speed scanning. Investigations at high and low temperatures. Attachments for spectrochemical analysis.

Accuracies and sample results.—Overall accuracy of reading. Reproducibility of result. Sample traces.

20. Z. MIHAILOVIC. *Utilisation des cristaux semi-conducteurs en radiocristallographie comme appareil de mesure des faisceaux diffractés de rayons X.*

Application des cristaux semi-conducteurs (CdS, LiF, ZnS, AgI, et AgCl) en radiocristallographie pour la détection et la mesure de l'intensité des faisceaux diffractés de rayons X.

Technique appliquée aux cristaux compteurs (réalisation des électrodes, schéma électrique, amplificateurs, etc.).

Etude du courant photoélectrique.

Le spectromètre de Bragg équipé avec un compteur à cristal. Diagrammes des spectres enregistrés.

21. F. EBERT. *Neue kristallographische Deutungsaufgaben an Rotationsdiagrammen, die mittels Zählrohrgoniometer erhalten werden.*

22. V. SCATTURIN. *Calibration of cylindrical Debye–Scherrer cameras against absorption errors.*

§ 1b. Techniques et méthodes

1. G. K. WILLIAMSON. *The use of Fourier analysis in the interpretation of line broadening in powder patterns.*

Some anomalies obtained in the practical application of Fourier-analysis methods to line broadening studies are briefly described. An investigation into the severity of some of the errors predicted by Eastabrook & Wilson has been made, using theoretical line shapes. Many of the results to which a physical significance has been attached are shown to be a consequence of these errors. The reliability of some past results is assessed and an alternative method of interpretation suggested.

2. E. JENSEN. *Particle-size requirements for accurate intensity measurements by the spectrometer X-ray method.*

It is sometimes overlooked that the conditions for accurate intensity measurements are, as regards particle size, much more rigorous in the spectrometer method than in the ordinary Debye method with rotating specimens.

Intensity measurements in three particle size fractions of powdered quartz ($k_{\text{average}} = 1{\cdot}0\mu$, $6{\cdot}5\mu$ and 18μ) with a commercial X-ray focusing spectrometer using flat non-rotating samples indicate that k_{average} should not be greater than a few microns if the precision of the instrument shall be fully utilised. At $k_{\text{average}} = 1{\cdot}0\mu$ the standard deviations of the integrated intensities are less than 2–3 % of results, but already at $k_{\text{average}} = 18\mu$ it rises to about %.

In order to establish more exact and general particle size limits an attempt has been made to derive a theoretical relation between the particle size k (= [particle volume]$^{\frac{1}{3}}$) and the relative standard deviation of the integrated intensity $\sigma I/I$. The relation which may be written $\sigma I/I = ck^{3/2}$, was deduced on the basis of the distribution of the number of particles oriented so that their reflexions would be picked up by the detector unit. The proportionality factor c may be calculated from physical properties of the material and the geometric instrument factors limiting the X-ray beams. The experimental and the calculated relative standard deviations agree within *c.* 25% of the calculated values; the underlying assumptions must therefore have been approximately fulfilled.

3. K. DRENCK. *A simple theory of particle-size line broadening as applied to flint.*

It is known that a crystal fragment may be described by the product of the density function $\varrho(x)$ for the infinite crystal and a shape function $s(x)$. The corresponding Fourier transform will be the shape transform $S(\xi)$ repeated at each reciprocal-lattice point with a weight given by the transform F_H of the infinite lattice.

A powder diagram contains information about $\int |S|^2 . d\sigma$ integrated along a sphere in Fourier space with radius $\xi = 2 \sin\theta$; if this radius is large compared with the size of S, the sphere can be approximated by a plane. Thus one gets the projection of $|S|^2$ on to a line through the origin and the point $[h, k, l]$. This yields information in real space about the convolution function $s^*s = \int s(x-y)\, s(y) dy$ along a line with the direction (h, k, l).

In a simple manner one gets a distribution function of particle 'diameters' from which it is rather difficult to

deduce information about the size of the particles and their shape unless some simplifying assumptions are made.

Measurements have been carried out with a modified GE Geiger-counter diffractometer on a series of specimens of flint with varying age. These show considerable differences in particle size.

The experimental setup is briefly described.

4. W. PARRISH & A. J. C. WILSON. *Some new minor geometrical aberrations in powder diffractometry.*

A ray leaving the point (u, v, w) on the target of an X-ray tube, being diffracted at the point (x, y, z) in the specimen, and passing through the point (ξ, η, ζ) of the receiving slit will be registered at an angle 2ψ related to the Bragg angle by $2\psi = 2\theta - 2\varepsilon$, where

$$2\varepsilon = 2xR^{-1}\cos\psi + (v+\eta)R^{-1} + y^2R^{-2}\sin 2\psi - y(u+\xi)R^{-2}\sin\psi + R^{-2}\{\tfrac{1}{2}[(\zeta-z)^2 + (z-w)^2]\cot 2\psi - (\zeta-z)(z-w)\operatorname{cosec} 2\psi\}:$$

R is the spectrometer radius and (u, v, w) *etc.* are referred to suitably oriented local coordinate systems. Examination of this equation shows that, in addition to the ordinarily recognized geometrical aberrations (L. Alexander, *J. Appl. Phys.* (1948), **19**, 1068; A. J. C. Wilson, *J. Sci. Instrum.* (1950), **27**, 321; J. N. Eastabrook, *Brit. J. Appl. Phys.* (1952), **3**, 349), displacement and/or broadening can be caused by (i) cross-linking between specimen 'length' and 'horizontal' focal extension; (ii) cross-linking between specimen 'length' and any inequality of the source–specimen and specimen–slit distances; (iii) missetting or variation of the 2:1 ratio.

The magnitude of these and the effect of the known angular variation of the intensity of the incident beam are discussed.

5. J. C. M. BRENTANO. *The advantages of a shift to shorter wavelengths in X-ray crystal diffraction.*

The choice of wavelength in X-ray diffraction is largely influenced by the response of the detector. Both the photographic film and the gas counter favor long wavelengths. Ladany and myself reported that scintillation counters can be used for the quantitative evaluation of intensities in X-ray diffraction (J. C. M. Brentano & I. Ladany, *Phys. Rev.* (1953), **92**, 850). By using thalliated sodium iodide the crystal can be made small (0·5 mm. thick for Mo $K\alpha$) so that the radioactive background, which is a volume effect, becomes negligible. The random thermal emission of electrons from the cathode of the photomultiplier, which constitutes another disturbing effect, can be eliminated with a discriminator by making the time constant of the amplifier circuit sufficiently small so that the number of thermoelectrons emitted for that time interval is small compared with the number of electrons released by one X-ray photon. For Mo $K\alpha$ radiation one X-ray photon releases about 15 photoelectrons (West, Meyerhof & Hofstadter, *Phys. Rev.* (1951), **81**, 141); discrimination can then be obtained with a time constant of 2 or 3 sec. The scintillation counter is then a simple device giving a high yield and a linear response up to counting rates of several thousand counts per second. We dispose thus of detectors adapted to various wavelengths; this suggests a revision of techniques.

While for any given lattice spacing the Bragg angle θ decreases with wavelength—with $\sin\theta$ proportionate to λ—the absorption coefficient decreases in a general way approximately with the third power of λ. Comparing *f* Cu $K\alpha$ and Mo $K\alpha$, corresponding $\sin\theta$ values for the latter are reduced by a factor of about $\frac{1}{2}$, while absorption coefficients—outside the range affected by selective photoelectric absorption, which in this case extends from *Z* 28 Ni to *Z* 39 Y—are reduced by a factor of approximately 8. With Mo radiation the thickness of the diffracting material can thus be increased eight times.

With powder methods this is an advantage which is felt when recording line widths. With the Debye rod *f* line contours are greatly affected by unevenness in the distribution of the powder. By disposing of larger volumes a more even distribution can be secured. Operating in the range of small angles, the loss of resolution resulting from the decrease of θ can be compensated by observing the pattern at a correspondingly greater distance without intensity loss, the pattern being projected on a circle of the same diameter. The following arrangement is then indicated: a narrow X-ray beam of rectangular cross section $a \times b$ with $a > b$ falls at right angles on a powder layer of such thickness that it reduces the intensity of the transmitted beam to $1/e$. The width b of the incident beam is less than the thickness of the powder layer and the diffraction pattern is observed as deflected in a plane normal to the height a of the beam. The diffracting volume can then satisfy in approximation the parafocusing condition (J. C. M. Brentano, *J. Appl. Phys.* (1946), **17**, 420), and a nearly symmetrical intensity distribution for each line results. Where high intensities are required the X-ray beam of rectangular cross section is replaced by one comprised between two concentric circles defined by a slit representing the section of an annulus, the curvature changing with the deflection angle. Slides will illustrate the arrangement.

For small-angle diffraction, when examining granulous materials with long wavelengths, it is not possible to normalize the diffraction pattern in terms of the intensity of the incident beam and in terms of the diffraction volume because of the unequal absorption for various parts of the specimen. This cannot be overcome by any averaging operation of rocking or sliding since the absorption is not a linear but an exponential function of thickness. By using a more penetrating radiation, so that the thickness of the material comprises many grains, this uncertainty can be greatly reduced. The writer, in observing by small-angle diffraction the strain of iron filings, has found great advantage in the past in using Mo $K\alpha$ radiation in combination with photographic methods. With the simple quantitative evaluation in the short-wave range offered by the scintillation counter it seems justified to draw attention to these conditions.

6. C. M. MITCHELL. *Precise parametric measurement at low θ values with the Debye–Scherrer camera.*

In order to obtain accurate $q(= 1/d^2)$ values over a complete pattern, a collimator has been designed and a systematic error derived which gives precise measurements down to low θ values. The camera has a particular application to the problem of unit-cell determination from the powder pattern.

The collimator gives an effective line source, controlled in position and dimensions, which, in order to obtain

optimum focusing, is adjusted to give a source on the film cylinder. Line profiles have been generated for monochromatic radiation and the effect of natural width on the profiles at high θ values determined. Source dimensions have been chosen, similar to those proposed by Ekstein & Siegel (*Acta Cryst.* (1949), **2**, 99) which give high resolution over the forward region, an invariant width at half-maximum intensity equal to the source width being obtained at low θ values, for specimens of high absorption.

The systematic line-centre displacement has been determined and the centre of density relation found in a general form containing terms for source and irradiated specimen area. This relation corresponds to Warren's function in the case of a point source and totally absorbing specimen. The line-centre displacement at any intensity level has been determined and the absorption shift for specimens of less than total absorption derived. The absorption shift relation is accurate over the full θ range for specimens of $\mu r \geqslant 8$.

It is shown that with a 114·59 mm. camera direct correction of the film can be made, without graphical extrapolation, to within 1:5,000 down to $\theta \approx 20°$, using an effective source width of 0·1 mm.

7. P. T. DAVIES. *An improved method of indexing powder diffraction patterns of orthorhombic crystals.*

A more powerful method of determining unit-cell dimensions of orthorhombic crystals has been developed from the method described by Lipson (*Acta Cryst.* (1949), **2**, 43). The problem is, given a set of values of $q(= \sin^2\theta$ or $1/d^2)$, to determine constants A, B, C such that every q can be expressed as $h^2A+k^2B+l^2C$ with integral values of h, k, l.

Lipson's difference diagram is used to obtain a list of values which recur several times among the differences Δq of any pairs of q. These values of Δq are plotted logarithmically on a second chart with the object of determining whether any groups of them are in the ratios of some members of the series 1, 3, 4, 5, 7, 8, 9, 11 etc. Such groups contain Δq values which are most probably of the form $q(h_2kl)-q(h_1kl)$, and each group gives a possible value for one constant A. After a quick screening of the trial A values, the most promising is used to calculate a set of values of $q(0kl)$. For a given A, each Δq of the form Ax (1, 3, 4, etc.) leads to a probable value of $q(0kl)$. The recurrence of certain values among the trial $q(0kl)$ provides a check on the correctness of A. Recurring values are taken as confirmed $q(0kl)$, and to them may be added any original $q < A$. The resulting set of $q(0kl)$ are indexed by standard procedures, e.g. Bunn's chart.

The method is illustrated by application to published data for potassium nitrate and uranium and to new data for ammonium metavanadate. It could also be used to determine the diad axis of a monoclinic crystal.

8. F. FOURNIER. *Note sur quelques appareils mettant en oeuvre les microtechniques rayons X.*

Résultats sur des cristaux mal organisés.

9. C. J. BALL & P. B. HIRSCH. *Miscellaneous applications of a microbeam technique.*

1. An inclusion in a steel specimen of size $100\mu \times 30\mu$, was examined in back reflexion, with a beam of diameter 100μ. The specimen was oscillated through $1\frac{1}{2}°$ about an axis passing through it, and from the spots on the film spacing values for several lines were deduced with an accuracy of $\frac{1}{2}\%$. The method of location of the beam is described.

2. Electrodeposited chromium films, of thickness 10–20μ, have been examined by a transmission method. A texture similar to that of a cold-worked metal has been discovered, grains of size 1μ clustering into groups of size 7μ. One film showed marked preferred orientation of a 'fibre' nature, which presented special problems.

3. The application of the technique to the study of silver bromide films is also discussed; very small beams are required to resolve the Debye–Scherrer rings into spots.

4. The texture of boron steels has been investigated.

10. E. W. RADOSLOVICH. *A geometrical structure-factor device.*

This device forms $\cos(hx+ky+lz)$ separately for ten atoms, and simultaneously presents these cosines ready for addition, for any given h, k, l. It contains one unit repeated ten times. This is made up of (1) a horizontal chart carrying a cosine table at 1·8° intervals (0·005 of the unit-cell dimensions), and a separate table (labelled ky) of angular intervals; (2) drums for winding this chart to left or right; (3) an origin marker whose position in front of the chart is determined by lz; (4) small lights (behind the chart), connected to a distribution board and switch. These lights can be switched on singly, in sequence; this sequence is determined by hx, the lights being connected up once only for a given calculation.

Thus, by the switching, all required values of $\cos hx$ could be lit up as h runs from 0 to 23. But, by first moving the chart by $(ky+lz)$, the values of $\cos(hx+ky+lz)$ are lit up instead.

Ten such units are stacked vertically and connected to the same switch. Each unit is set for its own ky and lz, and, by switching, $\cos(hx+ky+lz)$ is presented simultaneously for all ten atoms for each successive h. The device is accurate and not restricted to low (h, k, l); by repetition, 10, 20 or more atoms of the same kind can be included in the summation.

11. J. CLASTRE & R. GAY. *Machine à calculer les facteurs de structure.*

La machine se compose de plusieurs étages; chaque étage comprend 8 éléments qui correspondent à 8 couples d'atomes centrosymétriques. Pour chaque élément, on fixe, sur un limbe gradué au 100ème, un décalage initial $2\pi(hx_j+ky_j)$, et, sur un 2° limbe, l'angle $2\pi z_j$. Un excentrique, fixé sur le 2° limbe, donne les valeurs $\cos 2\pi(hx_j+ky_j+lz_j)$, l progressant par valeurs entières, grace à un axe moteur commun aux 8 éléments, tournant alternativement dans les deux sens. L'excentrique agit sur le piston d'une seringue. Les 8 seringues sont mises en rapport, par une canalisation commune, avec une seringue collectrice. Le déplacement du piston de cette dernière donne la contribution $\sum_j \cos 2\pi(hx_j+ky_j+lz_j)$ des 8 couples d'atomes. La précision est de l'ordre de 2% de la valeur maxima. Le calcul de 20 valeurs F_{hkl} appartenant à une même rangée prend 15 min. environ. Les atomes de natures différentes sont rapportées à des étages différents, ce qui permet de calculer $\sum_j Z_j \cos 2\pi(hx_j+ky_j+lz_j)$.

12. J. M. ROBERTSON. *A desk computer for Fourier analysis.*

Many computers, both analogue and digital, have been designed for Fourier operations. Analogue machines are generally of rather low accuracy, unless made with extreme precision and at great cost. Digital machines of the punched-card type are also costly, require a great deal of space, and demand skill and training on the part of the operator. Modern electronic computers have similar disadvantages for the crystallographer and usually lack storage space for Fourier operations. There is, therefore, need for a more compact device.

The digital computer now designed is non-electrical, and works by simple direct gearing, from the input feed to the output printing counters. It is the mechanical analogue of the usual strip methods, F values being fed in either singly or simultaneously, while the summation totals are printed out automatically. Five-figure accuracy is built into the gear trains. The machine is capable of speeds up to 6000 revolutions per minute, so that two-figure and three-figure coefficients can be set in a matter of seconds. The brief specification for the machine is an accuracy a thousand times greater than the usual strip methods and a speed ten times faster. It would, however, be slower if coefficients of more than three figures are employed. It requires no skill or training on the part of the operator.

13. A. S. DOUGLAS. *The use of digital computers in structure analysis.*

Kendrew & Bennett first demonstrated how a particular computer, the EDSAC, can be used to compute Patterson syntheses rapidly. It is relatively simple to extend their methods so as to carry out Fourier-series summations, such as are used to express the electron density or its derivatives. The calculation of structure factors in the general case presents a more difficult problem, owing to the tabular form of the atomic scattering factors. Nevertheless, Cruickshank & Ahmed at Manchester and Thompson, Caminer, Fantl, Wright & King, in the Lyons Electronic Office, have been able to set up complete systems for the 'refinement' of approximate structures of various space groups. A possible application, not yet carried out, is to the more accurate calculation of atomic scattering factors, which is believed important in the study of intermetallic compounds. Another possible application is to the computation of Karle–Hauptman probabilities, whilst the author has been developing, with Dr Cochran, a method, based on the sign relations of Cochran and Zachariasen, of using the EDSAC to determine systematically the signs of structure factors for crystals centrosymmetric in projection. The latter method has reached a stage where it has been possible, in a favourable case, to determine an unknown structure without using any other aid, but is, as yet, comparatively limited in scope.

14. A. S. DOUGLAS. *Application of the EDSAC to structure determination by a direct method.*

Cochran and Zachariasen have shown independently that the signs of the structure factors of a centrosymmetric structure tend to be related by the equations $S(h)\,S(h') = S(h+h')$. Woolfson has shown that the probability that each such equation is satisfied depends on $|U(h)\,U(h')\,U(h+h')|$. It is possible to assess the 'plausibility' that a given combination among the $S(h)$ for a structure is the correct one by evaluating

$$\chi \equiv \sum_{h,\,h'} Y(h, h')\,P(h, h')$$

where

$$Y(h, h') = S(h)S(h')S(h+h')\,,$$

and $P(h, h') = |U(h)U(h')U(h+h')|$. This can be carried out systematically for 20–30 different $S(h)$ by a digital computer, and those combinations for which χ is large can be selected. This may lead to a large number of combinations being picked out in unfavourable cases and other tests must be used to reduce the number of these. Further useful tests of plausibility, which can be mechanized, are to evaluate the 'zero checks' for the structure and to examine how far Sayre's equation is satisfied. Final selection can be carried out by inspection of Fourier maps of projections of the structures corresponding to various possible sign combinations. It is not easy, however, to identify the correct structure from projections, especially if only comparatively few of the $S(h)$ are used. Nevertheless, in a favourable case, arsonium bromide, it was possible to determine the correct structure by using the χ test alone. A test on the known structure of salicylic acid indicated that this could have been solved by application of all the tests discussed.

15. M. M. WOOLFSON & W. COCHRAN. *Some experience of direct methods of Fourier structure determination.*

Successful and unsuccessful applications of two direct methods (the EDSAC method and the use of permutation syntheses) will be described. The reasons for success in some problems and failure in others, and their bearing on the general situation with respect to solving the phase problem, will be discussed.

Some possible new methods of analytical attack will be indicated.

16. D. W. J. CRUICKSHANK. *The use of the Manchester University electronic digital computer in detailed structure refinement.*

A description will be given of three-dimensional structure refinement by successive cycles of structure-factor calculations and observed and calculated differential syntheses carried out on the Manchester University electronic computer. So far work has been done on 18 structures, involving 56 sets of structure factors (comprising in all about 300,000 atom structure factors) and 50 sets of observed and calculated differential syntheses. Including the development of the programmes, a total computer time of about 290 hr. has been needed for this work. Programmes just coming into operation include the calculation of electron-density sections in non-crystallographic planes, the calculation of isotropic or anisotropic thermal parameters, the calculation of structure factors with anisotropic thermal motion, and refinement in non-centrosymmetric space groups.

17. Å. ÅKESON. *Principles of an electronic apparatus for variation of structure factors and an iterative way of using it.*

Varying structure factors means (1) picking out one value—from say 6 values—for the structure factor of each atomic position, (2) adding these values to obtain the complete structure factor, (3) comparing this total

structure factor value with the observed reflexion intensity and then (4) doing this for various reflexions.

Substituting elementary structure factors by voltages, picking out the voltages and adding them by flip-flop circuits of the counter type and electronically comparing the sums thus obtained with the observed intensities, one can scan 10^5 different parameter (atomic structure factor) *combinations* per sec. or 10^9 in 3 hr. In 3 hr. such an apparatus can completely scan $9/\log 6 = 9/0{\cdot}78 > 11$ *parameters*, 6 *values* of each.

The sensitivity can be varied and thus the apparatus can be made to indicate agreement when the obtained complete structure-factor values are proportional—within *chosen* limits—to all reflexions or all except one or all except two.

Instead of having 6 values for each elementary structure factor and scanning all combinations of them, one could have 3 or 2 values of each and run the apparatus several times. For each new run the elementary structure factor potentiometers are reset so that the apparatus can test new parameter values, chosen at that side to which it moved during the preceding run. This means an increase of the number of parameter values scanned per atomic structure factor by two for each new run.

For example: In one *second* $5/\log 2 = 5/0{\cdot}30 > 16$ parameters, two values of each, can be completely scanned (in 3 hr. $9/\log 2 = 30$ parameters). Running the apparatus 5 times, 1 sec. for each run, would thus mean working through 16 parameters, 10 values of each, choosing the most favourable path through the field of parameter combinations. (Analogously running 5 times, 3 hr. for each run: 30 parameters, 10 values of each.—Completely scanning *all* these 10^{30} different combinations would take $10^{30-5} = 10^{25}$ sec. $= 3{\cdot}2 \times 10^{17}$ years.)

The number of reflexions simultaneously studied does not affect the time of electronic scanning but only the size of the apparatus.

18. J. W. JEFFERY. *Intensity measurement and absorption correction.*

The results of the first part of a programme designed to estimate the relative accuracy and efficiency of various methods of measuring integrated reflexions will be reported. The work consists of: (*a*) Grinding spherical crystals (diameter 0·1–0·25 mm.) of $Co[Hg(CNS)_4]$, a substance whose crystals are both highly symmetrical (space group $I\bar{4}$) and heavily absorbing ($\mu \sim 500$ cm.$^{-1}$); (*b*) The measurement of intensity from oscillation photographs and Weissenberg photographs of the zero layer about *c* for these spherical crystals by (i) estimation against a standard scale; (ii) photometry using the positive-film method; (iii) radioactive toning of the film and measurement of the β emission; (iv) direct photometry from an integrating Weissenberg photograph. In all cases the tetragonal symmetry is used to obtain internal evidence of consistency and results are obtained from different sizes of crystals, instruments (including X-ray tubes) and observers where possible.

19. T. NOGUCHI & A. F. MOODIE. *Non-linearity problem in an image-seeking machine.*

Minimum signals from any number of photo-cells are linearized at the last stage by suitably choosing the levels at which a contour line generator works.

20. G. VON ELLER. *Le photosommateur harmonique: applications et nouveau modèle.*

Un nouveau modèle de photosommateur harmonique (appareil pour le calcul par analogie optique des séries de Fourier bidimensionnelles) a été construit, qui se distingue du modèle expérimental par une précision meilleure, de plus larges possibilités de travail et une maniabilité plus grande. Les applications et méthodes sont cependant restées les mêmes; parmi les opérations de base sont à citer—outre le développement en série de Fourier—des techniques de densitométrie, de mesure des phases, d'exploration de séries à domaine étendu, de mise en évidence des lignes de niveau. Développées en cristallographie, ces manipulations nous ont permis, entre autres, le calcul optique de toutes projections et sections des espaces cristallins direct et réciproque (ou de leurs dérivés), la recherche des structures par essai et erreur, une extension de la technique de Hanson & Lipson de diffraction par quatre mailles, le parachèvement des structures par les séries 'différence'.

Sa précision fait du photosommateur un outil de travail efficace.

21. L. BRÚ, M. P. RODRIGUEZ & M. CUBERO. *Application of Eller's optical machine to the determination of crystal structures by the direct method.*

We show the possibility of obtaining the Buerger's image-seeking functions (sum, product and minimum) by using Eller's optical machine. These functions are obtained by appropriate translations of the Patterson projections and a series of successive or simultaneous photographic prints.

To get the minimum function it is necessary to obtain previously (always with the optical machine) the function $P(x, y) - P(x+u, y+v)$ which allows the selection of the corresponding Patterson's projections.

Applications are made.

22. L. BRÚ, M. P. RODRIGUEZ & A. L. L. CASTRO. *Application of Eller's optical machine to the determination of crystal structures by the trial-and-error method.*

We show a modification of Eller's optical machine that allows the calculation of the signs of the structure factors. It is also possible to get an approximate value of the factors that allow one to select or to exclude models of the structure.

The modification consists essentially in the addition of a gyratory sector placed before the photographic plate. The form of this sector depends on the atomic factor of the atom.

The basis of the method lies in the property that the atomic factor is a function only of the distance between the origin of the reciprocal lattice and the corresponding lattice point.

We present also an application of the method recently proposed by Woolfson of the permutation synthesis.

Applications are made.

23. L. BRÚ, M. P. RODRIGUEZ & M. G. GEA. *Applications of Eller's optical machine to the refinement of crystal structures.*

The purpose of this paper is to expose the possibility of using Eller's optical machine in the refinement of crystal structures by means of the synthesis $F_o - F_c$.

We study: (*a*) The influence of the translations of the atoms from their correct positions; (*b*) The influence of the temperature factor; (*c*) The presence of non-isotropic vibrations.

In all cases, the mistakes introduced in the calculated structure appear very clearly in the corresponding photographs.

Applications are made.

24. A. D. Booth. *The application of MAGIC to the determination of crystal structures.*

A short account of the features of the latest digital calculator based upon the design produced at Birkbeck College Electronic Computation Laboratory. MAGIC—or magnetic integer calculator—is a very small high-speed machine and its characteristics in Fourier synthesis and structure-factor calculation will be described.

25. A. D. Booth. *S. E. F. S.*

This machine uses a magnetic drum store to eliminate the synchronized oscillators used by Pepinsky. A model which will deal with four values of $F(h0l)$ has been constructed and its performance and possible future development will be discussed.

26. P. H. Dowling, C. F. Hendee, T. R. Kohler & W. Parrish. *Improved detectors for X-ray analysis.*

During the past decade Geiger-Müller counters have proven their usefulness and superiority to film in many fields of X-ray analysis. The two principal limitations have been (1) non-linearity (dead time 270 μ sec. with full-wave rectified copper target X-ray tube) which limits the accuracy of intensity measurements, and (2) they cannot be used to measure high intensities (exceeding 5000 counts/sec. without interposing absorbing filters to reduce the counting rate. Several schemes have been used to reduce the dead time but these were usually complicated and gave an improvement of perhaps a factor of five. These difficulties are overcome by side window proportional counters and scintillation counters and an extensive program on their development has improved them to the point where they are as practical and dependable as Geiger counters.

Since these detectors will soon be used widely in X-ray analysis we have studied their characteristics over a wide range of conditions encountered in powder and single-crystal diffraction and X-ray spectroscopy (fluorescence and absorption). The following factors were considered: linearity of response, quantum counting efficiency in the wavelength region 0·2–15 Å, stability, background, circuits and other practical requirements.

Both detectors have a dead time < 1 μsec., giving a linearity of better than 1% at 10,000 counts/sec. and counting rates in excess of 100,000 counts/sec. can be measured easily. The quantum counting efficiency of the NaI.Tl crystal itself can be made 100% for any wavelength. In the actual counter, the 0·005 in. Be window reduces the efficiency gradually with increasing wavelength to 80% at 3 Å, but the sensitivity is still so uniform as to make it ideal for X-ray spectroscopy. In the softer X-ray region 3·0–15 Å, it becomes more difficult to use because the pulses produced are of the same order of magnitude as the photomultiplier tube noise. Proportional or side-window Geiger counters are preferred for the longer wavelengths and the factor limiting the efficiency is the window absorption. Proportional counters 1 in. in diameter with about 30 cm. (Hg) pressure xenon have a spectral response nearly identical with the end-window argon Geiger counter (55 cm. Hg, 100 mm. long, 60% efficiency at Cu $K\alpha$). The lower efficiency for short wavelengths limits the usefulness of these counters in X-ray spectroscopy but is advantageous in diffraction work with Cu and longer wavelengths.

The pulse heights produced by proportional and scintillation counters are proportional to the energy of the incident X-rays. Hence they have the further important advantage over Geiger counters because the background from scattered X-rays, subharmonics in monochromator or single-crystal measurements, radioactivity in the specimen, cosmic rays, tube noise, etc. may be reduced or eliminated by simple electronic pulse-height discrimination. The wavelength (energy) resolving power of the proportional counter is about 2·5 times better than the scintillation counter, although the resolution of the latter is adequate for many problems.

27. R. L. Gordon & G. Nagelschmidt. *Application of X-ray diffraction to quantitative analysis of rocks.*

Two methods will be described. In the first, a photographic method, synthetic boehmite is used as an internal standard; either peak or integrated intensities may be compared. The second method utilizes Geiger–Müller counters to measure line intensities and the output of the X-ray tube; an internal standard can often be dispensed with, and the sample is then compared with a pure reference sample of the mineral to be determined. For accurate results (without internal standard) a correction for X-ray absorption in the sample is required; this may be based either on direct measurement of the mass absorption coefficient or on data available from other sources.

The techniques were developed for dust analysis in silicosis research, but can be used generally for analysis of clays, shales and similar sedimentary rocks. It was found in the course of the work that the intensity of quartz diffraction lines varies with particle size; there is a maximum in the region 2–5 micron. The fall in intensity at large particle diameters is due to extinction; that for very fine particles appears to be due to imperfections in the surface structure.

28. C. Alexanian. *Analyse quantitative des minéraux dans les roches au moyen des rayons X.*

Les échantillons sont examinés sous forme de plaquettes ($1 \times 2{,}5 \times 0{,}1$ cm.). Ces dernières sont préparées par tassement ou compression après un broyage de la roche. La granulomètrie de la poudre employée est uniforme, de 35 à 45 μ. Lorsque la roche est compacte et microcristalline, l'analyse se porte également sur des plaquettes taillées dans la masse même de la roche.

L'examen débute sous incidence rasante ($2\theta = 2°$). L'enrégistrement des raies de diffraction, en position et en intensité, exprimé sous forme de pics, s'opère par voie électronique. On mesure la hauteur, ou éventuellement, la surface de ces pics. Pour l'analyse, on s'attache aux pics les plus forts se trouvant, si possible, dans une même zone d'angles 2θ; pour le quartz 26,7°, la calcite 29,4°, la dolomie 31°, l'anhydrite 25,6°, le mica 27°. L'identification ou l'analyse qualitative s'effectue du

reste simulanément grâce à la présence des autres raies qui seraient caractéristiques aux minéraux respectifs.

L'évaluation finale est faite par la moyenne arithmétique de cinq mesures successives dont les valeurs sont rapportées à des courbes d'étalonnage préalablement établies. Les résultats numériques sont *excellents* pour un taux de 10 à 100% de présence dans une roche de 1, 2 ou 3 constituants. La précision varie alors de ±3 à ±1% sur le taux réél. Il y a indécision pour les taux inférieurs à 5%. Des exemples concrets intéressant la pétrographie, la géologie et les mines sont passés en revue.

§ 2. Progrès récents dans la détermination des structures

1. C. H. Carlisle & G. S. D. King. *A method of refinement for complex structures.*

Structure factors calculated by sampling a Fourier map on a sufficiently fine mesh are normally identical with those used in computing the map. If sampling is confined to those regions whose density is above a certain value the structure factors will be different from the values put into the map. The imposition of this restriction on the electron-density map takes into account the fact that in a real structure the electron-density distribution consists of peaks (not necessarily resolved atoms) surrounded by regions of low density. By using the new calculated phases a Fourier map is produced in which there are fewer spurious peaks below the minimum sampling level. Provided that in the initial Fourier map, which need be calculated from only a few reflections, a large proportion of the phases are nearly correct the process will refine to give a self consistent set of phases corresponding to a substantially correct electron density map.

The method is being applied to the *b*-axis projection of ribonuclease the refinement of which is described elsewhere. As an example the refinement of the *c*-axis projection of nicotinic acid starting with five reflexions of correct sign is given.

2. J. Karle. *Invariants and seminvariants for crystals in categories 2 and 3.*

The crystal structure alone does not determine the phases of the structure factors but rather the values of certain linear combinations of the phases, called the structure invariants. The values of the structure invariants are thus independent of the choice of origin. However, if the origin is restricted by selecting a functional form for the structure factor, there still exist linear combinations of the phases whose values are independent of the choice of origin consistent with the chosen functional form. These are called the structure seminvariants. For categories 2 and 3 (H. Hauptman & J. Karle, *Solution of the Phase Problem. I. The Centrosymmetric Crystal*, ACA Monograph No. 3.), the distinction between the structure invariants and seminvariants is non-trivial.

3. H. Hauptman. *Phase-determining relations in categories 2 and 3.*

The dependence of phase on the choice of origin is clarified by means of the introduction of special linear combinations of the phases, the structure invariants and seminvariants. Any solution of the phase problem must yield information concerning the values of the invariants and seminvariants rather than of the phases themselves. A solution of the phase problem by probability methods has already been described (H. Hauptman & J. Karle, *Solution of the Phase Problem. I. The Centrosymmetric Crystal*, ACA Monograph No. 3.), and involves the evaluation of certain simple definite integrals, called the mixed moments. As will be shown now, for categories 2 and 3, the mixed moments lead, in a non-trivial way, to the structure invariants and seminvariants discussed in the previous talk by J. Karle.

4. C. L. Christ, J. R. Clark & H. T. Evans. *Application of the Hauptman–Karle method of phase determination to the structure of colemanite,* $2CaO.3B_2O_3.5H_2O$.

The structure of colemanite has been determined directly from the distribution of the intensities, using the method of Hauptman & Karle.

Colemanite is monoclinic, $P2_1/a$, $a = 8{\cdot}743 \pm 0{\cdot}004$, $b = 11{\cdot}264 \pm 0{\cdot}002$, $c = 6{\cdot}102 \pm 0{\cdot}003$ Å, $\beta = 110° 7' \pm 5'$, $Z = 2$. Using the signs calculated by the H–K method, 944 terms were used to calculate electron-density sections over the *xz* plane at intervals of 1/60 for $y = 0$ to $y = 1/4$. These show the presence of infinite B–O chains running parallel to the *a* axis, the chain element consisting of a BO_3 triangle and two BO_4 tetrahedra. This gives a chain composition of $[B_3O_4(OH)_3]_n^{-2n}$. Each Ca^{++} is surrounded roughly octahedrally by one H_2O and five O. The formula for colemanite may thus be written $CaB_3O_4(OH)_3.H_2O$.

5. R. G. Howells. *The Application of the Sayre–Cochran sign relation to the structure of harmine.*

The alkaloid harmine, $C_{13}H_{12}ON_2$, crystallizes in the space group $P2_12_12_1$ and its unit-cell dimensions are $a = 19{\cdot}3$, $b = 9{\cdot}8$, $c = 5{\cdot}8$ Å.

No signs of *F*'s were known and none could be determined by means of Patterson projections. Systematic application of the Sayre–Cochran relation $S(H) = S(H').S(H+H')$ to the reflexions of largest intensity in the $[hk0]$ zone led to a knowledge of the signs of 41 structure factors. The resulting Fourier projection gave a trial structure which gave reasonable agreement with the observed structure factors. Refinement is proceeding by means of two-dimensional Fourier syntheses and $F_o - F_c$ syntheses.

6. Dorothy Wrinch. *On the interpretation of vector maps.*

In order to clarify the new situation in protein crystallography, this communication devotes some attention to vector distributions, contrasting them with vector sets.

For all crystals, vector map interpretations depend upon the (D, D_v) relation, where D is an electron-density distribution and D_v is the Fourier transform of $|T|^2$, where T is the transform of D. If D is resolved into sub-distributions such as K_f at x_f, y_f, z_f, $D = \Sigma(K_f \text{ at } f)$, then $D_v = \Sigma\Sigma(K_{fg} \text{ at } f-g)$ where K_{fg} is the image of K_f in K_g. In the case of atoms, the form of the K's is known at the start, say $K_f k_f \sim \exp(-p_f r^2)$ and so $K_{fg} \sim k_f k_g \exp(-p_{fg} r^2)$, where $1/p_{fg} = 1/p_f + 1/p_g$. The problem is then closely related to and may be attacked via a problem in vector sets, i.e. finding $d = \Sigma(k_f \text{ at } f)$, given $d_v = \Sigma\Sigma(k_{fg} \text{ at } f-g)$.

In protein crystallography, D is not resolved into

individual atoms and the K's are, at best, of relatively large extent. Information as to the electron-density distributions therein is the first objective. Since sufficiently near the origin $D_v = \Sigma K_{jj}$, the superposed self-images or vector maps of the K's, the first task is to make all possible inferences regarding the K's from this region of the vector map. But this is a problem of vector distributions not of vector sets.

It is readily seen that it is the whole topography of a K_v (the lie of the contours, the extent, nature of boundary, symmetry, etc.) and not merely the set of maxima, if any, which is the vector expression of a K distribution. One consequence of this situation is the fact that K_v's can have maxima which do not correspond in K to pairs of maxima related by the corresponding vector. The type of inference which is the basis of interpretations of vector sets has no analogue in vector distributions: it is not legitimate to infer from maxima of a K_v that K has related maxima or indeed any maxima at all.

This negative result destroys the case for rodlike polypeptides in protein crystals. Superseding this traditional picture is the new interpretation which infers, from vector maps which are neither uniaxial nor biaxial near the origin, the presence in the protein crystals of structures which are genuinely three-dimensional in nature.

7. V. Vand & R. Pepinsky. *Developments in the statistical approach to X-ray analysis.*

Statistical formulae, as developed by Hauptman & Karle, do not represent a general practical solution to the phase problem of crystallography, especially for the space group $P\bar{1}$. However, the statistical method may prove of use if applied with understanding of the problems involved. With this in view, more accurate distribution functions have been derived and maps which are related but superior to Harker maps have been constructed. These will be demonstrated.

8. D. Rogers. *An improved method of scaling intensities.*

The precision of Wilson's scaling method has been improved by two new procedures:

(1) The graph of $\ln(\langle I' \rangle / \Sigma f_j^2)$ versus $\sin^2\theta$ is linear only if $\sum_j f_j^2$ is based on f data appropriate to the structure. Strong curvature at low $\sin\theta$ has been found if Hartree f's are used for light atoms. The linear extrapolation back to $\theta = 0$ then gives rise to considerable error in the scaling factor. If $\ln(\langle I' \rangle / \Sigma Z_j^2)$ is also plotted the two curves have a common intercept and for structures consisting largely of light atoms this latter function is the more nearly linear of the two. This reveals any inappropriateness in the f curves assumed and provides a provisional empirical curve.

(2) The values of $\langle I' \rangle$ have always been evaluated in narrow ranges of $\sin\theta$ and it is often difficult to get smooth curves for the above functions, especially when there are few distinct intensities in a zone of high symmetry. The form of the curves for the important small-θ range is also very ill-defined. By a suitable transformation of the minimum profile of the origin peak of the Patterson function one obtains $k\sum_j f_j^2$ from which both k, the scaling factor, and an empirical f-curve can be obtained with a precision considerably better than has been possible hitherto.

9. H. Lipson. *Information obtainable from weighted reciprocal lattices.*

The reciprocal lattice of a crystal with each point weighted according to the intensity of the corresponding X-ray reflexion can be regarded as the sampled Fourier transform of the unit-cell contents. Drawings of these weighted reciprocal lattices may therefore give some information about the transform and thence about the arrangement of atoms to which it belongs. For example, if a structure contains two heavy atoms, the resultant fringes can be clearly seen; the positions of the heavy atoms can then be calculated, and the signs of the structure factors allotted by inspection.

Separate features of molecules can be detected. A straight chain of atoms gives rise to rows of strong reflexions in reciprocal space; the direction and spacing of the chain can thence be calculated. A benzene ring gives rise to a hexagonal arrangement of strong reflexions; the orientation of such a benzene ring can thence also be calculated.

It is hoped ultimately to be able to recognize complete structures from their X-ray diffraction patterns, and one of the objects of the present work is to gain as much experience as possible about the diffraction patterns of various types of structural features.

10. C. A. Taylor. *The application of optical transform methods to structures which contain non-planar molecules.*

The successful application of optical transform methods has, so far, been confined to structures containing planar molecules of which the general outline was known. The present contribution describes attempts that have been made to extend the technique to more complicated structures. Use is made of the general principle that the transform of a whole molecule is the vector sum of the transforms of the individual portions. It is thus possible to treat a complicated problem by considering first the shape of each portion of the molecule, then their positions with respect to each other, and finally the position of the complete molecule in the unit cell.

The difficulty of presenting the transforms of separate portions simultaneously to the eye in such a way that individual contributions at any point can be identified has been solved by making use of the principles of three-colour photography; a colour is associated with each portion and the resultant colour at any point gives the information required. The illustrations are from work on the structure of vitamin A acetate which has been carried out in collaboration with Mrs Olga Kennard.

11. E. J. W. Whittaker. *Diffraction by cylindrical lattices.*

Chrysotile is known to give sharp reflexions of the type $h0l$, and unsymmetrical diffuse reflexions involving a non-zero k index. It is also known from electron-microscope studies that the individual fibres of chrysotile are tubular in form, and it has been suggested that the layers of composition $Si_2O_5(OH)$–Mg_3–$(OH)_3$ are themselves curved (E. Aruja, Ph.D. Thesis, Cambridge, 1943). Evidence in support of this has been adduced (E. J. W. Whittaker, *Acta Cryst.* (1953), **6**, 747) from Fourier syntheses calculated from the intensities of the $h0l$ re-

flexions, and the validity of treating these sharp reflexions from a circular cylindrical lattice as ordinary crystal reflexions has been discussed theoretically (E. J. W. Whittaker, *Acta Cryst.*, in the press). However, there are good *a priori* reasons for supposing that a cylindrical lattice might take the form of a spiral cylinder rather than of a set of concentric circular cylinders; as the corresponding theory is intractable, recourse has been taken to the method of optical transforms, using the optical diffraction apparatus described by W. Hughes & C. A. Taylor (*J. Sci. Instrum.* (1953), **30**, 105). The results obtained from circular lattices confirm the theoretical conclusions, and it is shown that spiral lattices give closely analogous results.

The diffuse reflexions from these lattices have also been studied, and it is shown that the profiles of the diffuse reflexions from chrysotile differ considerably from those of either a circular or a spiral cylindrical lattice. The difference may be due partly to the occurrence of a distribution of fibre diameters in chrysotile, and partly to the occurrence of split fibres.

A number of interesting features occur in the optical transforms of the circular and spiral lattices which become explicable when the transforms of sets of points equally spaced round a single circle or spiral turn are considered. The results illustrate the theory of diffraction by a circle (V. A. Fock & V. A. Kolpinsky, *J. Phys. U.S.S.R.* (1940), **3**, 125) and by a circular arc (M. Blackman, *Proc. Phys. Soc.* B, (1950), **64**, 631).

12. R. HOSEMANN. *Korrektur des Babinet'schen Theorems.*

Das Babinet'sche Theorem, welches besagt, dass das Beugungsbild zweier zueinander komplementärer Schirme ausserhalb des Nullstrahles dasselbe sei, hat sich in den vergangenen hundert Jahren in vielen Fällen gewiss als 'fruchtbares Prinzip' im Sinne von Babinet erwiesen. Für die Strukturerforschung mittels irgendwelcher Strahleninterferenzen ist es aber deshalb korrekturbedürftig, weil eine quantitative Strukturanalyse auch einer quantitativen background-Analyse und einer Miterfassung von Beugungsnebenmaxima bedarf. Hierauf hat zuerst Boersch hingewiesen (*Z. Phys.* (1951), **131**, 78). Mit Hilfe von Faltungsintegralen gelingt eine einfache Berechnung der Streuintensität. Ist $\varrho(x)$ eine Ortsfunktion im physikalischen Raum (Ortsvektor x), die proportional ist zur Dichte der kohärente Streustrahlung erzeugenden Zentren und $\varrho_a(x)$ eine Ortsfunktion, die mindestens innerhalb des von $\varrho(x)$ beanspruchten Volumens V von konstantem Wert ist, ausserhalb eines Volumens $V_a \geqq V$ aber verschwindet, so ist $\varrho_b(x)$ dann im Sinne Babinets komplementär zu ϱ, wenn die Relation erfüllt ist

$$\varrho_b(x) = \varrho_a(x) - \varrho(x) . \tag{1}$$

Ist $R(b), R_a(b), R_b(b)$ die Fouriertransformierte von $\varrho, \varrho_a, \varrho_b$, also z.B.

$$R(b) = \int \varrho(x) \exp[-2\pi i(bx)] dv_x \tag{2}$$

und b der reziproke Ortsvektor im Fourierraum, so ist die von $\varrho(x)$ gestreute Intensität $I(b)$ gegeben durch (f_e^2 Polarisationsfaktor usf.):

$$I(b) = f_e^2 RR^*, \tag{3}$$

während die komplementäre Struktur eine Intensität $I_b(b)$ erzeugt

$$I_b(b) = f_e^2(RR^* + R_aR_a^* - R_aR^* - RR_a^*) . \tag{4}$$

Es wird allgemein bewiesen, dass $I_b(b)$ nur für

$$V_a >>> V \tag{5}$$

und bei Benutzung von Beugungsapparaturen endlicher Auflösung entartet zu

$$I_b(b) = f_e^2(RR^* + R_aR_a^*) , \tag{6}$$

sich also stets von $I(b)$ um den Term $R_aR_a^*$ unterscheidet. Insbesondere bei Anwendung auf Probleme der Kleinwinkelstreuung ist die Ungleichung (5) aber nicht erfüllt. Ein in der Literatur als 'Reziprozitätsgesetz' bekanntes Phänomen besteht darum nicht. Dann treten auch noch die weiteren Korrektursummanden in (4) ganz wesentlich in Erscheinung. Hierfür werden eine Reihe von lichtoptisch hergestellten Beugungsbeispielen erbracht.

13. R. HOSEMANN. *Bedeutung der Faltungsintegrale für die Strukturanalyse.*

Die Strukturanalyse mittels Röntgen- und Elektronen-Interferenzen lässt sich mit Hilfe von Faltungsintegralen bei genügender Genauigkeit der Messung der Intensitätsverteilung in einigen wesentlichen Punkten ausbauen und teilweise sogar gegenüber der heute benutzten Fouriersynthese vereinfachen. Insbesondere gelingt so eine quantitative Fehlerabschätzung des errechneten Strukturergebnisses. Ist

$$R(b) = \mathfrak{F}(\varrho) = \int \varrho(x) \exp[-2\pi i(bx)] dv_x$$

die Fouriertransformierte der unbekannten Struktur $\varrho(x)$, f_e^2 der Polarisations- und Thomsonfaktor, $\widehat{g_1 g_2}$ das Faltungsprodukt und $\overset{2}{\widetilde{g}}$ das Faltungsquadrat

$$\widehat{g_1 g_2} = \int g_1(y) g_2(x-y) dv_y ,$$

$$\overset{2}{\widetilde{g}} = \int g_1(y) g_2(x+y) dv_y ,$$

so liefert die Inverstransformierte der durch f_e^2 dividierten experimentell beobachteten Intensitätsverteilung $I(b)$ die sogenannte Q-Funktion, die mit der Pattersonfunktion in enger Verwandtschaft steht und nichts anderes ist als das Faltungsquadrat von ϱ

$$\mathfrak{F}^{-1} I/f_e^2 = Q(x) = \overset{2}{\widetilde{\varrho}} .$$

Gelingt es, aus $Q(x)$ durch einen dem Faltungsquadrat inversen Prozess die sogenannte Faltungswurzel zu bilden

$$\sqrt{Q}(x) = \varrho(x) ,$$

so ist damit die Strukturanalyse beendet. Es lässt sich allgemein beweisen, dass räumlich begrenzte $\varrho(x)$-Strukturen mit Symmetrie- oder Antisymmetriezentrum grundsätzlich auf diese Weise eindeutig bestimmbar sind.

Auf diese Weise lassen sich insbesondere auch parakristalline Strukturen analysieren. Bei kristallinen Strukturen bringt die Ersetzung der üblichen Fourierreihen durch Fourier- und Faltungsintegrale Vorteile. Insbesondere gelingt auf diese Weise auch in vielen Fällen eine Abschätzung des Abbrucheffektes. Aber auch homo-

metrische Strukturen lassen sich durch Faltungsintegrale in einfacher Weise erkennen und oftmals analysieren.

Durch zweidimensionale Modelle und deren lichtoptisch hergestellte Faltungsquadrate und Beugungsbilder werden die Zusammenhänge veranschaulicht.

§ 3. Structures des minéraux

1. P. A. SABINE & B. R. YOUNG. *Cell-size and composition of the baryte–celestine isomorphous series.*

Examination of a series of sulphates of barium and strontium from the West of England by chemical and X-ray powder methods has shown a correlation between cell-size and composition. When cell dimensions, calculated from spacings of indexed lines of powder photographs, are plotted against chemical composition a straight-line graph results, confirming that the series is isomorphous. The work forms part of an extensive investigation into the paragenesis of the minerals of the Bristol and Somerset coalfields.

2. C. KURYLENKO. *La syngénite.*

La syngénite ($K_2SO_4.CaSO_4.H_2O$) se présente sous forme de prismes incolores d'éclat vitreux. Les arêtes $a = 9{,}5_3$, $b = 7{,}1_2$, $c = 5{,}9_9$ kX. et $\beta = 105°$ sont déterminés à l'aide de la méthode de Weissenberg. Les diagrammes obtenus indiquent $(0k0)$ seulement pour $k = 2n$. Le groupe de recouvrement est C_{2h}^3–$P2_1/m$. Grâce à une centaine de taches de diffraction nous avons un diagramme de Patterson; il serait possible de définir approximativement les positions des atomes.

3. T. ITO. *The symplesite problem.*

The mineral of the composition $Fe_3(AsO_4)_2.8H_2O$ is dimorphous, one being triclinic (symplesite) and the other monoclinic (parasymplesite, a vivianite-like new mineral from Kiura, Japan) with the cell dimensions:

	Symplesite	Parasymplesite
a	7·85 kX.	10·25 Å
b	9·39 kX.	13·48 Å
c	4·71 kX.	4·71 Å
α	99° 55′	—
β	97° 22½′	103° 50′
γ	105° 51½′	—
Space group	$P\bar{1}$	$C2/m$
Z	1	2

The crystal structure of parasymplesite (worked out and published as of symplesite (H. Mori & T. Ito, *Acta Cryst.* (1950) **3**, 1)) bears a close resemblance to that of symplesite now to be reported. The former structure is a polysynthetic structure formed of the latter structure although the mode of H_2O linkage is not the same in them.

4. J. ZEMANN. *On the crystal structure of koechlinite,* Bi_2MoO_6.

Koechlinite was first described by Schaller on specimens from the Daniel mine, Schneeberg, Saxony. The composition of the orthorhombic, markedly pseudo-tetragonal crystals corresponds well to the formula Bi_2MoO_6. Lattice constants and diffraction group have been determined by Wolfe & Frondel as follows: $a = 5{\cdot}48$; $b = 16{\cdot}16$, $c = 5{\cdot}48$ kX.; diffraction group $Cmca$; $Z = 4$. These statements are confirmed from rotation, Weissenberg, and precession photographs.

The lattice constants correspond very closely to the cell found by Sillén & Lundborg for tetragonal La_2MoO_6, if one turns this cell by 45°. Ascribing to Koechlinite the crystal structure of La_2MoO_6 (with Bi on the positions of La), one gets (e.g. for all $h0l$ and hhl reflexions) a practically perfect correspondence of calculated and estimated intensities. That koechlinite does not have quite this structure is only evident from several very weak $0kl$ and hkl reflexions. The crystal structure of koechlinite is therefore closely related to that of La_2MoO_6.

5. G. F. CLARINGBULL. *X-ray study of raspite (monoclinic* $PbWO_4$).

6. H. STRUNZ. *Zur Systematik der Phosphatmineralien.*

Seit Erscheinen der 2. Auflage der *Mineralogischen Tabellen* (1949) sind auf dem Gebiet der Phosphatforschung wesentliche Fortschritte erzielt worden: (1) Diskreditierte Namen; (2) Neue Phosphatmineralien; (3) Vereinfachung bisheriger Formeln; (4) Neue Beziehungen der Isotypie und Homöotypie; (5) Strukturbestimmungen.

Zu (1)–(4) werden eigene Ergebnisse vorgelegt, desgleichen eine vereinfachte Systematik.

7. A. PABST. *Structures of some tetragonal sheet silicates.*

The phases $CaCuSi_4O_{10}$ ('Egyptian Blue'), $SrCuSi_4O_{10}$ and $BaCuSi_4O_{10}$ have been grown in single crystals. Their structure, in the space group $P4/ncc$, is similar to that of the mineral gillespite, $BaFeSi_4O_{10}$, previously established (A. Pabst, *Amer. Min.* (1943), **28**, 372). The properties are as follows:

	$CaCuSi_4O_{10}$ 'Egyptian Blue'	$SrCuSi_4O_{10}$	$BaCuSi_4O_{10}$	$BaFeSi_4O_{10}$ gillespite	Leached gillespite
a_0 (Å)	7·30±0·01	7·37	7·44	7·51	7·64±0·03
c_0 (Å)	15·12±0·02	15·57	16·11	16·07	15·10±0·05
$G_{obs.}$	3·06±0·02	3·32±0·03	3·47±0·03	3·402±0·004	1·9±0·1
$G_{calc.}$	3·09	3·32	3·52	3·407	2·15
N_0	1·636±0·003	1·628	1·632	1·621	1·449
N_e	1·591	1·588	1·593	1·619	1·441
O	'Deep blue'	Blue	Blue	'Deep rose red'	
E	'Pale rose'	Nearly colorless	Nearly colorless	'Pale pink'	

Gillespite is not known in good crystals. The artificial materials were all obtained in measurable crystals showing the forms {001}, {102} and {110} in the order of prominence predicted from the Donnay–Harker rule.

Gillespite is easily attacked by dilute mineral acids. The copper analogues are impervious to attack. This may be attributed to the superior stability of copper in 4-fold planar coordination. Such coordination is characteristic of divalent copper but unusual for ferrous iron.

Leached gillespite has been found to retain the silicate sheet structure of the parent material with only slight dimensional changes. The intensities of the *hk*0 spots indicate that the structure within each sheet is maintained. Extreme diffuseness of all other spots indicates that the stacking of the sheets is greatly disarranged.

8. J. ZUSSMAN. *Investigation of the crystal structure of actinolite.*

An amphibole with high water content, as shown by chemical methods, has been subjected to X-ray single-crystal analysis in one projection. The 'vacant position' which may have housed a water molecule or (OH) group is seen to be truly vacant, and atomic co-ordinates are compared with those found for tremolite (Warren) and crocidolite (Whittaker).

The distribution of ions among the different sites is also discussed.

9. J. ZUSSMAN. *Investigation of the crystal structure of antigorite (Mikonui).*

The cell dimensions given by Aruja are $a = 43{\cdot}5$ $b = 9{\cdot}26$, $c = 7{\cdot}28$ Å, $\beta = 91°24'$.

A Weissenberg (*h*0*l*) photograph clearer than those hitherto obtained has been indexed, and the intensities of reflexions measured visually. Trial structures of layers similar to those of kaolinite, but corrugated in different ways, have been conveniently tested by the 'optical transform' method of Hanson, Lipson & Taylor.

The relation of this mineral to other serpentines is discussed.

10. H.-G. HEIDE. *Die Struktur des Dioptas,* $Cu_6(Si_6O_{18}) \cdot 6H_2O$.

Es wurden Schwenk- und de Jong-Aufnahmen von Dioptas ausgewertet. Mit Patterson- und Elektronendichte-Projektionen kann die Lage aller in der Struktur vorhandenen Atome (mit Ausnahme der H) ermittelt werden. Es ergeben sich sechsgliedrige Ringe Si_6O_{18}. Zwischen den Ringen ist molekulares H_2O eingelagert, das jedoch nicht ohne weiteres durch die Ringe hindurchtreten kann, weil die zu passierenden Hohlräume verhältnismässig eng sind. Dadurch wird die schwere, nicht reversible Wasserabgabe des Dioptas erklärt, der nicht zu den Zeolithen zu rechnen ist. Die Orientierung der H_2O-Moleküle (Lage der H) lässt sich auf Grund ihrer Umgebung vermuten. Die Cu-Ionen, welche als Kationen die Ringe zusammenhalten, treten auch im Dioptas mit 6-zähliger Koordination in verzerrten Oktaederlücken auf. Die gefundene Struktur ist durch eine Statistik von Strukturfaktoren gesichert (reliability index = 0·16). Sie stimmt *nicht* überein mit der Struktur des Dioptas, welche von Butusov, Belov & Golovastikov (1952) angegeben wurde, und welche das Verhalten des H_2O schlechter erklärt, sowie eine unwahrscheinliche Koordination des Cu und unwahrscheinliche Atomabstände aufweist.

11. R. PULOU, M. ORLIAC & L. CAPDECOMME. *Sur les déformations du réseau des crandallites–deltaites et des wardites–millisites.*

Les phosphates alumino-calciques et alumino-calco-sodiques des types crandallite–deltaïte et wardite–millisite ne sont encore connus que par un petit nombre d'exemples. On sait toutefois que les crandallites et deltaïtes sont isostructurales avec symétrie rhomboédrique holoèdre, et que les wardites et millisites, isostructurales elles aussi, sont quadratiques avec la symétrie λ_4.

Les remplacements isomorphiques dans ces structures ont été peu étudiés. L'examen de divers échantillons nous a permis de constater l'ampleur des variations de compositions chimiques: substitution de Fe''' à Al, remplacements de Na^2 par Ca, introduction de Mg.

Ces variations de la composition chimique entraînent des modifications des paramètres cristallographiques extrêmement marquées sur les diagrammes de poudres. Les rapports *c*/*a* généralement attribués aux wardites et aux crandallites, sont respectivement de 2,68 et de 2,31. Ces ordres de grandeur sont tels que les variations résultant des substitutions dans le réseau entrainent des déplacements relatifs très sensibles dans certains couples de raies, avec parfois superposition et même inversion. Un minéral du groupe des crandallites nous a donné un diagramme simplifié de cristal quasi-cubique (rapport *c*/*a* voisin de 2,45).

12. G. PEYRONEL. *Recherches sur la structure cristalline d'un silicate naturel à composition quantitative inconnue.*

Le silicate naturel, bazzite, contient, d'après une détermination microqualitative (Artini), principalement du scandium et du fer, mais sa composition quantitative n'a pas pu être établie a cause de son extrême rareté.

Sur un échantillon unique on a établi, aux rayons X, que le minéral a une symétrie de diffraction hexagonale D_{6h}–6/*mmm*. Les dimensions de sa cellule élémentaire, $a = 9{\cdot}51$ et $c = 9{\cdot}10$ Å, sont très proches de celles du béryl. On a *hkil* = quelconque; 000*l* avec $l = 2n$. Le groupe de symétrie le plus probable est D_6^6–$P6_322$.

On va tâcher d'obtenir, par l'analyse Patterson, quelques renseignements sur le type d'anion silicate ainsi que sur la position et la nature des cations présents dans cette structure.

13. A. McL. MATHIESON & G. F. WALKER. *The crystal structures of normal and partially-dehydrated* Mg-*vermiculite.*

The single-crystal analysis of Mg-vermiculite which is monoclinic, $a = 5{\cdot}32$, $b = 9{\cdot}18$, $c = 2 \times 14{\cdot}4$ Å, $\beta = 97°$, has been reported (Mathieson & Walker, *Amer. Min.* (1954), **39**, 3). The principal interest lay in the distribution of exchangeable cations and water molecules in the region between the mica-like silicate layers. The cation and water sites were determined from the analysis, and the probable distribution of the available cations and waters over their respective sites was deduced.

Partial collapse of the mineral normal to 001 is effected by heat-treatment at 80° C. and the sharp spectra

can be indexed on the basis of a monoclinic cell, $a = 5{\cdot}32$, $b = 9{\cdot}18$, $c = 11{\cdot}8$ Å, $\beta = 90°$. The interlayer region of partially-dehydrated Mg-vermiculite contains only one sheet of water molecules arranged in a hexagonal network similar to that deduced for the water molecule sites in normal Mg-vermiculite. The water sheet lies at 2·43 Å from the oxygens of one silicate layer and 2·84 Å from those of the opposite layer. The latter distance is consistent with hydrogen-bonding between each water molecule and its related surface oxygen of the silicate layer, the relative disposition of the atoms being the same as in normal Mg-vermiculite. The short approach distance 2·43 Å occurs because the Mg cations are disposed between the water sheet and the surface oxygen sheet of the silicate layer, each cation being coordinated to three water molecules and three oxygen atoms.

The results of both analyses point to the importance, in the structure of layer-silicate minerals of this type, of hydrogen-bonding between water molecules and the surface oxygens of the silicate layers, and of the coordination behaviour of the cations.

14. H. D. MEGAW & C. H. KELSEY. *Cell dimensions of bultfonteinite.*

Bultfonteinite ($Ca_4Si_2O_{10}H_6F_2$) is triclinic, pseudo-orthorhombic. Accurate cell dimensions have been determined from high-angle reflexions by a method of successive approximations. The interaxial angles have been determined by the same method; the accuracy is greater than that of the goniometric study in the original description by Parry, Williams & Wright. The obvious choice of axes based on the pseudo-orthorhombic symmetry is incompatible with the convention that all interaxial angles should be greater than 90°, and the convention is therefore over-ridden in this case.

$a = 10{\cdot}992 \pm 0{\cdot}002$ Å	$\alpha = 93°57' \pm 18'$
$b = 8{\cdot}187 \pm 0{\cdot}002$ Å	$\beta = 91°19' \pm 2'$
$c = 5{\cdot}674 \pm 0{\cdot}001$ Å	$\gamma = 89°51' \pm 1'$.

The crystals are all twinned; there are two twin laws, imitating the higher symmetry, and the relative volumes of the components seem to depend on the magnitude of the departure from a 90° angle. Though oscillation photographs from a twin are more complex than those from a single individual would be, the interpretation is quite unambiguous.

The cell dimensions are related to those of afwillite, and so probably is the structure. The two minerals occur in the same locality and a chemical similarity was pointed out by Parry, Williams and Wright.

15. M. J. BUERGER & T. HAHN. *The structure of nepheline,* $KNa_3Al_4Si_4O_{16}$.

Nepheline belongs to space group $P6_3$ with $a = 10{\cdot}01$ Å and $c = 8{\cdot}405$ Å. The composition of nepheline is usually given as $NaAlSiO_4$ but implication maps, which readily located the metal atoms, showed that the alkali atoms occur in two different equipoints. The ideal formula is $KNa_3Al_4Si_4O_{16}$ with 2 formula weights per cell, in conformity with potassium content shown by analyses. One-quarter of the alkalis, silicons, and aluminums lie on special positions. The structure was determined by accepting the metal positions indicated by the implication maps, surrounding these by reasonable oxygen arrangements and by refining with successive Fourier syntheses. The structure is a silico-alumina tridymite framework, with alkali atoms occupying voids.

New Geiger-counter intensities were used for refinement by $\varrho_o - \varrho_c$ syntheses. The potassium location showed a negative anomaly of electron density; this was corrected by reducing the statistical number of potassium atoms in this site. A positive anomaly occurred near the threefold axis at $\frac{2}{3}, \frac{1}{3}, z$; this was corrected by moving the oxygen atom ideally situated on this axis to a statistical set of positions off the axis at 0·560, 0·230, z. This feature indicates that one variety of oxygen atom in the structure is in statistical disorder. When these anomalies are corrected the R factor for the $hk0$ reflections falls to 0·18. The refined structure and values for the Si–O and Al–O bond lengths were obtained by means of three-dimensional Fourier syntheses.

16. U. VENTRIGLIA. *La structure de la heulandite.*

L'auteur, au moyen d'analyses chimiques originales, de celles dans les ouvrages publiés, ainsi qu'au moyen de mesures absolues du volume de la maille élémentaire, établit que la formule constitutionnelle qu'il faut attribuer à la heulandite est $7SiO_2Al_2O_3CaO.6H_2O$. Les diagrammes de Laue et l'effet piézoélectrique vérifié ont permis d'établir que la symétrie de la heulandite n'est pas monoclinique holoédrique, d'après l'avis habituel, mais bien triclinique hémiédrique. Les photogrammes de Polany et les spectrogrammes de Weissenberg ont, d'autre part, confirmé les dimensions de la maille élémentaire; ils ont encore fait ressortir une pseudosymétrie monoclinique bien marquée: on a donc pris cette pseudosymétrie comme point de départ pour la résolution de la structure du minéral. On a, c'est-à-dire, admis que la structure de la heulandite peut être regardée comme étant une petite déformation d'une structure monoclinique.

Pour l'interprétation des données expérimentales on a eu recours aux synthèses de Patterson et Fourier et à la méthode des maxima avec la superposition des diagrammes des facteurs structuraux relatifs aux effets particuliers. La disposition des atomes, à laquelle on est parvenu ainsi, conduit à une structure caractéristique où les tétraèdres sont stratifiés suivant (010): les plans de deux couches qui se suivent sont espacés de $\frac{1}{2}b_0$. Dans ces plans se trouvent les $\frac{2}{3}$ des tétraèdres du minéral; ils sont placés de façon qu'ils forment un réseau avec des maillons hexagonaux. Chaque tétraèdre a donc trois ions d'oxygène en commun avec d'autres tétraèdres de la même couche et, par contre, un quatrième ion d'oxygène en commun avec un des tétraèdres résiduels, ne faisant pas partie de ces couches. Ces derniers, en liant entre elles les couches contigües, forment, à leur tour, des mailles hexagonales. Il en résulte une structure de tectosilicate avec des mailles hexagonales avec un entassement plus fort suivant (010). On peut justifier ainsi immédiatement le clivage parfait suivant (010), la pseudosymétrie monoclinique, les dimensions de la maille élémentaire et le contour hexagonal des cristaux. D'après cette structure Si et Al occupent les milieux des tétraèdres et pour chaque 2 Al un Ca occupe un des espaces entre les mailles hexagonales. Par conséquent, quant à l'eau, après un examen de toutes les hypothèses, celle de la présence dans le minéral des ions (OH) y comprise, on doit admettre que

l'eau ne prend pas part à la structure fondamentale du minéral et qu'elle est présente seulement comme H_2O.

17. S. W. Bailey & W. H. Taylor. *The structure of a triclinic potash felspar.*

Although the felspar structure has been known for twenty years, only an orthoclase, a sanidine and one form of anorthite have previously been examined by modern high-accuracy methods of structure-analysis. This paper describes the results of an accurate analysis of a triclinic potash felspar and in particular discusses the evidence thereby obtained for the ordered distribution of Al and Si atoms on the linked tetrahedra of the structural framework.

18. R. B. Ferguson, R. J. Traill & W. H. Taylor. *The albite structure.*

The structures of low-temperature and high-temperature albites have been determined as a part of a programme of high-accuracy analyses of important type-structures of the felspar group. The low-temperature albite is from Ramona, California, the high-temperature material was produced by thermal inversion of low-temperature albite from Amelia, Virginia. The structures will be discussed with special reference to the ordered distribution of Al and Si atoms, and in relation to current ideas about order–disorder transitions in felspars.

19. P. Gay. *X-ray investigations of the plagioclase felspars.*

Previous X-ray studies have shown that the plagioclase felspar series can be divided into three composition ranges within each of which a distinct structural type exists. The present work has investigated the occurrence of these structural types not only as a function of composition but also of temperature.

X-ray single-crystal methods have been used to examine a large number of felspars over a wide composition range. The specimens have been examined before and after being subjected to varying heat treatments. These results have been supplemented by those from specimens with differing geological histories. In this way it has been possible to study the structural changes which occur on the transition from the low to the high form of a particular felspar and to obtain some data on the temperature–composition fields of the various structural types. Some careful optical measurements have been made which confirm the X-ray investigation.

In particular it has been possible to show that felspars intermediate between the low and high forms can exist stably, and that a common high-temperature structural form exists over the series from albite almost up to pure anorthite. The latter resolves the apparent discrepancy between previous X-ray and thermal work. Some structural explanations of the various transitions are suggested.

20. N. V. Bielov. *Sur la structure de la néphéline et de quelques autres minéraux hexagonaux.*

§ 4. Structures des métaux et alliages

1. W. H. Taylor. *Electron configurations in some transition metal alloys.*

Attempts have recently been made to test the validity of the suggestion that electrons are absorbed by transition metal atoms in aluminium-rich alloys. In many cases a simple treatment of the Brillouin zone measurements provides support for the assumption of electron absorption but it is clear that there is need for a more fundamental theoretical discussion. Accurate structure analyses of Co_2Al_9, Mn_3SiAl_9, $MnAl_6$ and $Cr_4Si_4Al_{13}$ have shown that abnormally short contacts between a transition metal atom and some of the surrounding Al atoms appear to be characteristic of these structures. In addition, there is evidence for the absorption of about 2 electrons by the Co, Mn and Cr atoms in these alloys but the assumptions made in the course of the analysis require careful examination.

2. P. J. Black. *Electron transfer in intermetallic compounds.*

It has been suggested that, in aluminium-rich compounds of transition metals, electrons are absorbed to fill vacancies in the 3*d* shells of the transition metals. Attempts have been made to observe the effect directly from F_o and F_o-F_c syntheses. This evidence is examined critically. It is shown that errors in atomic scattering factors account for some of the evidence that was thought to indicate electron transfer. The possibility of detecting electron transfer effects is examined with particular reference to the work of Lonsdale & Bijvoet on lithium hydride.

3. P. J. Black. *Brillouin zones in intermetallic compounds.*

Measurements of Brillouin zones from X-ray data have been used to derive valencies for transition metals in intermetallic compounds, on the assumption that they are electron compounds. New measurements on several such compounds are presented and their interpretation by the electron absorption hypothesis is considered. These results indicate that the Brillouin zone analysis cannot be applied indiscriminately to these compounds and an attempt is made to define the limits of its validity.

4. P. Vousden. *The electron/atom ratio and localized bonds in metals.*

It is shown that the problem of alloy structures may legitimately be discussed in terms of electrons which are localized to the coordination polyhedra in the structure. This approach leads to a new division of the factors influencing crystal structure, which is closely related to the empirical division proposed by Hume-Rothery. The approach allows us to define the class of structures where the electron/atom ratio is important, and accounts for its relation to crystal structure without introducing the concept of Brillouin zones.

5. P. J. Black. *The structure of* $FeAl_3$.

The structure of this compound has been solved by Patterson methods. It is a complicated structure with a *C*-face centred monoclinic cell containing 100 atoms. The

structure is unusual in that it has close-packed regions, in which there are very short interatomic distances, separated by regions of misfit where the atom density is low. An analysis of the interatomic distances reveals a regular variation in the mean distance of an atom's neighbours with the number of these neighbours; possible explanations of this are discussed. An explanation of the twinning of $FeAl_3$ crystals is presented.

6. P. Vousden. *On the origin of the compounds of aluminium and the transition metals.*

It is shown that the common features of the group of complex alloys which aluminium forms with the transition metals Ni–Cr can be explained in terms of a strong interaction between the aluminium and the transition metal atoms. This interaction also accounts for all the evidence previously advanced in support of the electronic interpretation of these alloys. The relation of the strong interaction to the electronic structure is discussed and the special interest of these intermetallic compounds to the general theory of alloys is pointed out.

7. P. J. Black. *Relationships between the structure of intermetallic compounds.*

An attempt has been made to fit the structures of the aluminium-rich transition metal compounds into one geometrical scheme. It has been found that most of them are built by the stacking, in different sequences, of two simple plane patterns of aluminium atoms. Transition metal atoms are fitted between the layers and usually have nine or ten aluminium neighbours. The structures that cannot be included in this scheme are more directly related to the simple close-packed structures. The connection between this group and other intermetallic compounds is discussed in terms of these generalisations.

8. M. G. Bown. *On the crystal structures of* Al-*rich ternary alloys of* Al *and* Cu *with* Fe, Co *and* Ni.

The crystal structures of the ternary compounds which have been given ideal formulae $FeCu_2Al_7$, $Co_2Cu_5Al_{13}$ and $NiCu_3Al_6$ are described.

The cobalt compound is isomorphous with $FeCu_2Al_7$, the structure of which is known. This fact necessitates slight changes in the ideal formula and the corresponding electron/atom ratio.

The crystal structure of $NiCu_3Al_6$ is quite different. It is made up of cubes of Al atoms, most of which are centred by a heavy atom. The vacancies are regularly arranged, giving a true unit cell containing 125 small cubes.

It seems that in addition to electron concentration, the preferred coordination number of the transition metal atoms is an important factor in these structures.

9. J. A. Bland. *A suggested explanation of the occurrence of forbidden X-ray reflexions in the σ-phase.*

'Forbidden reflexions' in the Ni–V σ-phase reported by previous workers have been experimentally confirmed. Their explanation, which requires ordering in the structure, is critically examined. An alternative explanation based on the Renninger 'double reflexion' effect is proposed. The conditions for the occurrence of the double reflexions are discussed and shown to be particularly favourable in the present problem.

The two interpretations are compared by considering their adequacy in explaining all the observations. It is concluded that there is no reliable evidence for ordering in the Ni–V σ-phase.

10. J. Thewlis. *Crystal structure and metallic valency.*

The question of metallic valency is treated from the point of view of the resonating-valence-bond theory of Pauling, but without any assumptions as to the numerical values of metallic valency or single-bond radius.

It is shown that valencies, or at least a choice of valencies, may be allocated to certain allotropic metals from a knowledge of the crystal structure if it may be assumed that Pauling's equation is valid, that the single-bond radius of metal (corrected for temperature) is essentially constant for all valency states and that crystallographically equivalent atoms in a structure have the same, integral, valency.

For other metals a relation has been obtained between the linear coefficient of thermal expansion, the valency and the observed atomic size which makes it possible in many cases to allocate elemental metallic valencies.

The valencies worked out above are, in general, different from those put forward by Pauling and resemble more nearly the chemical valencies of the metals involved.

11. A. P. W. Spiegelberg, S. L. Å. Danielsson & H. Åström. *The crystal structure of some phases occurring in alloys of aluminium, iron and silicon and their relationship to other phases.*

The phases investigated are those (cubic, tetragonal and monoclinic) denominated *c*-AlFeSi, *t*-AlFeSi and *m*-AlFeSi (Phragmén, *J. Inst. Met.* (1950), **77**, 489) and characterized as follows: *c*-AlFeSi, $a = 12{\cdot}52$ kX.; *t*-AlFeSi, $a = 6{\cdot}11$, $c = 9{\cdot}47$ kX.; *m*-AlFeSi, $a = b = 6{\cdot}11$, $c = 41{\cdot}4$ kX. and $\beta = 91°$. In the order mentioned these phases are sometimes called α(Fe-Si) and β(Fe-Si) (Phillips & Varley, *J. Inst. Met.* (1943), **69**, 317) and δ (Gwyer & Phillips, *J. Inst. Met.* (1927), **38**, 29).

The phases are characterized by containing a transition element (iron) with the least absorbing power for valence electrons ever found in a separate ternary phase of aluminium, silicon and a transition element (Pratt & Raynor, *Proc. Roy. Soc.* A, (1951) **205**, 103). Though the determination of the atomic arrangement of these phases is not yet finished, some features and relationships—of interest in connection with the application of the band theory and with the knowledge of the transition from a more metallic to a lesser metallic atomic arrangement—already seem to appear and will be presented.

In revealing some of the relationships the method of Harker & Kasper for finding signs of the structure factors has played an important rôle.

12. R. Graham, G. C. S. Waghorn & P. T. Davies. *An X-ray investigation of the lead–platinum system.*

Three compounds of lead and platinum are shown to exist:

Pb_4Pt: Tetragonal, $a = 6{\cdot}64$, $c = 5{\cdot}97$ Å.
PbPt: Hexagonal, $a = 4{\cdot}24$, $c = 5{\cdot}48$ Å.
$PbPt_{5-7}$: F.-c. cubic, $a = 4{\cdot}05$ Å.

The cell dimensions of Pb_4Pt agree with those determined by Rösler & Schubert (*Z. Metallk.* (1951), **42**, 395), who also showed that its structure was similar to the *C*16 ($CaAl_2$) type. No other published X-ray data have been found for lead–platinum compounds.

The phase diagram of Doerinckel (*Z. anorg. Chem.* (1908), **54**, 358) appears to be essentially correct and the difficulties he experienced with platinum-rich mixtures have not been resolved. The diffraction pattern of the platinum-rich compound is compatible with an ordered or disordered structure but its exact composition has not been determined because of the difficulty of obtaining complete reaction. Superlattice lines would not be visible on the diffraction pattern owing to the closeness in atomic number of lead and platinum.

13. N. C. Baenziger & E. J. Duwell. *The crystal structures of some intermetallic compounds of mercury.*

The crystal structure of the intermetallic compound KHg was determined from precession-camera data. The triclinic cell has the dimensions, $a = 6{\cdot}62$, $b = 6{\cdot}91$, $c = 6{\cdot}94$ Å, $\alpha = 106°$, $\beta = 102°19'$, $\gamma = 92°48'$, $Z = 4$. A satisfactory structure was found in space group $P\bar{1}$.

The approximate structure was determined from Patterson projections and inspection of the (0*kl*) data. The atomic parameters were refined by electron density projections on (100) and (001) corrected by the 'back-shift' method.

The mercury atoms form groups of four similar to those formed in the Na_3Hg_2 structure except that the group is distorted from square. The Hg–Hg distances along the edge of the parallelogram are 3·03 and 3·08 Å, slightly longer than the closest Hg–Hg distance in mercury metal.

KHg_{11}, $SrHg_{11}$, and $RbHg_{11}$ all have structures similar to that of $BaHg_{11}$ reported by Peyronel (*Gazz. chim. ital.* (1952), **82**, 679).

14. R. Kiessling. *The nitrides and oxide–nitrides of tungsten.*

A tungsten oxide–nitride has been obtained by reducing ammonium paratungstate or tungsten trioxide with ammonia. The compound has a composition close to the formula $W_{0{\cdot}62}N_{0{\cdot}62}O_{0{\cdot}38}$ and belongs to the interstitial compounds. It has a defective *MX*-lattice with the sodium chloride structure. Only 62% of the *M*-positions are occupied at random by tungsten atoms, whereas probably all the *X*-positions are occupied, 62% by nitrogen atoms and 38% by oxygen atoms.

The γ-nitride in the tungsten–nitrogen system has been shown also to be an oxide–nitride. This phase has also a defective tungsten lattice, but the vacancies are ordered. Its ideal formula is $W_{0{\cdot}75}(N, O)_{1{\cdot}00}$, where the ration N:O is unknown but certainly greater than for $W_{0{\cdot}62}N_{0{\cdot}62}O_{0{\cdot}38}$.

15. B. Gale. *Integrated X-ray intensities from solid solution of copper–gold.*

16. G. Shinoda & Y. Amano. *Anomalous X-ray diffraction in* Al *and* Cu *single crystals.*

When an Al single crystal was rolled about 10% and set to reflect (333) with Cu $K\alpha$, several anomalous spots were observed besides the normal (333) spots due to $K\alpha_1$ and $K\alpha_2$. These are (1) a faint spot due to satellite $K\alpha_3$ and (2) doubletlike patterns crossing the normal (333) spots. The latter ones correspond to double diffractions of $(1\bar{1}1) \rightarrow (242)$ and $(\bar{1}11) \rightarrow (422)$. Also, when the crystal was rolled about 30% a nearly straight spot appeared between the (115) spots due to $K\alpha_1$ and $K\alpha_3$. This corresponds to double diffraction $(\bar{1}\bar{1}3) \rightarrow (222)$. The lattice constant calculated from the double diffraction condition becomes 4·0247 Å, and is much smaller than that of stress-free crystals. Therefore, the residual stress due to cold rolling is as follows: (1) longitudinal direction, compression of 68 kg.mm.$^{-2}$, (2) transverse direction, tension of 68 kg.mm.$^{-2}$ and (3) direction of thickness, almost zero.

Also, in a Cu single crystal, the double diffraction spot $(111) \rightarrow (\bar{1}\bar{1}3)$ was just outside the (004) spot, after rolling of several per cent. This was already found by Rachinger and considered as anomalous diffraction. The residual stress calculated from the double diffraction condition becomes 30 kg.mm.$^{-2}$ and is much smaller than that of Al.

17. G. S. Jdanov. *Structure atomique de quelques combinaisons métalliques de bismuth.*

18. R. J. Weiss. 3*d wave functions of iron.*

The absolute scattering factor of Fe for X-rays has been measured with Mo $K\alpha$ radiation. Cold-worked powders were used to eliminate extinction and Mo $K\alpha$ radiation was used to minimize both extinction and dispersion correction. A single crystal of Fe was used to place the powder data on an absolute basis. The scattering factor for the charge density of the argon core electrons (18) was subtracted from the experimental results, using a free-atom self-consistent-field calculation with exchange. Little change of the argon-core wave functions is expected in the solid. The remaining scattering factor is used to determine the wave functions of the *d* electrons with small overlap integrals. The resultant charge density agrees with neutron-diffraction results of Shull and indicates two unpaired *d* electrons with negligible overlap and the remaining six electrons with large overlap. The radial wave function of the two unpaired *d* electrons agrees also with the free-atom self-consistent calculations of Wood & Pratt.

§ 5. Structures non-organiques

1. I. Lindqvist. *On the crystal structures of* $AgSCN.2AgNO_3$ *and* $AgCN.2AgNO_3$.

AgI, AgCN and AgSCN can be dissolved in hot concentrated solutions of $AgNO_3$. The double salts $AgI.2AgNO_3$, $AgCN.2AgNO_3$ and $AgSCN.2AgNO_3$ crystallize from the

solutions. Single crystals of these salts give the following data:

$AgSCN.2AgNO_3$: $P\bar{1}$; $a = 7{\cdot}6$, $b = 7{\cdot}9$, $c = 6{\cdot}5$ Å; $\alpha = 85$, $\beta = 90$, $\gamma = 104°$; $N = 2$.

$AgCN.2AgNO_3$: $P2_1/n$; $a = 5{\cdot}30$, $b = 11{\cdot}34$, $c = 6{\cdot}20$ Å; $\beta = 101{\cdot}95°$; $N = 2$.

$AgI.2AgNO_3$: $P2_12_12_1$; $a = 7{\cdot}4$, $b = 12{\cdot}4$, $c = 7{\cdot}8$ Å; $N = 4$.

In $AgSCN.2AgNO_3$ the Ag and S positions have been determined. The S atoms coordinate four Ag atoms in a distorted tetragonal pyramid with S at the apex (Ag–S distances 2·4–2·8 Å). A reasonable arrangement of the SCN^- ions is suggested.

In $AgCN.2AgNO_3$ the Ag positions have been determined. Two principal possibilities are given for the arrangement of the CN^- ions, one of which is in good agreement with the structure of AgCN.

It is difficult to come to a definite decision about the structures but in any case they do not contain discrete Ag_3SCN^{2+}, Ag_3CN^{2+} or Ag_3I^{2+} groups, which have been assumed to exist in the solution.

The chemical bonds involved in the complicated complexes must be of a type which has not yet been treated theoretically (e.g. the S–Ag coordination).

2. Y. Saito, K. Nakatsu, M. Shiro & H. Kuroya. *Determination of the absolute configuration of the optically active complex ion,* $[Coen_3]^{3+}$, *by means of X-rays.*

Hitherto unrecorded double salts having the composition,

$2D\text{-}[Coen_3]Cl_3.NaCl.6H_2O$ and $2L\text{-}[Coen_3]Cl_3.NaCl.6H_2O$

were prepared, the crystal structures of which were completely determined using Fe $K\alpha$ radiation, except for the 'hand'. The space group is C_3^1–$P3$ with one formula unit in a cell of dimensions $a = 11{\cdot}45 \pm 0{\cdot}05$, $c = 8{\cdot}07 \pm 0{\cdot}03$ Å. The structure belongs very nearly to the space group C_6^6–$P6_3$, namely all the atoms except a sodium and a chlorine atom are arranged according to the symmetry $P6_3$. The five-membered cobalt ethylenediamine ring is not planar.

In order to distinguish between $(hkil)$ and $(hki\bar{l})$, the latter being equivalent to $(\bar{h}\bar{k}\bar{i}l)$ because of pseudo symmetry when l is even, use was made of Cu $K\alpha$ radiation which can just excite the cobalt atoms in the crystal. Slight but marked differences in intensities of the corresponding pairs of reflexions were observed on the oscillation photographs around the c-axis, and, furthermore, it was found that these inequality relations observed for one crystal were the reverse of those found for another enantiomorphous crystal. On the other hand, the intensity differences were calculated on the basis of a set of parameter values. The results were found to agree quite well with those actually found for D-crystal. Thus the absolute configurations of D- and L-$[Coen_3]^{3+}$ complex ion were successfully determined without ambiguity.

3. P. Herpin. *Structure de l'irido-trioxalate de potassium actif au moyen des rayons X.*

4. T. Rosenqvist. *Magnetic and crystallographic studies on the higher antimonides of iron, cobalt and nickel.*

These intermetallic compounds have been prepared: $FeSb_2$, $CoSb_{2-x}$, $CoSb_3$ and $NiSb_{2+x}$ ($x = 0{\cdot}1-0{\cdot}2$). For the first three compounds single crystals were obtained which were examined by optical goniometry and Weissenberg diagrams. $NiSb_{2+x}$ was studied by means of powder diagrams. The diantimonides all have the marcasite structure (space group V_h^2–$Pnnm$), and $CoSb_3$ has the skutterudite structure (space group T_h^5–$Im3$). The following values for the unit-cell dimensions and independent parameters u and v were obtained:

	a (Å)	b (Å)	c (Å)	u	v
$FeSb_2$	5·83	6·55	3·204	0·188	0·355
$CoSb_{2-x}$	5·596	6·373	3·370	0·195	0·360
$NiSb_{2+x}$	5·180	6·314	3·838	0·22	0·36
$CoSb_3$	9·036	—	—	0·343	0·157

The three last compounds were found to be very weakly para- or diamagnetic with susceptibility values between $+0{\cdot}1$ and $-0{\cdot}1 \times 10^{-6}$ independent of temperature. $FeSb_2$ is antiferromagnetic with an antiferromagnetic transition temperature of 500° C.

The magnetic data show that covalent bonds predominate in all compounds, and are formed by the d^2sp^3 orbitals of the transition metals and the sp^3 orbitals of antimony. The axial ratio of the marcasite compounds is determined by the number of uncompensated electron spins; antiferromagnetic interaction between these spins tends to shorten the length of the c axis. The relative stability of the marcasite, pyrite and skutterudite structures is discussed.

5. K. A. Wilhelmi. *On* $RbSb_3F_{10}$ *and its relation to other complex antimony* (III) *fluorides.*

The crystal chemistry of complex antimony (III) fluorides has been studied during recent years by the late Dr. A. Byström and his coworkers at the University of Stockholm. The compounds investigated are of the general formula $M_xSb_yF_{3y+x}$ where M is an alkali metal including NH_4^+ and Tl^+ and $x:y = 1:4$, $1:3$, $1:2$, $1:1$ and $2:1$.

The structural chemistry of the complex antimony (III) fluorides shows interesting features. The coordination number of the antimony atom is not constant but changes according to the formula type of the compound. Thus SbF_3 groups with C.N. = 3 were found to exist in SbF_3 (and also in $KSbF_4F_{13}$); $Sb_2F_7^-$ groups with C.N. = 4 in $CsSb_2F_7$; SbF_5^{2-} complexes with C.N. = 5 in K_2SbF_5; $(Sb_4F_{16})^{4-}$ complexes with C.N. = 5 in $KSbF_4$ and infinite chains of the composition $(SbF_4^-)_\infty$ with C.N. = 5 in $NaSbF_4$.

The investigation was recently extended to fluorides of the formula type MSb_3F_{10}. There are three isomorphous compounds ($M = NH_4^+$, Rb^+ and Tl^+) in this group. Weissenberg photographs indicated monoclinic symmetry, space group $P2_1/m$, with the dimensions $a = 7{\cdot}9$, $b = 13{\cdot}7$, $c = 8{\cdot}8$ Å, $\beta = 95°$ for $RbSb_3F_{10}$.

Accurate positions of the 12 Sb and 4 Rb atoms of the unit cell have been determined from Fourier analyses, which also have given approximate data for the F atoms.

The relation between the various structure types of the complex antimony (III) fluorides will be discussed.

6. K. Plieth & D. Balz. *Die Struktur des Kaliumnickelfluorids,* K_2NiF_4.

Die Kristalle werden als Erstausscheidung beim Abkühlen von $KF–NiF_2$ Schmelzen mit einem NiF_2 Gehalt zwischen 9,2 und 23,3 Mol % erhalten. Sie haben eine Dichte von 3,39 g.cm.$^{-3}$ und sind hellgrün gefärbt. Aus Laue-, Drehkristall- und Weissenbergaufnahmen konnte die Gittergeometrie abgeleitet werden. K_2NiF_4 kristallisiert im tetragonalen System mit $a_1 = a_2 = 3{,}99_8$; $a_3 = 13{,}05$ Å. Der Zellinhalt beträgt 2 Formeleinheiten K_2NiF_4. Wegen der Auslöschungen und einer Diskussion der speziellen Punktlagen kommen nur die wahrscheinlichen Raumgruppen: $D_{4h}(17)$; $D_4(9)$; $D_{2d}(11)$; $D_{2d}(9)$ und $C_{4v}(9)$ in Betracht. Die Intensitäten der Aufnahmen werden visuell gegen einen Stufenkeil geschätzt und auf Absorption korrigiert. Aus der Patterson-Projektion längs [010] können die Lagen der Atome einwandfrei ermittelt werden. Die endgültigen Parameter werden einer Fourierprojektion entnommen. Der Vergleich zwischen den beobachteten und den mit einem Temperaturfaktor multiplizierten, berechneten Strukturfaktoren fällt gut aus ($R = 0{,}11$). Die gefundenen Punktlagen der Atome sind in allen 5 Raumgruppen realisierbar.

7. H. Bode. *Über die Kristallstrukturen der Hexafluorozirkonate.*

Von den Strukturen der Kristalle mit der allgemeinen Formel M_2XF_6 sind verschiedene Typen bekannt. Bei einigen dieser Strukturen lässt sich die Baugruppe XF_6^{2-} erkennen. Liegt der Radienquotient Zentralatom–Ligand (X–F) in der Nähe der unteren, für die Koordinationszahl 6 zulässigen Grenze, so kennt man die trigonale K_2GeF_6-, die hexagonale Rb_2MnF_6- und die kubische K_2PtCl_6-Struktur. Bei vielen hierher gehörenden Stoffen handelt es sich um eine Polymorphie zwischen diesen Formen. Übersteigt dagegen der Radienquotient X–F den oberen Grenzwert für die Koordinationszahl 6, so treten Strukturen mit den Koordinationszahlen 8 und 9 auf (α–K_2UF_6; β_1- und β_2–K_2UF_6); irgendwelche Baugruppen lassen sich hierbei nicht mehr erkennen.

Mit dem Zirkon als Zentralatom des Komplexes liegt der Radienquotient etwas unterhalb der oberen Grenze der Koordinationszahl 6, und es treten hierbei wiederum neue Strukturen auf. Näher untersucht sind bisher das K_2ZrF_6 und das $(NH_4)_2ZrF_6$, die beide rhombisch (pseudohexagonal) kristallisieren, aber nicht isotyp sind. Für das Kaliumsalz gelten folgende Daten: $a = 6{,}60$, $b = 11{,}42$, $c = 6{,}96$ Å; $n = 4$, Raumgruppe D_2^5–$P222_1$; Anordnung der Atome: 4Zr(b); 4K(b) 0, y, $\frac{1}{4}$; 4K(a) 0, 0, 0. Die sechs Fluor umgeben das Zirkon in der Form eines Oktaeders, das in der Richtung einer dreizähligen Achse gestaucht ist. Betragen die Parameter der Zr- und K-Lagen genau $\frac{1}{3}$ bezw. $\frac{2}{3}$, so lässt sich die rhombische Zelle in eine hexagonale Zelle mit 2 Molekülen umformen; die Lage der Zirkonatome lässt sich durch die Koordinaten $\frac{1}{3}$, $\frac{2}{3}$, $\frac{1}{4}$; $\frac{2}{3}$, $\frac{1}{3}$, $\frac{3}{4}$ beschreiben. Die Parameter sind aber ein wenig von diesen Werten verschieden, sodass die Substanz nur pseudohexagonal ist. Für das Ammoniumsalz gilt: $a = 13{,}50$, $b = 11{,}68$, $c = 7{,}74$ Å, $n = 8$, Raumgruppe D_{2h}^9–$Pbam$ (mit anderer Koordinatenwahl), Anordnung der Zirkonatome: 2(a) 0, 0, 0; 2(b) 0, $\frac{1}{2}$, 0; 4(h) 0, $\frac{1}{4}$, $\frac{1}{2}$; die Fluor umgeben das Zirkon wie beim K-Salz. Vernachlässigt man einige schwache Reflexe, so erhält man eine rhombische Zelle mit $a = 6{,}75$ Å und $n = 4$. Diese Zelle lässt sich hexagonal umformen ($n = 2$); die Zirkonatome liegen in 0, 0, 0; 0, 0, $\frac{1}{2}$, die 4 Stickstoff in $\frac{1}{3}$, $\frac{2}{3}$, z, also verändert gegenüber dem K-Salz. Die Zelle mit 8 Molekülen lässt sich nicht mehr hexagonal umformen, ist aber immerhin noch pseudohexagonal.

8. J. Österlöf. *Crystal structure of* $Ag_2C_2.6AgNO_3$ *and* $2CuCl.C_2H_2$.

$Ag_2C_2.6AgNO_3$ is rhombohedral with one molecule per unit cell. The unit rhombohedron has dimensions $a = 7{\cdot}91$ Å $\alpha = 106°12'$. The space group is $R\bar{3}$. The linear group Ag–C≡C–Ag is placed along the space diagonal and is surrounded by six silver atoms and six nitrate groups.

$2CuCl.C_2H_2$ is hexagonal with six molecules per unit cell. The cell dimensions are $a_1 = 11{\cdot}8$, $a_3 = 6{\cdot}0$ Å. The space group is C_{6v}^4–$C6mc$. The structure can be seen as a derivate of the wurtzite structure type, where one-third of the copper and chlorine atoms are substituted by acetylene molecules. Each copper atom forms tetrahedrally directed bonds with three chlorine atoms and one acetylene molecule.

9. F. Mazzi. *The crystal structure of copper tetramine sulphate,* $Cu(NH_3)_4SO_4.H_2O$.

$Cu(NH_3)_4SO_4.H_2O$ is orthorhombic with: $a = 7{\cdot}07$, $b = 12{\cdot}12$, $c = 10{\cdot}66$ Å, $Z = 4$, space group D_{2h}^{16}–$Pmcn$.

The determination of the structure was made by two-dimensional Patterson and Fourier projections along [100] and [001]. The relative intensities of the reflexions were visually estimated from Weissenberg and precession photographs.

From the parameters of Cu and S measured in the Patterson projections, the signs of most structure factors were calculated. The refinement of the co-ordinates was carried on by means of the least-squares method.

In spite of the analogy of the formula,

$$Cu(NH_3)_4SO_4.H_2O$$

has a different structure from that of $Cu(H_2O)_4SO_4.H_2O$, in which the two additional bonds of the distorted octahedral group around Cu are saturated by O atoms of SO_4 groups.

In copper tetramine sulphate, Cu, which lies in a symmetry plane parallel to (100), has the four nearest NH_3 neighbours in square co-ordination and two more H_2O neighbours, lying in the same symmetry plane as Cu, which complete the distorted octahedral co-ordination group. Each H_2O molecule being in common with two Cu, a chain –Cu–H_2O–Cu–H_2O– is formed in the z direction.

S atoms lie also in a symmetry plane parallel to (100). The SO_4 group is tetrahedral with two O atoms in the same symmetry plane as S and two on opposite sides: each of these last O atoms is bound by a strong hydrogen bond to the same H_2O molecule co-ordinated by Cu atoms, forming a chain $\cdots H_2O \cdots O–S–O \cdots H_2O \cdots$ in the x direction.

Bond lengths and angles, as well as interatomic contacts, are normal.

10. R. Westrik & C. H. MacGillavry. *The crystal structure of the asbestos-like form of sulphur trioxyd.*

After many attempts, a needle of the asbestos-like form of SO_3 was successfully isolated in a capillary tube of thin-walled glass. Weissenberg diagrams about the needle axis showed that the crystal was a twin, which gave some difficulties in the interpretation.

The cell constants are: $a = 6{\cdot}20$ Å, b (needle axis) = 4·06 Å, $c = 9{\cdot}31$ Å, $\beta = 109° 50'$. Space group C_{2h}^5–$P2_1/c$; $Z = 4$.

The crystal structure was solved by Patterson and Fourier methods. The structure is built up out of chains along the needle axis, whose unit length contains two SO_4 tetrahedra linked in such a way that a spiral of –O–S–O–S– is formed. These chains have twofold screw symmetry. The cell contains two of these chains brought to coincidence by the glide plane c.

There is a significant difference between the S–O distances in the chain (1·61 Å) and the other S–O bonds (1·41 Å), just as was found in the structure of the ice-like modification of this compound.

11. R. Pascard. *Structure cristalline de l'acide sulfurique anhydre.*

Partie expérimentale.—Les cristaux d'acide sulfurique sont obtenus en refroidissant à 0° C. un liquide de composition aussi voisine que possible de la composition stoechiométrique. On amorce la cristallisation et on obtient assez facilement de fines aiguilles que l'on extrait du liquide à la pince.

SO_4H_2 cristallise dans le système monoclinique, groupe de symétrie Aa avec $a = 8{,}54$, $b = 4{,}70$, $c = 8{,}14$ Å, $\beta = 111° 25'$.

L'axe b coïncide avec l'axe des aiguilles.

Résolution de la structure.—On a résolu la projection de Patterson $P(x, z)$. Deux projections de Fourier successives suivies du calcul de la série différence permettent de tirer le maximum de précision à partir des données fournies par l'équateur $h0l$.

La projection de Patterson $P(x, y)$ est rendue confuse par suite de nombreuses superpositions, comme il a été confirmé par la suite. Nous avons donc calculé la fonction de Patterson à trois dimensions $P(x, y, z)$. Connaissant les coordonnées x et z la résolution est pratiquement immédiate. La coordonnée y est alors précisée au maximum en utilisant l'équateur $hk0$.

Amélioration des coordonnées atomiques.—Les positions obtenues précédemment subissent de légers déplacements après calcul de la série différence à trois dimensions. Malheureusement, cette série présente de nombreux pics résiduels qui masquent les pics hydrogène.

12. H. Seifert. *Deformationsvorgänge in Hydratstrukturen.*

Für eine vertiefte Erkenntnis der Rolle des Hydratwassers in Kristallstrukturen schien es lohnend, das Verhalten bei Deformationen der Kristalle zu studieren. Auf dem Kongress in Stockholm wurden darüber einige orientierende Mitteilungen bereits gemacht. Das Tatsachenmaterial muss indes reichlich und systematisch vermehrt werden, zumal Zweifel an der allgemeinen Giltigkeit bisher angenommener Leitsätze über Gleitmechanismen aufgekommen waren.

In der schon von Mügge & Johnsen durchgeführten Weise wurden in einer hydraulischen Presse in einem Presszylinder abgeänderten Modells Gleitungen bei hydrostatischen Drucken bis zu 10,000 atm. (und zusätzlichem kleinen Überdruck unbekannten Masses) erzielt bei Kupfervitriol, bei dem Tuttonschen Doppelsulfaten, bei Seignettesalz. Es wird die Gittergeometrie dieser Deformationen festgestellt und der Gleitmechanismus hinsichtlich des Anteils der Hydratwassermoleküle zu deuten versucht.

13. J. Clastre. *Structure de* $KOH.1H_2O$.

$KOH.1H_2O$ cristallise dans le système monoclinique avec le groupe de symétrie: $P2_1/c$–C_{2h}^5.

La maille élémentaire contient 4 molécules; elle est définie par les paramètres: $a = 5{,}795$, $b = 5{,}80$, $c = 7{,}88$ Å, $\beta = 109° 50'$.

Les clichés de diffraction ont été obtenus au moyen du rétigraphe de de Jong avec le rayonnement Mo $K\alpha$. Les synthèses de Fourier ont été effectuées uniquement par le photosommateur optique de G. von Eller. Les facteurs de structure ont été calculés automatiquement avec la machine à seringues à volume constant. Ces deux techniques ont permis de déterminer la structure sans faire appel aux calculs mécanographiques.

La structure a été résolue par l'interprétation de la fonction de Patterson, et par l'application de la méthode des superpositions. Le raffinement a été obtenu par améliorations successives des fonctions différences, et conduit jusqu'à une valeur du coefficient de reliabilité $R = 0{,}07$.

La structure est formée de feuillets de KOH liés par des lits de H_2O parallèles à (100). Les oxygènes forment des chaines en zig-zag –OH–OH_2–OH– parallèles à [001]. La coordinance du potassium est octaèdrique.

Les distances interatomiques sont les suivantes: K–OH = 2,91 et 2,795 Å, K–OH_2 = 2,84 Å, OH–OH_2 = 2,63 Å.

Les angles des liaisons entre les oxygènes sont: OH–OH_2–OH = 97°, OH_2–OH–OH_2 = 106° 45′.

L'étude précise des fonction différences montre que les atomes d'oxygène ne sont pas entièrement ionisés. On envisage également une agitation thermique non isotrope différente pour chaque atome.

14. P. Hemily. *Some remarks on the crystal structures of the sodium hydroxide hydrates.*

Crystal structures have been determined for the 4- and 7-molecule hydrates. Unit-cell parameters and space groups have been determined for four other hydrates.

15. K. W. Hedberg. *The molecular structures of ferrocene* ($FeC_{10}H_{10}$) *and nickelocene* ($NiC_{10}H_{10}$).

16. J. K. Dawson & R. W. M. d'Eye. *The hydrated tetrafluorides of uranium and plutonium.*

The tetrafluorides of uranium and plutonium form two hydrates. The higher one has the formula MF_4, $2{\cdot}5\,H_2O$ (where M = U or Pu) and the lower one forms a bivariant system between the limits MF_4, $0{\cdot}5\,H_2O$ and MF_4, $2{\cdot}0\,H_2O$. Analyses by chemical, X-ray diffraction and thermogravimetric methods indicate that the lower hydrate is produced in several ways: (1) Reaction of the metallic oxides with gaseous hydrogen fluoride in the temperature range 20–100° C. The hydrate is usually mixed with another complex which is believed to be $M(OH)F_3.HF$. (2) Addition of aqueous hydrofluoric acid to hydrochloric acid solutions of the quadrivalent ions at concentrations greater than 2 mg.ml.$^{-1}$. (3) Reaction of uranium dioxide with 40% aqueous hydrofluoric acid.

X-ray photographs indicate that the lower hydrate is simple cubic. A structure is proposed whereby the unit cell has $a = 5{\cdot}69$ kX. (UF_4, $1{\cdot}5H_2O$), with 2 moles per unit cell and giving calculated densities of 6·32 and 5·98 g.cm.$^{-3}$ for UF_4, $2H_2O$ and UF_4, H_2O respectively. The space group is O_h^5–$Fm3m$ with the U atoms randomly distributed on the 8(c) and the fluorine atoms on the 4(a) and 4(b) special positions. It is thought that the water molecules occupy vacant uranium sites and are hydrogen bonded to the fluorine atoms. The calculated interatomic distances for U–F, F–F and O–H–F are 2·46, 2·84 and 2·46 kX. respectively, and are compatible with those found in other uranium fluoride structures.

The PuF_4 lower hydrate is isostructural with the uranium lower hydrate with $a = 5{\cdot}63$ kX., the slightly smaller value being due to the decrease in size of the cation.

Indications were obtained that the ThF_4 hydrate system was dissimilar to the U and Pu systems.

17. R. B. Heiart & G. B. Carpenter. *The crystal structure of cyanogen chloride.*

In the analogous compound ICN, strong forces were found to act between the iodine atom of one molecule and the nitrogen atom of another. This study of ClCN was expected to provide a confirmation and extension of these observations.

Pure ClCN samples were sealed in capillaries and frozen in the X-ray camera by a jet of cold nitrogen. Rotation and oscillation photographs were prepared at about −30° C. Although the crystals were always twinned, it was possible to index the photographs. ClCN is orthorhombic with $a = 5{\cdot}68$, $b = 3{\cdot}97$, $c = 5{\cdot}74$ Å. The measured density, 1·55 g.cm.$^{-3}$, corresponds to 2 molecules per unit cell.

The systematic absences indicate the probable space groups to be $Pmmn$ or $Pm2_1n$. A Patterson projection along the c axis exhibited perfectly round peaks only, so that the linear molecules must lie parallel to c. This requires the space group to be $Pmmn$.

The expected length of the ClCN molecules is about 6·21 Å, but the length in the crystal is only 5·74 Å. This shortening verifies that strong forces act between ends of adjacent molecules.

Approximate atomic coordinates for one molecule (in fractions of a cell edge) are $z_{Cl} = -0{\cdot}14$, $z_C = 0{\cdot}17$, $z_N = 0{\cdot}37$, and $x = y = 0$ for each atom.

18. D. Grdenić. *The crystal structure of mercurous nitrate dihydrate,* $Hg_2(NO_3)_2.2H_2O$.

The elementary cell has the dimensions: $a = 8{\cdot}65$, $b = 7{\cdot}52$, $c = 6{\cdot}35$ Å, $\beta = 103{\cdot}8°$ and contains 2 formula units. The space group is C_{2h}^5–$P2_1/n$.

The $h0l$ and $0kl$ reflexions were recorded on the Weissenberg photographs using filtered Cu K radiation. The preliminary coordinates of the mercury atom were obtained from a Patterson synthesis on (010) and by the usual trial-and-error procedure.

The electron density maps on (010) and (100) were computed, using the signs of the mercury contributions only. The resolution of the water molecule and nitrate ion was satisfactory only in the (010) projection. Therefore it was possible to determine the position of water molecule and nitrate ion only approximately.

The mercury atoms are centrosymmetrically joined in pairs, the distance between them being 2·55 Å. The approach of the water molecule to the mercury atom amounts to about 2·2 Å and is therefore considerably shorter than the sum of van der Waals radii. Consequently, it is to be assumed that the lattice is built up of the oxonium ions H_2O–Hg–Hg–OH_2 and nitrate ions. The angle Hg–Hg–O is about 160°. This nonlinearity can be explained by the influence of the nitrate ion as well as by the fact that O–Hg bond is longer than the normal covalent bond (2·2 Å against 2·06 Å) and is therefore not truly covalent.

19. G. Carpeni. *Point isohydrique et nature des cristaux dans le système ternaire acide borique–borate monopotassique–eau.*

Les solutions aqueuses d'acide borique partiellement neutralisé par l'hydroxyde de potassium, sont le siège d'équilibres de condensations–dégradations, fonction, en particulier, des concentrations et du pH (ou du taux de salification $x = BO_3H_2K/BO_3H_3$ total): en dehors de l'acide BO_3H_3 et du sel *monomère* BO_3H_2K, ces solutions laissent, en effet, cristalliser aussi des sels *condensés* $B_5O_8K.aq(x = 0{,}2)$ et $B_4O_7K_2.aq(x = 0{,}5)$.

Cependant, quels que soient les composés boriques cristallisés utilisés pour la préparation des solutions, celles-ci se comportent d'un point de vue physicochimique général—électrométrique, conductimétrique, cryoscopique, etc.—d'une manière *univoque*, ce qui prouve qu'*en solution*, les équilibres électrolytiques de dissociation et de condensation–dégradation sont toujours les mêmes. Cette constatation, jointe à la présence d'un *point isohydrique* dans le réseau des courbes $pH = f(x)$, nous a incité à admettre qu'*en solution* le véritable pivot des équilibres est constitué par un sel condensé encore différent $B_5O_9HK_2.aq$, intermédiaire ($x = 0{,}4$) entre les sels cristallisés précédents ($x = 0{,}2$ et $x = 0{,}5$).

Cette conclusion, assez inattendue, est étayée par les résultats d'une analyse poussée des phases—solides et solutions—en équilibre à différentes températures. Le diagramme ternaire de solubilités du système BO_3H_3–BO_3H_2K–H_2O permet de préciser, entre autres, le domaine de stabilité probable du sel *solide* $B_5O_9HK_2.aq$, *prévu* par la théorie du point isohydrique mais impossible à obtenir cristallisé dans les conditions habituelles.

20. P. T. Davies, E. V. Garner & B. D. Caddock. *An X-ray study of the lead bromide rich region of the lead oxide–lead bromide system.*

The system has been studied by powder and single-crystal methods, preparations being made by various methods including solid-state reaction of lead oxide with lead bromide, and the decomposition of lead hydroxybromide, Pb(OH)Br. Lattice parameters were obtained by means of single crystal X-ray diffraction patterns for the following phases:

(*a*) $2PbO.PbBr_2$, orthorhombic, $P2_12_12_1$, $a = 9{\cdot}7$, $b = 12{\cdot}1$, $c = 5{\cdot}88$ Å.
(*b*) $4PbO.5PbBr_2$ (*R* phase), tetragonal, $P4/n$ or $P4/nmm$, $a = 12{\cdot}2$, $c = 8{\cdot}34$ Å.
(*c*) Probable composition $6PbO.7PbBr_2$ (*N* phase), monoclinic, *C*-face centred, $a = 16{\cdot}7$, $b = 5{\cdot}92$, $c = 20{\cdot}0$ Å, $\beta = 113{\cdot}5°$.

Previous studies of the system by thermal analysis and by X-rays were interpreted in terms of the formation of a congruently melting compound at $2PbO.PbBr_2$ and an incongruently melting compound at $PbO.PbBr_2$. The formation of $2PbO.PbBr_2$ is confirmed, but instead of a compound $PbO.PbBr_2$, the two compounds (*b*) and (*c*) are now found, and a modified phase diagram is proposed.

Other sets of lattice parameters which have been obtained in the course of the study include those for a hydrate of lead bromide (monoclinic primitive, $a = 12{\cdot}5$, $b = 4{\cdot}34$, $c = 12{\cdot}4$ Å, $\beta = 102°$) and for the chloride compound isomorphous with *N*-phase, probable composition $6PbO.7PbCl_2$ (orthorhombic, face centred, $a = 15{\cdot}7$, $b = 5{\cdot}82$, $c = 35{\cdot}3$ Å).

21. J. A. McMillan. *The crystalline structure of* AgO.

The pattern was obtained with Cu $K\alpha$, in a universal camera. AgO was prepared by boiling $NO_{11}Ag_7$ with water. Since it was impossible to obtain a single crystal of AgO, we had to interpret the powder pattern.

The structure being neither orthogonal nor trigonal, we resorted to the analogy between neighbouring elements of the same group in the periodical classification, and specially to the case of copper oxides. Thus we assumed that AgO would be isomorphous with CuO (tenorite), just as in the case of Ag_2O and Cu_2O. On this assumption, we modified the values of a, b and c of CuO in the ratio of the distances Ag–O and Cu–O in Ag_2O and Cu_2O, keeping constant the value of β. The values so obtained did not agree well with the experimental ones, but provided us with a criterion for indexing the lines.

After a few trials we arrived at a solution. The experimental structure factors checked against those calculated gave good agreement.

The proposed structure is C_{2h}^6–$C2/c$, with 4AgO groups per unit cell of $a = 5{\cdot}79$, $b = 3{\cdot}50$, $c = 5{\cdot}51$ Å, $\beta = 107° 30'$.

Ag: $\frac{1}{4}, \frac{1}{4}, \frac{1}{4}$; $\frac{3}{4}, \frac{3}{4}, \frac{1}{4}$; $\frac{3}{4}, \frac{1}{4}, \frac{3}{4}$; $\frac{1}{4}, \frac{3}{4}, \frac{3}{4}$.
O: $0, u, 0$; $0, u+\frac{1}{2}, \frac{1}{2}$; $\frac{1}{2}, \bar{u}, 0$; $\frac{1}{2}, \frac{1}{2}-u, \frac{1}{2}$; with $u = 0{\cdot}035$.
Ag–Ag = 3·26 Å; Ag–O = 3·14 Å; O–O = 3·50 Å.

22. P. B. Braun. *Structure determinations of barium iron oxides.*

In the system Ba–Fe–O a number of hitherto unknown compounds ($BaFe_{18}O_{27}$; $BaFe_{15}O_{23}$ etc.) have been found.

These hexagonal compounds have a long c axis (32·8 Å, 28 Å etc.). They consist of close-packed oxygen layers in different cubic and hexagonal sequences. In hexagonal parts of the stacking some of the O ions are replaced by Ba ions. The Fe ions are placed in interstices between the oxygens. Part of the structure within the cubic packed layers has a packing very similar to that of Fe_3O_4. As a whole, the structures are related to that of $BaFe_{12}O_{19}$ which is isomorphous with the mineral magneto-plumbite.

All of these substances have a strong tendency to crystallize in parallel intergrowths with each other on the (0001) surface. The structures have been solved with a minimum of *a priori* knowledge about the Ba:Fe:O ratios, largely by the use of one-dimensional methods.

The relationship between these different structures will be shown.

23. M. Edstrand. *On the structures of some compounds of antimony.*

I. The mixed lithium antimony(V)oxide $LiSbO_3$, is orthorhombic, space group *Pncn* with 4 formula units in the unit cell. The oxygen atoms form a distorted hexagonal close packing, with antimony and lithium in some of the octahedral holes. Antimony and oxygen form a staggered chain of octahedra along the needle axis of the crystal. The chains are coupled together by sharing corners. The structure is different from other known mixed oxides of the type M^ISbO_3.

II. The complex chloride of trivalent antimony $(NH_4)_2SbCl_5$ is monoclinic, space group $C2/m$ with 4 formula units in the unit cell. Approximate atomic positions have been determined by the vector-coincidence method. This shows that each antimony atom is surrounded by 5 chlorine atoms occupying 5 of the corners of an octahedron, resembling the configuration around antimony in K_2SbF_5. The Sb–Cl distances are of the same magnitude as in $SbCl_3$. We hope to be able to give the complete structure.

III. Some aspects of antimony(III)oxide halogenides: Needle shaped crystals of the idealized formula $Sb_8O_{11}X_2$ where X is Cl, Br or I have been prepared. They are monoclinic with 2 formula units in a unit cell with the needle axis (b axis) approximately 4·0 Å. It has, however, been found that the analyses indicate approximately 15·5 instead of 16Sb in the small unit cell. These two phenomena perhaps explain each other. If possible an approximate structure will be given and discussed in connection with the already published $Sb_4O_5Cl_2$ and SbOCl structures.

Probably some remarks on compounds of the type $NH_4Cl.As_2O_3$ also will be given.

24. S. Ohlberg. *The crystal structure of antimony pentachloride at −30° C.*

Single crystals of antimony pentachloride were grown by the usual low-temperature techniques. The unit cell is hexagonal with $a_0 = 7{\cdot}49$ and $c_0 = 8{\cdot}01$ Å. The space group is $P6_3/mmc$ and there are two molecules in the unit

cell. Intensity data were obtained from multiple-film Weissenberg (Cu $K\alpha$) and precession (Mo $K\alpha$) photographs. The antimony atoms were readily located in special positions from a Patterson projection, and the majority of the signs were thereby determined. The structure was subsequently refined by two-dimensional Fourier syntheses. Antimony pentachloride forms a molecular crystal and the trigonal bipyrimidal structure observed for the gaseous molecule is retained in the solid state. The bond distance between the antimony and the three basal chlorines is in good agreement with that found for the gas (2·31 Å). On the other hand, the bond distances between the antimony and the two apical chlorines is about 0·05 Å less than that found for the gas (2·43 Å).

25. M. G. HARWOOD. *The crystal structure of lanthanum strontium manganites.*

The crystal structure of lanthanum strontium manganites of formula $LaMnO_x$ has been examined as a function of the oxygen content. The value of x has been varied between 3·24 and 3·07. In all cases the structure is of the perovskite type with a small unit cell. At the oxygen-rich end of the system the symmetry is rhombohedral while at the other end it is cubic. An abrupt transition occurs between the two forms.

In the lanthanum manganite–strontium manganite system the perovskite phase is stable from 23% to 100% lanthanum manganite. At the lower limit of stability it is of cubic symmetry, the unit cell becoming rhombohedral between 50% and 60% lanthanum. Variations of the lattice parameters versus composition are indicated.

26. A. DURIF-VARAMBON, E. F. BERTAUT & R. PAUTHENET. *Propriétés cristallographiques et magnétiques de quelques nouvelles séries de spinelles mixtes.*

27. R. ROY. *The hexagonal–cubic transition in* $BaTiO_3$ *and the influence of various ions upon it.*

It has been shown that cubic $BaTiO_3$ undergoes a reversible reconstructive transition to the hexagonal form at 1460° C.

Phase equilibrium diagrams have been determined for 5 systems involving $BaTiO_3$ and the influence of additives on this transition is discussed. The inversion temperature is raised very sharply by most additives, the influence of $CaTiO_3$ being most remarkable, less than $\frac{1}{2}$ mole per cent raising the inversion more than 100° C. Stoichiometric excess of TiO_2 or additions of SiO_2, indeed of any small ions, raises the inversion temperature. K^+ appears to be the only ion which lowers the inversion temperature.

28. H. FISCHMEISTER & I. LINDQVIST. *The polymorphism of the sulfates* A_2SO_4.

With one exception (Na_2SO_4 III–V), the transitions of the sulfates A_2SO_4 are characterized by a close similarity of the structures related by them. The transitions low–high imply an increase in symmetry, brought about by relatively small (translative) displacements of the ions. Simultaneously, the orientation of the sulfate group seems to become disordered which increases the symmetry still further. (However, in all the sulfates so far investigated, completely free 'rotation' is sterically impossible.) For all the sulfates A_2SO_4 that have an hexagonal high-temperature modification, the symmetry of the low form can be derived from D_{6h}^4–$C6/mmc$. This is true for the isomorphous group K_2SO_4, Rb_2SO_4, Cs_2SO_4, Tl_2SO_4, the isomorphous pair Na_2CrO_4, Na_2SO_4 (metastable at room temperature), as well as the previously known hexagonal sulfates $KLiSO_4$ and the glaserite series

$$(KNaSO_4 \cdots K_3Na(SO_4)_2) .$$

Li_2SO_4 is cubic with the sulfate groups probably orientationally disordered, in f.-c. positions. Here too, the symmetry of the low-temperature modification is a subgroup of that of the high form, and the transition involves only small displacements.

For the transition III–V of Na_2SO_4, no such simple symmetry relation holds. The transition implies considerable changes of ionic positions and produces an essentially different type of lattice. It is sluggish.

Although no example of true stabilization of the hexagonal high-temperature forms of any sulfate A_2SO_4 is known, hexagonal Na_2SO_4 can be made metastable at room temperature by addition of Na_2CO_3. Whereas in the high form of Na_2SO_4 (I) complete replacement of the sulfate by the carbonate group is possible (Na_2SO_4 I and Na_2CO_3 I form a continuous series of mixed crystals), the Na_2SO_4 III arrangement can hold only up to *c.* 10% carbonate. At higher carbonate contents (*c.* 10... 70%), the burkeite structure (termed after the mineral $2Na_2SO_4.Na_2CO_3$) is more stable. Thus, when Na_2SO_4 I with more than 10% carbonate eventually does invert, it is to a burkeite rather than to an Na_2SO_4 III arrangement. The geometrical aspects of the replacement of SO_4'' by CO_3'' groups, and its stabilizing effect on the hexagonal form of Na_2SO_4 will be discussed.

29. G. LUNDGREN. *On the arrangement of the metal and oxide ions in some basic salts of tetravalent metals.*

The crystal structures of some basic sulfates and chromates of tetravalent metal ions have been determined to investigate what sort of arrangement the metal and the oxide or hydroxide ions form in them.

For Th^{4+} only a chain-like arrangement was found. In the crystals of $Th(OH)_2$, CrO_4H_2O and $Th(OH)_2SO_4$ the metal ions are situated on alternate sides of a double row of hydroxide ions, forming an infinite chain of the composition $[Th(OH)_2^{2+}]_n$.

For U^{4+}, with a smaller ionic radius than Th^{4+}, two arrangements were found. The first is isotypic with the $[Th(OH)_2^{2+}]_n$-complexes. It is found in $U(OH)_2SO_4$. The second is found in the crystals of $U_6O_4(OH)_4(SO_4)_6$, where there are finite groups of the composition $[U_6O_4(OH)_4]^{12+}$. Six uranium atoms, arranged in an octahedron, are joined by four oxide and four hydroxide ions forming a cube.

This second type of arrangement is also found for Ce^{4+} in $Ce_6O_4(OH)_4(SO_4)_6$. However, for Ce^{4+} (with an ionic radius only a little less than that of U^{4+}) no chains $M(OH)_2^{2+}$ occur. Instead a new chain-like ion $(CeO)_n^{2n+}$ is formed and is found in $CeOSO_4H_2O$. Here the Ce^{4+} ions form complexes only with oxide ions.

In addition to these compounds of the rather closely related elements Th, U and Ce the crystal structure of $TiOSO_4.H_2O$ has been determined. In this salt the metal and oxide ions are arranged in zigzag rows –Ti–O–Ti–O–.

Investigations on basic zirconium chromates and on vanadyl sulfates are also in progress. Preliminary results show that for Zr^{4+} the arrangement is quite different from those mentioned above, the Zr atoms being arranged in infinite chains or in two-dimensional infinite networks.

30. W. H. Zachariasen. *The crystal chemistry of compounds containing groups* $(XO_2)^{+2}$ *or* $(XO_2)^{+1}$, *when* X = U, Np, Pu, Am.

Considerable experimental evidence has been obtained on the structure of uranyl compounds and of related compounds of hexavalent and pentavalent transuranic elements containing radicals $(XO_2)^{+2}$ or $(XO_2)^{+1}$, where X = Np, Pu or Am.

Both the $(XO_2)^{+2}$ and the $(XO_2)^{+1}$ groups are collinear. The collinear structure of the groups $(PuO_2)^{+1}$ and $(AmO_2)^{+1}$ was recently demonstrated in the compounds $KPuO_2CO_3$ and $KAmO_2F_2$.

In addition to the two strong primary bonds to the uranyl oxygen atoms the uranium atom forms four, five or six secondary bonds to fluorine atoms or to other oxygen atoms. Considerable variation in the length of primary as well as secondary bonds has been observed (Tables 1–3). This variation is much greater than can be accounted for by changes in the coordination number.

Table 1. *Primary bond length*, U–O

Compound	Bond length (Å)	Bond strength
$MgUO_2O_2$	1·92±0·02	1·33
$CaUO_2O_2$	1·91±0·10	1·25
$K_3UO_2F_5$	1·75±0·04	1·63

Table 2. *Secondary bond length*, X–O

Compound	Number of bonds	Bond length (Å)	Bond strength
$MgUO_2O_2$	4	2·18±0·02	0·83
$CaUO_2O_2$	6	2·29±0·02	0·58
$KPuO_2CO_3$	6	2·55±0·05	0·25

Table 3. *Secondary bond length*, X–F

Compound	Number of bonds	Bond length (Å)	Bond strength
$K_3UO_2F_5$	5	2·24±0·02	0·55
UO_2F_2	6	2·50±0·05	0·33
$KAmO_2F_2$	6	2·47±0·05	0·29

On the assumption of detailed balancing of valences it is possible to deduce the strength of the various bonds in an independent manner (Tables 1–3). It is seen that there is a close correspondence between bond length and bond strength.

31. S. B. Levin. *Synthetic manganese dioxide for dry cells.*

32. Y. Ginetti. *Structure cristalline du métagermanate de cuivre.*

La littérature chimique mentionne comme germanate de cuivre un composé que Schwartz a obtenu par réaction en phase aqueuse et dont la formule peut, à la rigueur, se laisser interpréter comme étant celle d'un orthogermanate de cuivre à l'état hydraté. Des essais ont été tentés en vue de l'obtention d'un germanate de cuivre non hydraté (par voie ignée) et ont donné des monocristaux d'un composé que l'on identifia comme étant le métagermanate de cuivre anhydre $CuGeO_3$.

Le groupe de recouvrement est C_{2v}^2. Le cristal appartient donc à l'antihémiédrie du système orthorhombique.

Les valeurs des paramètres sont: $a = 4{,}8\pm0{,}05$, $b = 8{,}5\pm0{,}05$, $c = 2{,}93\pm0{,}05$ kX. Il y a deux molécules par maille-unité.

Des projections de Patterson $hk0$ et $hk1$ permettent de localiser les atomes lourds. Les coordonnées des atomes d'oxygène sont fixées par 'trial-and-error'.

La structure obtenue met en évidence l'existence d'une chaîne de tétraèdres GeO_4 plus simple que la chaîne des pyroxènes.

33. Y. Ginetti. *Structure cristalline du métagermanate de sodium.*

Notre travail venait d'être commencé lorsque nous eûmes connaissance de la publication de Grund & Pizy (*Acta Cryst.* (1952), **5**, 837) portant sur la structure cristalline du métasilicate de sodium.

Les résultats acquis jusqu'à présent montrent une grande analogie entre ces deux composés aussi bien en ce qui concerne les paramètres et le groupe de recouvrement que la projection de Fourier $hk0$.

34. R. C. L. Mooney, H. Kissinger & A. Perloff. *X-ray analysis of orthophosphates of some trivalent elements.*

The anhydrous orthophosphates of scandium, gallium, indium and trivalent thallium were prepared by a method consisting essentially of heating a mixture of phosphoric acid and the appropriate oxide or metal to moderately high temperatures in hydrothermal bombs for a week or more. In general, the products were well crystallized powders, though small single crystals were grown in some cases.

The structural parameters of $InPO_4$ and hexagonal $GaPO_4$ were determined from Fourier analysis of Weissenberg spectrometer data, and those of the other compounds from powder patterns taken on a Geiger-counter spectrometer. The temperature stability ranges of $GaPO_4$ were investigated by means of a series of powder patterns taken at small intervals between room temperature and 1200° C.

The results of the structure determinations will be presented. Some crystallographic data are as follows:

	Cell size (Å)	Z	Space group	Type
$ScPO_4$	$a = b = 6{\cdot}57$ $c = 5{\cdot}79$	4	$I4amd$	Zircon
$GaPO_4$ (Stable)	$a = b = 4{\cdot}92$ $c = 11{\cdot}10$	3	$P321$	Berlinite (high quartz)
$GaPO_4$ (Metastable)	$a = b = 6{\cdot}95$ $c = 6{\cdot}87$	4	$C222_1$	Low cristobalite
$GaPO_4$ (High)	$a = 5{\cdot}06$ $c = 7{\cdot}16$	2	$I\bar{4}$	BPO_4 (High cristobalite)
$InPO_4$	$a = 5{\cdot}31$ $b = 7{\cdot}85$ $c = 6{\cdot}77$	4	$Cmcm$	$CuCrO_4$

	Cell size (Å)	Z	Space group	Type
$TlPO_4$	$a = 5{\cdot}39$ $b = 8{\cdot}01$ $c = 7{\cdot}07$	4	*Cmcm*	$CuCrO_4$
$CrPO_4$ (Unstable)	$a = 5{\cdot}15$ $b = 7{\cdot}77$ $c = 6{\cdot}11$	4	*Cmcm*	$CuCrO_4$

35. P. M. DE WOLFF & L. WALTER-LÉVY. *Structure de quelques halogénures basiques de magnésium.*

Les structures des divers halogénures basiques de magnésium ont été établies et comparées à celle de $Mg_2(OH)_3Cl,Br.4H_2O$ (*Acta Cryst.* (1953), **6**, 40).

On peut distinguer quatre classes, ayant en commun un habitus en aiguilles et la présence de la même 'substructure' qui se manifeste dans la projection (010), b étant l'axe des aiguilles. Cette propriété est dûe à la présence d'éléments prismatiques dérivés d'une couche de brucite et liés entre eux par des liaisons hydrogène.

I. *Hydrates de* $Mg_2(OH)_3X$.—Les chaines doubles trouvées dans le sel à $4H_2O$ forment également la base de deux autres hydrates à 3 et à $2H_2O$. Les atomes halogènes se trouvent entre les chaines ($4H_2O$), en font partie dans des positions liées à $1Mg(2H_2O)$, ou sont réparties entre ces deux situations ($3H_2O$).

II. *Hydrates de* $Mg_3(OH)_5Cl$.—La structure des hydrates à 4 et $3H_2O$ est analogue à celles des hydrates correspondants de $Mg_2(OH)_3X$, mais les chaines sont constituées par trois rangées d'octaèdres.

III. *Hydrates de* $Mg_3(OH)_4X_2$.—Il en existe deux à 4 et à $2H_2O$ contenant des chaines triples comme ceux de la classe II.

IV. *Hydrate de* $MgX_2.9Mg(OH)_2$ à $5H_2O$.—Ici la couche de brucite n'est pas formée de rubans, mais comme plissée par des dislocations périodiques. Les liaisons hydrogène se forment entre les arêtes de deux couches consécutives.

36. K. ERIKS, P. A. HOWELL & W. N. LIPSCOMB. *Molecular and crystal structures of two boron hydrides in the* B_6–B_9 *range.*

A B_6 hydride, presumably B_6H_{10}, crystallizes in the orthorhombic space group $Cmc2_1$, with four molecules in a unit cell of dimensions $a = 7{\cdot}50$, $b = 9{\cdot}23$ and $c = 8{\cdot}50$ Å. The molecule is required to have Cs symmetry, and can be visualized as a pentagonal pyramid, the cap of the icosahedron, by adding one B atom to the B_5 arrangement of B_5H_{11}. The three nearest hydrogen atoms to this newly-added boron atom are removed, and two are attached by single bonds to this boron atom. This newly-added BH_2 group lies in the symmetry plane of the molecule and the new B is joined to the apex B by a normal covalent bond and to the two next nearest B atoms by an open three-center bond. Bonding in the remainder of the molecule is very similar to that in B_5H_{11}. While we are not yet certain of this hydrogen arrangement it reduced the value of R from 0·16 to 0·135 for the 144 observed reflections.

A higher hydride, presumably containing 8 or 9 boron atoms, is undergoing analysis by three-dimensional Patterson methods. About 500 general *hkl* reflections obtained from a crystal with melting point about −20° C. indicate four molecules in the space group $P2_1/n$ with unit cell parameters $a = 11{\cdot}80$, $b = 6{\cdot}94$, $c = 11{\cdot}25$ Å and $\beta = 109°\ 35'$.

37. P. BLUM & E. F. BERTAUT. *Boracites de quelques métaux de transition.*

Morphologie et structure des boracites de formules générales A_2O_3, B_2O_3, nMO, où $n = 2$ ou 4, A = V, Ti, Fe et M un cation bivalent.

38. P. BLUM & E. F. BERTAUT. *Structure de* $FeNaO_2$ *orthorhombique.*

39. M. HAMELIN. *Étude des réactions à l'état solide à hautes températures dans le système* TiO_2–Al_2O_3–Cr_2O_3.

Des mélanges d'oxyde de titane, d'alumine et d'oxyde de chrome traités de 10 min. à 3 heures entre 1400 et 1600° C. ont donné les résultats suivants:

L'affinité de l'alumine et du sesquioxyde de chrome se traduit par la formation de solutions solides Al_2O_3–Cr_2O_3 dans une grande partie du domaine ternaire.

Le composé $TiO_2.Al_2O_3$ se forme dès les faibles teneurs en alumine dans la partie riche en oxyde de titane, et dans le domaine des teneurs élevées en alumine.

Par contre, nous ne retrouvons que dans un très petit domaine la phase correspondant à $2TiO_2.1Cr_2O_3$. Elle semble constituer un état intermédiaire dans la formation d'un composé qui se constate dans un domaine du système ternaire TiO_2–Al_2O_3–Cr_2O_3, qui est aussi important que celui des solutions solides Al_2O_3–Cr_2O_3. Ce composé n'a été obtenu dans le système binaire TiO_2–Cr_2O_3 qu'après une fusion au four solaire.

§ 6. Structures organiques

1. D. R. HOLMES. *The crystal structure of polycaproamide: nylon* 6.

The crystal structure of nylon 6 $(-NH(CH_2)_5CO-)_p$ has been determined by interpretation of the X-ray diffraction patterns given by drawn, rolled fibres. The determination was part of a programme to investigate the relation between structure and physical properties, in particular melting point. Nylon 6 melts 50° C. lower than its isomer nylon 66 $(-NH(CH_2)_6NH.CO(CH_2)_4CO-)_p$; it had been suggested that this was due to deficient hydrogen-bond formation in nylon 6 crystallites.

The unit cell contains eight chemical units

$$(-NH(CH_2)_5CO-)$$

and is monoclinic with $a = 9{\cdot}56$, $b = 17{\cdot}24$, $c = 8{\cdot}01$ Å, $\beta = 67\frac{1}{2}°$. Calculated density = 1·231 g.cm.$^{-3}$. Observed density for a drawn monofilament = 1.16 g.cm.$^{-3}$. The

structure consists of planar chains of CH_2 groups and amide groups tilted 7° from the (001) plane. Alternate chains in this plane are oppositely directed, an arrangement which allows all hydrogen bonds to be made perfectly. The hydrogen bonded sheets of atoms are packed in an 'up-and-down' staggered configuration along the *c* axis. Distances between atoms in neighbouring molecules are all normal van der Waals contact distances, except for the N–H · · · O distance of 2·81 Å. It appears, from a general survey of polyamide melting points published elsewhere, that the determining factor is the number of CH_2 groups between the amide 'anchor points'—polymers with odd numbers of CH_2 groups melt lower than those with even numbers. The present work shows that the odd number of CH_2 groups in this polymer does not lead to deficient hydrogen-bond formation, and that the lower melting point of nylon 6 as compared with nylon 66 must be ascribed to some other cause.

Most samples of polycaproamide contain varying amounts of another crystal form (the β-form) in which the side-by-side packing of hydrogen-bonded sheets is different. The staggered packing scheme along the *c* axis is abandoned and all hydrogen-bonded sheets are at the same height in the cell. Details are given of the changes in the X-ray pattern during the conversion of the β to the normal α form.

2. S. C. Nyburg. *A statistical structure for crystalline rubber.*

The crystal structure of natural rubber proposed by Bunn is largely correct but invokes quite large bond distortions. The crystal structure has been re-examined using a quantitatively estimated set of intensities. The method of obtaining corrected intensity estimates is given in detail. One remarkable feature is the extremely small number of *hk*0 reflexions (*z* is the fibre axis). It is confirmed that if a structure of conventional type is present then only a distorted molecule of the type proposed by Bunn can adequately account for the *hk*0 intensities. Moreover, the agreement will never be good since the experimental data require the molecules to have *mm* symmetry in *z* projection, and this is not possible on stereochemical grounds. The impasse can only be resolved by assuming a statistical structure.

Statistical structures giving the required symmetry are discussed and it is shown that only one is possible. This allows an undistorted molecule to have its conventional position or to be mirrored in a plane parallel to *y*. The structure is discussed in detail. The structure factor discrepancy falls from 0·58 (Bunn) to 0·31. This comparatively large discrepancy is attributed mainly to approximations made in deriving intensity values and to absorption.

3. T. Petitpas. *Structure de la cellulose* II.

La cellulose régénérée 'Fortisan' fournit un modèle exceptionnellement bien orienté de cellulose II (mercerisée). Les diagrammes de diffraction ne présentent pas de phénomène gênant d'étalement et de recouvrement de strates. Aussi on a pu mesurer les intensités des taches discrètes de huit strates, en utilisant la méthode d'équi-inclinaison. Ces mesures ont servi à calculer la section méridienne de la fonction de Patterson cylindrique. La décroissance rapide des intensités, dans la direction radiale, fait que les pics observés sont mal résolus et ne peuvent pas être interprétés directement. Notre méthode d'analyse consiste à construire des sections méridiennes des fonctions de Patterson synthétiques d'après le modèle d'Andress pour l'ensemble du motif et le modèle plus récent de Meyer & Misch pour une chaîne unique et de confronter ces sections à la section expérimentale. Cette confrontation conduit à modifier quelque peu la structure de la chaîne unique (celle-ci est sensiblement distordue) et à modifier la disposition relative des deux chaînes dans la maille.

4. G. Fournet, J. Rogue & P. Antzenberger. *Étude du diagramme équatorial complet de la diffusion des rayons X par des fibres de cellulose (ramie) sèches et mouillées.*

A partir du diagramme équatorial complet de diffusion des rayons X nous avons cherché, non pas à préciser un modèle idéal de structure cristalline de la cellulose, mais à obtenir le maximum de renseignements possibles sur la structure réelle des fibres de ramie. Dans ce type d'étude des substances mal cristallisées il faut considérer les données de la diffusion des rayons X comme un tout et les utiliser globalement; un travail de ce type a déjà été effectué sur les carbones graphitisables (R. Franklin, *Acta Cryst.* (1951), **4**, 253). A la différence de ces derniers corps la cellulose contient plusieurs espèces d'atomes; pour obtenir de façon classique *les fonctions de répartition des centres d'atomes* il faut donc faire l'hypothèse que les variations en fonction de l'angle des facteurs de structure des atomes constituants sont semblables (à des facteurs *z* près); cette méthode vient d'être utilisée lors d'une étude de la ramie sèche. Pour nous affranchir de cette hypothèse—partiellement vérifiée dans le cas de la cellulose—nous avons considéré la *fonction de répartition des densités électroniques*. Cette fonction peut s'obtenir directement à partir de l'expérience; nous avons développé par ailleurs une méthode qui permet de calculer la fonction correspondant à un modèle quelconque. Le modèle de cellulose que nous avons adopté est le suivant: il n'y a pas d'ordre à grande distance radial et l'ordre à petite distance est celui correspondant au modèle de Meyer et Misch. Les premières comparaisons entre notre courbe théorique d'une part et nos deux courbes expérimentales d'autre part sont satisfaisantes, l'accord étant meilleur pour la ramie humide.

5. G. Fournet & P. Antzenberger. *Étude de la diffusion des rayons X aux petits angles par la cellulose (ramie) à différents taux d'humidité.*

Nous avions déjà obtenu en *valeur absolue* les courbes de diffusion centrale relatives à la ramie sèche et mouillée (humidité relative 100%), et montré que les intensités correspondant à la ramie mouillée étaient beaucoup plus élevées que celles de la ramie sèche (facteur de l'ordre de 4). Pour connaître le mécanisme de l'augmentation de l'intensité, nous avons établi en *valeur absolue* les courbes correspondant à des taux d'humidité intermédiaires (33, 58, 79 et 90%). L'ensemble de ces courbes montre que, pour un angle donné, l'intensité varie lentement de 0 à 33%, très peu entre 33 et 58%, puis très rapidement

au-delà. Il semble que les grandes valeurs observées dans la diffusion centrale de la ramie mouillée ne puissent être attribuées à une pénétration de l'eau dans le réseau; par contre, elles correspondent pour la plus grande part à l'absorption dite 'condensation capillaire'.

6. M. Oberlin & J. Méring. *Détermination de la répartition latérale des chaines cellulosiques dans la ramie sèche.*

La fonction $P'(r)$ de répartition des projections horizontales r des distances interatomiques est directement déduite des données de photométrie précise de la tranche équatoriale du diagramme de diffraction d'un paquet de fibres de ramie déshydraté à 60° C. dans le vide.

La courbe $P'(r)$ a été tracée pour les distances r comprises entre 0 et 55 Å. Cette courbe est confrontée aux éléments de la fonction $P'(r)$ synthétique construite d'après le modèle structural idéal de Meyer & Misch. Ces éléments comprennent: (*a*) les distances interatomiques horizontales à l'intérieur d'une chaîne unique; (*b*) les distances horizontales entre les atomes d'une chaîne et les atomes appartenant à chacune des chaînes voisines successives du réseau de la cellulose.

La confrontation montre qu'on arrive à un accord satisfaisant entre la répartition expérimentale et la répartition synthétique à condition d'affecter la contribution de chaque type de voisinage de coefficients de fréquence traduisant les dimensions limitées des domaines cristallisés.

Les coefficients de fréquence déterminés par cette confrontation conduisent à la statistique des répartitions des épaisseurs [001] des cristallites. Ces dimensions s'étendent entre 24 Å et 44 Å—35% de la substance ne participe pas à l'organisation cristalline tridimensionnelle. Ce dernier chiffre est en accord avec les résultats des déterminations physicochimiques (sorption et densité) de Hermans et ses collaborateurs.

7. C. Legrand & G. Costes. *Transformations du polytéréphtalate d'éthylène glycol en fonction de la température.*

On a observé que des échantillons de films de polytéréphtalate d'éthylène glycol, correspondant à une viscosité intrinsèque de 0,60, sont susceptibles de présenter selon les conditions d'évolution thermique, des structures différentes.

Par fusion suivie de refroidissement brusque, on obtient une structure amorphe caractérisée par deux halos. Par des chauffages de durée convenable au-delà du point de transition apparent du second ordre (environ 75°), une structure cristalline apparaît, identique à celle que l'on obtient par étirage à froid, avec cette différence que les films ne présentent pas d'orientation privilégiée.

Les durées nécessaires à la cristallisation aux diverses températures ont été déterminées par les mesures des volumes spécifiques à ces températures. Ces durées décroissent rapidement depuis la température de 80° C. jusqu'à 180° C.

La structure cristalline paraît de mieux en mieux définie quand la température de cristallisation augmente. On peut distinguer deux domaines de température: de 80 à 220° C. l'ordre cristallin croît lentement; au-delà de 220° C., il progresse plus rapidement. Ce résultat est en bon accord avec ceux que l'on obtient par les mesures de volumes spécifiques par dilatométrie cubique.

Le comportement de ce polymère en fonction de la température semble se différencier nettement de celui d'autres polymères comme le nylon ou les polyéthylènes.

8. M. P. Gupta. *Structures of* Rb- *and* K-*hydrogen fumarates.*

Rubidium hydrogen fumarate is triclinic, with two molecules of $RbC_4H_3O_4$ and one molecule of fumaric acid ($C_4H_4O_4$) of crystallization in the unit cell. The fumarate radical and the fumaric acid molecule are planar and closely similar, both having the *trans* configuration; but their orientations in the unit cell are quite different. Short H bonds, 2·57 Å in length, link the fumarate groups along the [010] directions in two rows separated by a short van der Waals distance, at $z = \frac{1}{4}$ and $z = \frac{3}{4}$ approximately. These rows are cross-linked by the fumaric acid of crystallization which joins the fumarate group at 0, 1, $\frac{1}{4}$ to that at 1, 0, $\frac{3}{4}$, also by short H bonds. The Rb ion is co-ordinated by seven O atoms at distances varying from 2·88 to 3·09 Å, the shortest bond being to the fumarate group to which it formally belongs. The overall length of the fumarate group indicates that there is considerable resonance in the C.C:C.C chain, the bond lengths being 1·45–1·41 Å for the 'single' and 1·32 for the 'double' bond. Potassium hydrogen fumarate is in some ways structurally similar to rubidium hydrogen fumarate, but is not isomorphous with it.

9. J. M. Robertson, H. M. M. Shearer & J. S. Broadley. *The structure of β-succinic acid: a three-dimensional survey.*

The special interest of the succinic acid structure concerns the length of the central C–C bond, which might be expected to show a contraction due to hyperconjugation, by analogy with the geranylamine hydrochloride and dibenzyl structures. To obtain information on this point and in order to study the fine structure of the carboxyl group, a three-dimensional Fourier analysis of β-succinic acid has now been completed, and corrections calculated by the method of differential synthesis on the Manchester electronic computer. Electron-density sections through the mean plane of the central carbon atoms, and through the mean plane of the carboxyl groups, have been evaluated. The length of the central C–C bond, first obtained as 1·47 Å, increases to 1·52 Å as a result of finite-series corrections, and may not be significantly shorter than the normal single bond. The next bond, to the carboxyl carbon, is significantly shortened to 1·48± 0·01 Å. The carbon–oxygen distances in the carboxyl group are 1·31±0·01 Å and 1·25±0·01 Å, in agreement with other dimeric carboxylic acids. There is also evidence regarding the position of the hydrogen atom in the hydrogen bond.

10. A. J. Richard. *Structure cristalline de l'acétaldéhyde à −140° C.*

Préparation des cristaux.—On utilise un capillaire de Pyrex, monté sur une chambre de Weissenberg, équipée

d'un appareillage pour les basses températures. Un courant d'azote, à température stable et réglable de 0° C. à −160° C., permet d'obtenir des monocristaux d'acétaldéhyde et de les conserver pendant l'exposition aux rayons X.

Résolution de la structure.—Système: orthorhombique, groupe *Pna*, non centrosymétrique.

Interprétation quantitative de la fonction de Patterson à trois dimensions, calcul des séries de Fourier et de séries différences (méthode de Cochran) en projection et à trois dimensions, avec localisation sans ambiguïté, malgré le problème des phases, des atomes d'hydrogène.

Résultats.—Les molécules CH_3CHO sont disposées le long des axes hélicoïdaux d'ordre $\frac{1}{2}$, d'une manière qui paraît favorable au phénomène de polymérisation en longues chaînes mis en évidence par M. Letort et par M. W. Travers. Les longueurs des liaisons dans le cristal, C–C = 1,47±0,02 Å, C = O = 1,25−0,02 Å semblent appuyer cette hypothèse.

Les molécules présentent un plan de symétrie contenant deux des atomes d'hydrogène. La rotation libre du groupe CH_3 semble nettement exclue dans le cristal.

L'utilisation des facteurs de diffusion atomique du carbone et de l'oxygène, donnés par McWeeny, améliore l'ensemble des facteurs de structure calculés et permet de réduire notablement la valeur moyenne de la densité électronique résiduelle dans la série différence.

11. M. R. Truter. *The crystal structure of sodium formaldehyde sulphoxylate*, $NaHSO_2.HCHO.2H_2O$.

The chemical behaviour of sodium formaldehyde sulphoxylate is consistent with its formulation as a sodium salt, the anion being either (*A*)-$[OSOCH_2OH]^-$ or (*B*)-$[O_2S–CH_2OH]^-$. The substance crystallizes as the dihydrate, giving orthorhombic crystals, space group *Pbca*. The structure was solved by Patterson and Harker syntheses and refined by Fourier projections which showed clearly that (*B*) was the correct formulation of the ion. Accurate refinement was carried out by three-dimensional differential Fourier syntheses.

12. E. von Sydow. *On the crystal structures of some phases of long normal chain carboxylic acids.*

As a continuation of a work published in *Arkiv Kemi* the crystal structures of the different phases of long normal chain carboxylic acids are being investigated. There are at least six different crystal forms. One of these, the *C*-form of even-numbered acids, is determined by Vand *et al.* At present four different forms are being investigated, using single crystals and powder methods. Crystal preparation is very difficult. Form *A'* of odd acids is triclinic with a triclinic packing of the hydrocarbon chains, form *B'* of odd acids is triclinic with an orthorhombic packing of the chains and form *B* of even acids is monoclinic with the same orthorhombic packing.

The variation of unit-cell dimensions for one crystal form with different carbon content has been studied with powder methods. Form *C* of even acids is studied and all dimensions turned out to depend on the carbon content, so that the form cannot be called strictly homologous. This is probably the case with every crystal form.

13. Y. Tomiie, C. H. Koo & I. Nitta. *The crystal and molecular structure of diformylhydrazine*, CHO–NH–NH–CHO.

The dimensions of the bimolecular unit cell are $a = 8{\cdot}939\pm0{\cdot}004$, $b = 6{\cdot}253\pm0{\cdot}002$, $c = 3{\cdot}565\pm0{\cdot}002$ Å, $\beta = 112{\cdot}5°$, and the space group is C_{2h}^5–$P2_1/a$. We have determined a greater part of the signs of large U_{hk0}, U_{h0l} and U_{0kl} by the inequality method, using Sakurai's chart. By the usual procedure, we have obtained the final electron-density distributions projected on the (001), (010) and (100). By many (F_o-F_c) syntheses, we refined the atomic parameters and also obtained the positions of the hydrogen atoms. The *R* factors of F_{hk0} and F_{h0l}, including hydrogen atoms, are 8% and 11% respectively at present. The bond distances and bond angles are N–N (1·38 Å), N–C (1·32 Å), C–O (1·21 Å), N–H...O (2·80 Å), N–N–C (115·5°) and N–C–O (124°).

The structure of this molecule is a planar S shape with a centre of symmetry. This shape is rather remarkable for a derivative of hydrazine. The repulsion between the two lone pairs on two nitrogen atoms must be very strong because these lone pair orbitals are pure $p\pi$ state. However, if the –CHO radicals attract the part of lone pair electrons on nitrogen atoms, the character of the conjugation will appear and this structure will become stable. We have calculated and confirmed the stability of this molecule by a simple m. o. method.

14. D. W. J. Cruickshank & G. A. Jeffrey. *A refinement of the crystal structure analysis of geranylamine hydrochloride.*

A three-dimensional analysis of the crystal structure of geranylamine hydrochloride was published by Jeffrey in 1945 (*Proc. Roy. Soc.*, A (1945), **183**, 388). Among the interesting features were the apparently short C_5–C_6 bond, joining the two isoprene units, and its coplanar arrangement with the adjacent C_3–C_5 and C_6–C_7 bonds. The analysis has been refined by four cycles of observed and calculated differential syntheses carried out on the Manchester University electronic computer using F_c's allowing different temperature factors (*B*) for each atom. In agreement with the earlier electron-density maps, a considerable increase of *B* is found along the chain from the nitrogen, the variation being from 4·2 to 11·4. A consequence is that the peaks not near the nitrogen have low curvatures and high co-ordinate standard deviations, despite that of Cl being only 0·0025 Å. The important C_5–C_6 length is revised from 1·44 Å to 1·537 Å, with e. s. d. 0·045 Å, so that there is no significant shortening; however, the $C_3C_5C_6C_7$ group remains planar.

15. O. Kennard & J. Walker. *The crystal structure of amidinium carboxylates: an investigation of S-methylthiuronium p-bromobenzoate.*

In reporting upon the facile crystallization of amidine salts of carboxylic acids (J. Walker, *J. Chem. Soc.* (1949), p. 1996), it was pointed out that the resonance characteristics of the amidinium group and the carboxylate ion were complementary. The case of crystallization observed in such salts was interpreted in terms of association of anion and cation in solution into doublet ion-pairs of a relatively rigid oriented type (I), and that crystallization then proceeded by hydrogen bonding between the lateral

amidinium hydrogen atoms and the oxygen atoms of carboxylate groups in neighbouring doublet ion-pairs.

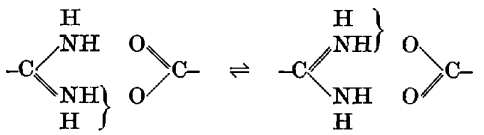

(I)

To examine this thesis the unit-cell dimensions of a number of amidine salts were measured and of these S-methylthiuronium *p*-bromobenzoate, $CH_3S.C(:NH)NH_2$, $Br.C_6H_4.CO_2H$, was chosen for detailed examination. The structure is being determined by means of electron-density projections along two crystallographic axes. These projections were solved directly using the heavy-atom method, no chemical assumptions being required. Owing to considerable overlap in one projection use is being made of 'higher-layer-line' projections to refine the co-ordinates. The salt 'molecules' lie along the *c* axial direction and are linked by both inter and intra molecular hydrogen bonds. The hydrogen bonded oxygen and nitrogen atoms form two sets of infinite sheets lying in planes inclined $\sim 40°$ to the *b* crystallographic axis. Some implications of the structure will be discussed.

16. J. L. Amorós & J. J. Coves. *Structure of the cyanacetylhydracide.*

The crystal structure of the cyanacetylhydracide has been investigated by single crystal methods:

$$a:b:c = 0{\cdot}9105:1:0{\cdot}8771,\ \beta = 63°29';\ Z = 4.$$
$$a = 8{\cdot}21\pm0{\cdot}04,\ b = 8{\cdot}85\pm0{\cdot}04,\ c = 7{\cdot}49\pm0{\cdot}02\ \text{Å}.$$

Holoedric monoclinic class. Space group $P2_1/a$.

The analysis of the structure from Patterson synthesis using Buerger's 'minimum function' gave the position of the atoms into the molecule; they are being refined by Fourier techniques.

17. T. C. Downie & J. C. Speakman. *The crystal structure of Feist's acid.*

In 1893 Feist prepared an acid which was for many years thought to be a methyl *cyclo*propene derivative of formula I. Recently Ettlinger (J. Amer. Chem. Soc. (1952), **74**, 5805), after reconsidering the chemical evidence, has argued that Feist's acid is in fact a methylene *cyclo*propane derivative (II).

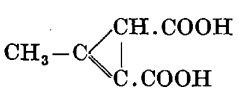

(I)

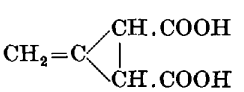

(II)

Since 1949 we have been studying this acid and certain of its salts by X-ray methods. The free acid belongs to the triclinic system, with $P\bar{1}$ as the probable space group, and with two molecules in a unit cell of dimensions, $a = 4{\cdot}8$, $b = 7{\cdot}6$, $c = 9{\cdot}1_5$ Å, $\alpha = 95°$, $\beta = 96°$, $\gamma = 78°$. We have recently succeeded in obtaining an electron-density projection on a plane perpendicular to the *a* axis. In this nearly all the atoms are resolved, and the three-carbon ring is clearly discernible. The molecule is however tilted at about 45° to the plane of projection, so that we were unable to deduce with certainty from its aspect whether the structure was (I) or (II). Nor were the other two principal projections decisive, since in them there is heavy overlapping of atoms. But, on the basis of the agreement between observed and calculated (*hk*0 and *h*0*l*) structure amplitudes, it seems likely that Ettlinger's formula ((II) in its *trans* configuration) is correct.

18. O. Hassel. *Recent results of structural determinations of molecules containing six-membered rings.*

Investigations of molecular and crystal structures of compounds containing six-membered rings of the cyclohexane type have been continued in the Oslo Chemistry Department by means of electron diffraction, X-ray crystallography and other methods. The substances studied are derivatives of cyclohexane—among them the new isomer of benzene hexachloride of m.p. 90° C. —and molecular compounds of 1·4 dioxane. In the case of the simple 1·2 dichloro-derivatives of cyclohexane, new detailed investigation of the compounds in the gaseous state have been carried out, using the newly constructed diffraction equipment of the Oslo Institute for Physical Chemistry.

19. W. R. Blackmore. *The crystal structures of Di-p-tolyl telluride, selenide and sulfide.*

Di-*p*-tolyl telluride, selenide and sulfide form orthorhombic crystals, space group $P2_12_12_1$ with four molecules in the unit cells of dimensions

	a (Å)	*b* (Å)	*c* (Å)
di-*p*-tolyl telluride	25·33	8·05	6·01
di-*p*-tolyl selenide	25·12	7·99	5·88
di-*p*-tolyl sulfide	25·07	7·92	5·81

The crystal structures of these compounds have been determined, the positional parameters being refined by double Fourier series based on 299, 401 and 284 terms respectively, derived from visual intensity measurements by two independent observers. Further refinement was carried out for each structure by the method of least squares. The bond lengths found for Te–C, Se–C and S–C are 2·05, 1·93 and 1·75 Å, and the angles C–*X*–C where *X* = Te, Se, S are 101°, 106° and 109° respectively.

20. W. Hoppe. *Die Struktur von Tetramethylnaphtazarin.*

Röntgenstrukturuntersuchungen an Naphtazarin sind von Interesse wegen der allgemeinen Molekülgestalt und wegen der Frage einer innermolekularen Wasserstoffbindung zwischen benachbarten O- und OH-Gruppen des Chinon- bzw. Hydrochinonringes. Da später geplante optische Messungen Schichtenstrukturen mit parallel gelagerten Molekülen uns besonders interessant erscheinen lassen, haben wir Kristalle des Tetramethylderivats des Naphtazarins zur Strukturuntersuchung herangezogen mit der Hoffnung, dass durch Einbau der Methylgruppen analog wie beim Übergang von Benzol zu Hexamethylbenzol eine Schichtenstruktur entstehe.

Die Kristalle sind rhombisch-pseudohexagonal mit $a = 17{,}47\pm0{,}15$, $b = 9{,}94\pm0{,}15$, $c = 6{,}76\pm0{,}07$ Å und

enthalten 4 Moleküle pro Elementarzelle. Die Raumgruppe ist D_{2h}^{15}. Weissenbergaufnahmen nach dem Mehrfilmverfahren werden zur Intensitätsauswertung integrierend ausphotometriert. Wegen der Strukturfaktorengleichheit für alle $l = 2n$ einerseits und alle $l = 2n+1$ andererseits ($n = 0, 1, 2, \ldots$) sind die Moleküle eben und liegen senkrecht zur c-Achse in parallelen Schichten mit dem halben c-Abstand. Aus Symmetriegründen müssen die Moleküle entgegen der klassischen chemischen Schreibweise ein Symmetriezentrum besitzen. Eine 'trial-and-error'-Analyse ergibt die Art der Anordnung der Moleküle in diesen Schichten.

Für die Bestimmung der genauen Molekülgestalt sind dreidimensionale Fourierschnitte mit $z = 0$ oder $z = \frac{1}{2}$ besonders vorteilhaft, die mit einem mechanischen Fourierrechengerät des Verfassers berechnet wurden.

Die Strukturanalyse wurde gemeinsam mit L. Camerer und A. Friedle durchgeführt.

21. S. C. Wallwork. *The structures of layer-type molecular complexes.*

The determination of the crystal structure of phenoquinone

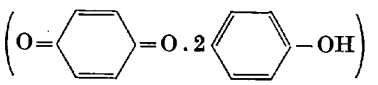

which has been reported previously, and preliminary work on other quinhydrones and complexes formed by trinitrobenzene, has established that the fundamental structural feature in both these series of molecular compounds is the plane-to-plane stacking of alternate polarizing and polarizable molecules.

Detailed structures of two further examples of these series of complexes are now being completed. Although they have the same fundamental arrangement of molecules, suggesting that the molecules are again held together by polarization bonding, they show interesting differences in detail:

Hexamethylbenzene–chloranil

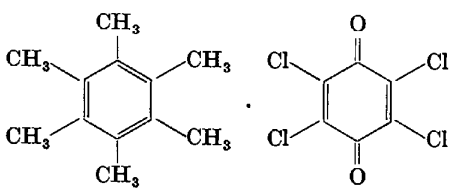

$P2_1/c$; $a_0 = 7{\cdot}30$, $b_0 = 8{\cdot}64$, $c_0 = 15{\cdot}26$ Å, $\beta = 106°$. Two formula units per cell. Molecules in special positions—chloranil at 0, 0, 0 and $0, \frac{1}{2}, \frac{1}{2}$; hexamethylbenzene at $\frac{1}{2}, 0, 0$ and $\frac{1}{2}, \frac{1}{2}, \frac{1}{2}$. Structure established by trial-and-error method involving Fourier projections, section and lines together with a generalized projection and difference syntheses.

Molecules are stacked alternately in columns parallel to the a axis, but tilted through approximately 14° from the position where they would be perpendicular to the a axis. Perpendicular spacing between adjacent parallel molecules c. 3·54 Å.

Anthracene–trinitrobenzene

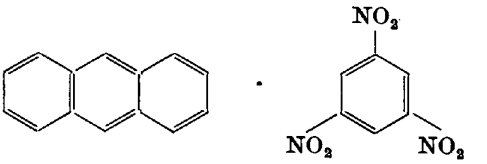

$C2/c$; $a_0 = 11{\cdot}69$, $b_0 = 16{\cdot}35$, $c_0 = 13{\cdot}23$ Å, $\beta = 133\frac{1}{2}°$. Four formula units per cell. Molecules in special positions—TNB at $0, y, \frac{1}{4}$; $0, \bar{y}, \frac{3}{4}$; $\frac{1}{2}, \frac{1}{2}+y, \frac{1}{4}$; $\frac{1}{2}, \frac{1}{2}+\bar{y}, \frac{3}{4}$; anthracene at 0, 0, 0; 0, 0, $\frac{1}{2}$; $\frac{1}{2}, \frac{1}{2}, 0$; $\frac{1}{2}, \frac{1}{2}, \frac{1}{2}$. Structure established by trial-and-error as for the hexamethylbenzene–chloranil complex.

Molecules are stacked alternately in a staggered manner in columns parallel to the c axis and are tilted about 6° from the position where they would be perpendicular to the c axis. Perpendicular spacing between adjacent parallel molecules c. 3·29 Å.

Comparison of these two structures with those of phenoquinone and quinhydrone suggests that the detailed molecular arrangement adopted in each case is a compromise between the requirements of polarization bonding and steric repulsion (and hydrogen-bonding in the case of the quinhydrones).

22. W. Nowacki. *The crystal structure of xanthazol monohydrate.*

Xanthazol monohydrate (I), $C_4H_3N_5O_2.H_2O$, is triclinic with $a = 9{\cdot}67$, $b = 10{\cdot}71$, $c = 5{\cdot}24$ Å, $\alpha = 100°\ 52'$, $\beta = 141°\ 54'$, $\gamma = 87°\ 01'$, $Z = 2$, space group $P\bar{1}$ (according to an intensity statistics). The structure was found by means of a three-dimensional Patterson synthesis and independently by the method of inequalities and that of Zachariasen, which yielded the signs of about 200 reflexions. The structure was refined by means of two three-dimensional Fourier syntheses, the R-value of the second being 0,14. (I) is a typical layer structure, the two molecules lying almost in a plane and being held together by H bonds, the distance between the layers being 3·1 Å. It corresponds to a packing of ellipses which was predicted theoretically. The molecule itself is almost planar (±0·1–0·5 Å). The calculations of the syntheses and of the structure factors were made on IBM punched-card machines.

23. J. Toussaint. *Étude radiocristallographique de l'hétérocycle γ-pyrone.*

La 2–6 diméthylthiopyrone est la molécule la plus simple contenant l'hétérocycle pyrone. Les cristaux sont tricliniques holoédriques. La maille-unité, qui contient deux molécules, est caractérisée par les dimensions suivantes: $a = 7{,}66$ Å, $b = 9{,}69$ Å, $c = 5{,}40$ Å, $\alpha = 88$, $\beta = 105$, $\gamma = 109°$.

La maille déterminée par [410], b, c est quadruple et pseudo-monoclinique; le plan ($\bar{1}40$) est presque perpendiculaire à l'axe b. Le plan des axes optiques est parallèle à ce plan qui est également de pseudo-symétrie pour le Patterson $l = 0$.

L'interprétation des réflexions intenses ($\bar{2}01$), ($\bar{2}80$) et de la symétrie pseudo-monoclinique, révélée à la fois par les radiogrammes et les propriétés optiques, fournit l'orientation approximative des molécules. Celles-ci sont

quasi-parallèles au plan ($\bar{2}01$); leur plan médian est parallèle à ($\bar{1}40$).

L'interprétation de Patterson $l = 0$ ainsi que quelques 'trial and error' donnent les coordonnées de l'atome de soufre. La connaissance de ces dernières jointes à l'orientation moléculaire fixent la position de la molécule avec suffisamment de précision pour l'utilisation de la technique de Fourier.

Les principales liaisons de l'hétérocycle sont caractérisées par les distances interatomiques suivantes: C_4–S = 1,68, C_2–C_3 = 1,36, C_2–O = 1,37, C_3–C_4 = 1,42 Å.

La forme du cycle s'explique parfaitement par l'existence du phénomène de résonance entre différentes structures électroniques. La contribution la plus importante est fournie par la structure non-polaire (environ 60%). Les structures polaires dans lesquelles le soufre porte une charge négative et l'oxygène une charge positive confèrent à la molécule un moment électrique dipolaire très élevé.

24. W. T. Eeles. *The structure of 4–5 dimethyl phthalic thio-anhydride.*

This substance is a member of a class of compounds in which there is a sulphur atom substituted in a phthalic anhydride skeleton. A structure determination by X-ray methods has shown conclusively that the sulphur atom is part of the five-membered ring.

The compound crystallizes in the space group $P2_1/c$ with $a = 4{\cdot}1$, $b = 13{\cdot}6$, $c = 16{\cdot}7$ Å, $\beta = 92°$.

The sulphur atom was located by means of Patterson projections and a trial structure was deduced from a Buerger minimum function formed from the [100] Patterson projection. Refinement is proceeding by means of two-dimensional Fourier syntheses and $F_o - F_c$ syntheses.

25. D. C. Phillips. *The polymorphism of acridine.*

Three distinct polymorphic forms of acridine, $C_{13}H_9N$, are now being examined in detail. They are:

	a (Å)	b (Å)	c (Å)	β	Space group	Z
II	16·34	18·90	6·08	95° 5′	$P2_1/a$	8
III	11·41	5·99	13·69	98° 37′	$P2_1/n$	4
IV	15·75	29·43	6·20	—	$P2_12_12_1$	12

A complete three-dimensional analysis has been made of acridine III, the simplest form, and a detailed description of the structure will be presented. Examination of its thermal properties has shown the way in which it is transformed, at about 45° C., into acridine II.

Acridine II is stable throughout the temperature range 20–105° C. Its structure has been determined by trial-and-error methods, and a three-dimensional refinement is in progress.

Acridine IV sublimes slowly even at 20° C. and is transformed into acridine II at about 70° C. The projection of the structure on (001) has been determined.

The relationships between the three forms will be described.

26. R. F. Entwistle, W. G. Ferrier & J. Iball. *Some similarities in the diffraction patterns of organic compounds.*

In a series of investigations of the structures of some aromatic hydrocarbons remarkable similarities have been observed between the diffraction patterns from single crystals of compounds which have molecules of roughly the same size and shape. This is so in spite of the unit cells being of different size and of having different space groups. Two pairs of compounds will be mentioned as examples.

(1) *Chrysene and* 1:2-cyclo*pentenophenanthrene.*—In order to bring out the similarity it is necessary to take a non-primitive cell for the latter compounds. If a cell centred on the B face is used, however, the weighted reciprocal lattices are seen to be strikingly similar and this of course means that although chrysene has a molecule with a centre of symmetry occupying a centre of symmetry in the unit cell while the other compound is asymmetric and not even planar, they are arranged in space in a very similar manner. Two-dimensional Fourier projections will show the relationship between the two structures.

(2) *Anthracene and di-hydroanthracene.*—Again the space groups are different, $P2_1/a$ in one case and $P2_1$ in the other. There is no centre of symmetry in the latter case but the packing is very similar in the two compounds. In the $hk0$ zone, for example, the structure factors are almost identical, and in other zones there are marked resemblances. When more detailed comparisons are made, however, differences are observed which suggest that the molecule of dihydroanthracene has a different shape from that of anthracene.

27. J. Toussaint. *Étude radiocristallographique du p-nitrophénol (variété métastable).*

Le p-nitrophénol est dimorphe monotrope. Les deux variétés sont monocliniques.

	Stable	Métastable
Dimensions de la maille	a = 11,8 Å	a = 15,4 Å
	b = 8,9	b = 11,2
	c = 6,17	c = 3,8
	β = 106° 52	β = 106° 55
$a:b:c$	1,3419 : 1 : 0,6930	1,3836 : 1 : 0,3398
Groupe d'espace	$P2_1/n$	$P2_1/a$
Z	4	4

Il n'existe pas de relations simples entre les réseaux des deux formes.

Il faut, par conséquent, reviser les idées anciennes concernant le polymorphisme paramorphique du p-nitrophénol. Cette assertion basée sur le fait que les rapports des paramètres des deux modifications sont multiples très simples l'un de l'autre, n'est pas confirmée par les valeurs absolues des axes.

La variété métastable du p-nitrophénol se présente sous forme polymère à l'état solide. Les molécules associées par les groupes OH et NO_2 forment des chaînes qui s'étendent parallèlement à l'axe a du cristal. La molécule est plane dans les limites des erreurs de mesure. L'axe moléculaire parallèle à (001) est incliné sur l'axe a d'un angle de 24°.

28. P. G. Taylor. *The derivation of the crystal structure of trinitrotoluene from the three-dimensional Patterson.*

Samples of 2:4:6 tri-nitro-toluene were found to crystallize from chloroform at room temperatures in an orthorhombic cell, containing eight molecules, of dimensions 14·85, 19·78, 5·96 Å. The space group was indicated as either D_{2h}^{11} or C_{2v}^{5}.

The Patterson synthesis was computed in three dimensions using Cu K diffraction data. From an examination of the Harker-type vectors it could be deduced that the non-centric space-group C_{2v}^{5}–*Pba* was present. Certain features of the Patterson enabled the orientation and relative position of the two independent molecules to be deduced. The position of the carbon rings in the cell and the positions of the remaining atoms were then arrived at by use of Patterson evidence, assisted by trial-and-error work.

Agreement of calculated and observed structure factors indicates that the structure is correct, but cannot be determined with high accuracy until three-dimensional refinement work is undertaken. Some interesting modifications in the bond lengths, notably those of the carbon ring, appear to be present.

29. D. M. Burns & J. Iball. *The determination of the atomic coordinates of fluorene.*

The structure of fluorene has been completed by two-dimensional Fourier syntheses down each of the three crystallographic axes. Refinement of the atomic coordinates was carried out by (*a*) the application of the least-squares method (*b*) repeated Fourier projections followed by F_c syntheses to correct for series-termination errors. The results obtained by these two methods were then compared with the atomic coordinates obtained from the final F_o syntheses making systematic correction for the effect of nearest neighbouring peaks in the F_o maps.

There does not seem to be any systematic connection between this method of correcting for overlapping peaks in the Fourier map and the corrections given by an F_c synthesis. It is not true, in this particular case at any rate, that an F_c synthesis automatically corrects for overlapping of peaks.

The errors in the final coordinates have been estimated by statistical methods and by calculating the distances of the individual atoms from the mean plane of the molecule which is apparently planar. The r.m.s. deviation of atoms from the mean molecular plane is 0·031 Å, using corrections indicated by an F_c synthesis, but only 0·017 Å if corrections for overlapping are applied directly.

30. L. L. Merritt & C. Guare. *La structure cristalline du salicylaldoximate de nickel.*

La structure cristalline du salicylaldoximate de nickel, $Ni(C_7H_6O_2N)_2$, a été déterminée par les méthodes du monocristal. La maille élémentaire est monoclinique avec $a = 13{,}63$, $b = 4{,}89$, $c = 10{,}20$ Å, $\beta = 110°\ 26'$. Le groupe spatial est $P2_1/n$–C_{2h}^{5}; $Z = 2$.

Les positions des atomes ont été déterminées par des projections de densité électronique sur le plan (010) et par des sections de Fourier à trois dimensions. Ces positions ont été raffinées par la méthode des moindres-carrés.

Les taches de diffraction ont été enregistrées sur quatre films superposés; leurs intensités ont été estimées par comparaison visuelle avec une échelle photographique.

Le molécule est plane et les liaisons autour de l'atome de nickel sont en position *trans*. Les angles O–Ni–N et O–Ni–N′ sont respectivement 95° et 85°. Dans le cycle de chélation chaque simple liaison est inférieure de 0,1 Å environ à la simple liaison normale tandis que chaque double liaison dépasse de 0,1 Å la double liaison normale. Ceci montre qu'il y a vraisemblablement résonance dans le cycle de chélation.

Chaque molécule possède deux courtes liaisons hydrogène, 2,45 Å environ. Ces liaisons hydrogène unissent l'oxygène phénolique d'un groupe salicylaldoxime a l'oxygène du radical oxime de l'autre groupe salicylaldoxime. La longueur de cette liaison hydrogène a été vérifiée par l'absorption dans l'infrarouge du complexe.

31. P. Franzen. *Structure determination of hexaethylbenzene.*

32. H. v. Eller. *Structure de colorants indigoïdes.*

La structure de l'indigo a été déterminée à partir de cristaux monocliniques ($P2_1/c$) par la méthode d'essai et d'erreur. Les calculs successifs de densité électronique et la détermination des signes des facteurs de structure, puis le calcul de fonctions ($\varrho_o - \varrho_c$) ont été effectués optiquement à l'aide du photosommateur harmonique. L'erreur quadratique moyenne est de 0,03 Å. La distance de 2,83 Å, caractéristique d'une liaison hydrogène, sépare l'oxygène cétonique de deux groupes imine, l'un d'une même molécule, l'autre d'une molécule voisine.

La comparaison est faite entre cette structure et celle du sélénoindigo, déterminée par la méthode de l'atome lourd, où les distances entre les atomes d'oxygène et de sélénium sont très courtes.

33. G. v. Eller. *Structure cristalline du chlorhydrate de paratoluidine.*

Le chlorhydrate de paratoluidine (H_3C–C_6H_4–NH_2) (HCl) cristallise dans le système monoclinique (groupe spatial $P2_1/c$) avec quatre molécules par maille: $a = 9{,}07$, $b = 9{,}33$, $c = 9{,}85$ Å, $\beta = 108{,}7°$; densité 1,1927 g.cm.$^{-3}$.

La recherche de la structure a été conduite de façon classique (méthode de l'atome lourd), *mais uniquement par voie optique*, au moyen du photosommateur harmonique, en opérant par essai et erreur. Le parachèvement a été effectué en faisant alterner les photosommes de séries 'différence' et les calculs arithmétiques des facteurs de structure. La moyenne quadratique de l'erreur est d'environ 0,015 Å. L'atome d'azote du radical plan (H_3C–C_6H_4–N) est relié à trois ions chlore par l'intermédiaire de liaisons hydrogène.

34. T. H. Goodwin. *Calculation of bond lengths in conjugated structures.*

Complementary to the X-ray crystallographer's work of measuring atomic co-ordinates, bond lengths and bond angles is the wave mechanician's task of calculating these, though there is at present no possibility of evaluating atomic co-ordinates in crystals. The simplest approximation of all starts from counting the number of times a given bond is represented as a double bond in the set of canonical structures, but in view of the possibility that

each electron may be found anywhere in space, the molecular orbital approach, in which every electron is partially associated with every nucleus, is clearly a more logical, possibly a more rigorous but certainly a more laborious, approximation. This method has already been applied, e.g. by Coulson, Daudel, Robertson and others to naphthalene, anthracene, coronene, etc.

The present writer has applied it to the molecules of flavanthrone, $C_{28}H_{12}O_2N_2$ (I) (structure determination by Stadler, *Acta Cryst.* (1953), **6**, 54), acedianthrone, $C_{30}H_{14}O_2$ (II) (structure determination by Friedlander, Goodwin & Robertson, *Acta Cryst.* (1954), **7**, 127), furoic acid, $C_5H_4O_3$ (III), and benzanthrone, $C_{17}H_{10}O$ (IV), with the following results for the first two (calculations not yet complete for furoic acid; structure determination incomplete for benzanthrone):

	Flavanthrone	Acedianthrone
Bonds in asymmetric unit	20	20
Experimental uncertainty in bond lengths (Å)	±0·05	±0·06
Number of bonds calculated within 0·03 Å of measurement	12	9
Number of bonds calculated within experimental uncertainty	15	17

These results suggest that molecular orbital calculations made before a structure determination is complete may well suggest the directions in which atomic coordinates should be adjusted in refining a crystal structure.

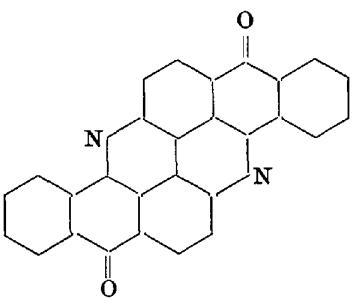

I

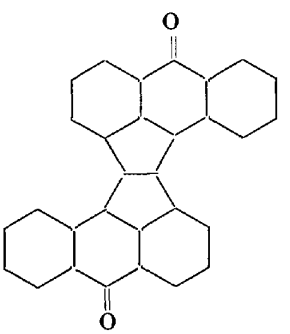

II

III 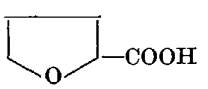

IV 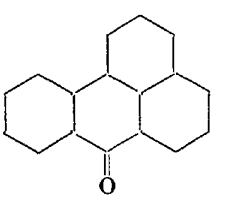

35. J. M. Lindsey. *The crystal structure of codeine.*

Codeine hydrobromide dihydrate and codeine hydroiodide dihydrate crystallise from water as orthorhombic needles with almost square cross section. The space group of each is $P2_12_12_1$, $Z = 4$, and the cell dimensions are

$C_{18}H_{21}O_3N.HBr.2H_2O$: $a=6·82$, $b=13·10$, $c=20·86$ Å.
$C_{18}H_{21}O_3N.HI.2H_2O$: $a=6·83$, $b=13·44$, $c=21·38$ Å.

The positions of the halogen atoms have been determined from Patterson projections on (100) and (010) and the signs of the structure amplitudes by the isomorphous-replacement method. Electron-density projections have been refined by repeated F_o and F_o-F_c syntheses.

The electron-density projection on (100) shows nearly all atoms clearly resolved and confirms the existence in the solid state of the molecular configuration suggested by Rapoport & Lavigne from chemical evidence.

36. W. Traub. *The crystal structure of biotin.*

37. M. Huber & W. Cochran. *Crystal structure of bromothymidine.*

The structure of 5′-bromo–5′-deoxythymidine has been determined, for each of two crystalline modifications, by two-dimensional projections and generalized projections of the electron density. Accurate measurement of bond lengths has not been attempted. There are a number of points of interest in the molecular configuration; for instance, the ribose and thymidine residues are in the 'standard' configuration which has been found for all nucleosides and nucleotides so far investigated. From the system of hydrogen bonds, some conclusions can be drawn about the tautomeric form of the molecule. The structures are of interest in connection with current theories of the structure of nucleic acid.

38. A. M. Abd El Rahim. *The two-dimensional analyses of β-amyrin and α-amyrin, using the heavy-atom technique.*

Recently the suggested stereochemistry of oleanolic acid, a member of the β-amyrin series was put forward as:

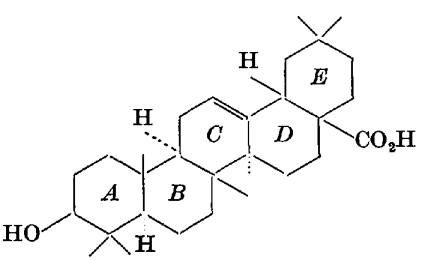

An X ray study of the iodoacetate of oleanolic acid has been carried out. The orthorhombic crystals, with cell dimensions: $a = 7·70$, $b = 16·11$, $c = 25·14$ Å, belong to the space group $P2_12_12_1$, with $Z = 4$. Using the heavy-

atom technique, together with successive refinements, it has been possible to show from electron-density map on (100) that the above suggested formula is essentially correct.

A detailed study along similar lines is at present being undertaken on the iodoacetate of α-amyrin. The crystals are orthorhombic with cell dimensions: $a = 8{\cdot}08$, $b = 22{\cdot}23$, $c = 33{\cdot}34$ Å, and space group $P2_12_12_1$, with $Z = 8$. Preliminary electron-density maps have already been obtained on (100) showing the molecule with little overlap and with the possibility that this projection shows the molecule in two orientations.

39. R. H. Moffett. *The structure of longifolene hydrochloride*, $C_{15}H_{25}Cl$.

This tricyclic sesquiterpenoid crystallizes in the space group $P2_12_12_1$ with $a = 8{\cdot}505\pm0{\cdot}003$, $b = 9{\cdot}760\pm0{\cdot}002$, $c = 16{\cdot}674\pm0{\cdot}003$ Å.

Its chemical constitution, previously unknown, has been determined by comparison of two projections, obtained with the aid of the isomorphous hydrobromide, and by the use of an error synthesis. The molecular constitution has been described in a preliminary note (R. H. Moffett & D. Rogers, *Chem. Ind. Rev.* (1953), p. 916). Refinement has been carried out by difference syntheses, and it became necessary to take account of the considerable anisotropy in the thermal motion of the halogen atom.

The formation of longifolene hydrochloride by a rearrangement from the parent hydrocarbon, longifolene, will be mentioned briefly, and there will also be some discussion of bond lengths and bond angles derived from the two projections.

40. Y. Sasada & I. Nitta. *Crystal structure of sodium tropolonate.*

As a part of the fundamental studies of the so-called tropoloid compounds, we have determined the accurate crystal and molecular structure of sodium tropolonate in which tropolone behaves as anion. This substance is a very stable yellow needle crystal and the dimensions of the unit cell, containing four formula units and of the space group symmetry $P2_1/c$, are $a = 13{\cdot}91$, $b = 3{\cdot}67$, $c = 11{\cdot}69$ Å, $\beta = 93{\cdot}0'$.

The inequality method provided a key to structure analysis, and the approximate structure was obtained from the ordinary Fourier projections along three principal axes. After this, successive (F_o-F_c) and three-dimensional Fourier syntheses were calculated, and parameter values of all atomic coordinates, including hydrogen, were estimated with considerable accuracy.

The planarity of seven-membered carbon ring, expected from many organic and physico-chemical investigations, was established. Bond lengths are discussed in comparison with those in tropolone hydrochloride, in which tropolone behaves as cation, and in aromatic compounds. The results of molecular orbital treatment and infra-red absorption are also taken into consideration. The sodium ion is surrounded by six oxygen atoms at distances 2·4–2·7 Å and the orientation of tropolonate and sodium ions explains the cleavages parallel to (010) and (100).

41. J. Fridrichsons & A. McL. Mathieson. *The crystal structure of* DL-*isocryptopleurine methiodide.*

DL-*iso*Cryptopleurine methiodide, a derivative of L-cryptopleurine, is monoclinic with $a = 9{\cdot}95$, $b = 24{\cdot}2$, $c = 9{\cdot}95$ Å, $\beta = 112°$ and space group $P2_1/n$. Because of the failure of chemical studies to reveal the structure of cryptopleurine and *iso*cryptopleurine, an X-ray analysis has been carried out, based solely on the empirical formula, $C_{25}H_{30}O_3NI$, and using no assumptions regarding structure, bond lengths and angles. The crystal structure has been solved in a direct manner by the use of the 'heavy' atom technique combined with a new application of generalized projections, the principle of which is as follows. The data from the n different layers about one axis, e.g. nkl can be combined to yield n different generalized projections down the a axis, $\varrho_n = \sqrt{(C_n^2+S_n^2)}$. Since only Fourier terms whose signs can be considered fixed by the iodine contribution are used in the syntheses, each projection will be in error to a certain extent. However, errors occurring in each projection will not coincide because each projection is derived from a different set of data. It is therefore possible to combine the n projections by a minimum or summation function and extract the correct atomic locations y, z in this projection area. The approximate x parameters can then be assessed from $C_1(y, z)$ and $S_1(y, z)$ and refinement carried through.

The improved resolution of generalized over normal projections will be shown.

42. T. H. Doyne, S. Hirokawa & T. Watanabé. *The crystal structure of* L-*glutamic acid and zinc asparatate tri-hydrate.*

The unit-cell dimensions and space groups of L-glutamic acid (new form) and zinc asparatate tri-hydrate are:

L-Glutamic acid (new form)	Zinc asparatate tri-hydrate
$a = 5{\cdot}17$ Å	$a = 9{\cdot}46$ Å
$b = 17{\cdot}34$ Å	$b = 7{\cdot}92$ Å
$c = 6{\cdot}95$ Å	$c = 11{\cdot}58$ Å
$\beta = 90°$	$\beta = 90°$
$Z = 4$	$Z = 4$
$\varrho_{exp.} = 1{\cdot}575$ at 20° C.	$\varrho_{exp.} = 1{\cdot}97$
M.w. = 147	M.w. = 255
Space group—$P2_12_12_1$	Space group—$P2_12_12_1$

Dimorphism of L-glutamic acid was found. One form has the same unit cell dimensions and the space group as reported by Bernal while the new form has the aforementioned unit cell dimensions and the space group. Using the Fourier series method, atomic coordinates were obtained for L-glutamic acid (new form) by three projections and for zinc asparatate tri-hydrate by two projections.

43. R. Pepinsky & P. F. Eiland. *X-ray analyses of biochemical compounds.*

The steric conformation of tropine is established by an analysis of tropine.HBr; the six-membered ring is in a chair form, and the hydroxyl group is trans to the amine bridge (with R. Sloan). The structure of actithiazic acid, a new thiazolidone antibiotic, is established from the K and Rb salts (with J. Turley). The examination of two stereoisomeric pyridyl antihistamines (substituted propenes) reveals that the β form, which is the less potent physiologically, has pyridine and pyrrolidino groups on

the same side of the double bond; chemical evidence then affirms that the very active α-isomer has these groups in *trans* arrangement (with J. Rathlev). The complete analysis of α-methyldihydrothebaine methiodide confirms the structure proposed by Robinson (with D. Smits and J. A. Goedkoop). A projection of podophyllotoxin bromacetate is in agreement with the structure proposed by Hartwell & Schrecker (with W. G. Perdok). Some features of the structure of desoxynupharidine are established from the HCl salt (with Y. Okaya). The general stereochemistry of aureomycin is established via a study of the HBr salt (with T. Watanabe and T. Doyne).

Crystallographic data is presented for thymidine, several derivatives of jervine, castoramine.HSO_4, streptamine.2HCl, radicinin dihalides, salts of erythromycin, polypeptides obtained by thermal cleavage of ergotamine and ergocornine, hydrohalides of α-methyldihydrothebaine, and a series of hydrohalides of terramycin, aureomycin and achromycin.

44. D. W. Smits & R. Pepinsky. *The crystal structure of α-methyldihydrothebaine methyliodide.*

The crystal structure of α-methyldihydrothebaine methyliodíde has been determined by X-ray diffraction, using the heavy-atom technique. The compound crystallizes in space group $P2_1$, with $a = 11{\cdot}06$, $b = 8{\cdot}75$, $c = 10{\cdot}54$ Å, $\beta = 94°32'$. There are two molecules per unit cell.

Three-dimensional data were collected from Weissenberg photographs in 1950 by J. A. Goedkoop, using quite small crystals and Cu $K\alpha$ radiation. Since only about 40% of the *h0l* reflections were recorded on these films, new zero-layer-line *b*-axis Weissenberg photographs were taken, using a larger crystal ground cylindrically along this axis. The intensities were carefully estimated against a series of intensity-calibrated reflections and absorption corrections were made for this zone.

The position of the iodine atom was determined from the three-dimensional Patterson synthesis, already computed by Goedkoop on X-RAC. A Fourier projection on (010) was then made, assigning to the structure factors the signs of the iodine contributions. A model of the molecule, based on the structure proposed by Robinson, could be fitted on to this map.

The atomic *x*, *z* coordinates were refined by consecutive Fourier syntheses and structure-factor calculations. An improved agreement between the calculated and observed structure factors was obtained by assuming an anisotropic temperature factor for the iodine atom.

The *y* coordinates could be obtained from a three-dimensional Fourier synthesis, with the phases based on the iodine contributions only. From this synthesis, which represented the superposition of the optically active molecule and its centrosymmetrical image, the atomic positions for an individual molecule were found with the aid of the model.

The further refinement of the coordinates was established by consecutive two- and three-dimensional structure-factor calculations, the latter made on IBM machines, two- and three-dimensional Fourier syntheses, computed on X-RAC, and difference syntheses. During this refinement it appeared that the temperature factor to be applied to the new *h0l* data from the cylindrical crystal was different from that to be used for Goedkoop's *hkl* data. This discrepancy is probably due to the neglect of an absorption correction for the latter data. After applying an appropriate absorption correction to these data a reliability index of 15·2% was reached for the *hkl* reflections; for the *h0l* reflections a reliability index of 10·8% was obtained.

The molecule contains two non-coplanar benzene rings and a chain of five atoms between these rings, which forms with four atoms of the benzene rings a nine-membered ring. The methyl group of the methyliodide molecule is bonded directly to the nitrogen atom, leaving an I^- ion. This iodine ion is surrounded by three positively charged amino groups, a phenolic hydroxyl group, and an oxygen atom of a methoxy group. The molecules are arranged in sheets parallel to (100); in each sheet they are connected by the iodine ions. These ions also connect the sheets two and two, thus forming layers each consisting of two sheets; van der Waals forces connect these layers.

§ 7. Structures des proteines et structures des composés analogues

1. W. L. Bragg & M. F. Perutz. *A Fourier projection of haemoglobin on the* 010 *plane.*

I. *Transform of haemoglobin projected on the* 010 *plane.*— Horse haemoglobin forms monoclinic crystals with two molecules in the unit cell and symmetry *C*2, the molecules lying on twofold axes of symmetry. The projection of the molecule on 010 thus has a symmetry centre, and its transform consists of positive and negative areas separated by nodal lines where *F* passes through zero. The spaces between the molecules are filled with water, the average density of the protein being greater than that of the surrounding water. Within the limits of resolution considered here, this water may be considered as a uniform background to the molecule. The transform thus has a maximum at the origin equal to the difference between the average electron density of protein and water multiplied by the volume of its molecule. The inner part of the transform such as the central positive maximum and surrounding negative ring is largely determined by the overall shape of the molecule, whereas its outer regions are for the most part due to the interference of waves arising from variations of density within the molecule.

The monoclinic crystals under varying conditions assume a series of forms owing to changes in the monoclinic angle β, while the sheets of molecules in the *c* planes retain their arrangement unaltered. This makes it possible to explore the values of *F* along the *a* layer lines, and so to outline a series of nodes and loops representing sections of the transform along these layer lines. The 'wave-number' of these nodes and loops is determined by the overall shape and size of the molecule. Their delineation shows where changes of sign in *F* occur, and is a step towards the complete determination of all signs and so towards the solution of the structure described in the following paper.

The replacement of water by salt solution diminishes the difference in density between protein and surrounding liquid. The resulting changes in the values of *F* outline

Modification	Solvent	Space group	Z	a_0 (Å)	b_0 (Å)	c_0 (Å)	β
I	50 vol. % n-C_3H_7OH, pH = 6–8, Ni^{++} = 1–6 per mole of protein	$P2_12_12_1$	4	37·2	44·5	75·7	—
II	50 vol. % $(CH_3)_3COH$	$P2_1$	2	30·2	38·4	53·2	105·85°
III	50 vol. % n-C_3H_7OH	$P2_1$	4	42·9	45·4	77·2	114·31°
IV	50 vol. % n-C_3H_7OH	$P6_222$	24	88·3	—	112·6	—
V	70 vol. % HO-$(CH_2)_3$-OH	$C222_1$	8	31·6	62·0	121·8	—

the transform corresponding to a 'ghost' molecule which has the outer shape of the haemoglobin molecule but a uniform interior.

II. *Sign determination by the isomorphous-replacement method.*—Horse haemoglobin combines with two molecules of paramercuri-benzoate or with two silver ions. Crystals of these heavy metal compounds are exactly isomorphous with normal haemoglobin crystals but exhibit significant changes in the intensities of many reflexions. The changes in $F(h0l)$ were used to determine the x and y parameters of the pair of heavy atoms attached to each haemoglobin molecule; this was done both for the normal wet lattice and for one of the acid-expanded lattices. The positions of the heavy atoms proved to be slightly different in each case, giving rise to three sets of diffraction fringes, each set making measurable contributions in different areas of the reciprocal net.

In each case the isomorphous substitution allowed the signs of just over two-thirds of the reflexions to be found with certainty. Between them the three sets of diffraction fringes determined the signs over the entire area of the $h0l$ plane so far investigated. These signs were then superimposed on the waves of the transform described in § I. All the sign relations established by the transform method were confirmed and the remaining uncertainties cleared up. Comparison of the transform with the three sets of isomorphous-replacement results allowed the consistency of the signs to be rigorously checked; not a single inconsistent sign was found.

In the normal wet lattice the mercury and the silver compounds between them allowed the signs of 87 out of 94 reflexions to be found with certainty. This suggests that the isomorphous-replacement method may offer a way of finding the phases in protein crystals even when practical difficulties preclude the use of the transform method.

Fourier inversion of the molecular transform gives an electron-density map of a single row of molecules in projection on the 010 plane. This map shows a molecule of irregular outline and complex internal structure seen at a resolution of about 4 Å. Owing to this limited resolution and to the great depth of material projected neither polypeptide chains nor haem groups can as yet be recognized. Along the c direction the molecular dimensions can be measured with accuracy; along the a direction this is not yet possible, owing to overlap of neighbouring molecules in projection. Indications of the length of the molecules in that direction are obtained from the Fourier of a lattice slightly shrunk along a. An interesting feature of the projection is a hollow at the central dyad where the thickness of the molecule is apparently reduced to 32 Å. It is not yet clear what this hollow represents.

A full account of this work will appear in the *Proceedings of the Royal Society*, A.

2. D. Harker. *X-ray crystallography of five forms of the protein ribonuclease.*

Ribonuclease can be crystallized from mixtures of water and water-soluble organic substances. Depending on pH, organic substance and the addition of other, minor constituents, one or the other of five different crystalline forms of ribonuclease is obtained. The above table presents typical examples. The implications of these and other data with regard to the structure of this protein will be discussed.

3. C. H. Carlisle, M. Ehrenberg & H. Scouloudi. *Some further observations on the structure of crystalline ribonuclease.*

The evidence obtained so far on the examination of electron-density maps on (100), (010) and (001) of the crystal conform to the view, previously put forward, that ribonuclease is largely composed of a flat chain of the 2_7b type. The evidence at this early state appears to suggest the presence of one polypeptide chain composing the molecule which folds back on itself to give a parallel hexagonal close packing of chains. In doing this the electron-density maps suggest distortions of the chain which are probably due to the packing of the side chains and its necessity to turn back on itself at the folds. Some of these conclusions will be supplemented as far as possible with supporting arguments from a three-dimensional Patterson synthesis of the crystal.

4. J. G. White. *Recent X-ray work on the air dried crystals of vitamin B_{12}.*

Work has continued on the B_{12} structure on the basis of the partial structure tentatively suggested. Further calculations, using the phases of the cobalt atom and planar group alone, have been carried out in the regions believed to be occupied by the benzimidazole and sugar, and appear to confirm the positions postulated for these groups.

An attempt has been made to fill in the rest of the structure by adding into the phase calculations possible atomic positions suggested by successive Fourier series. Complete three-dimensional Fouriers have been computed with the phase angles of 59, 78 and 104 atoms respectively, and in addition several partial three-dimensional Fouriers of particular regions in space at intermediate stages. These have been interpreted both by trying to place side chains in the molecule and also by placing isolated atoms without regard to chemical connection. Changes in one part of the original planar group have been observed on refinement.

Calculated R factors and their significance at various stages are discussed.

5. G. S. D. King. *Preliminary X-ray investigation of some lysozyme salts.*

Crystals of lysozyme iodide have been examined in the wet and dry forms. The cell dimensions have been measured approximately using a 3 cm. radius camera with the following results:

	a (Å)	b (Å)	c (Å)	β (°)	c sin β (Å)	Space group	Z
Wet	28	62	75	114	62	$P2_1$	4
Dry	26	62	35	118	31	$P2_1$	2

This suggests that in the wet cell two molecules with slightly different orientations are related by a translation $\frac{1}{2}c$. The drying process would then align the molecules, thus halving the cell. These results are similar to those found by Carlisle for the bromide.

It is hoped that a comparison of the Patterson functions of the wet and dry forms of the two salts will lead to an analysis of the structure.

6. M. F. Perutz. *Phase transition in protein crystals.*

Protein crystals show discontinuous lattice changes in response to changes in their suspension medium. The effects of pH, electrolyte concentration and humidity are discussed.

7. P. M. Cowan, A. C. T. North & J. T. Randall. *New light on the structure of collagen.*

High-angle X-ray diffraction photographs of rat-tail-tendon collagen, held under tension during exposure, show improved orientation which depends on the amount of stretching; best results have been obtained at about 8% extension. Layer-line spacings increase on stretching, but only by about two-thirds of the observed fibre extension.

Low-angle spacings also vary with extension, values as great as 760 Å for the fibre period having been observed. Here, however, the percentage increase in spacing is about 90% of the percentage extension of the fibre.

The relative intensities of orders of the low-angle spacing of air-dried fibres suggest a scattering unit measuring 210–240 Å in the fibre direction. The low-angle scattering round the central maximum indicates a crystallite size of about 200 Å by 65 Å in dried material. Nevertheless, over 30 orders of the low-angle spacing are sharp and clearly visible.

The interpretation of the X-ray data in terms of molecular models is discussed with reference to both the large scale architecture and the atomic configuration of polypeptide chains. No model yet proposed is in agreement with all the observed facts.

8. U. W. Arndt & D. P. Riley. *Two-component structure for collagen.*

The polypeptide chain folding in collagen is considered to be of two types, regular and disordered, possibly corresponding to interbands and bands. X-ray scattering evidence which favours a γ-helix type of configuration in the ordered component is presented. Every third residue in the helix is either exceptionally heavy or exceptionally light. The less ordered component is considered to contain all the proline and hydroxy-proline.

9. G. N. Ramachandran. *Structure of the collagen group of proteins.*

A re-examination of the wide-angle X-ray pattern of collagen indicates that the observed reflexions could be indexed on the basis of a hexagonal unit cell with $a = 12-16$ Å and $c = 9{\cdot}0-9{\cdot}5$ Å. The meridional arcs of spacing 4·0 Å and 2·86 Å are indexed as 112 and 113, and their non-meridional nature is confirmed by a calculation of the expected angular spread. A structure, composed only of *trans*-amino acid residues, is proposed, which fits the above unit cell. It consists of 9 residues per cell, arranged in the form of three helical chains (symmetry 3_1), linked together to form a cylindrical rod. The pitch of each chain is equal to c and the three chains are also related to each other by the symmetry 3_1. Two of the three NH groups per turn in each chain are linked by hydrogen bonds to an oxygen in another chain; the third group points outward from the cylinder and is in such a position that a proline ring can be formed there. One out of every three α carbon atoms is such that none of its hydrogens can be replaced by an R group, another takes part in forming the proline ring, while the third has a general R group attached to it. These are in agreement with the amino-acid composition of collagen. Since all the NH and CO bonds are practically perpendicular to the c axis, the observed infra-red dichroism is explained. Structure-factor calculations show reasonable agreement with observation. Thermal contraction and limited extensibility of collagen are also explained.

10. R. E. Franklin & R. G. Gosling. *The Patterson function of sodium desoxyribonucleate.*

It has been shown that sodium desoxyribonucleate (SDN) exists in two distinct structural forms. Structure A has a water content of about 40%, is stable at r.h. 75% and is highly crystalline. Structure B exists at higher r.h. and its water content may vary widely. B has a lower degree of order than A but is important because it is probably more closely related to DNA in living matter.

The X-ray fibre-diagram of B is typical of a helical structure, and is consistent with the main features of the Watson & Crick model. The molecule is shown to contain two co-axial helical chains of radius 8·5 Å and pitch 33·1 Å, with 10 residues per turn of each chain. Since the change $A \rightleftharpoons B$ is readily reversible it follows that A must also contain a two-strand helix. Owing to the greater amount of information obtainable from the X-ray diagram of the crystalline form, A was chosen for detailed study.

The cylindrical Patterson function of A suggests strongly that the phosphorus atoms lie on two equally spaced co-axial helices of pitch 28·1 Å and radius 9·0 Å, each having 11 phosphorus atoms per turn. Phosphorus atoms in the two strands of the helix lie directly above one another. Density measurements and the unit-cell dimensions show that the sugar and base residues must be turned inwards towards the axis of the helix. In addition, the space group ($C2$) requires that the sequence of the atoms in the two phosphate–sugar chains should run in opposite directions.

This model is shown to be in good agreement with the three-dimensional Patterson function, and the application of superposition methods provides further confirmation of the correctness of the parameters quoted.

The relative value of the cylindrical Patterson, the three-dimensional Patterson, and other possible methods in investigations of this type will be discussed.

11. M. H. F. Wilkins. *Structure of deoxypentose nucleic acids and nucleoprotein.*

X-ray diffraction studies have been made of two crystalline forms of deoxypentose nucleic acid fibres and of deoxypentose nucleoprotein. To fit the data, molecular models have been built of helical structures basically similar to that suggested by Watson & Crick. The transform of the models has been calculated and compared with the observed three-dimensional diffraction intensity data. (This aspect of the work is described by Dr W. E. Seeds.) The crystalline structure is independent of nucleotide ratio from ratio guanine–adenine of 0·5:1 to 1·8:1, the specimens of nucleic acid being supplied mainly by Dr G. L. Brown of our Laboratory and Drs L. D. Hamilton and G. L. Barclay of the Sloan Kettering Institute. Most of the interpretation has involved direct and detailed comparison of the three-dimensional data with the Fourier transform of slightly deformed helices. Oriented nucleoprotein in intact sperm heads gives 14 reflections which have been indexed. Comparison of spacings observed by means of X-rays and of water-content in sperm-head nucleoprotein and sodium nucleate show that the protein is fitted around each nucleic acid helix.

12. W. E. Seeds. *Molecular model building in relation to the structure of the sodium salt of deoxypentose nucleic acid.*

Molecular models of the sodium salt of deoxypentose nucleic acid have been built to conform to the experimental X-ray data. The molecular models consist essentially of two polynucleotide chains hydrogen-bonded together in the manner suggested by Watson & Crick. The pairs of bases are coplanar, and are tilted at about 65° to the fibre axis for the more perfect of the two crystalline forms; this model, as a whole, corresponds closely to the structure derived from the X-ray data. A probable mechanism for intermolecular binding is suggested by the model, and it has also been possible to determine fairly precisely the position of the water and the sodium ions in this structure. The diffraction from the hydrated and less perfect crystalline form, and from nucleoprotein, will be discussed in relation to the observed X-ray data.

13. M. M. Woolfson. *The structure of adenylic acid 'b'.*

Adenylic acid '*b*' crystallizes with an estimated 1·5 molecules of water for each molecule of acid. The unit cell data are: $a = 10{\cdot}06$, $b = 6{\cdot}30$, $c = 11{\cdot}84$ Å; $\beta = 92{\cdot}5°$. The space group is $P2_1$.

The structure was determined by two-dimensional Fourier analysis. The projection along the short axis established the chemical form of the molecule. The y coordinates were determined from both the other projections, in one or other of which most of the atoms were resolved. The configuration of the molecule was found to substantially confirm that already assumed for the structure of DNA.

Bond lengths, bond angles and the formation of hydrogen bonds will be discussed.

14. W. Traub. *A preliminary X-ray study of wheat protein.*

Chemical studies of flour and wheat protein indicate that the wide differences in baking quality between different flours depend primarily on the protein rather than the starch fractions, and, moreover, on the structural features rather than the amino-acid composition of the former.

Gluten, the washed-out protein fraction of flour is divisible into gliadin (soluble in 70% ethanol), and glutenin (insoluble). Both are, however, complex mixtures of different proteins and are obtained as amorphous powders.

Powder photographs of gluten, gliadin and glutenin from different wheat varieties show diffuse rings in the 5 Å and 10 Å regions, which appear to be inappreciably affected by attempts at mechanical orientation. There is, however, a spacing at 45 Å which in thin gliadin films is oriented equatorially.

In gluten decomposed under toluene, a sharp 4·67 Å line appears, giving the characteristic disoriented β picture of the *k–m–e–f* group of proteins.

Gluten decomposed under the action of bacteria leaves a residue, which yields a high proportion of fat on hydrolysis. The 5 Å and 10 Å rings disappear in this residue, but several sharp lines appear including a greatly enhanced 45 Å line, and several higher orders of it.

K. Hess & E. Niemann have suggested a gluten model of parallel polypeptide chains linked by perpendicular side chains 45 Å long. This model is discussed with reference to the above results.

15. B. W. Low & F. M. Richards. *The permeability of protein crystals.*

Protein crystals in equilibrium with their mother liquor contain large amounts of water of crystallization; they are usually soft and fragile. Optical and X-ray diffraction studies show that in this 'wet' crystal state the molecules are highly oriented in the crystal lattice. 'Wet' protein crystals are permeable to a wide variety of solute molecules, and they equilibrate rapidly when immersed in media of different composition from that of their mother liquor. When the crystals are removed from solution they lose some water of crystallization and the crystal lattice shrinks. 'Air-dried' crystals are rather hard and horny, and show evidence of intermolecular disorientation.

It appears established that the gross features of the intramolecular protein structure remain unchanged when the crystals swell and shrink. Protein molecules, on the current coiled polypeptide chain model, have a complex and indented surface and the disorder on drying protein crystals is probably due to intermolecular side-chain entanglement. Important aspects of the protein crystal lattice structure are concerned with the nature of the intermolecular forces in the 'wet' state, and with the

geometry of the intermolecular holes or channels. The work to be reported here is part of a study of this problem.

The water in β-lactoglobulin crystals has been replaced by a series of less polar organic solvents. The observed shrinkage at the end of the solvent exchange increased as the polarity of the solvent decreased while the disorder was more marked in the more polar solvents. Although varying degrees of reversibility were found in the unit-cell dimensions on returning the crystals to their mother liquor, the disorder never decreased and generally increased.

The permeabilities of 'wet' crystals of insulin, β-lactoglobulin and human serum dimer albumin to polysaccharide molecules of graded size have been investigated. Within the limits of the uncertainty of the exact size and shape of these molecules, the protein crystal lattices appear to be able to accommodate molecules of sizes roughly equivalent to the maximum changes in intermolecular distances observed on drying.

X-ray crystallographic methods have been used to follow the changes in unit-cell size and to observe disorientation effects within the crystal lattice. Density measurements, for the most part, have been used to follow the changes in crystal composition.

16. J. C. Kendrew, R. G. Parrish & M. M. Bluhm. *New crystal forms of myoglobin.*

About a dozen new crystal forms of myoglobin have been discovered; an account will be given of some features of interest encountered in the study of these, and of their bearing on the problem of the molecular structure of this protein.

17. W. Traub. *The crystal structure of biotin.*

The main points of interest in the crystal structure of β biotin or vitamin *H*, ($C_{10}H_{16}O_3N_2S$), are the steric configuration about the three asymmetric carbon atoms and the mode of intermolecular hydrogen bonding.

The orthorhombic unit cell, containing 4 molecules, has the space group $P2_12_12_1$ with $a = 5{\cdot}17$, $b = 10{\cdot}33$ and $c = 21{\cdot}00$ Å.

By the analysis of all the Harker and zero sections of the three-dimensional Patterson synthesis, a trial structure was obtained.

This was confirmed and refined by Fourier projections along the *a* and *b* axes, and finally by three-dimensional Fourier syntheses.

This work confirms the chemical structure deduced for biotin by Hofmann, du Vigneaud and others. The molecule has the *cis* configuration at the junction of the two five-membered rings, and the aliphatic carbon chain has a *trans* configuration with respect to the nitrogen atoms of the ring system (or *cis* with respect to the hydrogen on the neighbouring carbon atom).

The crystal is held together by a strong system of hydrogen bonds.

18. C. Robinson. *Spherulites and paracrystalline structures in solutions of synthetic polypeptides.*

Solutions of the synthetic polypeptide poly-γ-benzyl-L-glutamate in certain organic solvents (e. g. methylene chloride) when above a certain critical concentration separate into two phases. The more concentrated phase is spontaneously birefringent and separates in the form of spherulites which under favourable conditions coalesce to form a 'cream'. These spherulites show spiral structures which are visible in natural light. A similar spiral arrangement is seen from whatever direction the spherulite is observed; the explanation of this paradoxical observation seems to lie in the fact that each spherulite shows a 'fault' in the spiral structure which runs the length of one radius. The distance between the convolutions of the spiral is constant and highly reproducible, though dependent on solvent and (apparently) molecular weight. Values as high as 0·02 mm. for this periodicity have been observed. Parallel lines are also seen in the cream and the distance between these is the same as the distance between the convolutions in the cream. When the spherulites are seen between crossed polaroid it is found that the retardation observed along any radius passes through a number of local maxima and minima. If the cream is allowed to approach equilibrium in a rectangular cell, equidistant layers parallel to the walls of the cell are formed, and uniformly coloured areas are observed between crossed polaroid which can be shown to be due to high form—optical—rotation, as in the so-called cholesteric mesophases. Some preliminary conclusions about the nature of these remarkable structures will be given.

19. U. W. Arndt & D. P. Riley. *X-ray scattering characteristics of some polypeptide chain configurations.*

Calculations have been carried out by a modification of the Debye method of the X-ray scattering characteristics of the following models of folded polypeptide chains:

Helices: α, π, γ, 4_{13}, 3_{10}, 3_8.
Ribbons: $2_7 b$.
Sheets: Pleated β-sheets (parallel and anti-parallel).

The calculations include the C_β atoms and embrace their two alternative positions in the case of the first 5 helices listed. Such calculations represent the X-ray scattering which would be obtained if the polypeptide chains were scattering independently and possessed random orientation; it is shown that such calculations approximate to the scattering observed from randomly oriented molecules in a powder sample of an amorphous protein or synthetic polypeptide preparation, when allowance is made for inter-chain interferences due to packing of the folded chains in the molecule.

For the purposes of comparison with observation an analysis of the scattering curves presents a more sensitive method than an examination of observed and calculated radial distribution functions. It is shown that the former method is inherently capable of distinguishing between even very similar configurations if close attention is paid to minor features of the scattering curves. Of the proteins and synthetic polypeptides examined experimentally, a small number gave rise to scattering curves characteristic of a β structure containing more or less fully extended polypeptide chains; the majority of the remainder, including all the corpuscular proteins examined, corresponded most closely with the curves calculated for the Pauling, Corey & Branson α-helix. The collagenous proteins are considered in a separate communication.

20. R. E. Franklin. *X-ray diffraction studies of tobacco mosaic virus.*

X-ray fibre diagrams of tobacco mosaic virus (TMV) have previously been studied by Bernal & Fankuchen and by Watson.

Photographs of TMV gels (digested with trypsin) have now been obtained showing 300–400 sharp maxima distributed over some 25 layer lines, and extending to spacings of about 3 Å (2 Å on the meridian).

The rod-shaped virus particles in the gel specimens are aligned accurately parallel to one another, but are probably in rotational disorder about their long axis. Moreover, the low-angle spacings show that the particles are uniformly dispersed in the gel. The diffracting unit therefore consists of a single virus particle.

The general features of the X-ray diagram strongly indicate that the diffracting unit has a helical structure. There is reason to believe that each particle (of diameter 150 Å) has a single helical axis, and that the highly detailed diffraction pattern is, in fact, the Fourier transform of a single giant helical molecule.

Intensities are being measured, and a cylindrical Patterson function will be shown at the meeting. This is a particularly powerful method of investigating this type of structure, since any set of vectors related by the helical axis are coincident in the Patterson function.

The sharpness of the diffraction pattern and the low level of background scattering indicate a very high degree of order in the virus particle.

Changes in the diagram which occur when the gel is dried or is subjected to mild denaturing treatment have been studied, and it is hoped that these will help in the general interpretation of the structure.

§ 8. Ordre-désordre et déformations dans les structures cristallines (polygonisation)

1. J. Despujols. *Anomalie des taches de Laue de cristaux épais.*

P. Lucasson et moi-même avions déjà trouvé, pour des cristaux épais de quartz et d'aluminium, une variation d'intensité le long des taches de Laue, qui apparait souvent comme une véritable démultiplication. Les renforcements d'intensité aux extrémités des taches sont connus depuis longtemps et attribués aux perturbations du réseau au voisinage des faces du cristal. Murdock a donné une explication pour un troisième renforcement situé au milieu de chaque tache.

Dans nos expériences, le nombre des composantes varie entre 2 et 10, pour des épaisseurs comprises entre 3 et 12 mm. Nous avions tenté d'expliquer de phénomène en supposant que ces cristaux étaient formés de régions de perfections différentes; la désorientation de ces régions les unes par rapport aux autres étant très faible ou nulle.

Une étude systématique a été entreprise sur divers cristaux: quartz naturel ou synthétique, calcite, diamant, béryl, aluminium, etc. Il a été vérifié sur certains échantillons que les désorientations possibles d'une région à l'autre du cristal étaient inférieures à une minute. Dans ces conditions, les diagrammes de Laue focalisés (méthode de Guinier & Tennevin) ont pu être appliqués à l'étude de ces cristaux dans leur épaisseur.

L'essai d'explication antérieur est repris et discuté.

2. P. B. Hirsch & A. Kelly. *The structure and strength of cold-worked metals.*

The results obtained by the micro-beam technique are related to the microscopic observations of slip. The boundaries and 'particles' in cold-worked metals are identified respectively with the slip bands and the regions between the slip bands. The particle-size against strain curve is explained in terms of data on the amount of slip per slip band. The strain hardening of metals is thought to be due to crossing slip bands which provide obstacles to further slip. The dislocations are considered to be piled up on the slip bands over a length equal to the particle size (or slip band spacing), and the yield stress is calculated using Frank's criterion for the stress concentration necessary for the formation of a new dislocation loop. The stress–strain curves computed in this way for aluminium and iron from the experimental data on particle size agree well with those experimentally observed.

3. P. B. Hirsch, A. Kelly & J. W. Menter. *An electron-optical study of beaten gold foil.*

It is shown how the method of counting spots can be used to determine the particle size on electron-diffraction transmission photographs. The particle size of beaten gold foil is found to be $\sim$ 2000 Å. Both extinction and refraction must be taken into account in the calculations. Electron micrographs show a pronounced structure of sets of parallel lines, whose smallest spacing is $\sim$ 200 Å. Combining electron diffraction and microscopy, these lines have been shown to be traces of 111 planes. It is thought that this structure may be due to slip and the contrast mechanism is considered. Surface replicas indicate slip in certain regions. The high resolution of the technique with regard to step heights is discussed.

4. Z. Nishiyama & M. Yamamoto. *On the sub-structure in sodium chloride crystals.*

The cleaved surface of sodium chloride crystals, both rocksalt and artificial, was observed by means of X-ray diffraction microscopy (Berg–Barrett method). The X-ray tube used was provided with a rotating iron target, the focus being $3 \times 0{\cdot}2$ mm. in apparent dimension. The distance from the target to the specimen was 460 mm. The X-ray pattern taken of the (420) or (440) reflexion revealed the sub-grain structure very clearly. The following results were obtained: (1) In the artificial crystals, the dimension of the sub-grains was 0·5–5 mm. and the maximum difference in orientation of the sub-grains was 40–50′. In some specimens there were finer domains in the sub-grains. The size of these finer domains was several times 0·01 mm. in diameter. The difference in orientation, if any, among the finer domains was not revealed within the resolving power of the camera used (2′). (2) In the rocksalt crystals, the dimension of sub-grains and the orientation difference among them were of the same order as in the artificial crystals. The finer domains were not found in the natural crystal.

5. J. Intrater & S. Weissmann. *Subgrain structure in single aluminum crystals.*

By means of a double-crystal-diffractometer (spectrometer) technique the subgrain structure of a bent aluminum single crystal, 99·98% pure and heated at 620 C. for 18 hr. was revealed in the form of a multimodal intensity distribution curve. Through the proper combination of Geiger-counter and film techniques structural details of the subgrains have been studied. Thus it has been shown that the cyclic peaks obtained by the Geiger-counter technique correspond to the preferential clustering of the subgrains at intervals of 7′. A combination of discrete specimen and film shifts disclosed the angular misalignment of the individual subgrains which, expressed in terms of the halfwidth of their reflection curves, ranged from 1·5 to 2′. Metallographic correlation with the X-ray data has been obtained.

6. P. A. Jacquet. *Recherches expérimentales sur la déformation plastique et la polygonisation de la solution solide polycristalline cuivre–zinc à 35% de zinc.*

L'emploi du polissage électrolytique et d'une méthode d'attaque extrêmement sensible a permis de révéler dans la masse d'une microéprouvette de laiton α polycristalline soumise à une très faible traction, les perturbations structurales qu'accompagnent les lignes de glissement apparaissant sur la surface. Ces perturbations sont localisées par des microfigures de corrosion mesurant 0,07–0,5 micron, plus ou moins espacées sur les glissements.

En faisant subir aux éprouvettes déformées des recuits étagés entre 200 et 600° la répartition des micro-domaines d'attaque évolue jusqu'au stade ultime du recuit à 600° où ils définissent une sous-structure typique de l'état polygonisé, d'ailleurs visible sur les diagrammes de rayons X en retour.

Les attaques sélectives sont par conséquent en relation avec la distribution de certaines dislocations. La méthode proposée permet de suivre cette distribution depuis l'état de très faible déformation jusqu'à l'état polygonisé, ce qui apporte d'intéressantes précisions sur les étapes précédant la polygonisation typique.

7. G. D. Rieck. *Fragmentation in wolfram crystals.*

Laue diagrams were made of W crystals in·recrystallized lamp filament wires, using an X-ray beam collimated through a 50 μ capillary of 20 mm. length, so that sealed-off X-ray tubes could be used although their focal spot is not homogeneous. Differences in orientation of 1–2′ could be observed.

The crystals showed often Laue diagrams with double spots, split in the direction of the wire axis, with angular differences of 0·2–2°. After cold bending over 90° with a radius of 1–3 mm., fragmentation was found, which was more clearly seen after restretching the crystals, for then the deformation asterism diminished. The fragmentation occurred mainly in two directions. One corresponds with the normal breaking up of the lattice in the direction of bending. The other was approximately perpendicular to the latter and gave small lines parallel to the wire axis, arising from particles with orientation differences of 2–8′ and dimensions of 10–25 μ.

Bearing in mind the double spots often occurring in unbent wires and the fact that during drawing contaminations in the wire will have been stretched out in the wire direction, we may assume a predisposition of the crystals to break along planes parallel to the axis.

8. P. Lacombe & A. Robillard. *La croissance des monocristaux d'aluminium.*

Étude par rayons X et microscopie de la répartition des impuretés au cours de la solidification de monocristaux d'aluminium.

Rôle des différentes impuretés et de leur répartition sur les imperfections de structure des cristaux.

9. A. R. Weill. *Mise en évidence de la polygonisation de l'uranium par les rayons X.*

On a cherché une méthode de diffraction de rayons X facile à mettre en oeuvre et permettant de reconnaitre les différents modes de polygonisation correspondants à des traitements thermiques différents. L'essentiel de la méthode consiste à préparer par dissolution électrolytique une pointe très fine et à l'examiner ensuite par la méthode de Debye–Scherrer.

En opérant avec la radiation du molybdène on peut suivre l'évolution de la polygonisation existant dans un barreau filé au cours des traitements successifs par cycles thermiques. On s'attachera particulièrement à observer les variations de fragmentation des astérismes en même temps que celle de l'allure des réflexions fournies par la radiation caractéristique.

La méthode s'applique également à l'étude des textures de laminage ou de recristallisation, mais il est préférable dans ce cas de recourir à la radiation du cuivre. Enfin dans certains cas la technique de préparation de l'échantillon permet d'obtenir soit un monocristal, soit un petit nombre de cristaux faiblement désorientés les uns par rapport aux autres. Dans les quelques exemples examinés il apparait que l'échantillon de volume très réduit est chaque fois bien représentatif et de la matière analysée, et du traitement qu'elle a subi.

10. G. Fournet. *Théorie des modifications ordre–désordre dans les substances contenant n sortes d'atomes.*

Dans la plupart des études théoriques sur les phénomènes coopératifs (modifications ordre–désordre, magnétisme etc.) il est toujours supposé que le nombre d'espèces de particules présentes est égal à deux. Dans la solution apportée par Yvon par exemple on peut s'apercevoir que cette hypothèse est *essentielle* et que toute généralisation simple est impossible.

Dans le cadre du modèle d'Ising nous nous sommes proposés de chercher une solution générale et exacte dans le cas où il existe n espèces de particules; nous avons obtenu ce résultat par une adaptation convenable de la théorie des fluides à n sortes de particules de Yvon. Dans l'équation de *l'ordre à grande distance* nous avons pu grouper les différents termes d'après le nombre de nœuds distincts qu'ils font intervenir et nous avons établi les règles qui permettent de calculer ces termes en tenant compte des énergies qu'échangent entre eux les différentes particules en position de premiers, deuxièmes, etc. voisins.

L'équation de *l'ordre à petite distance* peut s'exprimer sous une forme de structure analogue.

L'ensemble de ces résultats permet en particulier l'étude des ferrites.

11. E. F. Bertaut. *Théorie simplifiée de la transformation ordre–désordre dans les surstructures ioniques.*

12. J. Méring & J. Longuet-Escard. *Effets de la répartition spatiale des défauts dans les empilements désordonnés.*

Généralisation des calculs de Landau. Discussion des effets interférentiels des différentes fonctions de répartition des défauts. Rôle de la nature des défauts.

13. J. Longuet-Escard & J. Méring. *Empilements désordonnés formés au cours de la croissance des cristallites dans les sols d'hydroxydes.*

Application des méthodes quantitatives de diffraction des rayons X à l'étude statistique de la croissance par fusionnement des cristallites dans $Ni(OH)_2$. Détection des défauts créés par les impuretés emprisonnées.

14. A. Durif-Varambon & E. F. Bertaut. *Sur les composés du type* A_5LiO_8 *et* $ALiO_2$.

15. M. Hoch & H. L. Johnston. *Order–disorder transitions in the germanium–oxygen and zirconium–oxygen systems.*

High-temperature X-ray diffraction studies on the solid solutions of oxygen in germanium and zirconium (in which the metal–oxygen ratio is 1:1) showed reversible order–disorder transitions. In the germanium–oxygen system, the germanium lattice disappears at the melting point of pure germanium (965° C.) and a liquid-like structure is visible, although the sample is solid. In the zirconium–oxygen system, we have at 1575° C. a simple cubic structure, which at 1970° C. transforms into a body-centred cubic structure.

16. P. T. Davies & C. Orman. *The superlattice of di-ammonium lead bromide.*

Colourless acicular crystals of $2NH_4Br.PbBr_2$ have been prepared from aqueous solution, and single-crystal rotation and Weissenberg photographs have been obtained. The principal unit cell was found to be orthorhombic with $a = 13{\cdot}2$, $b = 8{\cdot}84$, $c = 4{\cdot}84$ Å and space group *Pba* or *Pbam*. Rotation photographs about the three principal axes show superlattice layer lines corresponding to planes in the reciprocal lattice at $h = \frac{1}{4}, \frac{1}{2}, \frac{3}{4}$, at $k = \frac{3}{12}, \frac{6}{12}, \frac{9}{12}$ with less intense ones at $\frac{2}{12}, \frac{4}{12}, \frac{8}{12}$ and $\frac{10}{12}$, and at $l = \frac{4}{11}$ and $\frac{7}{11}$. This suggests a superlattice unit cell with $a_1 = 4a = 52{\cdot}8$ Å, $b_1 = 12b = 106{\cdot}0$ Å, $c_1 = 11c = 53{\cdot}2$ Å. Weissenberg photographs confirm the existence of the superlattice, but show the lattice to be more complicated than at first supposed because weaker reflexions also occur in reciprocal-lattice planes at $k = \frac{1}{12}, \frac{5}{12}, \frac{7}{12}, \frac{11}{12}$ and at $l = \frac{3}{11}, \frac{5}{11}, \frac{6}{11}, \frac{8}{11}$ although their intensity is not sufficient for them to be recorded on the rotation photographs.

17. P. Andersen. *The structure of mixed crystals in the system* $MnCl_2+LiCl$.

The $MnCl_2+LiCl$ system has been examined by differential thermal analysis and by X-ray exposures using a high-temperature X-ray powder camera. The results of these examinations indicate a very small mutual miscibility of the two components at room temperature. Yet a very narrow homogeneous range of miscibility has been found in the neighbourhood of the mole fraction for $LiCl = \frac{2}{3}$ (Li_2MnCl_4). This phase has a $MnCl_2$-like structure with $c/a = 4{\cdot}90$, corresponding to ideal cubic close packing. At temperatures above 440° C. two homogeneous regions of miscibility have been found. In the $MnCl_2$-rich region the axial ratio increases towards 4·90 with increasing LiCl content, while the LiCl-rich region has been found to be pure cubic. On increasing the temperature, the transition between the two phases is accompanied by a slight absorption of heat, and the change in volume has been found to be continuous within the limits of error. The powder photographs of the $MnCl_2$-rich region show some strong lines, which, taken alone, may be indexed cubically and in respect only to the intensities deviate from the photographs of pure LiCl. Further, some weak lines are observed which lower the symmetry from cubic to trigonal. The intensity of these 'superlattice' lines gradually decreases with increasing temperature and the lines disappear at the transition temperatures.

These facts indicate that the transitions mentioned are of the second order, and they are discussed in relation to order–disorder phenomena.

18. B. Hagene & R. Freymann. *Absorption hertzienne et défauts de réseau.*

I. *La spectroscopie hertzienne est un procédé de choix pour l'étude des défauts de réseau.*—La diffraction des rayons X, la spectroscopie infra-rouge et Raman (spectres de vibrations)—ainsi que la résonance paramagnétique électronique et nucléaire—sont des moyens d'étude des solides supposés parfaits; dans ces diverses méthodes, les défauts de réseau n'apparaissent que comme un effet du second ordre.

Au contraire, les propriétés diélectriques d'un solide constituent un effet du premier ordre permettant d'étudier les imperfections de réseau. La spectroscopie hertzienne complète les données de la spectroscopie de fluorescence en fournissant (indirectement) les niveaux d'énergie du solide étudié.

II. *Faits expérimentaux.*—La spectroscopie hertzienne met en évidence des bandes d'absorption (bandes de Debye) des solides: pour une température donnée, la variation de l'absorption diélectrique ε'' en fonction de la fréquence présente en général un ou plusieurs maxima. Ces maxima se déplacent vers les basses fréquences quand la température diminue.

Divers types de solides (*à l'état de poudre*) ont été étudiés jusqu'à présent et plus particulièrement à Rennes: composés monoatomiques: bore et sélénium (Meinnel); cristaux ioniques: NaCl (Breckenridge & Meinnel); semiconducteurs: ZnO (Freymann, Freymann, Rohmer & Tiennot); oxydes d'uranium (Rolland & Langevin); Cu_2O (Daniel); CdO (Hagene); oxydes de fer (Hagene); ferrites de Ni, Co, Zn, ... (Kamiyoshi).

La glace, de nombreux composés organiques, présentent également une absorption dans le spectre hertzien.

III. *La représentation* $\log \nu_c$–$1/T$.—La théorie qui rend compte du phénomène Debye par les défauts de réseau donne, pour la fréquence ν_c à laquelle se trouve un maximum de l'absorption (à la température T) la formule: $\nu_c = Ae^{-U/kT}$, où A est une constante caractérisant le solide et U *l'énergie d'activation de diffusion du défaut de réseau.*

Par conséquent, une réprésentation $\log \nu_c$–$1/T$ devra donner *des droites dont la pente est proportionnelle à l'énergie d'activation* U.

IV. *Détermination des niveaux d'énergie des solides* (*exemple*: ZnO).—L'absorption en ultra-violet donne, entre les bandes de valence et de conduction, une différence d'énergie de 3,2 eV.; la fluorescence met en évidence, entre ces bandes de valence et de conduction, la présence d'un intervalle de 2,5 eV. D'autre part, la vibration infra-rouge du réseau de ZnO (Parodi) fixe un niveau d'énergie séparé de celui de la bande de conduction par 0,05 eV.

La spectroscopie hertzienne donne des énergies d'activation de 0,18–0,23–0,29–0,34 ou 0,40 eV., qui mettent en évidence d'autres niveaux que ceux donnés par les méthodes antérieures.

Un autre exemple est celui des oxydes de fer: nous avons trouvé des énergies d'activation de 0,1 eV. pour Fe_3O_4, 0,4 eV. pour Fe_2O_3 α et 0,07 eV. pour Fe_2O_3 γ.

19. P. B. Hirsch. *A structural model of coal.*

The X-ray scattering has been studied for a series of vitrains of varying rank. From the scattering at high angles the diameters of the aromatic lamellae and the percentages of carbon in the ordered form are determined. Up to 89 % C there is little growth of the layers with rank; the diameter of the aromatic lamellae is ~ 8 Å. Anthracitization is accompanied by a rapid increase in layer diameter. The nature of the packing of the coal molecules is determined from the scattering at moderately low angles. The aromatic lamellae occur in groups of two or more stacked parallel to each other; the ordering of the layers increases with rank. At 89 % C the groups of layers form a liquid structure, the average distance between the groups being ~ 20 Å. The layers are preferentially orientated parallel to the bedding plane and the degree of preferred orientation increases with rank. The scattering at very low angles, which has been measured up to spacings of ~ 5000 Å, suggests a very wide distribution of pore sizes. The total low-angle scattering indicates the existence of disc-like cracks preferentially orientated parallel to the bedding plane. The structural changes occurring during coalification are discussed.

20. R. Renninger. *Zu den Reflexionseigenschaften (Umweganregung, Intensitäten, (222)-Reflex) der beiden Diamant-Typen für Röntgenstrahlen.*

Es wird mittels registierender (Zählrohr-)Intensitätsmessungen an einer Anzahl von Vertretern der beiden Diamant-Typen (Oktaeder von etwa 0,5 mm. Kantenlänge aus der Sammlung des University College, Prof. Lonsdale, London) festgestellt, dass die Unterschiede beider Typen, soweit sie *röntgenographischer Natur* sind, sich völlig durch das bekannte verschiedene Ausmass ihrer Mosaikstruktur deuten lassen, d.h. dass der röntgenographische Befund keinerlei Hinweis auf einen eigentlichen Strukturunterschied, eine Verschiedenheit der Elektronendichte-Verteilung gibt. Die Absolut-Intensität der (222)-Interferenz ist bei beiden Typen ungefähr gleich, während diejenige der übrigen Interferenzen bei der Type II um ein Mehrfaches höher ist als bei der Type I. Entsprechend tritt Umweganregung ('indirect reflexion') an (222) bei Type II mit einer um den Faktor 10–15 stärkeren Intensität auf als bei Type I. Die stärksten Umweganregungs-Maxima (Cu $K\alpha$, Umweg über (331)–(11$\bar{1}$)) erhöhen die direkte (222)-Intensität bei Type I etwa auf das Doppelte, bei Type II auf das 10–15-fache. Intensitätsvergleich (integrales Reflexionsvermögen, Bademethode) der verschiedenen Interferenzen zeigt bei Type II, dass diese sehr nahe dem Extrem des 'Idealen Mosaikkristalls' ('ideally imperfect' crystal) liegt. Dies erlaubt eine Errechnung des (222) F-Wertes, der sich, in guter Übereinstimmung mit dem früheren Ergebnis des Verfassers (*Z. Kristallogr.* (1937), **97**, 107) zu etwa 1,2 Elektronen/Zelle ergibt.

21. R. E. Franklin & M. Méring. *La structure de l'acide graphitique et de ses dérivés.*

Nous avons étudié aux rayons X les différents composés interlamellaires de graphite et oxygène, et spécialement l'acide graphitique. Nous discutons de la nature de la liaison entre les couches de carbone et celles d'oxygène.

22. J. Kakinoki & Y. Komura. *Intensity of X-ray diffraction by a one-dimensionally disordered crystal: rhombohedral case.*

On calculating the intensity of diffuse X-rays due to the stacking faults, as in SiC, we needed to solve such difference equation as

$$x_n + x_{n-1}p_c + x_{n-2}p(p_c - p_h) = hp_c,$$

in which the elements in x_n concern the probablities of finding the same kind of layer at the $(j+n)$th position as that at the jth, $h = x_0$, $p = p_c + p_h$, and p_c and p_h are the probabilities of continuing in cubic and hexagonal manners respectively.

In this case the intensity distributions are the same for the two cases $k-h = 3m \pm 1$. But when the fundamental regular structure is the rhombohedral type, they must be different. In the regular cubic order, for example, when the three sets of $A\,B\,C$, $B\,C\,A$ and $C\,A\,B$ exist, the remaining three sets of $A\,C\,B$, $C\,B\,A$ and $B\,A\,C$ do not exist. Corresponding to this fact, if we divide the six sets of layers belonging to the same cubic–hexagonal order into two groups, then the above matrices are also divided into two. After all, we get such two simultaneous difference equations as

$$x_n + x_{n-1}p_c + (x_{n-2}p_c + x'_{n-2}p'_h)p_c - (x'_{n-2}p'_c + x_{n-2}p_h)p'_h = hp_c,$$
$$x'_n + x'_{n-1}p'_c + (x'_{n-2}p'_c + x_{n-2}p_h)p'_c - (x_{n-2}p_c + x'_{n-2}p'_h)p_h = h'p'_c,$$

and spur $\bar{V}FP^n$ in the intensity equation becomes

$$\mathrm{sp}\,\bar{V}FP^n$$
$$= \tfrac{1}{2}V_0V_0^*[\tfrac{3}{2}\mathrm{sp}(x_n + x'_n) - 1 \pm \tfrac{1}{2}\sqrt{3}i\{\mathrm{sp}(x_n - x'_n) - \mathrm{sp}(h - h') + 4\mathrm{sp}(x_{n-1}p_c - x'_{n-1}p'_c) - 2\mathrm{sp}(x_{n-1} - x'_{n-1})\}]$$

for $k-h = 3m\pm1$ respectively. These results contain the former as a special case by omitting the primes.

23. J. Kakinoki & Y. Komura. *Intensity of X-ray diffraction by a one-dimensionally disordered crystal: some examples in* SiC.

For simplicity, we describe only the case of the hexagonal–cubic (*hc*) structure. Putting

$$p = \begin{matrix} \\ c \\ h \end{matrix}\!\!\begin{matrix} \begin{matrix} c & h \end{matrix} \\ \begin{pmatrix} \beta & 1-\beta \\ \alpha & 1-\alpha \end{pmatrix} \end{matrix} \quad p_c = \begin{pmatrix} \beta & 0 \\ \alpha & 0 \end{pmatrix} \quad p_h = \begin{pmatrix} 0 & 1-\beta \\ 0 & 1-\alpha \end{pmatrix},$$

the characteristic equation to be solved and the simultaneous equations for determining the coefficients c_ν accompanying x_ν become

$$\det|x^2 1 + xp_c + p(p_c - p_h)|$$
$$= x^4 + \beta x^3 - (1-\alpha+\beta)(1-\alpha-\beta)x^2 + (1-\alpha)(\alpha-\beta)x + (\alpha-\beta)^2 = 0,$$

$$\Sigma c_\nu = 1, \quad \Sigma x_\nu c_\nu = \frac{-1}{2}, \quad \Sigma x_\nu^2 c_\nu = \frac{2-\alpha-2\beta}{2(1+\alpha-\beta)},$$

$$\Sigma x_\nu^3 c_\nu = \frac{-(1+\alpha-\beta-3\alpha\beta)}{2(1+\alpha-\beta)}.$$

For the fundamental regular structure of *hc*-structure where $\beta = 0$ and $\alpha = 1$, x_ν's and c_ν's can be solved to be

$$x_1 = 1, \; x_2 = -1, \; x_3 = i, \; x_4 = -i,$$
$$c_1 = \tfrac{1}{16}, \; c_2 = \tfrac{9}{16}, \; c_3 = c_4 = \tfrac{3}{16}.$$

For the diffuse line we may put

$$\alpha = 1-\Delta\alpha, \; \beta = \Delta\beta, \; \omega = \tfrac{1}{2}(\Delta\beta - \Delta\alpha), \; \delta = \tfrac{1}{2}(\Delta\alpha + \Delta\beta),$$
$$x_1 = 1-\varepsilon_1, \; x_2 = -(1-\varepsilon_2), \; x_3 = i+\varepsilon_3, \; x_4 = -i+\varepsilon_4,$$
$$c_1 = \tfrac{1}{16}(1+\Delta_1), \; c_2 = \tfrac{9}{16}(1+\Delta_2), \; c_3 = \tfrac{3}{16}(1+\varepsilon_3), \; c_4 = \tfrac{3}{16}(1+\varepsilon_4),$$

where $\omega, \delta, \varepsilon$ and Δ are small quantities. Substituting these values into the above equations, and omitting the higher order of $\omega, \delta, \varepsilon$ and Δ, we get

$$x_1 = 1-\tfrac{3}{2}\delta, \; x_2 = -(1-\tfrac{1}{2}\delta), \; x_3 = x_4^* = -\tfrac{1}{2}\omega + (1-\delta)i,$$
$$c_1 = \tfrac{1}{16}(1-\tfrac{3}{2}\omega), \; c_2 = \tfrac{9}{16}(1-\tfrac{1}{2}\omega), \; c_3 = c_4^* = \tfrac{3}{16}(1+\omega+i\tfrac{1}{2}\delta).$$

From these values the diffuse term can be calculated as

$$D(\varphi) = \frac{3}{64}\delta \frac{8+4\delta+6\omega-(4-8\omega)\cos\varphi-(\delta+16\omega)\cos^2\varphi}{\sin^2\varphi\,(\cos\varphi+\frac{1}{2}\omega)^2}$$

except $\varphi = 0$, π and $\pm(\frac{1}{2}\pi+\frac{1}{2}\omega)$, where they are

$$D(0) = \frac{4-3\delta-6\omega}{48\delta}, \quad D(\pi) = \frac{9(4-\delta-2\omega)}{16\delta},$$
$$D(\pm(\tfrac{1}{2}\pi+\tfrac{1}{2}\omega)) = \frac{3(2-\delta+2\omega)}{16\delta}.$$

Concerning the calculations for the cases of *hcc*- and *hchcc*-structures we say only that it is very laborious to calculate without making the assumption that the continuing probabilities of $h \to h$ and $cc \to c$ are zero.

24. K. Dornberger-Schiff. *Structure determination of disordered crystals.*

If the electron density of a diffracting body is composed of identical units arranged in parallel, i.e. $\varrho(r) = \sum_j \varrho_0(r-v_j)$, the amplitude of the diffracted beam (measured in terms of the amplitude of a beam diffracted by an electron) is equal to the product of the Fourier transform $F(r^+)$ of the distribution $\varrho(r)$ (the structure factor), and the 'lattice' factor $G(r^+)$, which is the Fourier transform of the point function $\sum_j \delta(r-v_j)$, where

$$\delta(r) \begin{matrix} = 0 \text{ for } r \neq 0 \\ \neq 0 \text{ for } r = 0 \end{matrix}$$

and

$$\int \delta(r)dv = 1.$$

If the end points of the vectors v_j lie on a lattice (as in the case of one-dimensional disorder discussed by Wilson, Jagodzinski, Méring and others), $G(r^+)$ is periodic with periods of the lattice reciprocal to it. This periodicity of $G(r^+)$ can be used to split the experimentally determined intensity $I(r^+)$ into factors $I(r^+) = |F(r^+)|^2 . |G(r^+)|^2$.

The knowledge of $|F(r^+)|^2$ between the reciprocal-lattice points can be used to resolve in part the ambiguity inherent in the Patterson function of the crystal.

The transform $T(r)$ of $|G(r^+)|^2$ is the *Faltung* of $\sum_j \delta(r-v_j)$ with itself:

$$T(r) = \int \sum_i \sum_j \delta(r+r'-v_j) . \delta(r'-v_i)dr'.$$

Thus it can be interpreted similarly to a Patterson and gives all the directly obtainable information on the character of the disorder present.

25. K. Kimoto & H. Morimoto. *Stacking faults in very small crystals of gold.*

Germer & White (*Phys. Rev.* (1941), **60**, 447) reported that the electron-diffraction patterns from evaporated thin films of face-centred cubic metals show anomalous intensities. The intensity of the (200) ring is especially weak compared with the normal intensity. They based their explanation on the size of the crystals. Kimoto (*J. Phys. Soc. Japan*, (1953), **8**, 762) studied the same phenomenon with silver and said it was due to stacking faults in the crystals. He measured the intensities and then compared them with theoretically calculated intensities for assumed structures of crystals.

In the present work we studied the same phenomenon with gold. In interpreting the pattern, however, we made no assumption concerning the structure of crystals, performing a Fourier analysis of the measured intensities. We followed Kimoto's experimental procedure. A camera provided with a rotating sector was used to photograph electron-diffraction patterns. Then microphotometer records of the diffraction patterns were converted into the intensity distribution curves. We analysed these curves by a Fourier method with the aid of punched cards. The radial distribution function thus obtained revealed the existence of the interatomic distances corresponding to stacking faults.

26. R. S. Pease. *X-ray examination of irradiation effects in boron compounds.*

The effects of displaced atoms produced in BN, B_4C, SrB_6, TiB_2 and ZrB_2 by the $B_{10}(n\alpha)$ reaction, have been studied by X-ray powder photographs up to doses at which, on the average, each atom has been displaced from a lattice site about once. Changes in unit-cell dimensions of the order of 1 %, and, in some cases, pronounced line broadening are produced; the main feature all results have in common is that the effects are rapid at low doses, and either cease at, or occur only very much more slowly beyond, a dose of the order of 2×10^{18} thermal neutrons/cm.^{2}. This phenomenon is attributed to a saturation of the concentration of interstitial atoms, so that the principal features of the crystal structure are preserved even at the highest doses obtained. The saturation arises essentially because interstitial atoms return to surrounding lattice sites when these become vacant. A detailed model has been worked out for the case of BN, which accounts for the orders of magnitude of the effects observed.

27. G. J. Dickins. *Ordering in the σ phases.*

28. U. Korhonen. *On the determination of the atomic scattering factors on the basis of the measured structure factors by using Fourier series.*

The writer has developed a method for the determination of the atomic scattering factors of an ion in a crystal lattice when the structure factors are known. Assuming, for the sake of simplicity, that the ion of which the atomic scattering factors $f_{(hkl)}$ are required is situated at the origin, we can write

$$f_{(hkl)} = \frac{4\pi R^3}{3V} F_{(hkl)} + \sum_{h'k'l'} \frac{F_{(h'k'l')}}{V} \frac{Rd^2}{\pi} \left(\frac{\sin 2\pi R/d}{2\pi R/d} - \cos 2\pi R/d \right). \quad (1)$$

Here, $F_{(h'k'l')}$ is the structure factor for the reflexion $h'k'l'$, R is the ionic radius of the ion considered, V is the volume of the unit cell, and $d = d_{(h-h',k-k',l-l')}$ is the distance of repetition of the lattice planes $(h-h', k-k', l-l')$.

In order to show the practical importance of series (1), the writer proceeded in the following way. He calculated the structure factors $F_{(h'k'l')}$ of NaCl by using the atomic scattering factors of Na^+ and Cl^- obtained from Hartree's self-consistent field and by using the mean-square displacements for the same ions measured by Wasastjerna. The values of $F_{(h'k'l')}$ were calculated up to 777. The writer then calculated back the atomic scattering factors $f_{Cl^-,(hkl)}$ of Cl^- for the $h00$ reflexions up to 800 by means of these values for $F_{(h'k'l')}$ and by using the value 1·84 Å for R. The original values were thus obtained within the limits of the calculating accuracy.

To show that series (1) gives a result which, between certain limits, is independent of the value for R, the writer calculated the values of $f_{Cl^-,(hkl)}$ using the value 1·64 Å for R, a value smaller by 12·5 %; in other words, the volume of the ionic sphere was diminished by a third. The atomic scattering factors of Cl^- obtained in this way were practically the same as those obtained by using the value 1·84 Å for R.

The writer finally calculated the atomic scattering factors of Cl^- for $h00$ reflexions up to 500 by using the values of $F_{(h'k'l')}$ measured experimentally by Wasastjerna for the NaCl crystal and by using the values 1·84 Å and 1·61 Å for R. The values obtained practically coincided this time, too.

29. T. Ll. Richards & D. E. Yeomans. *Principle of the unextended cone in the plastic deformation of metal crystals.*

The unextended cone of plastic deformation can be defined for any small increment of finite strain on the basis that, with no change in volume, an extension increment e is accompanied by a lateral contraction of $\frac{1}{2}e$. Consequently directions at angles of $\cot^{-1}\sqrt{\frac{1}{2}}$ with the axis of extension, which are unchanged in length, generate the surface of the unextended cone. Plastic deformation of homogeneous solids takes place by shear, in directions and on planes which are directly related to the unextended cone. Most metals having a face-centred or body-centred cubic structure, however, are elastically and plastically anisotropic with a minimum Young's modulus in a ⟨100⟩ direction, so that a stress applied to a single crystal in any direction extends the crystal preferentially along the nearest ⟨100⟩ direction. It can be demonstrated that all the shear elements of the various modes of crystallographic shear in cubic metals are such that the shear direction and/or normal to the shear plane lies in or near the surface of the unextended cone of strain along the nearest ⟨100⟩ direction.

30. R. E. Smallman. *The effect of cold work on integrated intensities in the spectra of metals.*

Geiger-counter measurements have been made of the changes produced by cold work on the integrated intensities in the Debye–Scherrer spectra of several metal powders. It is shown that the effect of cold work on extinction entirely masks the intrinsic effect of cold work on the integrated intensities of the lines. With molybdenum powder the combination of surface roughness and large absorption coefficient produce abnormally low intensity values for the low-angle lines similar to extinction.

Several alternative corrections have been applied to the intensity results, since there is very little agreement on the nature of extinction or the correction. The differences principally concern the variation of extinction losses with diffraction angle. A new method has been adopted to assign an unambiguous extinction coefficient to the results, thereby eliminating some of the alternative corrections. It is shown that the effect of cold work is to decrease the corrected line intensities of aluminium, α-brass, iron and molybdenum by about 5 %, which is independant of the type of extinction assumed. On the other hand, the lines develop 'tails' which are so long that they overlap sufficiently to cause a detectable rise in the background level; the total reflected intensity therefore remains approximately constant.

Brief reference is made to the analysis of line widths and line shapes and it is shown that the results support the dislocation theory of plastic deformation. Approximate values for the density of dislocations are given.

31. A. Merlini. *Effect of zinc content on rolling and annealing texture of α brass.*

Earlier investigations by the photographic method suggested that the change-over of the annealing texture from the copper-type to the brass-type takes place at lower zinc contents than the corresponding change in the deformation texture. This result would be difficult to reconcile with the 'oriented growth' theory of annealing textures.

The quantitative pole figures determined in the present work show that the changes with zinc content of both deformation and annealing texture are gradual, extending over a wide concentration range, and that the changes in the annealing texture correspond to changes in the deformation texture.

32. H. Wilman & R. P. Agarwala. *Surface deformation caused on iron crystals by very light unidirectional abrasion.*

The deformation caused by a single 10 in. stroke on 0000 emery paper at 50 g.cm.$^{-2}$ pressure, on electropolished roughly (107) and (110) surfaces of iron single crystals, has been investigated by electron diffraction. The nearly (107) face was abraded along directions near [$\bar{1}$10], [$\bar{2}$10] and [100], and the observed large rotations of the fragments were found to be about [110], [120] and [010] axes respectively, with little spread from the mean. The (110) face, when abraded along [$\bar{1}1\bar{2}$] and [$\bar{1}$11], showed large rotations about well-defined axes which were parallel to [1$\bar{1}\bar{1}$] and an axis near [$\bar{3}3\bar{4}$] respectively. Of these results, similar to those we have found previously, most could possibly correspond to lamellar rotational slip.

An apparently abnormal case was observed in abrading the (107) face along [$\bar{1}$00], which gave unusually obscure disorientation until after etching down to a level where the disorientation was reduced to only a few degrees rotation; the diffraction patterns indicated that parts of the lattice had rotated about an axis estimated to be near [451], while other parts had rotated about the axis [4$\bar{5}$1] symmetrically disposed across (010) which was parallel to the abrasion direction and normal to the surface. This [451] rotation may be due to flexural translational slip on ($\bar{2}$13) along the usual slip direction, [1$\bar{1}$1].

The presence of γ-iron was also shown both in the surface layers, and also below the rotationally disturbed layer of α-iron, in a strong orientation.

33. T. Mukai. *Oxide-film effect on the plastic deformation of aluminium single crystal.*

By employing Prof. T. Fujiwara's method I prepared two kinds of aluminium single-crystal plates. With these plates the stress–strain curves were obtained and the broken fracture of the oxide film and plastic deformation of the body crystal were observed by electron-microscopical and X-ray examinations. By comparing these results it was found that the oxide film on the surface makes the surface layers of the body single crystal so hard that it influences the tensile strength of the specimen, and that the broken fracture of the oxide film has a definite relation to (*a*) the inclination of the slip plane to the crystal surface, (*b*) the slip direction and (*c*) the thickness of the film.

34. T. Fujiwara, I. Ogura, Y. Takano & T. Yamashita. *On the elongation and fracture of an aluminium single-crystal plate.*

By Fujiwara's method, many single-crystal plates of aluminium, 99·99 % in purity, were produced in definite crystallographic orientations.

When these specimens were stretched lengthwise, their stress-strain curves were obtained by measuring the tensile strength, and the deformation behaviour in the interior and exterior of the specimens at each stage of the stretching were studied by taking X-ray radiographs and by observing the slip lines and bands with a microscope and an electron microscope.

By comparing these results it was found that according to the crystallographic orientation of the plate the manner of the work hardening of the single-crystal plate was quite different. It can be concluded that the manner of the hardening depends upon the number of active slip planes and the existence of multiple slip.

35. G. A. Homes. *L'investigation de l'état structural des cristaux métalliques par les ultrasons.*

La mesure du coefficient d'amortissement des ultrasons permet de déceler certains troubles dans les cristaux métalliques liés à des modifications d'état structural.

§ 9. Liquides; cristaux liquides; phases amorphes

1. P. Chatelain. *Sur les propriétés optiques des liquides nématiques et la structure du 'monocristal liquide'.*

Le monocristal liquide est un milieu fluide, homogène à l'échelle macroscopique, présentant une seule direction d'isotropie; la connaissance de sa structure nécessite: (1°) celle du nombre des molécules dont les axes font avec l'axe d'isotropie un angle θ donné (fonction de répartition); (2°) celle du mode de groupement des molécules ayant sensiblement même orientation.

L'extension des théories optiques classiques à un tel milieu permet de relier les valeurs des indices principaux à la fonction de répartition, et de calculer la valeur moyenne de $\sin^2\theta$ pour diverses valeurs de la température; de plus, l'accord entre les résultats théoriques et expérimentaux est meilleur en admettant que les molécules voisines sont sensiblement parallèles; rien cependant ne permet de déterminer la distance minima séparant deux molécules non parallèles.

Au contraire, la grande intensité de la lumière diffusée et la dissymétrie des diagrammes de diffusion, imposent le groupement des molécules en paquets ou 'essaims' de 0,2 μ de diamètre, dans lesquels les axes des molécules sont sensiblement parallèles à l'axe du paquet.

La valeur élevée du coefficient de dépolarisation (de l'ordre de 8 pour les faibles angles de diffusion), s'interprète par une diffusion due aux fluctuations thermiques d'orientation de l'axe des paquets, l'agitation thermique écartant au maximum de 40° cet axe de l'axe d'isotropie.

2. P. B. HIRSCH. *The application of Fourier-transform methods to the study of 'amorphous' materials.*

It is shown that Fourier transform projections can be used to determine the dimensions and the distances between structural units occurring in 'amorphous' substances which show preferred orientation. The method is applied to study the packing of aromatic lamellae in coals. From the transforms the spacings between the layers and the distribution of layers as a function of the numbers of parallel layers per group can also be determined.

3. S. N. BAGCHI. *Limitations of Debye's interference theory of liquids.*

It is proved that Debye's theory is valid under the following three assumptions which are seldom realized in nature: (1) Lattice distortions of the first kind (thermal displacements, effects of mixed paracrystallites, etc.) and the existence of polydisperse clusters are neglected. (2) The zone of interaction of a particle is small compared to the volume of each of the paracrystalline lattices. That means, the (000) reflexion lies outside the domain of observation. (3) The *a priori* distance statistics is the same for any and every particle and is taken to be spherically symmetric.

Generally valid relations between the intensity distribution and the *a priori* distance statistics in general are deduced. These equations under the three above assumptions degenerate to the well-known equation of Debye & Menke. The effect of these approximations is the smearing out of the *a priori* distance statistics—the *W*-function. The calculated *W*-function is, therefore, more damped than the actual function and its value at any point, as well as the integral value of a hump of the *W*-function, is smaller than the actual value. In other words, these approximations give rise to an apparently greater statistical fluctuation (distortions of the second kind) than actually is the case.

It is also shown that Debye's theory is inherently incapable of explaining the low-angle scattering characterized by monotonicly increasing intensity with decreasing scattering angle, since the intensity function discussed by Debye is zero for the scattering angle zero.

4. R. HOSEMANN. *Klärung des Trialismus kristallin–flüssig–amorph.*

Die Strukturerforschung mittels Röntgen- und Elektroneninterferenzen hat gezeigt, dass es viele Stoffe gibt, die der Kristallgittertheorie von v. Laue–Ewald–Bragg genügen, während gewisse Flüssigkeiten in erster Näherung nach einer von Debye–Menke–Zernicke–Prins entworfenen Gittertheorie diskutiert werden können. Die Interferenzen an Gasen, Dämpfen und die Kleinwinkelinterferenzen gewisser 'Festkörper vom Gastyp' verlangen eine weitere Interferenztheorie, mit deren Ausarbeitung Guinier, Hosemann, Shull, Roess u.a. beschäftigt waren.

Viele Realstoffe, vor allem Flüssigkeiten und hochmolekulare Stoffe, lassen sich aber nicht befriedigend in einen dieser drei Prototypen einreihen. Die Gittertheorie des idealen Parakristalls und der polydispersen Haufwerke gibt eine Lösung des Problems. Man unterscheidet demnach neben Gitterstörungen 1. Art, zu denen die thermischen und chemischen Gitterstörungen gehören, die Gitterstörungen 2. Art, hervorgerufen durch verschiedene Form und Grösse der einzelnen Gitterzellen sowie die Statistik der Grössenverteilung der einzelnen Gitterbereiche und ihre wechselseitige Anordnung, die durch ein mehr oder weniger gestörtes Übergitter in Rechnung gestellt werden kann. Schon ein einzelner derartiger Gitterbereich erzeugt im allgemeinen Fall neben kristallinen, flüssigkeitsartigen und amorphen Interferenzen auch Reflexe, die in gewissen Richtungen des Fourierraumes partiell 'röntgenkristallin', in anderen partiell 'röntgenflüssig' und in wieder anderen partiell 'röntgenamorph' sein können. An Hand von lichtoptisch hergestellten Beugungsbildern zweidimensionaler Modelle wird die Vielzahl derartiger Strukturtypen dargestellt und erläutert, wie man die Röntgendiagramme auswerten kann, wobei die oben erwähnten Prototypen nur mehr die Rolle von entarteten Sonderfällen spielen.

5. G. DALLINGA. *X-ray analysis of some complexes in solution.*

Solutions of iodine in benzene and mesitylene, in which part of the iodine is present in the form of a complex with the solvent molecules, were examined with the aid of X-ray methods. The diagrams obtained with Cu $K\alpha$ and Mo $K\alpha$ radiation were subjected to Fourier analysis. The maxima in the Fourier curve correspond to the interatomic distances occurring in the system.

It could be demonstrated that the structure of the iodine–benzene complex is less compact than is often assumed, the shortest carbon–iodine distance being 3·93 Å, i.e. about 0·1 Å less than the sum of the van der Waals radii. Moreover, we think that the iodine molecule has not a fixed orientation with respect to the benzene nucleus. The shortest C–I distance in the iodine–mesitylene complex is 3·84 Å, which is a little shorter than that of iodine–benzene. It has further been found that the I–I distance is shorter in this complex.

We also started an investigation of the pyridine–iodine complex in solutions. It is probable that the distance of 2·90 Å found is an I–I distance, which would reveal a considerable distortion of the iodine molecule. The distance found might be explained by the occurrence of a I_3^- ion in the solution.

6. J. S. DAVE. *Mixed liquid crystals.*

§ 10. Verres

1. A. SMEKAL. *Vitreous states generated by lattice plasticity.*

In contrast to normal crystal plasticity, lattice plasticity demands work of the order of the melting heat. Therefore, vitreous states have been generated by suitable mechanical treatment of substances fulfilling appropriate bonding conditions.

2. K. FAJANS. *Structural viewpoints concerning a general theory of glasses.*

According to Tammann (1903), all liquids can be expected to solidify as glasses under appropriate conditions of supercooling. Among numerous other substances,

water, ethanol and some saturated hydrocarbons are now known to form glasses. Therefore, the theory of the vitreous state should be concerned with the great differences in conditions under which various liquids solidify as glasses.

The outstanding measurable property involved is the viscosity of the supercooled liquid near its freezing point. The main structural factor appears to be the symmetry of the force field around the constituent units (atoms, ions or molecules) whose mutual displacements are involved in crystallization. For instance, the extraordinary fluidity of He II, i.e. the negligibly small activation energy of the motion of helium atoms within this liquid, implies the nearly perfect spherical symmetry of these only very slightly deformable atoms. On the other hand, if the energy of interaction between the constituent units differs markedly, depending upon which parts of these units are adjacent, the activation energy of their displacement becomes significant. As a result, the viscosity increases and the attainment of the spatial order of the thermodynamically more stable crystal is impeded.

Examples, including organic hydroxyl compounds in which the proton bridges influence the viscosity, and inorganic oxides whose crystals consist of molecules $(M^{3+})_4(O^{2-})_6$, will be discussed.

3. H. RICHTER. *Struktur des glasigen* B_2O_3.

Aufnahmen mit monochromatischer Cu- and Mo-Strahlung an sehr dünnen plattenförmigen Präparaten von glasigem B_2O_3 zeigen ein Streubild, wie man es bei festen amorphen Stoffen ganz allgemein beobachtet. Bei Berücksichtigung der äusseren Interferenzen (grosse $\sin\theta/\lambda$-Werte) liefert die zugehörige Kurve der radialen Dichteverteilung eine ganze Reihe ausgeprägter Maxima, d.h. im glasigen B_2O_3 liegt offenbar eine hohe Ordnung der Atome vor. Eingehende Untersuchungen haben weiter gezeigt, dass der Grundbaustein des B_2O_3-Glases durch ein flaches Tetraeder (Abstände: B–O = 1,38 Å; O–O = 2,39 Å und Höhe H = 0,4 Å) dargestellt wird. Diese BO_3-Tetraeder sind zu Schichten von mehr oder weniger regelmässiger Bauweise miteinander verbunden und im kürzesten Schichtabstand (= 1,85 Å) zu sehr dünnen Schichtpaketen aneinander gelagert.

§ 11. Transformations thermiques

1. H. SAALFELD & H. JAGODZINSKI. *Solubility and precipitation of* Al_2O_3 *in* Mg-Al-*spinels.*

The Al-Mg-spinel can dissolve an excess of alumina (ratio $MgO:Al_2O_3$ ranging from 1:1 to 1:7) which is precipitated in crystallographic directions by heat treatment. Analogous phenomena are well known in metal-phases. The optical and X-ray behaviour of these spinels has been studied. The following stages of the precipitation process by heat treatment may be distinguished:

(1) 600–800° C.—Heating for some hours produces unsymmetrical diffuse scattering around distinct X-ray reflexions. This may be the result of incipient precipitation.

(2) 800–1150° C.—Heat treatment for 1 hr. is sufficient to distinguish optically a new phase (transition phase). It is an anisotropic lamellae system parallel to the spinel planes {113}. An enormous number of reflexions rendered the X-ray investigation very difficult. By a new method, yielding the identical points of the 12 different orientations by symmetry operations of the spinel lattice, it was possible to find a twinned triclinic cell of which two axes are nearly parallel to two [113] directions and one axis is nearly parallel to [112]. The lattice constants are five times those of the corresponding spinel spacings. As the associated streaks prove, there exist intimate relations between the strained spinel lattice and the new phase. Measurements of the lattice constants during the precipitation mechanism give rise to the assumption of a nearly pure Al_2O_3-modification.

(3) 1150–1500° C.—The transition-phase disappears and the precipitation to α–Al_2O_3 takes place. The spinel lattice is no longer strained. Measurements by Eppler show that the important hardness increase coincides with the appearence of the lamellae system. The behaviour of hardness in the nucleation state is now being investigated. The mechanism of precipitation is accompanied by thermoluminescence, the spectral distribution of which was measured. Examinations of the (OH)-content by infrared absorption established the existence of two (OH) frequencies at 2·8 μ and 3 μ. The (OH) content varies as a function of heat-treatment. These investigations, too, are not yet completed.

2. S. CAILLÈRE & F. KRAUT. *Transformation de quelques minéraux manganésifères sous l'action de la chaleur.*

Il a été montré antérieurement que, sous l'action de la chaleur, la polianite se transforme en braunite, puis en haussmanite.

Or, les manganates, en particulier la hollandite et la coronadite, possèdent une structure cristalline très voisine de celle de la polianite. Cette analogie nous a suggéré l'idée d'étudier le comportement thermique de ces minéraux et de chercher à identifier les composés qui prennent naissance au cours du chauffage.

L'analyse thermique différentielle fait apparaître un domaine de stabilité s'étendant jusqu'à environ 600° C. Entre 600 et 1000° C. se manifestent des phénomènes endothermiques correspondant à un premier stade de transformation, aussi bien pour la polianite que pour les deux manganates. Enfin, au delà de 1000° C., se produit une nouvelle modification qui se traduit sur les courbes par un accident endothermique extrêmement important.

Par ailleurs l'etude thermopondérale permet de suivre quantitativement ces transformations. Les pertes de poids enregistrées sont dues principalement au départ de l'oxygène et caractérisent dans une certaine mesure les composés de néoformation.

En étudiant aux rayons X les poudres chauffées on détermine avec plus de certitude ces substances.

Enfin, l'examen microscopique des éprouvettes portées aux différentes températures de transformation confirme le diagnostic et montre le mode d'association des nouveaux constituants.

3. H. WILMAN & T. DE S. MUTUCUMARANA. *The thermal transformations of mica between* 200 *and* 650° C.

It is found by electron diffraction that cleavage faces of muscovite mica, when heated *in vacuo* or in air for $\frac{1}{2}$–3

hr., first show a change of surface structure at about 200° C., a hexagonal structure being formed, with a between 5·3 and 5·5 Å and c between 6·9 and 7·4 Å, orientated with the basal axes parallel to those of spacing 5·18 Å of the mica cleavage face. Similar lattices, though with several major variations in structure as shown by the relative spot intensities, were found up to nearly 550° C., where a complete change in pattern occurred, corresponding to an epitaxially orientated structure which was orthorhombic, or nearly so, with axial lengths near 7·4, 9·6 and 12·9 Å.

After heating mica for 3 hr. in the region of 650° C. the decomposition product again gave a different type of pattern, corresponding to a similar orthorhombic structure, with axial lengths near 9·9, 13·3 and 7·7 Å, but in different epitaxial orientation relative to the main mica substrate. These decomposition products are presumably due to a progressive dehydration of the mica, but identification of their composition is difficult owing to lack of data for comparison. Mica heated to 850° C. became too wrinkled and rough-surfaced to yield a clear pattern.

4. H. F. W. Taylor. *Dehydration mechanisms of the hydrated calcium silicates.*

The dehydration of single crystals of hydrated calcium silicate minerals has been studied by X-ray, electron-microscope, and electron-diffraction methods. In some cases the product is an unoriented aggregate, but more often it is a single or twinned crystal having a definite orientation relative to that of the initial material. In these cases, a close relation exists between the unit cells of initial and final materials.

Earlier X-ray studies yielded incomplete information, especially with the fibrous compounds, because these are frequently available only as polycrystalline aggregates which give only rotation photographs. In several of these cases (okenite, tobermorite, foshagite) more complete information has now been obtained by electron-diffraction, using the three-stage electron microscope.

The transition afwillite $\rightarrow \gamma$-Ca_2SiO_4 has been examined in some detail, because the crystal structures of both compounds are known. The (010) and (10$\bar{1}$) directions of the afwillite become respectively the (100) and (001) directions of the γ-Ca_2SiO_4. The atomic movements needed to effect the change have been determined. The subsequent change to rankinite has also been examined..

The occurrence in the neighbourhood of transition temperatures of 'extra' X-ray reflexions, not attributable to either of the pure phases, is noted and their possible significance is discussed.

§ 12. Diffusion aux petits angles; diffusion en dehors des réflexions sélectives

1. W. A. Wooster. *An instrument for the study of central sections of diffuse reflexion surfaces.*

2. H. Curien. *Diffusion des rayons X par le sodium.*

On a préparé des monocristaux de sodium dans des moules plats à fenêtres en nickel très mince, et on a étudié la diffusion des rayons X par transmission. On a ainsi tracé des courbes de diffusion le long des directions importantes dans le réseau réciproque. On constate que les pouvoirs diffusants du deuxième et du trosième ordre dépassent largement, pour la plupart des mesures, ceux du premier ordre. On calcule *a priori* avec une bonne approximation ces pouvoirs d'ordres supérieurs à partir des constantes élastiques. On peut ainsi interpréter l'ensemble de la diffusion des rayons X par l'agitation thermique dans le sodium à température ordinaire.

3. P. Olmer & H. Robert. *Diffusion des rayons X par les ondes d'agitation thermique.*

Les résultats qui avaient été primitivement obtenus sur l'aluminium pour la direction [100], sont complétés par une étude précise de la diffusion pour des vecteurs de diffusion coïncidant avec une axe ternaire [111]. Les plans d'ondes acoustiques coïncident alors avec les plans d'empilement compacts de la structure.

Caractéristiques de la diffusion aux limites de la zone. Conséquences sur les courbes de la dispersion de vitesse.

4. K. Kranjc. *Influence de la densité apparente d'un système hétéro-dispersé sur la diffusion des rayons X aux petits angles.*

On étudie expérimentalement l'influence du rapprochement systématique des 'particules' d'un système hétéro-dispersé sur la forme de la courbe de diffusion et sur l'intensité des ondes diffractées sous les petits angles. En tassant de plus en plus d'hydroxyde d'aluminium très finement divisé dans un volume donné, on a obtenu des échantillons de densité relative allant de 0,026 à 0,89. Des diagrammes de diffusion des rayons X de douze de ces échantillons ont été faits. Sur aucune des courbes de diffusion on n'aperçoit de maximum d'intensité. L'allure générale des courbes ne varie pas beaucoup d'une courbe à l'autre, ce qui est en accord avec les prévisions théoriques (Guinier, 1943; Fournet, 1951; Hosemann, 1939, 1950).

Les résultats d'analyse quantitative d'après les méthodes de Hosemann (1950) et Porod (1951–3) sont comparés entre eux et aussi avec la photographie obtenue au microscope électronique. Pour l'échantillon de densité faible les deux méthodes donnent la taille moyenne de l'élément structural environ 90 Å, en bon accord avec l'image électronique. La taille augmente avec la densité apparente de l'échantillon. Ce résultat s'explique par l'association des particules provoquée par la compression de la substance.

Le rapprochement des éléments structurals diminue l'intensité des ondes diffractées, ce qui est en accord qualitatif avec certaines considérations théoriques. L'étude quantitative de cette influence montre une diminution de l'intensité avec la densité relative approximativement exponentielle. Tout se passe comme si le coefficient d'absorption massique était augmenté. Quant à l'influence combinée de l'absorption et des interférences, l'expérience montre un maximum d'intensité des ondes diffractées pour l'échantillon de densité relative 0,2 et non 0,5, généralement admise.

5. R. Smoluchowski, Y. Y. Li & W. H. Robinson. *Small-angle X-ray scattering by lattice imperfections.*

It is pointed out that a Fourier inversion of the intensity distribution of X-ray scattering, taking the small-angle scattering alone, gives the electron-density function of the continuum approximation. The procedure of including only the central scattering is practicable, when none of the Bragg peaks of the lattice diffraction occur at such a small angle that their scattered intensity overlaps the central scattering. A general discussion of the choice of the sign of the phase factor in the Fourier transformation and of its experimental consequences is given. The analysis is applied to scattering in a supersaturated alloy and to a discussion of some of the approximate formulae used in fitting experimental data. When the electron-density function of the scattering center has an odd symmetry with respect to one of the coordinate variables, conclusions can be drawn about the scattered intensity distribution without actually knowing the density function. The most interesting case of an odd symmetry is the edge dislocation. Various experimental results recently obtained on metallic and non-metallic imperfect solids will be presented and discussed.

6. P. B. Hirsch. *The measurement of low-angle scattering by the double-crystal spectrometer technique.*

The double-crystal spectrometer has been used to measure diffuse scattering up to spacings of several thousand Ångströms. The extension of the method to even larger spacings is discussed. It is also shown how the total scattering, measured by the Warren method, can be used to determine the shapes of the structural units responsible for the low-angle scattering in substances which exhibit preferred orientation. Some applications of these methods are described.

7. J. Laval. *Intensité des rayons X diffusés par un cristal sous l'effet de l'agitation thermique.*

§ 13. Croissance des cristaux

1. C. S. Brown, R. C. Kell & L. A. Thomas. *The growth of large quartz crystals.*

The growth of large quartz crystals on seeds cut perpendicular to the trigonal axis has been described previously. Subsequent work has achieved two main results: the growth of crystals substantially larger than those obtained in the earlier work and the successful use of low-grade sources of silica, native to the United Kingdom, instead of high-grade melting-quality quartz from Brazil.

Crystals weighing about 150 g. are now being grown on a pilot scale in a period of 30 days using autoclaves having a 63 mm. bore. This size of crystal is large enough for the majority of piezoelectric purposes in radio communications. Certain applications, including those in carrier telephony, require larger crystals and this has prompted an investigation using autoclaves having 100 mm. bore. In such autoclaves crystals weighing over 700 g. have been grown in 40 days.

Quartz crystals have been grown from flint, from quartzites of varying composition and even from granite. Depending on the nature and the amount of impurity in the source material the crystals may be strained or flawed owing to the inclusion of impurity atoms. However, certain modifications of the growth process have enabled these defects to be overcome, yielding crystals of good quality. Work now in progress promises to reveal the nature of the impurities which most affect the growth of quartz.

2. C. S. Brown & L. A. Thomas. *The response of laboratory-grown quartz to irradiation with X-rays and other radiations.*

It has been shown previously that the darkening produced in quartz when irradiated with X-rays is dependent on the presence of impurities incorporated during growth. Moreover, a quartz crystal grown in the laboratory under optimum conditions is not appreciably darkened by exposure to X-rays for a period which normally induces substantial darkening in natural quartz, e.g. a dose of 5×10^6 R.

The continuation of the investigation has shown that laboratory-grown quartz can be made to darken either by a sufficiently long exposure to X-rays, about twenty times the normal dose, or by irradiation with high-energy electrons or thermal neutrons. However, the saturation darkening is still only about one-fifth of that produced in a typical natural quartz crystal.

In contrast to the laboratory-grown quartz of good quality, crystals grown from impure source materials, such as flint, darken readily when exposed to X-rays, the darkening forming a characteristic pattern directed along the trigonal axis. This pattern no longer occurs when quartz is grown from flint using a modified process which produces high quality crystals. The characteristic darkening patterns can also be produced by the intentional introduction of impurities into the quartz lattice during growth. There also appears to be a close correlation between the darkening and the strain patterns observed when the crystals are viewed in polarised light.

A tentative explanation is given of the form taken by the darkening which accounts for the manner in which the impurities are adsorbed.

3. A. R. Verma. *Interferometric studies of crystal growth.*

The growth of long-chain compounds, e.g. palmitic acid crystals grown from dilute solutions, has been studied by the application of multiple-beam interferometry. It is found that these crystals grow by the screw-dislocation mechanism, exhibiting growth spirals on the basal planes (*ab* planes).

The measurement of spiral step heights by the application of multiple-beam internal interference fringes has been carried out. The measured step heights are discussed in relation to the size of X-ray unit cell.

The formation of large dislocation groups, their movement and macroslips have been illustrated.

The birefringence of thin crystals has been measured for different wavelengths in the visible region by the application of the multiple-beam fringes of equal chromatic order for doubly silvered crystals.

4. I. M. Dawson. *The formation of dislocations in crystals of long chain compounds.*

The electron microscope has been used to study the growth of crystals of long-chain paraffins, acids, alcohols

and esters. Using shadowcasting techniques, it is possible to resolve molecular layers on crystal faces and measure the height of growth steps under varying conditions for growth.

Micrographs have now been obtained which show how dislocations are formed in crystals of the ester, *n*-propylpentacontanoate. Growth appears to start from monomolecular sheets of the ester which first form as nuclei. As these sheets grow out, lattice misfit occurs at the edge of the sheet. The dislocation thus formed is then built in to the body of the crystal by continued growth. Secondary dislocations can arise in the same way at the edge of growth steps in large crystals.

The mechanism is probably a general one for the formation of screw dislocations in crystals.

5. A. R. Lang & B. Chalmers. *Imperfections in lead single crystals grown from the melt.*

Imperfections in lead single crystals grown from the melt have been studied by the methods used by Teghtsoonian & Chalmers in the case of tin (*Canad. J. Phys.* (1951), **29**, 370; (1952), **30**, 388). Single crystals grown in the form of flat bars show a macromosaic or lineage structure consisting of 'striations' about 1 mm. in width rotated relative to each other by angles of up to a few degrees about the growth axis. If a wide crystal is grown from a narrow seed the new material shows no striations until a certain length has grown. The length of this coherent region, called the 'incubation distance', and the form of the subsequently developing striations have been studied under a variety of growth conditions. For all orientations, at growth speeds above about 10 mm. per minute, striation boundaries are closely aligned with the growth axis. At lower speeds the boundaries form an irregular pattern. Incubation distance is decreased when growth rate is increased and when temperature gradients are decreased. A modified Berg–Barrett X-ray technique enables orientation differences to be measured and indicates the local degree of crystal perfection. Observations are in general accord with Teghtsoonian & Chalmers' explanation of the behavior of tin: vacancies formed at the solid–liquid interface aggregate into discs which subsequently collapse to form edge dislocation half-loops, dislocations of the same sign later aligning themselves as low-angle boundaries. However, the behavior of lead is generally more complex than that of tin.

6. S. B. Levin. *Crystal-growth improvements over the Verneuil method.*

7. B. Honigmann. *Züchtung grösserer Einkristalle von Hexamethylentetramin aus der Dampfphase.*

Die Kristallzüchtung erfolgt in evakuierten Glasröhrchen in einem Metallblockthermostaten. Gekühlt wird durch eine Kupferplatte (10×10 mm.), die an die Röhrchenwand angedrückt wird und deren Temperatur geregelt und gemessen werden kann.

Keimbildungshäufigkeit und Wachstumsgeschwindigkeit werden durch Fremdadsorptionsschichten beeinflusst. Grössere, fehlerfreie Kristalle konnten bisher nur in nicht ausgeheizten Rohren, in die die Substanz unter Hochvakuum einsublimiert worden ist, gezüchtet werden. Desgleichen nimmt die Tendenz zur Fehlerbildung mit steigender Temperatur merklich ab.

Von Wichtigkeit ist ferner die Form der Isothermen. An den Kristallflächen, die Isothermen schneiden, treten Temperaturdifferenzen auf. Diese führen bei Überschreiten eines kritischen Wertes zur Fehlerbildung am Kristall. Bei der Plattenkühlung liegen die Isothermen etwa parallel zur Unterlage. Dabei gelingt die Züchtung grösserer plattenförmiger Kristalle (bis $10 \times 10 \times 3$ mm.), sofern die Keime in geeigneter Orientierung zur Unterlage aufgewachsen sind. Dabei muss eine Kristallfläche etwa parallel zur Unterlage liegen.

Mit der beschriebenen Apparatur gelingt ferner die Beobachtung zahlreicher Oberflächeneffekte wie z.B.: Ausbildung von Vizinalflächen, Wachstumsschichten, Fehlerbildungen und deren Auswirkung auf die Wachstumsgeschwindigkeit usw.

8. R. Renninger & B. Krause. *Kristallgitter-Model aus schwimmenden Pentaerythrit-Kristallen infolge von elektrischer Aufladung bei der Kristallisation.*

Bei der Kristallisation von Pentaerythrit aus wässeriger Lösung ordnen sich die an der Oberfläche schwimmenden Kristallkeime, falls sie einheitliche Grösse haben, regelmässig an zu einem hexagonalen Gitter ähnlich demjenigen der Seifenbläschen beim Bragg–Nie'-schen Modell. Ursache sind elektrische Aufladungen der wachsenden Kristalle. Die mit vertikaler tetragonaler Achse schwimmenden Kriställchen erweisen sich als an ihren Köpfen negativ aufgeladen. Geht das Wachstum in Wiederauflösung über, so kehrt sich das Ladungsvorzeichen um. Die Potentiale der Kristalle erreichen Werte bis zu mehreren hundert Volt, sie sind proportional deren Kantenlängen. Da das elektrische Feld nur im Luftraum herrscht, konnte nicht eindeutig entschieden werden, ob die Aufladung unipolar ist, oder etwa echten Dipol-Charakter hat. Verschiedene Hinweise sprechen aber für ein homogen räumliches 'Einfrieren' von negativen Ladungen beim Wachstum, und damit für Zusammenhänge mit dem Costa Ribeiro'schen 'thermo-dielektrischen Effekt'.

9. L. Graf. *Das Verhalten der nieder indizierten Ebenen bei verschiedenen Wachstumsgeschwindigkeiten.*

Nieder indizierte Ebenen weisen bekanntlich ein geringes Adsorptionspotential auf. Dies hat zur Folge, dass die Art ihres Wachstums von der Anzahl der pro Zeiteinheit auf ihnen adsorbierten Atome abhängt. Bei geringer Anzahl ist die Keimbildungswahrscheinlichkeit auf ihnen gleich Null und es erfolgt kein Wachstum in Normalenrichtung, nur eine Vergrösserung der Fläche. Bei grösserer Anzahl kommt es auf den Ebenen zu einer Keimbildung mit tangentialem Auswachsen des Keims, d.h. es tritt (atomares oder lamellares) Schichtwachstum auf, die Ebenen wachsen in Normalenrichtung durch Parallelverschiebung zu sich selbst. Bei hoher Zahl pro Zeiteinheit adsorbierter Atome wird jedoch die Wahrscheinlichkeit einer Keimbildung auf den Ebenen trotz ihres geringen Adsorptionspotentials so gross, dass sich gleichzeitig sehr viele Keime bilden. Ihr tangentiales Auswachsen ist aber nicht mehr bedeutungsvoll, da sie

sich durch Anlagerung weiterer Atome viel rascher in der Normalenrichtung der Ebene weiterentwickeln. Die Wachstumsgeschwindigkeit der einzelnen Keime ist dabei unabhängig von einander und wird nur von den an dem betreffenden Keim herrschenden Wachstumsbedingungen bestimmt. Daher bleiben die Ebenen nicht erhalten, sondern es bilden sich beliebig gekrümmte, kristallographisch undefinierte Flächen. Die äussere Begrenzungsform eines Kristalls wird dann von der Grenzflächenspannung, der Wachstumsanisotropie und der Ableitungsgeschwindigkeit der Kristallisationswärme (bezw. Diffusionsgeschwindigkeit bei wässerigen Lösungen) bestimmt. Es bilden sich hierbei Dendriten mit krummen, kristallographisch undefinierten Flächen.

10. H. Wilman & T. H. V. Setty. *Crystal growth in electrodeposits on single-crystal substrates.*

Previous work in this laboratory has demonstrated how the main factors influence the structure of crystalline electrodeposits, and in particular has distinguished two types of growth—'lateral growth' and 'outward growth' —with characteristic orientations. The present experiments and electron-diffraction observations show more quantitatively the effects of bath composition, deposit thickness, current density, temperature and substrate nature, in the case of deposition of silver from the argentocyanide bath upon smooth electropolished (110), (111) and (100) faces of silver single crystals.

It is also shown that between the initial growth which is orientated parallel to the substrate lattice, and the randomly-orientated polycrystalline layer which develops with increasing deposit thickness at the higher current densities, there is an intermediate twinned layer. This onset of twinning, in conjunction with 'outward growth' conditions, (high current-density etc.) appears indeed to be the cause of the development of the random layer. The dependence of the critical current density above which twinning occurs, upon the substrate face, bath temperature, etc. is determined.

11. H. Wilman & M. S. A. Khan. *The structure and growth of metal layers formed by chemical replacement from solution.*

Earlier experiments on chemically formed deposits were made with polycrystalline substrates. In the present experiments, the structure of gold, silver and platinum deposits, respectively, formed by chemical replacement from solution upon atomically smooth electropolished (111), (100) and (110) faces of copper single crystals, is determined by electron diffraction. It is shown that, as tends to occur in other types of deposition, in particular electrodeposition, the deposits grow initially in epitaxial orientation relative to the substrate, then with increasing deposit thickness twinning occurs and a wider and wider spread of orientation develops. A proportion of close-packed hexagonal structure was present, however, in certain of the deposits, in epitaxial orientations showing it had been formed as initial nuclei, not as a faulting of the f.-c. cubic structure.

In the case of gold deposited on Cu (111) and Cu(110), the orientation is of parallel {111} and {110} type respectively. On Cu (100) the deposit from gold cyanide was initially {111}, orientated with a cube-face diagonal parallel to one of those of the copper surface. This is evidently due to primary deposition on a very thin layer of Cu_2O present initially, which is also in this {111} orientation on the copper surface. Later growth was in parallel {100} orientation, evidently directly on the copper.

Deposits from gold chloride solution on Cu (100) showed only the {111} orientation and were associated with formation of much Cu_2O.

12. T. Ichiki & H. Fujiwara. *To produce thin single crystal foil of aluminium having any desired crystallographic orientations.*

By using Fujiwara's method we have succeeded in producing aluminium single-crystal foils ($0{\cdot}05 \times 6 \times 100$ mm.^{3}) having definite crystallographic orientations in the following manner:

First many slender pieces ($1 \times 5 \times 100$ mm.^{3}) of aluminium were cut from commercial plate (1 mm. in thickness, 99·5% in purity); then each was reduced to 0·05 mm. in thickness by rolling, after suitable intermediate annealing. These thin rolled foils were cut in lengths of 200 mm. and, after suitable anneal, were stretched lengthwise about 2·5%. Secondly, a foil treated in this way was held between two aluminium plates (0·25 mm. in thickness and having the same form and nature as those of foils), to which composite specimen we applied Fujiwara's method.

13. J. C. Monier & R. Hocart. *Épitaxies et recouvrements de liaisons.*

A l'interprétation réticulaire classique des épitaxies, nous proposons d'ajouter une précision nouvelle; celle des recouvrements géométriques de liaisons du support et du dépôt.

Ces recouvrements permettent plusieurs justifications:

1°. Justification de certains accolements par des plans réticulaires qui n'apparaissent dans le faciès du cristal porté que lors du dépôt orienté. Exemple du chlorure cuivreux de faciès $\frac{1}{2}(111)$ qui donne sur le clivage (110) de la blende une épitaxie par (110). Exemple de la sénarmontite Sb_4O_6, de faciès (111) qui s'accole sur (110) de la blende, également par (110).

2°. Justification de l'orientation unique observée dans le cas où la réitération que laisse prévoir la symétrie des réseaux des plans d'accolements n'a pas lieu. Exemple du chlorure cuivreux, de faciès $\frac{1}{2}(111)$, accolé par (110) sur (110) de la blende en donnant une seule orientation de triangles isocèles. Exemple de l'arsénolite, de faciès (111), accolé par (111) sur (111) de la fluorine, en donnant une seule orientation de triangles équilatéraux.

14. A. Oberlin & R. Hocart. *Épitaxies étudiées au microscope électronique et par diffraction électronique.*

Le graphite est clivé en feuillets assez minces pour servir de support utilisable en microscopie électronique. Il est employé comme porteur épitaxique pour l'étude de quelques microcristaux.

Des particules de MoO_3 obtenues par sublimation et d'or préparé par réduction en solution, s'orientent sur le graphite. D'autres exemples sont examinés avec les mêmes méthodes.

Les concordances réticulaires sont établies au moyen de la diffraction électronique.

15. J. VON VULTÉE. *Über die orientierten Verwachsungen von Rutil in Quarz.*

Zehn Vorkommen von Blauquarz wurden mikroskopisch untersucht. Die Richtungen der Nadelachsen der im Blauquarz orientiert eingelagerten Rutile wurden auf dem Universaldrehtisch bestimmt. Es konnten elf Verwachsungsgesetze mit insgesamt 55 Nadellagen nachgewiesen werden. Weitere Beobachtungsergebnisse beziehen sich auf die vermutbaren Zusammenhänge zwischen den Bildungsbedingungen des Blauquarzes und der Länge der eingelagerten Rutilnadeln und auf ein wahrscheinliches Zwillingsgesetz des Rutils mit einem Winkel von 169° zwischen den *c*-Achsen der Individuen.

Die mikroskopische Untersuchung von acht Vorkommen von Rosenquarz zeigte, dass bei stärksten Vergrösserungen durchaus gleichgeartete Einlagerungen einer nadelförmigen Komponente zu beobachten sind. Dass es sich dabei ebenfalls um Rutile handelt, konnte wie beim Blauquarz durch Debye–Scherrer-Aufnahmen der Rückstände nach dem Abrauchen des Quarzes mit Flussäure gezeigt werden.—Zu einer Vermessung der Nadellagen auf dem *U*-Tisch sind die Rutile im Rosenquarz zu klein. Es ist jedoch möglich, aus dem Asterismus an Rosenquarzkugeln auf die Orientierung der eingeschlossenen nadelförmigen Komponente zu schliessen. Eine Untersuchung von 64 Rosenquarzkugeln aus den Sammlungen des Heidelberger Mineralogischen Institutes zeigte, dass die zu beobachtenden Lichtkreise an den Kugeln auf neun Verwachsungsgesetze schliessen lassen, die sämtlich mit Verwachsungsgesetzen in Blauquarzen übereinstimmen.

Um neben den Orientierungen zum Quarz als Wirtmineral und der lichtmikroskopisch messbaren Länge der Rutilnadeln auch eine Aussage über die Nadeldicke machen zu können, wurden von Blau- und Rosenquarzen elektronenoptische Aufnahmen gemacht. Es zeigte sich, dass die Durchmesser der Nadeln bei Blauquarzen zwischen 0,02 und 1 μ schwanken. Ein Häufungswert der Nadeldurchmesser liegt bei etwa 0,3 μ. In Rosenquarzen konnten im Regelfall Nadeldurchmesser zwischen 0,01 und 0,2 μ festgestellt werden. Im reinen, klaren Rosenquarz besitzt die weitaus grösste Anzahl der Rutilnadeln einen Durchmesser von 0,05 bis 0,07 μ.

Die strukturgeometrischen Analogien zwischen dem Quarz als Wirtmineral und dem Rutil als Gast werden für die einzelnen Verwachsungsgesetze aufgezeigt. Abschliessend folgen einige Bemerkungen zur Frage der Färbung des Rosenquarzes.

16. J. BARDOLLE & J. BÉNARD. *Sur quelques aspects cristallographiques et morphologiques de la réaction de formation du protoxyde de fer à la surface du fer.*

Des échantillons de fer monocristallins ou comportant au plus quelques cristaux d'assez grandes dimensions sont oxydés à haute température sous pression réduite d'oxygène.

Sous très basse pression (10^{-3} mm. de Hg environ) à 850° C. on peut observer après un temps variable (de 10 minutes à plusieurs heures) la formation de germes d'oxydes en épitaxie avec le métal sous-jacent. L'orientation de ces germes est étudiée. De plus leur nombre par unité de surface, variable d'un cristal à l'autre est déterminé pour différentes orientations de la surface métallique initiale.

Sous des pressions un peu plus élevées (10^{-2} à 10^{-1} mm. de Hg) dans les mêmes conditions de temps et de température on obtient une couche continue de protoxyde de fer, également en épitaxie avec le métal sous-jacent. Vers 750–850° C. il est même possible d'obtenir un monocristal de protoxyde sur un monocristal de métal. Ce dernier résultat permet une étude précise de l'orientation cristallographique du réseau de l'oxyde par rapport à celui du métal. Les relations d'orientations ainsi mises en évidence sont rapprochées des aspects morphologiques observés.

17. G. I. FINCH, M. V. GHARPUREY & A. GOSWAMI. *The initial stages of epitaxial crystal growth.*

The orientation of an overgrowth crystal formed on a single-crystal substrate is primarily determined by the orientation and spacing of the atom pair constituting the primary crystal nucleus. Stresses due to misfit between overgrowth and substrate may be relieved by an appropriate change in orientation of the growing crystal.

18. G. I. FINCH & A. GOSWAMI. *The structure of tin deposits.*

A comparative study of tin deposits formed by electrodeposition, displacement and hot-dipping shows that the deposit can be formed either by the laying down on the basis metal of successive densely packed layers (lateral growth), or by the building up of crystals along densely packed atom rows normal to the surface (outward growth). Lateral, but not outward, growths conform epitaxially to the substrate crystals. Thin layers produced by hot dipping are epitaxial.

19. A. P. KAPOUSTINE. *Étude expérimentale de l'influence des ultrasons sur la cinétique de la cristallisation.*

20. M. FRANÇON, S. GOLDSZTAUB & R. KERN. *Étude des cristaux par interférométrie.*

Les auteurs appliquent différentes méthodes interférentielles à l'étude de la qualité des faces cristallines et de la croissance des cristaux à partir de leurs solutions.

Parmi ces méthodes il en est une nouvelle, basée sur les interférences en lumière polarisée et applicable aux objets isotropes.

21. G. NOMARSKI. *Étude de la croissance des cristaux par interférence en lumière polarisée.*

Pour l'observation en lumière réfléchie des figures de croissance visibles sous divers grossissements, on propose une méthode de contraste interférentiel dont l'application se ramène à l'adjonction d'un dispositif optique simple à un microscope quelconque équipé pour les examens en lumière polarisée.

Le même dispositif, qui se place entre l'objectif et l'illuminateur vertical du microscope à réflexion n'exige aucune limitation du faisceau. Il permet, en lumière blanche, la mesure des discontinuités observées depuis quelques Ångströms jusqu'à quelques microns.

On donnera quelques exemples d'application, tirés de l'étude des cristaux de carbure de silicium qui présentent des figures de développement très différents à des échelles variables.

22. G. Pfefferkorn. *Das Wachsen von Metalloxydkristallen nach elektronen-mikroskopischen Untersuchungen.*

Auf Oxydhäuten wachsen sublichtmikroskopisch kleine Nadeln und dünne Blättchen. Die Abhängigkeit des Wachstums nach Länge und Dicke und die Abhängigkeit weiterer Oberflächenerscheinungen von äusseren Bedingungen wird untersucht, und ist ein Beweis für die Oberflächendiffusion von Bausteinen.

23. P. Hamard. *Formations cristallines tubulaires de l'hexaméthylene-tétramine-triphénol: problème de croissance.*

Par cristallisation rapide, l'hexaméthylène-tétramine-triphénol cristallise en bottes d'aiguilles. En cristallisation lente, il donne des prismes allongés, tous creux, à section extérieure hexagonale. Le tube intérieur présente l'aspect d'une pyramide hexagonale allongée, terminée à l'extrémité ouverte par un plan en biseau à 51° des génératrices extérieures. La formation tubulaire, dont ce corps paraît un prototype parfait, est relativement fréquente.

La régularité du développement de cette formation nous paraît difficilement interprétable par les théories habituelles de la diffusion.

Par analogie avec la théorie de Kossel qui envisage, dans le cas des cristaux cubiques homopolaires, des forces de liaison également réparties autour d'une particule élémentaire et des forces d'agrégation sensiblement équivalentes suivant les deux ou trois directions d'un système de composantes, on pourrait chercher à interpréter l'existence des formations en aiguille et tubulaire par une force d'agrégation à forte prépondérance dans le sens de l'allongement.

L'influence relative de cette composante principale et des composantes secondaires conjuguées varie largement avec la nature de l'espèce chimique possédant cette propriété. Cette force prépondérante correspond aussi à la possibilité de déformations mécaniques permanentes dans le cas de certaine symétrie (urée). Par ailleurs, la prépondérance considérable d'une force d'agrégation ne paraît pas compatible avec la théorie du grossissement par nucléations bidimensionnelles.

Le type de structure décrit pose un problème dont la solution pourrait contribuer à l'interprétation du grossissement des édifices fibreux.

24. G. Deicha. *La genèse des groupements cristallographiquement définis de cristaux droit et gauche, observée sur l'exemple du chlorate de sodium.*

Les macles où se trouvent associées les variétés *d* et *g* d'une même espèce cristalline apparaissent comme un intermédiaire entre les macles *s.s.* associant des individus cristallins semblables et les groupements épitaxiques d'espèces différentes. L'étude expérimentale de la cristallisation de ClO_3Na (tétartoédrie énantiomorphe cubique) montre que la formation de macles associant individus droit et gauche peut être obtenue en faisant varier le degré de sursaturation. Ce résultat est un nouvel exemple de l'influence du déséquilibre cristallogénétique sur l'orientation mutuelle *s.l.* Les mêmes expériences permettent de préciser les relations entre sursaturation et formation de lacunes de cristallisation.

25. M. Drechsler. *Schmalfilm: Adsorption und Diffusion auf Einkristallflächen.*

In Feldelektronenmikroskopen wird die flächenspezifische Adsorption und Oberflächendiffusion an den Beispielen W auf W und Ba auf W gezeigt. Aufgedampfte adsorbierte W-Atome wandern gemäss den Verweilzeiten und den Platzwechselenergien flächenspezifisch und in Vorzugsrichtungen. Ba-Atome zeigen auf W-Flächen charakteristische Verweilzeiten. Die Linie monoatomarer Ba-Bedeckung wandert entsprechend den flächen-spezifischen Oberflächendiffusions-Koeffizienten. Einkopierte Zahlenwerte sowie ein Modell ermöglichen Vergleiche mit theoretischen Werten.

26. M. Drechsler. *Messung strukturabhängiger Platzwechselenergien mit dem Feldelektronenmikroskop.*

Flächenspezifische Platzwechsel- und Bindungsenergien von arteigenen und nicht arteigenen Atomen auf Einkristallflächen werden vereinfacht berechnet durch Summation der Bindungsenergien zu den nächsten Nachbarn.

Im Feldelektronenmikroskop werden zeitlich räumliche Veränderungen adsorbierter Einzelteilchen und Schichten als Funktion der Temperatur auf mehreren Einkristallflächen gemessen und daraus Platzwechselenergien und Platzwechselrichtungen bestimmt. Im Falle der untersuchten Systeme Barium auf Wolfram und Wolfram auf Wolfram stimmen gemessene und berechnete Platzwechselenergien überein. Diese Messungen ermöglichen es auch, die verschiedenen Gitterstrukturen der einzelnen Flächen festzustellen bzw. zu bestätigen.

27. M. Drechsler & R. Vanselow. *Die Wachstumsform von Tantal-Einkristallen im Feldelektronenmikroskop.*

Mit dem Feldelektronenmikroskop werden Temper- und Wachstumsformen von Einkristallen aus Ta sowie aus W, Mo, Ni u.a. beobachtet. Als Ta-Wachstumsflächen treten bei einem Vakuum von 10^{-10} mm. Hg nur noch 011 und 001, dagegen nicht 112-Flächen auf. Dies steht im Gegensatz zu Messungen an Ta bei weniger gutem Vakuum sowie zu bisherigen Messungen an anderen kubisch raumzentrierten Kristallen, stimmt aber unmittelbar mit der Theorie von Stranski überein.

28. C. A. Rush. *Moving bubbles in negative crystals.*

A motion picture showing the rapid movement of gas bubbles in liquid-filled crystal cavities is presented. The cavities are negative crystals, and appear to be filled with mother liquor from the crystallization. The gas bubble is either air or the vapor phase of the liquid. The movement is presumed to be Brownian in nature, as modified by the proximity of the cell wall, and is very rapid for bubbles below two microns in diameter. Larger bubbles show slower movement, and above 25 microns no perceptible motion is noted. Examples of organic and inorganic laboratory crystals are shown.

§ 14. Diffraction des neutrons

1. J. A. Goedkoop & A. F. Andresen. *The crystal structure of copper hydride.*

The crystal structure of CuH, about which conflicting information appears in the literature, was reinvestigated

with X-ray and neutron powder techniques. The X-ray diagram was taken with a G. E. Geiger-counter goniometer and confirmed the hexagonal structure as given by Wyckoff with $a = 2{\cdot}920$, $c = 4{\cdot}614$ Å. Samples produced in the usual way, i.e. by adding hypophospherous acid to a copper sulphate solution, show considerable line broadening, and contain several per cent metallic copper. The neutron diffraction data were obtained at the Kjeller 250 kW. heavy-water reactor. They are consistent with the wurtzite structure assumed by Wyckoff. Work on the deuteride will be reported.

2. G. E. Bacon. *The ferroelectric structure of potassium dihydrogen phosphate.*

Neutron diffraction measurements of the (*hk*0) and (*h*0*l*) reflections of KH_2PO_4 have been carried out at 20, −140 and −180° C., using a neutron wavelength of 0·8 Å which permitted the study of interplanar spacings down to 0·45 Å. 'Normal' and 'difference' Fourier projections have been constructed on the (001) and (010) planes. In the ferroelectric state the crystal was maintained as a single domain under the influence of constraint and an electric field, evidence of the domain structure and orientation being obtained from the shape of the rocking curves. Certain pairs of reflections, such as 16,0,0 and 0,16,0, which are of equal intensity in the tetragonal state, are very sensitive to displacement of the hydrogen atoms. In the orthorhombic ferroelectric state they are quite unequal, becoming, for this particular example, in the ratio of 1:7. Reversal of the electric field reverses the structural asymmetry and domain orientation and interchanges these intensities, the ratio becoming 7:1.

3. R. Pepinsky & B. C. Frazer. *Miniaturized goniometers for neutron single-crystal diffraction.*

Use of LiI(Sn and Eu) scintillating crystals coupled to photomultipliers, and miniature high-pressure enriched-BF_3 counters, permits development of miniature single-crystal neutron diffraction goniometers. In the case of the scintillation detectors, the entire miniature goniometer is placed within a shielded region with 4-in.-thick walls of Pb and 4-in.-thick LiF embedded in paraffin. No shielding is required around the goniometer when the small BF_3 counter, encased in a B_4C-in-plastic shield, is used. Measurements with both types of detectors at the Brookhaven Reactor are illustrated. It is shown that the miniature counters have sensitivity and background comparable with standard large BF_3 counters.

The great advantages of these miniaturized goniometers lie in their small size and weight, low cost, and ease with which three-dimensional measurements can be accomplished with their use.

Two laboratory-constructed models of these goniometers are illustrated. These have been constructed at The Pennsylvania State University. A third instrument is also illustrated, which consists of a General Electric X-Ray Spectrogoniometer, modified according to Zachariasen's design for three-dimensional single-crystal measurements, but with B_4C-in-plastic slits for neutron collimation, and with a miniature BF_3 counter enclosed in a shield of similar material.

4. P. A. Egelstaff & G. L. Squires. *A thermal neutron analyser.*

A pulsed beam of thermal neutrons from the Harwell Linear Accelerator is allowed to fall on the rotating cadmium shutter of a slow neutron chopper. In this way a pulsed monochromatic beam of neutrons is produced. A crystal is placed in this beam, and the neutrons scattered at a selected angle are then analysed according to their time of flight from the crystal to a detector. Thus the wavelength spectrum of the scattered neutrons may be measured as a function of the scattering angle and the incident neutron wavelength. Such measurements provide information on the relation between the frequency and wavelength of elastic waves in the crystal lattice.

Some preliminary measurements will be presented.

5. P. A. Egelstaff. *Inelastic scattering of cold neutrons by liquids.*

When a cold neutron is scattered by a liquid it is possible for one or more quanta of vibrational energy (phonons) to be transferred to it. By measuring the cross section and the gain in energy we may obtain the approximate size of any groups of atoms in the liquid which are more tightly bound to one another than to their neighbours. If the energy spectrum is measured in detail we will also be able to determine the bond strength.

As a first step in the experimental study of this subject the average energy gain ($\bar{T}$) of 15° K. neutrons scattered by metals is being measured. Some results will be given on the variation of $\bar{T}$ with sample temperature for Pb and Zn near their melting points.

6. A. Herpin. *Étude théorique de la diffusion inélastique des neutrons par un monocristal.*

7. R. D. Lowde. *The scattering of neutrons by magnetic spin waves.*

The magnetic disorder which thermal agitation induces in a magnetic lattice can be analysed into spin waves. At temperatures not too near the Curie point or the Néel point, these waves may be represented as Fourier components of the motion of the array of spins; from this point of view they are the analogues in magnetism of the simple harmonic modes of vibration in lattice dynamics. Like the vibrational modes, the spin waves are also associated with definite momentum and energy, and in just the same way they give rise to characteristic diffuse reflexions by inelastic scattering when a magnetic crystal is exposed in a neutron beam.

Within an order of magnitude the spin wave reflexion intensities are found to be comparable with those of phonon scattering; thus the spin wave reflexions hold out the possibility of studying magnetic coupling forces by diffuse scattering methods. The cross section is, however, small—in iron about 0·002 barns per atom—and so exploitation of this potentiality is difficult. Nevertheless, it has been possible to isolate the spin wave part of the diffuse reflexion 110 in the Laue diffraction pattern of

iron, using the dependence of the cross-section on the magnetization direction of the crystal. Theoretical formulae will be given and compared with observation.

8. G. L. SQUIRES. *The scattering of slow neutrons by lead in the region of the melting point.*

The total cross-section of lead for neutrons with an average wavelength of 8·3 Å has been measured as a function of the temperature of the lead. Measurements have been made at temperatures from 20 to 550° C.

The cross-section is found to increase at the melting point.

9. L. M. CORLISS & J. M. HASTINGS. *A neutron-diffraction study of zinc ferrite at low temperatures.*

Recent neutron-diffraction measurements (J. M. Hastings & L. M. Corliss, *Rev. Mod. Phys.* (1953), **25**, 114) have confirmed the earlier X-ray result that zinc ferrite has the normal spinel structure, in which the diamagnetic zinc ions occupy the tetrahedral or *A* sites and the trivalent iron ions occupy the octahedral or *B* sites. According to the Néel theory of ferrimagnetism, there is, in addition to the dominant antiferromagnetic interaction between magnetic ions on *A* sites and those on *B* sites, a weaker antiferromagnetic coupling between magnetic moments on *B* sites alone. Since the *A*–*B* interaction is absent in zinc ferrite, this compound is ideally suited to observing the subsidiary *B*–*B* interaction, and might well be expected to exhibit antiferromagnetism at sufficiently low temperatures.

At room temperature, powder patterns show no evidence of coherent magnetic scattering. Experiments designed specifically to measure the diffuse scattering show no evidence of short-range order and permit an assignment of the ideal paramagnetic moment of $5\,\mu\beta$ to the Fe^{+3} ions. A low-temperature cryostat employing thin aluminum windows made it possible to obtain powder diffraction patterns down to liquid-helium temperatures. Peak intensities and positions obtained from runs at 77° K. and 48° K. are identical with those obtained at room temperature. At about 20° K. the general level of paramagnetic scattering decreases noticeably and a diffuse maximum appears in the low-angle region. At 4·2° K. a reasonably well-defined set of superlattice lines is present while the peaks corresponding to the original spinel structure are unchanged.

The transition which occurs in the neighborhood of 6–10° K. is interpreted as antiferromagnetic in origin. Experiments recently completed by Mr Friedberg at the Carnegie Institute of Technology, utilizing a portion of the neutron diffraction specimen, indicate a substantial heat capacity anomaly at 8·3° K., in confirmation of the diffraction result. The extra diffraction lines cannot be indexed on the original spinel unit cell. Possible models of the spin arrangement will be discussed.

§ 15a. Biocristallographie

1. H. v. PHILIPSBORN. *Biocristallographie.*

Les termes biophysique, biochimie et d'autres composés avec 'bio' sont usuels, mais pas encore le terme 'biocristallographie'. Les cristaux formés dans l'organisme sont rencontrés par beaucoup de spécialistes, mais le 'stroma organique' est seul mentionné.

2. J. BARRAUD. *Biocristallographie de l'ossification.*

Nous présentons une hypothèse tendant à expliquer une des phases de l'ossification par un mécanisme purement cristallographique. Cette hypothèse nous a été suggérée par un rapprochement entre les données suivantes:

1°. Le cartilage est très pauvre en phosphore inorganique, pauvre en calcium, relativement riche en soufre. Celui-ci appartient à des ions sulfuriques fixés sur une hexosamine, la chondroïtine avec laquelle ils constituent *l'acide chondroïtine sulfurique* (ACS).

2°. L'os, au contraire, est très riche en phosphore et en calcium, très pauvre en soufre.

3°. La brushite, PO_4HCa, $2H_2O$, dont le rôle est admis au cours de la calcification, a une maille presque rigoureusement identique à celle du gypse, SO_4Ca, $2H_2O$:

Gypse: $a = 10{,}47$, $b = 15{,}15$, $c = 6{,}51$, $d(001) = 7{,}578$ Å, $\beta = 151° 38'$.
Brushite: $a = 10{,}47$, $b = 15{,}15$, $c = 6{,}37$, $d(001) = 7{,}57$ Å, $\beta = 150° 8'$.

On peut donc imaginer que:

(1°) l'ACS du cartilage fixe le calcium du milieu circulant pour donner un *chondroïtine sulfate de calcium*; (2°) à la surface de celui-ci s'édifient (épitaxie?) quelques couches de *sulfate de calcium* (gypse); (3°) du fait, de l'identité des mailles, le gypse sert de germe pour la cristallisation de la brushite à partir des ions PO_4^{---} du milieu circulant; (4°) par enrichissement progressif en calcium, la brushite donne, par exemple, du phosphate tricalcique α, puis de l'hydroxyapatite, d'où édification du 'sel de l'os'.

Nous ne voulons voir là, pour le moment, autre chose qu'une *hypothèse de travail*, mais celle-ci suggère un certain nombre d'expériences, la plupart du domaine de la cristallographie, dont il reste à attendre le verdict.

3. A. S. POSNER. *The carbonate content of bone, teeth and allied phosphate minerals.*

A report upon the crystallographic investigation of the nature of carbonate found in the mineral portion of bone and teeth as well as the mineral which resembles them (francolite). X-ray diffraction and infra-red spectroscopy were used to prove the presence of calcite and magnesite in these materials. This lends support to previous chemical and physical data which indicated the presence of admixed carbonates in a general matrix of apatite in these substances.

4. J.-G. HELMCKE. *Biokristallographische Einlagerung anorganischer Verbindungen in organische Hartsubstanzen.*

Die Kristallisationen weichen bei den unterschiedlichen organogenen Hartsubstanzen voneinander ab. Beim Wachstum der Perlmutter erfolgt die Ausfällung des Kalziumkarbonats in der Modifikation des Aragonits aus einem kalkhaltigen Schleim, in dem statistisch (räumlich und zeitlich) einzelne Keime auftreten, an die sich die Kalziumkarbonationen anlagern. Die wachsenden Kri-

stalle treiben die organische Substanz vor sich her, sodass diese sich zwischen den Einkristallen des Aragonits ablagert. Bei der seitlichen Berührung der Einkristalle treten Kompromissflächen auf, die von der typischen Kristallisationsform des Aragonits unabhängig sind.

In Zähnen und Knochen der Säugetiere vollzieht sich die Ausfällung des Hydroxylapatits nicht (wie bisher angenommen) in vorgebildete organische Strukturformen, sondern unter kolloidchemischen Bedingungen. Innerhalb eines von den Zellen ausgeschiedenen Gels ordnen sich die Kristallite, den Zugspannungen entsprechend, an. Als kleinste Bauelemente bilden sich Einkristalle, die nicht zu hexagonalen Apatitprismen anwachsen können, sondern deren Grösse durch Verarmung des umgebenden Gels an geeigneten Ionen frühzeitig begrenzt und deren Tracht durch organische Lösungsgenossen bestimmt wird. In Modellversuchen konnten entsprechende Kristallisationen von Hydroxylapatiten erzielt werden.

Die Kieselsäureverbindungen sind in elektronenmikroskopisch amorphem Zustande in die Diatomeenschale eingelagert und bilden eine Schaumstruktur, die ihre Parallelen sowohl in organische Membranen als auch in Kieselsäuregelen besitzt. Mit ihnen haben die Diatomeenschalen das Adsorptionsvermögen und ein selektiv wirkendes Membranpotential gemeinsam (Es wurden Potentiale von 4 bis 15,4 mV., positiv für Kationen, zwischen 1/100 und 1/1000 NaOH ermittelt). Die Diatomeenschale wird aufgrund ihrer chemischen Bauelemente, sowie ihres mikromorphologischen Gefüges aktiv in den Stoffaustausch zwischen dem Protoplasma und dem umgebenden Wasser eingreifen.

5. H. Seifert. *Über die Bedeutung der Kristallstruktur für die Silikose.*

Lange herrschte bezüglich der Ätiologie der Silikose die 'Löslichkeitstheorie' (Gardner, King). Ihr zufolge sollte aus den silikatischen Fremdpartikeln, vornehmlich dem Quarz, im Lungengewebe die Kieselsäure in Lösung gehen und in dieser Form ihre toxische Wirkung entfalten. Seit dem 1. Staublungenkongress in Münster 1949 machte sich wachsender Widerstand gegen diese Auffassung geltend, zumal sie keine erfolgreiche Therapie und Prophylaxe gezeitigt hatte. Zunächst unabhängig voneinander, später gemeinsam entwickelten R. Jäger und Verfasser eine neue Theorie. Sie machte auf den bisher gänzlich vernachlässigten kristallinen Charakter der eingeatmeten Fremdteilchen aufmerksam und legt den Hauptwert auf die strukturgebundenen und strukturgelenkten Grenzflächenprozesse, vergleichbar den Elementarprozessen der heterogenen Katalyse wie beim Kristallwachstum bzw. der Kristallauflösung. Entscheidend für den Ablauf der Silikose sollen die spezifischen selektiven Adsorptionen von Partikeln des biologischen Milieus sein, die so zur Einleitung bestimmter Reaktionsketten führen, die eine Umlenkung gewöhnlicher Reaktionsketten bedeuten, nicht so ganz unähnlich dem Verlauf bei den Viruserkrankungen. Die selektiven Adsorptionen werden dabei im wesentlichen mit Strukturentsprechungen im Sinne der Epitaxie oder auch niederer Grade begründet, so dass die Vorgänge im ganzen Spannbereich zwischen Langmuir-Orientierung und orientierten Verwachsungen liegen.

Mit den feinstrukturellen Einzelheiten der Quarzgrenzflächen im Sinne dieser Theorie hat man sich bisher nicht ernstlich beschäftigt. Einige Andeutungen im Schrifttum nehmen lediglich Bezug auf die bekannten Gitterkonstanten a_0, c_0 des Quarzes. Diese zunächst notwendige Grundlage für die Erforschung aller Adsorptions- und Orientierungseffekte wird in Beispielen vorgeführt und diskutiert. Die Folgerungen scheinen wertvoll für die Beurteilung der bisher vorliegenden experimentellen Untersuchungen zur Adsorption an Quarzoberflächen. Strukturelle Beziehungen von Dimensionen der Quarzstruktur zu Molekül- und Kristallstrukturen von Molekülarten des biologischen Milieus werden untersucht.

Der direkte experimentelle Nachweise der postulierten Grenzflächenprozesse wird begreiflicherweise sehr schwierig sein. Wir sind in mehrfacher Hinsicht um solche Untersuchungen bemüht. Es sei nur gesagt, dass, wie wohl kaum anders erwartet werden konnte, einfache Versuche der Erzielung von Epitaxie bis jetzt noch nicht positiv ausgefallen sind.

6. A. V. Shubnikov. *L'antisymétrie des figures finies.*

7. S. N. Bose. *Appareil pour l'analyse des spectres d'émission transitoires. Son emploi dans l'étude de la thermoluminescence.*

§ 15b. Symétrie et morphologie; divers

1. W. Nowacki. *On the number of different space groups.*

It is shown with the aid of the *Hauptpunkte* of Weissenberg that there are 219 non-holomorphous space groups, i.e. 219 different space groups in the abstract group-theoretical sense, these groups being the 230 crystallographic space groups minus the 11 groups which occur as enantiomorphous pairs.

2. E. Tavora. *Multiplication tables for the crystallographic point-groups.*

Multiplication tables were constructed for the proper cyclic and non-cyclic point groups and for the improper ones which have a 1:1 isomorphism with the former groups. Furthermore, if properly handled, these tables may also be used for operations with the remaining improper groups of which the inversion is an element.

The highest order of the groups for which the tables were specially prepared is 24 (simply isomorphic groups 432 and $\bar{4}3m$) but, as remarked, it is possible to utilize the same tables for improper groups up to the order 48 (groups $m3m$) provided the peculiar nature of the modifications introduced is taken into account.

Defining relations based upon a maximum of three generating cyclic groups were established, which enable one to rebuild with ease any of the given tables.

The symbolism of the abstract groups was throughout used to identify their elements but its direct correspondence with that of the crystallographic point groups of the same structure (Hermann–Mauguin notation) is clearly shown.

The direct inspection of the tables provides readily interpretable information as to the nature, order and elements of the point-groups; to the isomorphism relationships; to the nature, number, order, index and ele-

ments of the subgroups; to the nature, number and order of the classes of conjugate elements and of the conjugate subgroups; to the allowed expansions of the groups in cosets; to the number of Abelian groups; to the existing Sylow groups; to the constituent elements of the intersections; to the identification of the normalizer elements and of the normalizer groups; to the invariant subgroups; to the establishment of factor-groups etc.

A tentative complementary nomenclature to the international symbolism of the point groups was suggested and largely employed and accounts for the unequivocal identification of the group elements referred to specific symmetry directions.

Either the groups of the real unitary matrices, or of the dyadic matrices which are isomorphous with the point groups and which constitute their representation of dimension 3, may be used to perform the product of elements.

From the calculated tables the determination of the irreducible representations, and consequently of the character tables, becomes a simple task.

3. S. BHAGAVANTAN. *Crystal symmetry and photoelasticity.*

Crystals of the T and T_h classes in the cubic system are expected to differ from those of the T_d, O and O_h classes in respect of their photoelastic behaviour. Many experiments have been performed and the results confirm this expectation. Similarly, crystals of the C_{3h}, C_6 and C_{6h} classes of the hexagonal system are expected to differ from those of the four other classes in that system in respect of their photoelastic behaviour. Experiments, performed for the first time with apatite belonging to the C_{6h} class, confirm this.

4. C. HERMANN. *Some crystallographic problems which are easily solved in terms of 'gitterkomplexe'.*

Gitterkomplexe (or simple representative crystal structures) are most useful for describing the properties and mutual relations of space groups. They offer a successful way of attacking the problem of homometric structures.

5. C. HERMANN. *A nomenclature for 'gitterkomplexe'.*

By extending the generally accepted descriptions of *Gitterkomplexe*, such as the translation lattices, the hexagonal close packing, or the diamond lattice, a nomenclature of all *Gitterkomplexe* will be proposed, short and descriptive enough to be useful in structural research.

6. P. HARTMAN. *Morphology of isostructural crystals.*

Crystals of isostructural compounds sometimes show different morphologies. Any geometrical theory that relates morphology to structure (e.g. the theories of Niggli and of Donnay–Harker) must fail here to give an explanation.

A qualitative explanation can be given when the bonds in the structure are considered. Different strength and different type of corresponding bonds affect the relative importances of periodic bond chains and hence the faces parallel to these chains. In this way the differences in morphology between the pairs halite–galena, aragonite–cerussite and hauerite–pyrites can be understood. In these pairs the bond type in the former mineral is more or less covalent. In each case it appears that certain zones, which were unimportant in the former mineral because of the interaction of ions with like charge, become more important in the latter mineral.

7. A. R. VERMA. *Polymorphism and polytypism in crystals with large unit cells: correlation between X-ray and interferometric data.*

SiC and long-chain organic molecules are two substances very suitable for this study of polymorphism and polytypism. Both are known to grow by the spiral mechanism of crystal growth. Formation of the different polytypes of SiC, some with very large unit cells, has been suggested by Frank to arise from the screw dislocations, whose pitch determines the size of the unit cell. Interferometric and X-ray techniques have been used for the study of SiC crystals and an attempt has been made to correlate the two data.

In the case of long-chain molecules (palmitic and stearic acids) it is observed that they occur in at least two stable polymorphs at room temperatures. These polymorphs give rhomboidal crystal plates with different profile angles. Small crystals ($\sim$ 100 microns) have been examined (*a*) by the application of multiple-beam interferometry to study their surface structure and (*b*) by fine-focus X-ray beams for the measurement of their unit-cell sizes. The X-ray data, the measured spiral step heights and other growth features can all be explained only by recognizing polytypism in addition to polymorphism in these crystals.

8. W. G. PERDOK. *On the relation between crystal structure and crystal morphology.*

Some new ideas on crystal morphology are given, relating crystal structure and crystal shape on an energy base. Anomalies in the earlier geometrical theories of Bravais–Donnay–Harker and of Niggli can be understood and often removed by applying these new ideas. Their main feature is the rule that high-energy bond chains govern the morphology rather than the highest reticular densities or the shortest distances along lattice rows.

The morphology of a crystal can be deduced from a set of periodic bond chain vectors (p.b.c. vectors), the most important zones being parallel to these vectors. The faces can be divided into three classes: F (flat) faces, containing two or more co-planar p.b.c. vectors; S (stepped) faces, containing one vector, and K (kinked) faces containing no vector at all.

The most prominent faces belong to the F faces, the K faces being not observed or very rare; the other faces are S faces.

Some examples will be given; in general it is difficult to give a quantitative order of importance for the zones and the faces, because no quantitative data on bond energies in crystal structures are available.

9. M. A. JASWON. *Structural properties of lattice planes.*

A mathematical investigation is made of the arrangement of lattice points in a lattice plane of Miller indices (*hkl*), for any type of crystal structure. Primitive vectors for the plane cannot be obtained explicitly in terms of h, k and l, but it is possible to lay down a simple proce-

dure for determining them in any given case. When one of the indices is unity, i.e. the indices are $1, k, l$, the primitive vectors can be defined in terms of k and l. The stacking properties of the (hkl) series of planes is also investigated, and admits of a general solution subject to the same limitations as for the preceding problem. The analysis is readily extended to cover the case of lattices with one or more bases.

Out of several possible applications, the results are illustrated by an analysis of atomic movements in deformation twinning. Given the plane of twinning, and not making use of the concept of a second undistorted plane, it is possible to calculate the direction and magnitude of the macroscopic twinning shear in such structures as zinc, bismuth, diamond, calcite, β-tin and α-uranium. The concomitant heterogeneous atomic movements are analysed in detail, and it is found that these are always such as to be facilitated by compressive stresses applied normally to the twinning plane. The lack of decisive evidence for a critical (twinning) shear stress is attributed to the effect of the normal stresses. In the case of c.-p.h. structures of $c/a = \sqrt{3}$, heterogeneous movements alone suffice to cause twinning; no macroscopic deformation should be observed in such cases, but the existence of a twin could be inferred by X-ray techniques.

10. H. WONDRATSCHEK. *On the description of physical properties of crystals by surfaces.*

Physical properties of crystals, which shall be described by surfaces, have to follow some conditions. A convenient description will be obtained if exactly one value of the property is related to every radius vector from the origin. The actual values of matter tensors, however, generally depend on two directions, namely on the position of the orthogonal coordinate system referred to.

Let the z axis of the coordinate system lie in the direction considered. In this case either (1) the x and y axes must be fixed by a supplementary condition or (2) the expression to be described has to be invariant under arbitrary rotations of the coordinate axes.

Let us investigate case (2). Exactly those combinations of tensor components, invariant under the rotations of the cylinder group, allow the required description by surfaces. The cylinder axis in the z direction will be represented by

$$x \to x\cos\varphi + y\sin\varphi;\ y \to -x\sin\varphi + y\cos\varphi;\ z \to z;\ \varphi < 2\pi/s;$$

where s is the order of the tensor.

A complete set of linear cylinder invariants I_v of any tensor can be obtained immediately by transformation on complex principal axes. No difficulties created by intrinsic symmetries of the tensor will arise.

The number of independent I_v can be derived most easily by the usual methods of group theory.

Cylinder invariants of higher than first degree can be derived too. Examples will be given.

The most simple surfaces may be obtained by postulating $r = \pm 1/\{|I_v|\}^{1/s}$, or applying spherical coordinates $r = I_v$.

11. R. RENNINGER. *Absolut-Vergleich der stärksten Röntgenreflexe verschiedener Kristalle.*

Die Tatsache, dass das 'integrale Reflexionsvermögen' für die Röntgeninterferenzen unter bestimmten Bedingungen, etwa solchen der symmetrischen Bragg-Reflexion einen definierten, theoretisch beherrschten Höchstwert, nämlich für den 'idealen Mosaikkristall', hat, lässt es sinnvoll erscheinen, nach einem Kristall mit dem absolut höchsten Reflexionsvermögen (für eine bestimmte Wellenlänge) zu suchen, auch in Hinblick auf die Frage nach geeignetem Material für Monochromator-Kristalle. Eine Berechnung der Absolut-Intensitäten einer Reihe von Reflexen mit Cu-Strahlung hat u.a. folgende Ergebnisse: Steinsalz (200) 31, LiF (200) 93, Pentaerythrit (002) 115, Quarz (101) 43, Al (200) 29, Cu (200) 71, Diamant (111) 120, Graphit (002) 620, jeweils $\times 10^{-5}$. Für grobe Abschätzung lässt sich eine Näherungsformel angeben, wonach die Werte proportional sind dem Netzebenen-Abstand sowie dem Quadrat der mittleren Elektronendichte, umgekehrt proportional dem Absorptionskoeffizienten. Das überragend hohe Reflexionsvermögen von Graphit (bestätigt durch Absolutmessungen an Spaltflächen von natürlichem Ceylon-Graphit) liesse diesen als idealen Monochromator erscheinen, wenn er in genügend gut gewachsenen Einkristallen zur Verfügung stünde. Dem als Monochromator vielfach verwendeten Pentaerythrit steht als gleichwertig LiF (auch NaF) gegenüber, mit dem Vorteil, dass es nicht wie jenes unter der Röntgen-Bestrahlung 'verwittert', und dass es sich durch Schleif- und Polierbehandlung auf das hohe Reflexionsvermögen bringen lässt ohne allzu grosse Einbusse an Reflexions*schärfe* (Halbwertsbreite $< \frac{1}{3}°$).

12. R. RENNINGER. *Zwei Arten der Verzwillingung von Pentaerythrit.*

Die aus wässeriger Lösung ausfallenden Kristalle von Pentaerythrit (Raumgruppe $I\bar{4}$), quadratische Doppelpyramiden oder Säulen parallel zur c-Achse, mit Querschnittkante parallel (100), sind vierfach unterteilt durch Diagonal-Flächen parallel (110). Diese Unterteilung zeigt sich deutlich an Spaltplättchen senkrecht zur c-Achse, sowohl im Ätz-Bild als im Polarisationsmikroskop. Röntgenographisch (im Laue-Bild) sind die Felder nicht unterscheidbar. Dies beweist, dass es sich nur um Verzwillingung nach der (001)-Ebene handeln kann. Ausser dieser Vierlingsbildung ist vielfach noch eine zweite Art von Unterteilung feststellbar, die sich aber in keinerlei optisch erkennbaren Grenzflächen äussert, dafür andererseits im Röntgenbild sichtbar wird und dort eine Verzwillingung nach der (100) bezw. (110) Ebene anzeigt. Die Grenzfächen dieser Verzwillingung verlaufen unregelmässig in allen Richtungen, bezw. sind möglicherweise überhaupt verwaschen.

13. R. BRILL & S. ZAROMB. *Solid solutions of* NH_4F *in ice.*

The phase diagram of ice–NH_4F was investigated by determining the solidus curve of this system. Solid solutions between ice and NH_4F are formed between 0 and about 10% NH_4F. Measurements of the dielectric constants of these solid solutions in dependency upon the concentration of NH_4F, the frequency of the alternating current and the temperature showed that the activation energy of dipole rotation in ice is lowered appreciably by the presence of very small amounts of NH_4F. At a concentration of 10^{-5} mol. NH_4F the activation energy

amounts to about 2 kcal. whereas its value for pure water is 13 kcal. The effect might be explained by the assumption of lattice distortions in ice caused by the presence of NH_4^+ and F^- ions.

14. A. J. FRUEH. *The application of 'zone' or 'band' theory to problems of sulphide mineralogy.*

The metallic or semi-metallic characteristics of many sulphide minerals, demonstrated by such properties as ductility, metallic lustre and low electrical resistivity, are evidence of the metallic nature of their chemical bonds. This justifies a limited application of the electronic theories of the metallic state to problems involving these minerals.

The important Brillouin zones, the volume of the zones and the electron-to-atom ratio necessary to fill them have been determined for some of the minerals of the copper–iron–sulphur system. With the assumption that all the outer-shell electrons of the elements of the system can contribute to the free electrons composing the Fermi body, the electron-to-atom ratios were calculated. The following table summarizes the data:

Mineral	Electron-to-atom ratio	Indices of forms determining principal zones	Electron-to-atom ratio of filled zone
Chalcopyrite ($CuFeS_2$)	4	{112}, {200}, {004}	1
		{204}, {220}	4
Bornite (Cu_5FeS_4)	3·2	{311}, {222}	0·5
		{400}	1·6
		{440}	3·2
Digenite (Cu_9S_5)	2·8	{200}	1·4
		{220}	2·9
Chalcocite (Cu_2S)	2·7	{102}, {110}	1.7
		{103}, {110}	3·3
Covellite (CuS)	3·5	{102}, {103}	0·5
		{110}, {006}	1·5

These minerals exhibit the properties of intrinsic semiconductors and therefore it is assumed that free-electron states exactly fill one of the zones, with an energy gap between the filled zone and the next higher zone. In the field from digenite to chalcopyrite the same basic structural type is maintained, despite the increase in the iron-to-copper ratio by the omission of sufficient metal atoms to avoid increasing the electron-to-atom ratio beyond the capacity of the filled zone. The existence of two structurally different types of sulphur in covellite, and possibly in chalcocite, is used to explain the apparent discrepancy between the zone capacity and the electron-to-atom ratio of these minerals.

15. K. SCHUBERT. *Über die Ortskorrelation der äusseren Elektronen in Kristallstrukturen, insbesondere bei metallischen Phasen.*

Berücksichtigt man die Wechselwirkung im Elektronengas in qualitativer Weise, so kommt man zum Begriff eines Gases mit Ortskorrelation. Idealisiert man die Ortskorrelation als Punktgitter im Raume, so gelangt man zu folgenden Forderungen an das 'Elektronenplatzgitter':

(1) Die Elektronenplätze sollen möglichst nahe den Valenzschalen der beteiligten Atome liegen.

(2) Die elektrostatische Energie des Elektronengitters soll klein sein. Es ist günstig, wenn den Elektronenplätzen Spine zugeordnet werden können derart, dass ein +Spin von möglichst vielen −Spinen umgeben ist.

(3) Die Zahl der besetzbaren Elektronenplätze soll möglichst mit der Zahl der räumlich zu korrelierenden Elektronen übereinstimmen.

(4) Die Gültigkeit von geometrischen oder dem Bandmodell entnommenen Strukturargumenten soll durch die Ortskorrelation nicht beeinträchtigt werden.

(5) An einer Ortskorrelation nehmen im allgemeinen ganze Gruppen von Elektronen teil, die durch die Zahl von im kugelsymmetrischen Einzentrenproblemen miteinander entarteten Einelektronen-Eigenfunktionen gegeben sind.

Die Elektronenplatzgitter haben lediglich symbolische Bedeutung. Es kann, aber muss ihnen nicht ein Gitter der Elektronendichte im Kristall entsprechen. Die Anforderungen bewirken, dass es nicht selbverständlich ist, dass zu einer Struktur eine befriedigende Ortskorrelation gefunden wird. Es zeigt sich, dass es auch Verbindungen gibt, in denen Elektronen die üblicherweise nicht zu den Valenzelektronen gezählt werden, an der Ortskorrelation teilnehmen. Ein solcher Bindungszustand möge Durchdringungskorrelation genannt werden, weil er dem Bindungszustand in den sogenannten Durchdringungskomplexen der Chemie der wässrigen Lösung entspricht. Für die Durchdringungskorrelation ist die vollständige Komplettierung der Edelgaschale des Komplexkerns also in unserem Beispiel des Cu nicht erforderlich.

Ebenso wie die Ortskorrelation der Atome beim Schmelzen bzw. Verdampfen eine sprunghafte Anderung erleidet, hat man auch bei der Durchdringungskorrelation solche Änderungen zu erwarten. Man kann eine grosse Zahl von Umwandlungen im festen Zustand als Aufhören der Durchdringungskorrelation bei ansteigender Temperatur deuten.

16. R. RENNINGER. *Quantitative observation of the asymmetrical Darwin–Ewald–Prins–Kohler diffraction pattern from perfect crystals.*

In experimental realization of an idea formerly published by the author (*Z. Kristallogr.* (1938), **99**, 181) measurements have been made with a triple reflexion device. The first two reflexions (from two extremely sharply reflecting crystals in (1, +1)-double reflexion) serve as source of a beam of very small angular and spectral width, used as primary beam for measuring the diffraction pattern of a third crystal, if this diffraction pattern is of greater angular width than that of the first two crystals. In this way, using the second-order reflexion of two good calcite crystals for the first double reflexion in (2, +2)-position (with at half maximum in (2, −2)-position $2\frac{1}{2}''$), it has been possible with Cu $K\alpha$ radiation to observe quantitatively the characteristic asymmetrical diffraction pattern of the first-order reflexion of calcite as calculated from the dynamical theory (width $7\frac{1}{2}''$). The kind of measuring can be signified as a triple reflexion in (2, +2, ±1)-position.

Surprisingly the cleaving faces of calcite are found to

be not parallel to the net planes. Irregularities in the orientation of the faces are no indication of parallel irregularities in the orientation of crystal blocks.

17. G. BORRMANN & H. WAGNER. *Zur Diskussion der dynamischen Theorie der Röntgenstrahl-Interferenzen.*

(1) Die planparallele Kristallplatte. (*a*) Grenzfall verschwindend kleiner Absorption. Der Strahlenfächer bei Existenz von nur einem Wellenfeld; der Fächer bei Überlagerung zweier Felder. (*b*) Grenzfall extrem hoher Absorption. Der Strahlweg des Feldes kleinster Absorption; Weg längs der reflektierenden Netzebene; Weg grösster Abweichung von der Netzebene.

(2) Der beliebig begrenzte, stark absorbierende Kristall. Der auf den Strahlweg bezogene Absorptions-Koeffizient. Kurven gleicher Eindringtiefe im Strahlenfächer. Ermittlung des Wellenfeldes kleinster Absorption, seines Strahlwegs und seines Absorptionskoeffizienten, im Beispiel des Kristallkeils. Der Halbkugelkristall als einfachstes Modell zum Studium der Röntgenoptik des stark absorbierenden Idealkristalls.

18. G. BORRMANN & G. HILDEBRANDTS. *Einige Ergebnisse der Durchstrahlung grosser Kalkspatplatten.*

Nachweis der Wellenfelder; der Strahlweg im Kristall; Messung des effektiven Absorptionskoeffizienten. Die Feinstruktur der Interferenzlinien und ihre Beziehung zum Kristallwachstum. Die Wirkung eines Temperaturgradienten auf die übernormale Durchlässigkeit.

19. C.-R. MINGINS. *Effects of granularity in titanate ceramics.*

The granular structure of polycrystalline titanate ceramics makes itself evident whenever energy is propagated through such materials, whether the energy comes by way of mechanical or thermal waves from without or by way of the internal electromechanical conversion of applied fields. Whichever may be the case, the relation of grain size to wavelength is important. When the waves are long, the granules act as scattering centers for them, but when the waves are short, the propagation process is evidently a diffusion which is dependent upon the mean free path for the energy quanta. The transmission functions for these two types of phenomena are quite different. When the crystal cells in the tetragonal phase have been left to assume free orientation, there may well be, in addition to the granular boundaries, buffer regions between domains to be reckoned with, analogous in part to Bloch walls in ferromagnetics. Mechanisms which might permit this will be discussed. Mention will also be made of other processes probably operative.

Photographs have been obtained with the electron microscope at Tufts College showing the form of the granules and giving some notion of how they fit together.

20. C. M. MITCHELL. *The derivation of the physical properties of oriented materials from the principal pole distributions.*

A method is described for calculating certain directional properties of oriented materials from a knowledge of the orientation texture and the principal coefficients of the single crystal.

It is shown that the probability distribution of the unit cell can be derived from two orthogonal principal pole distributions, of density ϱ_i and ϱ_j as

$$\sigma_{ij} = \varrho_i \varrho_j \Big/ \int_0^{4\pi} \varrho_i \left\{ \int_0^{2\pi} \varrho_j . d\delta \right\} . d\Omega \, ,$$

where $d\Omega$ is the element of solid angle about ϱ_i and δ is the angular rotation of the associated pole ϱ_j in the orthogonal plane.

Where the physical property has a tensor form, the component along a given symmetry axis in the orientation texture can be calculated, for any unit cell orientation, from the principal coefficients and, since the probability of the unit cell having this orientation is known, the mean axial coefficient can be derived. The treatment will be valid providing grain-boundary effects are not encountered.

The derivation of thermal and electrical conductivity and thermal expansion coefficients in rolled metals is described and from this a theory of thermo-elastic effects is obtained.

21. J. LIETZ. *Über die Verfärbung einiger Silikate durch Bestrahlung.*

Es wird berichtet über Färbung der Silikate Quarz, Topas, Zirkon und Kunzit durch Bestrahlung. Die Verfärbung wird teilweise durch ultraviolettes Licht, teilweise durch harte Röntgenstrahlen und γ-Strahlen hervorgebracht. Die Absorptionsmessungen erfolgten mit einem Spektralphotometer zwischen 10.000 und 2.250 Å für die verschiedenen Schwingungsrichtungen der Kristalle bei Temperaturen von $-160°$ C. bis hinauf zur Temperatur der Zerstörung der Färbung bei *c.* 300° C.

Es zeigte sich, dass die scheinbar kontinuierlich von *c.* 1,2 eV. zum Ultraviolett ansteigende Absorption bei allen untersuchten Silikaten auf die Überlagerung von 3 bis 4 glockenförmigen Resonanzbanden mit unterschiedlicher Höhe und Halbwertsbreite zurückgeführt werden kann. Das Verhalten der Resonanzbanden bei verschiedenen Temperaturen und bei Bestrahlung wird untersucht und wahrscheinlich gemacht, dass bei allen vier Silikaten durch Bestrahlung gleichartige Farbzentren entstehen.

22. E. JENSEN. *Effect of hydrofluoric acid etching on the X-ray diffraction intensity of powdered quartz.*

Quantitative determination of quartz by the X-ray powder method are usually referred to standard samples of powdered rock crystals. It has been claimed, however, that the individual crystals in such powders are not homogeneous but are covered with a Beilby layer which depresses the diffraction intensity as compared with that of crystals from which the surface layer has been removed by hydrofluoric acid etching.

To test this alleged 'non-homogenity', samples of an approximately monodisperse quartz fraction (average particle size $\sim$ 1·4 microns) were etched in solutions of increasing hydrofluoric acid concentrations. Assuming a

uniformly thick layer being removed from all particles the amounts of quartz dissolved (5–38 %) correspond to layers of 100–900 Å depth. Reflexion intensities were measured before and after the etching with a General Electric Geiger-counter X-ray spectrometer using Cu $K\alpha$ radiation and flat non-rotating samples. The lines $(10\bar{1}1)$ and $(11\bar{2}2)$ and their backgrounds were scanned at a rate of 2° per min.; line-counts minus background-counts then give the integrated intensity. The results show that etching with hydrofluoric acid has no significant effect on the reflexion intensity; it is concluded therefore that a Beilby layer thick enough to influence the X-ray reflexion intensity does not exist on powdered quartz crystals.

§ 16. Diffraction électronique

1. A. Boettcher & H. Treupel. *Einige Beispiele kontinuierlicher Gittertransformationen.*

Mit einer für die Untersuchung des Ablaufs von Gittertransformationen besonders geeigneten Elektronenbeugungsanordnung wurden die thermischen Umwandlungen der Kupfer- und Silber-Selenide und -Sulfide untersucht. Dabei wurde einerseits gefunden, dass bei einigen dieser Stoffe mehr Modifikationen bestehen, als bisher aus Röntgenuntersuchungen bekannt war, andererseits einige Umwandlungen durch die kontinuierliche Änderung von Gitterparametern gekennzeichnet sind. Umwandlungen dieser Art werden gezeigt bei Silber- und Kupfer-Selenid sowie beim Silbersulfid.

Es wird der Versuch einer Deutung solcher kontinuierlicher Gitteränderungen gemacht. Die Strukturen dieser Stoffe sind nach älteren Untersuchungen dadurch gekennzeichnet, dass für die Metallionen eine grössere Zahl von möglichen Gitterplätzen angegeben werden, als aufgrund der stöchiometrischen Verhältnisse besetzt werden können. Nimmt man an, dass die Gitterparameter einiger Modifikationen innerhalb gewisser Grenzen von der Verteilung der Metallionen abhängig sind, lassen sich die beobachteten Gitteränderungen so deuten, dass während einer Temperaturbehandlung ein langsamer Übergang der Metallionen von einer Gruppe von Plätzen auf eine andere erfolgt, der zu einer kontinuierlichen Änderung der Gitterparameter führt in ähnlichem Sinne wie bei einem Mischkristall, bei dem die Konzentration der gelösten Komponenten laufend geändert wird.

2. L. Wegmann. *Un diffractographe électronique pour enregistrement continu.*

L'intérêt pour les phénomènes de transformation de phase s'accroissant de plus en plus, la diffraction électronique en reçoit une impulsion nouvelle, car le microlaboratoire, comme M. Trillat a dénommé cette méthode, offre les possibilités les plus commodes et les plus simples pour observer de telles réactions.

Afin de pouvoir enregistrer précisément chaque transformation, Boettcher et Thun ont développé le nouveau procédé de la *diffraction cinématique*. Etant donné que l'on travaille le plus souvent avec des diagrammes Debye–Scherrer isotropes, sans texture, l'information est donnée exclusivement par les diamètres et les intensités des anneaux. Une section du diagramme en forme d'une bande effilée contenant un diamètre, renferme toute l'information.

Cette bande, pratiquement d'une seule dimension et contenant une série de points de différentes intensités, donne lieu à une deuxième dimension, qui permet l'enregistrement continu.

En pratique, une fente mobile, placée sur un diamètre du diagramme, quelques millimètres au dessus du film photographique, laisse libre cette bande étroite. Le film se déroulant dans la direction perpendiculaire à la fente, l'enregistrement consiste en une série de tangentes aux anneaux du diagramme Debye–Scherrer. Tant que le diagramme ne varie pas, les lignes de l'enregistrement continu sont parallèles à la direction du mouvement du film. Une transformation de phase se manifeste soit par une déviation de cette direction (changement des constantes du réseau), soit par l'apparition de nouvelles lignes, les anciennes disparaissant. Pour éviter des variations artificielles des lignes, la tension des électrons doit être stabilitée et l'avancement du film doit se faire bien régulièrement.

Le diffractographe électronique Trub, Tauber, qui possède tous les accessoires nécessaires pour l'examen des transformations de phase (comme par ex. les têtes goniomètriques avec chauffage et refroidissement, le canon à ions pour décharger les isolants ou attaquer les métaux) est maintenant adapté à la méthode de la diffraction cinématique.

Le nouveau dispositif consiste en une cassette pour l'enregistrement continu avec mécanismes du mouvement du film et du changement des fentes. Le réservoir du film est prévu pour 2 m. de film. La vitesse de déroulement varie entre 4 et 40 mm. par seconde. Quatre fentes de formes différentes peuvent être changées ou écartées sous vide. Conjointement avec les diaphragmes de l'anode et du condenseur électromagnétique, avec la tension et avec l'intensité de l'émission de la cathode froide, la luminosité est règlable à l'optimum pour chaque procédé.

Le diffractographe électronique Trub, Tauber, adapté à l'enregistrement continu, répond aux exigences les plus récentes de la diffraction électronique.

3. J. J. Trillat. *Sur l'enregistrement continu des diagrammes de diffraction électronique.*

En utilisant une méthode indiquée par Boettcher, on peut suivre aisément d'une façon continue l'évolution d'un grand nombre de réactions ou transformations de structures.

4. J. J. Trillat & N. Takahashi. *Étude par diffraction électronique de l'évolution des alliages légers.*

On montre comment l'évolution des alliages légers peut-être étudiée à partir de films constitués par les métaux de base après vaporisation dans le vide.

5. W. C. Bigelow & L. O. Brockway. *Electron-diffraction investigation of the minor phases of heat-resistant alloys.*

The influence of high-temperature ageing treatments on the development of minor phases in 16-25-6 and Inconel-*X*

heat-resistant alloys has been investigated. The minor phases were identified by the electron-diffraction method of Heidenreich, Sturkey & Woods (*J. Appl. Phys.* (1940), **17**, 127) and the microstructures of the alloys were studied by electron and optical microscopy. These results were correlated with the high-temperature properties of the alloys as determined by the metallurgical studies of Freeman and associates. For each alloy, specimens aged 1, 10, 100 and 1000 hr. at 1200°, 1400°, and 1600° F. were studied. The specimens were prepared for examination by special etching procedures following electrolytic polishing with perchloric acid reagents.

In the 16-25-6 alloy an $M_{23}C_6$ carbide is the predominate minor phase formed during the first few hours of ageing at each temperature. This carbide transforms to an M_6C carbide when the periods of ageing extend to approximately 10, 100 and 1000 hours for temperatures of 1600°, 1400° and 1200° F., respectively.

TiN, CbN, and $M_{23}C_6$ were identified as minor phases in all of the specimens of the Inconel-*X* alloy aged at 1200° and 1400° F. In the specimens aged at 1600° F., only TiN and CbC were identified, indicating that the $M_{23}C_6$ dissolves at this higher temperature and that the carbon released combines with the Cb, transforming the CbN to CbC. Electron micrographs also indicate the presence of a γ' phase based on Ni_3Al (Taylor & Floyd, *J. Inst. Met.* (1953), **81**, 451), although this phase could not be distinguished from the matrix phase by electron diffraction.

6. S. Yoshida. *Electron diffraction by electropolished surfaces and mean inner potentials of silver and copper.*

Electropolished surfaces of metal single crystals usually give electron-diffraction spots which are elongated towards the shadow edge. The elongation shows that the surfaces are nearly flat, but they are slightly undulating. An undulating surface is composed of minute facets which make small angles with the macroscopic surface. Kranert, Leise & Raether (*Z. Phys.* (1944), **122**, 248) estimated the angles to be $1 \sim 2°$ for an electropolished copper single crystal. However, they had to assume a certain value for the mean inner potential of copper.

In this work the author has derived a simple, approximate relation between the mean angle (δ) made by minute facets with the macroscopic surface and the mean inner potential (V), assuming a simple model for a slightly undulating surface. Using this relation, he tried to determine δ and V without assuming either of them by taking an electron-diffraction rotation photograph of an electropolished surface of a metal single crystal.

Measurements were made for (100) surfaces of silver single crystals and (100) and (110) surfaces of copper single crystals. They were mechanically polished and then electrolytically polished under proper conditions. The values of inner potentials obtained are 22 V. for silver (100) surface and 11 V. for copper (100) surface and 8–14 V. for copper (110) surfaces. The mean angle δ obtained ranges from 17° to 3° according to the condition of surfaces.

7. K. Kambe. *Simultaneous reflexions in electron diffraction.*

The dynamical theory of electron diffraction, applied to the case where two Bragg reflexions take place simultaneously, has shown that we can get information about the phases of structure factors by observing diffraction patterns of simultaneous reflexions. To illustrate the phenomenon we take up a typical case and show that the theoretical result is verified by the observation of convergent beam (Kossel–Möllenstedt) diffraction pattern. The diffraction fringes in flecks of this pattern have the form of hyperbolae near the point of simultaneous reflexions, provided the structure factors of the two reflexions V_h and $V_{h'}$ are sufficiently much smaller than $V_{h-h'}$. The theory shows that two branches of the hyperbolae lying inside and outside of the two bands (Kikuchi line pairs) of indices h and h' have the intensities proportional to $|V_h+V_{h'}|$ and $|V_h-V_{h'}|$, respectively, at their vertices.

We have used graphite as a specimen, and made two (211) reflexions occur simultaneously. There are two combinations of them, in which $h-h' = (110)$ and $h-h' = (100)$. The structure factors V_{110} and V_{100} are considerably larger than V_{211} in absolute value. When $h-h' = (100)$ the structure factors of the two reflexions have the same sign, so that the inner branch is strengthened and the outer branch weakened. When $h-h' = (100)$ the two structure factors have different signs, and the intensity relation is reversed. We found the same intensity variation at the crossing points of Kikuchi lines in both transmission and reflexion photographs.

8. S. Goldsztaub & P. Michel. *Étude de la formation d'alliages en couches minces par évaporation des constituants purs dans le vide.*

Des alliages en couches minces ont été préparés de deux manières différentes par évaporation dans le vide des constituants purs:

1°. On évapore simultanément les deux métaux purs. On constate que le mélange des vapeurs donne toujours des alliages mais généralement on obtient seulement des phases à structure simple (cubique centrée, cubique à faces centrées, hexagonale compacte). Les raies des diagrammes sont généralement floues indiquant des dépôts mal cristallisés. Par vieillissement, les raies s'affinent et les phases complexes apparaissent.

2°. On évapore successivement les deux constituants: certains systèmes seulement forment alors des alliages. On peut montrer que l'extrapolation à température ordinaire des valeurs des constantes de diffusion rend compte des résultats obtenus. La connaissance de la valeur de cette constante permet de prévoir la formation d'alliages et inversement l'obtention d'alliage permet d'en fixer l'ordre de grandeur.

9. I. L. Karle. *A new diffraction effect with electrons.*

Two previous investigations of the structure of I_2 vapor indicated that the electron-diffraction pattern was in good agreement with the usual scattering theory for electrons. From the diffraction pattern a value for the interatomic distance was determined which agreed with the result from spectroscopic investigations. Electron-diffraction photographs of iodine were taken in this Laboratory at 20 kV. and 40 kV. and it was observed that the scattering pattern differed considerably from the

theoretical expectations. The nature of this deviation was a large and easily measurable phase shift which has never before been encountered in molecules possessing like atoms. This may be a phenomenon which appears with highly polarizable substances. It does not appear in O_2 and Br_2 with 40 kV. electrons. The probable reasons why the previous authors have missed this effect are lack of sufficient data and a method of analysis which does not involve the direct comparison between experimental and theoretical intensity curves. This experimental observation is important not only because of its relationship to the analysis of diffraction patterns but also because it might add complications to the explanation of phase-shift effects in molecules composed of different kinds of atoms. A qualitative explanation for this effect can be made on the basis of the change of the electron distribution about the atoms in a molecule as the molecule vibrates.

10. Y. Morino & E. Hirota. *The generalized mean amplitudes of thermal vibration in polyatomic molecules and its influence upon the electron diffraction.*

A method of calculating the mean amplitudes, parallel, perpendicular and crossed, are derived, and James's theory on the influence of molecular vibration upon the diffraction pattern is revised.

11. L. O. Brockway. *The electron-diffraction study of organic fluorides.*

Recent investigation of the fluoromethanes by the sector-microphotometer modification of the electron-diffraction method for gases shows that the C–F distance ranges from 1·391 Å in CH_3F to 1·323 Å in CF_4. These values are compared with 1·31–2 Å previously observed in fluoroethylenes.

The effect of fluorine substitution on the C–Cl distance in CH_3Cl is contrasted with the effect of chlorine substitution. The CCl distances are: CH_3Cl, 1·784 Å; CF_3Cl, 1·753 Å; CCl_4, 1·766 Å. The decrease in the F–C–F angle to 108·5° in CF_3X compounds is compared with the increase of the ClCCl angle to 110·4° or more in CCl_3C compounds.

The effect of fluorine substitution on C–C distances is also discussed.

12. J. W. Midgley & H. Wilman. *The crystal growth, unit cell and structure of thin films of tetra-tetramethylene-tetradecane and tetra-pentamethylene-tetradecane.*

Microscopic and electron-diffraction investigations have been made on the process of crystallization of these long-chain hydrocarbons, which have recurrent cyclic side groups. The effect of rubbing the film unidirectionally is also shown.

Tetra-tetramethylene-tetradecane films formed by condensation *in vacuo* on a substrate such as polished stainless steel become retracted into lenses about 4 μ in diameter and about 4 μ apart. Electron diffraction indicates that the structure is then amorphous, with the molecules unorientated. After 10–15 min. a remarkable form of crystallization begins. One lens crystallizes, then 5–30 sec. later an adjacent lens migrates towards it and crystallizes, a similar process being repeated at irregular intervals of up to 30 sec. until the whole film has crystallized. The crystals have at first irregular shapes, and some have curved faces, but after some hours they have become block-like in form by surface diffusion. It is suggested that the lens migration occurs as a result of bombardment of the lenses by molecules diffusing across the substrate surface to the growing crystals. The migration may be assisted by the lens spreading towards the centre of heat generated by the crystallization.

In both materials, rubbing the film results in strongly one-degree-orientated crystals with no azimuthal preference. The planes parallel to the substrate have a spacing of 19·7 Å, which indicates that the molecules are orientated with the chain axes normal to the substrate, or nearly so. The lateral spacings show that the side groups of adjacent molecules must be interleaving.

13. O. Bastiansen. *Recent developments of the method of electron diffraction in gases.*

A new electron-diffraction apparatus designed and constructed at the Chemical Institute of the University of Oslo will be described. The apparatus has up to the present time been used mainly for gas work. The instrument has enabled us to increase the accuracy of our intensity determinations and to enlarge the intensity interval by a considerable amount. The result of this improvement is (1) a greater accuracy in the absolute determination of molecular dimension parameters, (2) a greater resolution power, (3) the possibility of a quantitative study of molecular vibrations. The improvements will be illustrated by examples.

14. G. C. S. Waghorn, P. T. Davies & R. W. Wilson. *Calibration of the type* EM3 *electron microscope.*

Calibration of electron microscopes for diffraction is most commonly done by reference to an internal standard, and for accurate work this is obviously highly desirable. For many purposes, however, this method may not be suitable and the procedure described below has been found to be more convenient. It has been applied successfully to the Metropolitan Vickers EM3 and depends on the fact that the magnification varies with objective lens current. Diffraction patterns are obtained of standards, for example NaCl, at a particular value of objective lens current. In dealing with samples, the pattern is first obtained in the usual way and then the objective lens current is adjusted to bring it to the fixed standard value. Although this procedure may defocus the specimen for microscopy it is shown that consistent diffraction patterns result. If the specimen is defocused too much, distortion of the diffraction pattern is observed, and it is convenient to calibrate the instrument at various values of objective lens current so that it is possible to work at a more suitable value for a particular sample.

This method may be applied to microscopy if accurate magnifications are desired.

15. H. Wilman & A. P. B. Sinha. *Some thermal transformations studied by electron diffraction.*

Electron diffraction has been used to study the reversible transformation of cuprous sulphide and silver sulphide heated *in vacuo*. Cuprous sulphide heated *in vacuo* at about 300° C. in presence of excess sulphur was first converted to CuS, then on further heating lost

sulphur and reverted to f.-c. cubic Cu_2S which was initially stable at room temperature; but after more heating and loss of sulphur was f.-c. cubic above a transformation temperature which progressively rose to a limit of about 250° C. Below the reversible transformation temperature the lattice was found to be tetragonal with about the same a axis and axial ratio 2·0. The orthorhombic structures previously described were not observed.

In the case of silver sulphide the reversible transformation from monoclinic to b.-c. cubic (a = 4·865 Å) occurred at about 180° C. in agreement with previous data. On progressive heating *in vacuo* at 180–200° C. further, little or no change in transformation temperature occurred. On heating at 350° C. to 400° C. for 1–2 min., the lattice was transformed irreversibly to f.-c. cubic (a = 5·412 Å). Similar films prepared on rocksalt cleavage faces or on pyrex glass surfaces, however, when heated at 400° C. for 5 min. were decomposed to silver.

16. H. Yoshioka. *The effect of absorption on electron diffraction.*

The effect of absorption on X-ray diffraction by crystals was studied by Molière. According to him, the effect can be represented by means of complex structure factors. Using a method similar to that of Molière, we have studied the effect of absorption on electron diffraction. In this case the effect cannot be represented by means of an imaginary part of the periodic electric potential of the crystal as it introduces into the dynamical theory a set of new complex coefficients C_{hg} which are not constant but depend upon the positions of wave points on a dispersion surface. When a Bragg reflexion is excited, the mean inner potential V_0 is modified to V_0+C_{00} for incident waves and to V_0+C_{hh} for reflected waves. The hth and $-h$th Fourier coefficients V_h and V_{-h} are modified to V_h+C_{h0} and $V_{-h}+C_{0h}$, respectively. Because of these modifications, the two waves which exist when a Bragg reflexion is excited are absorbed to different degrees. That sheet of the dispersion surface which lies on the side of the lattice origin corresponds to the rapidly attenuating wave; the other sheet corresponds to the slowly attenuating wave.

§ 17. Étude des minéraux argileux

1. J. Méring. *Conférence générale.*

2. B. Nagy & W. F. Bradley. *The structural scheme of sepiolite.*

An idealized structural scheme for sepiolite is deduced from the observed X-ray diffraction effects in the zero layer line of diagrams obtained from several natural fibres. The structure consists of a centered array of linked chains of composition $H_6Mg_8Si_{12}O_{30}(OH)_{10}$, somewhat similar to those found in attapulgite, the chains serving to enclose a second centered array of channels in which molecular water is disposed.

The $hk0$ projection is orthogonal with a = 13·4 and b = 27 Å. The skeletal chains are centered about 0, 0, z and $\frac{1}{2}$, $\frac{1}{2}$, z. Mg sites for each chain are at $x = 0$ and $y = 0, \pm\frac{1}{18}, \pm\frac{2}{18}, \pm\frac{3}{18}$, and $\pm\frac{4}{18}$. Oxygen and hydroxyl, Si, and oxygen, in layers, fill out each chain coordinated as in a mica or a chlorite, and the eight oxygens at $\frac{1}{4}$, $\frac{1}{4}$, z are each links common to two chains. The water channels are centered about $\frac{1}{2}$, 0, z and 0, $\frac{1}{2}$, z.

The disposition of the eight octahedral ions (mainly Mg) indicated by chemical analysis among the nine positions available in the schematic chain is not specified.

The quality of agreement between calculated and observed $hk0$-type intensities is illustrated. It is considered to adequately confirm the idealized section. It seems probable that the entire structure is in $C2/m$.

3. T. Sudo. *Long spacings at about* 30 Å *confirmed from certain clays from Japan.*

Certain specimens of the fireclay from the Kurata Mine, Yamaguchi Prefecture, show the X-ray powder lines of montmorillonite, disordered kaolinite, and of 29·8 kX.(±0·5 kX.). The basal reflexion of the montmorillonite is 14·7 kX.(±0·2 kX.), which is unaffected by heating at 300° C. about 1 hr., and is replaced by the 11·7 kX. line in the temperature range of 500–700° C. The 11·7 kX. line completely disappeared at 900° C. and the clay transformed to mullite at 1100° C. The 9·6 kX. line of a dehydrated montmorillonite never appeared. The treatment of the clay with ethylene glycol caused the 14·7 kX. line to be replaced by the 15·6 kX. (±0·3 kX.) line. The 29·8 kX. line completely disappeared at 300° C. and the line shifts to 32·3 kX.(±0·5 kX.) by the treatment with ethylene glycol. To account for these unusual X-ray properties as well as others, two kinds of crystal lattices were considered; one is the usual montmorillonite lattice (M-lattice) with two sheets of water molecules; its cell height is 15·5 kX.; the other is an unusual lattice (G-lattice) showing a configuration represented by a gibbsite layer interleaved between two adjacent silicate layers; its cell height is about 14·0 kX. The 29·8 kX. line is considered to be caused by a superlattice composed of these two kinds of unit cells. Similar long spacings are discovered and suggested in clays from the other several localities of Japan.

4. R. Greene-Kelly. *The structure of some montmorillonite complexes.*

The sorption complexes of montmorillonite and cyclic organic compounds have been studied by X-ray spacing measurements and one-dimensional Fourier synthesis. The results with aromatic molecules have shown that two orientations are common. The first, which is generally stable at low surface concentrations, has the plane of the ring of the molecule parallel to the plane of the silicate sheet but at higher surface concentrations the molecules often reorient so that their planes are perpendicular to that of the silicate sheet. In the latter configuration the molecules appear to avoid positioning atoms with electron excesses in contact with the oxygen atoms of the silicate sheet. Saturated ring compounds although puckered also show similar behaviour. It has been possible to distinguish between the polar and equatorial configurations of substituted alkane rings and to show that the larger of the two groups attached to a carbon atom occupies the equatorial position preferentially when the molecule is sorbed. Comparison of the results obtained with aliphatic

chains and rings have suggested that the former are also puckered when sorbed, neighbouring carbon atoms being in contact with different silicate sheets. The contact distances between the silicate sheet oxygens and the sorbed molecules have been confirmed as being shorter than the normal van de Waals distance. It has been found, however, that the calculated shortening does not vary much between complexes provided the correct structure is allocated.

5. H. Pezerat & J. Méring. *Influence des substitutions isomorphes sur les paramètres de structure des phyllites.*

Les résultats de synthèse de Fourier unidimensionnelle (projection de ϱ sur la perpendiculaire au plan des feuillets) sont donnés pour la pyrophyllite, la montmorillonite, la muscovite. Pour ces trois minéraux les taux de substitution sont respectivement: 0, 0,3–0,4 et 1. On peut donc observer les effects de la charge négative des feuillets sur les ordonnées z des plans d'atomes. Détermination précise des valeurs de z et discussion des résultats.

6. W. von Engelhardt. *Quantitative X-ray analysis of clays.*

Using recording spectrometers with Geiger–Müller-counters it is now possible to measure X-ray intensities more easily and accurately than by photographic and microphotometric methods. Therefore we have tried to develop a suitable technique for quantitative mineral analysis of clays with the Norelco X-ray spectrometer.

Examples of quantitative analyses of natural clays will be shown.

7. D. M. C. MacEwan. *Some Fourier transform methods for the study of clay minerals.*

8. M. Nakahira. *The polymorphism of sericite.*

For many of the sericite crystals from the Unnan Mine, Shimane Prefecture, Japan, there could be found both a two-layered (muscovite-type) and a three-layered (pseudo-trigonal) structure, or an intermediate type of these two.

In the intermediate structure, the (025), ($11\bar{4}$) and (114) reflexions of the two-layered structure were diffuse or disappeared, while others showed no variation in regard to positions of spots. These can be explained geometrically from the relation between the two- and three-layered types.

The structures can be explained as follows:

(1) If a mica layer be twinned on composition plane (001) with [310] as the twinning axis and then be twinned in the opposite direction with the same axis, the two-layered structure would be produced ($A\,B\,A\,B\,A\ldots$ sequence).

(2) If this twinning operation be repeated in one direction, the net result would be such that the twinning axis itself is operated by a threefold screw axis perpendicular to the layer; thus, the three-layered structure would be produced ($A\,B\,C\,A\,B\,C\,A\ldots$ sequence).

(3) The intermediate type is a mixture of these two sorts of sequence, and the diffuseness of (025) etc. of the two-layer type will depend on the frequency of the $A\,B$ sequence.

9. G. Honjo, N. Kitamura & K. Mihama. *A study of clay minerals by means of single-crystal electron-diffraction patterns.*

Electron-diffraction diagrams from individual crystallites of clay minerals were obtained by means of a three-stage electron microscope of le Poole's scheme and a shadow-microscope of Hillier & Baker's scheme.

A variety of the kaolin-group clay minerals which is distinguished by the elongated crystallites of a tubular habit of rolled sheet crystal have been studied. As expected from the habit, the diffraction diagrams of the crystallites show features similar to those of rotating single crystal. The indices of the axis of rotation, or the axis of elongation of the crystallites, were determined from the diagrams. For almost all crystallites examined this axis was the [0, 1] axis of the kaolin layer, but it was the [1, 0] or the [3, 1] axis for a few per cent of the crystallites.

The sample kaolins from different origins show different degrees of crystallization. The diffraction diagrams, however, reveal for all of them a structure having a period about 14·4 Å in the direction of the stacking of the kaolin layers, a structure which has not been reported previously. This structure was confirmed also by the X-ray powder method. It is a triclinic structure with a unit cell similar to that of kaolinite but the c-period is twice as long as that of the latter.

10. L. A. Romo & R. Roy. *Synthesis stability and properties of layer silicates.* VII. *Anion exchange and cation replacement as studied by infra-red spectroscopy.*

Utilizing the large number of synthetic layer silicates containing ions differing considerably in nature, infra-red absorption patterns have been studied with the following purposes:

1. Empirical correlation of the absorption bands due to various bonds as they are influenced considerably by the cations present in the octahedrally and tetrahedrally coordinated positions, with the structure-type remaining constant.

2. OD–OH exchange in these minerals as a function of time and temperature. At temperatures near 300° C. nearly complete exchange occurs in a few hours with all the clay minerals.

3. Confirmation of extensive F–OH exchange in the clay minerals studied at a series of temperatures by other methods including analysis, titration of exchanged OH, X-ray patterns etc.

11. U. Hofmann. *Einfluss der Kristallgestalt auf die kolloiden Eigenschaften des Tons.*

Der seit langem bekannte Einfluss der Morphologie (Kristallgestalt) der Tonmineralien auf die kolloiden Eigenschaften und die technische Brauchbarkeit eines Tons wurde an gemahlenem Kaolin (Schnaittenbacher OF) untersucht.

Durch trockenes Mahlen (I) wurde im wesentlichen der Durchmesser der Plättchen verkleinert; durch nasses Mahlen (II) wurde im wesentlichen die Dicke der Plättchen verkleinert.

Im Einklang damit ist die Änderung folgender kolloider Eigenschaften:

Das thixotrope Volumen wächst bei II stärker als bei I,

weil die Gerüste aus den dünnen Plättchen voluminöser werden.

Die Menge der austauschfähigen Kationen wächst bei I stärker als bei II, weil die Kationen bei Kaolinit bevorzugt an den Rändern der Plättchen gebunden sind.

Die Trockenschwindung wächst bei II stärker als bei I, weil die Biegsamkeit der Plättchen mit der Verringerung ihrer Dicke zunimmt.

Dementsprechend wächst die Trockenfestigkeit bei II stärker als bei I.

Die Festigkeit feuchter Massen wächst bei I und II etwa gleichmässig, weil die Zunahme der austauschfähigen Kationen die erhöhte Biegsamkeit der Plättchen kompensiert.

Die entsprechende Untersuchung von 25 verschiedenen Tonen und Kaolinen gibt einen ähnlichen Einblick in die Bedeutung der Morphologie.

12. S. Goldsztaub, S. Hénin & R. Wey. *Sur l'adsorption d'ions phosphoriques par les argiles.*

L'adsorption d'anions phosphoriques par des argiles minéralogiquement définies dépend du pH de la suspension. Dans l'intervalle de pH compris entre 3 et 6 l'adsorption est forte et présente un maximum pour pH 4. (Montmorillonite Na et Ca–Kaolinite Na et Ca). L'adsorption ne peut se faire par l'intermédiaire des cations échangeables, l'argile H adsorbe toujours plus de $PO_4H_2^-$ que l'argile Na ou Ca. Il n'y a point d'insertion de phosphate entre les feuillets de la montmorillonite dont les propriétés de gonflement restent normales. En bloquant les ions Al de la surface de l'argile par adsorption soit d'ions F^- soit d'aluminon, l'adsorption de $PO_4H_2^-$ est inhibée. Une hectorite–Na ne contenant pas d'Al octaédrique, ne fixe point de phosphate en milieu acide. La quantité d'ions $PO_4H_2^-$ adsorbée est en rapport avec le nombre d'ions Al superficiels de la montmorillonite.

Pour des pH voisins de la neutralité et pour des pH > 7, l'adsorption de phosphate dépend de la nature du cation présent dans la suspension. Il y a formation d'un composé insoluble du type hydroxy–apatite en présence de montmorillonite–Ca. Les ions Ca de la montmorillonite n'interviennent pas dans cette précipitation et l'apparition de la seconde phase cristalline n'altère point les propriétés de la montmorillonite.

13. H. R. Samson. *Flocculation characteristics of kaolinitic clays.*

A correlation has been traced between the mineralogical constitution of a series of china clays, their flocculation characteristics, and their capacity to absorb anionic dyes. The results emphasize the marked influence of the presence of traces of montmorillonite and illite on the behaviour of these kaolinitic clays, as well as variations found between different samples of pure kaolinite.

All these observations are in turn related to a new interpretation recently proposed of the distribution of positive and negative electrostatic charges at the surfaces of kaolinite crystals.

14. U. Ventriglia. *Les variations chimiques et structurales des différents minéraux des argiles.*

Dans l'état actuel des connaissances, il paraît nécessaire d'éclarcir les rapports structuraux et génétiques qu'il y a entre les différents minéraux des argiles (siallites) de façon que l'on puisse soit expliquer, soit prévoir les différentes associations naturelles ainsi qu'interpréter les résultats des synthéses. En essayant d'arriver à cet éclaircissement on parvient à la conclusion que chaque composant des argiles ne peut pas être regardé comme ayant une structure cristallographique carrément distincte de celles des autres composants; mais au contraire tous les minéraux argileux que l'on connaît forment quelques groupes seulement, que l'on peut distinguer entre eux tout au moins au moyen des leurs caractéristiques roentgenographiques. Cependant, ces groupes même, ne sont point fermés ou isolés mais ils peuvent s'entremêler. Quant aux minéraux du groupe de la kaolinite, on peut résumer les conclusions par l'affirmation que (1°) la pholérite, si l'on la regarde comme étant une siallite ayant un rapport $SiO_2:Al_2O_3$ inférieur à 2, possède la structure de la kaolinite avec une substitution partielle de Si par de l'Al; (2°) l'anauxite se distingue de la kaolinite du fait que quelques positions d'Al ne sont point occupées, et de ce fait quelques positions de (OH) ne le sont pas non plus. Quant aux minéraux du groupe de la montmorillonite, l'hypothèse de Hofmann et d'autres, de Marshall & Hendricks n'est point satisfaisante, parce qu'elle ne rend pas compte de toutes les propriétés de ces minéraux et surtout de leur capacité à l'échange des bases; on doit supposer, de préférence, une structure analogue à celle des micas (muscovite, paragonite, etc.), les montmorillonites ne se distingueraient de ceux-là qu'à cause d'un moindre nombre de Si, ceux-ci remplacés par de l'Al, ce qui aurait comme conséquence un nombre réduit de gros cationes dans la montmorillonite en comparaison des micas et par là un parfait clivage suivant (001). Cette interpretation, que j'ai avancéé dès 1945 et que les études faites jusqu'à ce jour n'ont pas contredite, paraît être actuellement la plus logique. On vient de la noter, en effet, de fraîche date dans quelques ouvrages généraux au sujet des argiles. Ce point de vue explique d'une façon intelligible l'adsorption de la part des siallites ainsi que le comportement des argiles qui renferment de l'illite seulement comme composant argileux; en effet, dans le clivage des lamelles des minéraux argileux du type séricitique les lamelles qui en dérivent auraient une distribution de l'ion K sur les surfaces (001) qui s'approcherait du type particulier aux montmorillonites: on devrait attribuer à cette distribution les phénomènes d'adsorption, de gonflement et les autres caractéristiques qui sont de même communes aux argiles illitiques.

15. R. E. Grim. *Conférence générale.*

16. R. Glaeser & J. Méring. *Isothermes d'hydratation des montmorillonites bi-ioniques* (Na, Ca).

Dans un travail récent les auteurs ont montré que les différences de comportement entre la montmorillonite-Na et la montmorillonite-Ca peuvent s'expliquer par l'impossibilité de neutraliser *localement*, par un cation bi- ou polyvalent, les charges négatives créées par les substitutions isomorphes.

Il existe toutefois un taux critique α, tel que dans une montmorillonite-fCa-$(1-f)$Na le calcium se comporte

comme le sodium aussi longtemps que f reste $< \alpha$. La valeur de α est calculable *a priori*, en admettant la répartition désordonnée des substitutions Mg → Al.

L'expérience confirme ce calcul, ce qui consolide l'hypothèse de départ sur le rôle de la répartition des charges. L'évolution des isothermes d'hydratation sous l'effet de la variation du taux f permet de préciser ce mécanisme.

17. S. Caillère, A. Oberlin & S. Hénin. *Étude au microscope électronique de quelques silicates obtenus par synthèse à basse température.*

Une méthode de synthèse de certains minéraux argileux à partir de solutions extrêmement diluées a été décrite antérieurement. Les produits préparés ont été examinés au microscope électronique.

A pH 8 ils ont l'aspect de feuilles de papier froissé assez indépendant des quantités de SiO_2 et de MgO, utilisées. A pH 9 les préparations ont l'aspect d'astérisques dû à la superposition de particules allongées. Ce sont toujours des montmorillonites.

A pH 6–7 on observe deux phases, l'une colloidale l'autre ayant l'aspect de baguettes probablement constituées par des feuillets enroulés. Le diagramme de rayons X est nettement différent du précédent; il s'agit peut-être de sépiolite.

L'introduction de fer et d'alumine à des pH variables mais toujours supérieurs à 7 donne soit des montmorillonites, soit des 'chlorites gonflantes' dont l'aspect général reste celui du papier froissé, les plis étant toutefois plus marqués.

Enfin les produits de composition Si, Al et Mg à pH 8 et en présence de KCl sont constitués par des particules en forme de feuillets étalés, leur diagramme de rayons X est celui d'un mica.

A 20° C. des composés obtenus à partir de solutions renfermant Si et Mg ont des cristallites rappelant encore l'aspect du papier froissé, mais qui se présentent avec des contours polyédriques.

A 100° C. les produits préparés en présence d'une forte concentration de NaCl apparaissent macroscopiquement comme des micas altérés, bien que la cristallisation d'après l'examen aux rayons X soit parfois nettement moins bonne que dans les autres essais, il faut encore les rapprocher des montmorillonites.

18. H. van Olphen. *Interlayer forces in bentonite.*

The forces between unit layers of a bentonite particle when in aqueous suspension are analyzed.

From experimental observations, the general qualitative shape of the net potential curve of interaction may be derived.

The long-range interaction is then computed from electric double layer repulsion and van der Waals attraction. It is concluded that there is a considerable adsorption potential of the exchangeable ions to the layer surface ($\approx$ 0·2 eV.). The consequences for ion exchange are briefly discussed.

The short-range interaction energy is computed for two models: either the adsorbed cations are unhydrated or they are at least partially hydrated. Van der Waals attraction, electrostatic interaction and hydration energies, are considered in the computation. The results are compared with the interaction curve derived from the experimental water-vapor adsorption isotherm. It appears that within the limits of the experimental results, both models are acceptable.

Although there is a correlation of bentonite hydration energy with the hydration energy of the exchangeable ions present, this would not constitute positive evidence of ion hydration. A secondary effect of the type and size of ion on the formation of ideal Hendricks' water layers, and thus of their bonding energy to the clay surface is also possible.

19. S. Caillère, S. Hénin & J. Esquevin. *Transformation expérimentale de certaines chlorites ferrifères en nontronite.*

Les 'chlorites gonflantes' ont été préparées au laboratoire en précipitant un hydroxyde entre les feuillets de la montmorillonite puis découvertes dans la nature dans des marnes du Keuper et dans les minerais de fer de Lorraine (Angevillers). Cette dernière mérite à peine son nom de 'chlorite gonflante' puisque même une ébullition prolongée en présence d'une solution de $MgCl_2$ ne lui permet pas de gonfler dans l'eau glycérolée. Un traitement déferrifiant à l'hydrosulfite de sodium transforme une partie de l'échantillon en nontronite que l'on peut reconnaître grâce à ses propriétés de contraction et de gonflement intrastructural.

Soumis à une électrodialyse prolongée, l'échantillon se transforme complètement en nontronite ainsi que le montrent aussi bien l'étude thermique que roentgenographique. Rappelons qu'une telle transformation paraît impossible avec une chlorite vraie. Au contraire les 'chlorites gonflantes' préparées par voies artificielles peuvent être aisément retransformées en montmorillonite par dissolution de l'hydroxyde précipité entre les feuillets.

Un traitement analogue a également été appliqué à une 'chlorite gonflante' provenant des marnes du Keuper et dans ce cas encore il a été possible d'obtenir un minéral montmorillonitique.

20. R. Roy. *Systematic syntheses, equilibrium thermal decomposition and phase relations of typical clay minerals.*

Under controlled conditions of temperature (up to 900° C.) and high water pressure (up to 3000 atmospheres) the various layer silicates can be synthesized with controlled compositions involving many different ions. The change of various properties such as lattice constants, morphology, 'expansion' with ethylene glycol has been studied as a function of the size and nature of ions present, for the serpentine–kaolinite group, the montmorillonite group and micas and chlorites.

The phase equilibrium relationships in the systems Al_2O_3–SiO_2–H_2O, MgO–Al_2O_3–SiO_2–H_2O and Na_2O–Al_2O_3–SiO_2–H_2O have been determined, thus determining the temperature and pressure limits of stability of endellite, kaolinite, serpentine, montmorillonites of various composition and two series of chlorites. The existence of two series of isomorphous chlorites helps to clarify several problems concerning these minerals. The bearing of these data on currently-used identification procedures for clays is discussed.

21. M. NAKAHIRA. *On the thermal transformation of kaolinite and halloysite.*

X-ray diffraction methods were used to obtain information about the so-called 'meta-kaolin' state. Specimens were heated slowly (2° C./min.) to 570° C., 700° C. and 950° C. and soaked at these temperatures for 3 hr. Supplementary specimens were heated to comparable temperatures and withdrawn without soaking to examine the variations of diffraction patterns before and after the prolonged heating.

From the variations of intensities and line profiles of such reflexions as (00l), (020), (060) and (20l), it was concluded that, in kaolinite, the x and z coordinates of all atoms and also the y's of Al atoms seemed to change easily, while the y's of oxygen atoms were not so seriously affected during the heating. This could be seen from the diffraction features that the (020) reflexion, though rather two-dimensional, always persisted clearly at about its original position, while those of (00l), (060) and (20l) were easily weakened (diffuse) or disappeared. The most probable explanation is that, in the meta-kaolin state, Si and Al atoms can easily migrate or exchange in the oxygen frameworks; the oxygen atoms themselves only move each other in the direction parallel to the b plane. At 950° C. a minor amount of mullite could be detected.

In halloysite, only a very diffuse band with its peak near 4·0 Å appeared at each of the above mentioned temperatures.

22. R. ROY. *New data on the thermal decomposition of kaolinite and the absence of an 'amorphous' stage.*

23. G. BARBIER. *Extension des échanges d'ions dans des argiles de sols par alternances de déssication et d'humectation.*

Les alternances de dessication et d'humectation provoquent tantôt un passage de K échangeable à l'état non échangeable, tantôt le passage inverse (sans doute par mise en communication temporaire de surfaces externes et internes qui ne sont pas au même niveau d'activité). L'emploi d'isotopes ($^{32}PO_4$) permet de percevoir en quelque sorte ce double mouvement en une seule opération, c'est-à-dire qu'il révèle une extension de l'autodiffusion par ces alternances (ou par ébullition). Les mêmes alternances libèrent également des ions boriques.

24. P. URBAIN. *Distinction des ions du réseau et des ions adsorbés.*

25. U. VENTRIGLIA. *La plasticité des argiles.*

La plasticité, envisagée comme une capacité à subir des déformations permanentes et visqueses, pour des efforts supérieurs toutefois à une limite fixée et finie, peut-être caractérisée par une expression du type

$$\frac{\tau^n/\eta^* - (\tau - f)^n/\eta^*}{f/G}$$

où τ est la contrainte au cisaillement, η^* la viscosité apparente, f la limite de glissement, G le module d'élasticité à la limite de glissement et n une constante. (Si l'on fait $n = 1$, η^* devient égal à la viscosité η.) Dans le domaine qui est le plus intéressant, à cause de ses applications, on peut caractériser la plasticité par le rapport $G/\eta = f/\eta\gamma_f$ (G = mobilité), où f est la limite de glissement (c'est-à-dire l'effort unitaire tangentiel τ au-dessus duquel commencent les déformations permanentes), et γ_f est la déformation qui correspond à f.

Une analyse du caractère des argiles et de leur comportement en présence de l'eau, fait voir que le mélange argile–eau correspond tout à fait aux conditions générales implicites dans le concept de plasticité, à condition que le rapport quantitatif réciproque entre la masse solide et celle liquide soit compris dans des limites convenables.

La structure réticulaire des minéraux argileux, considérée de par elle-même, mais surtout par rapport au liquide du mélange pâteux, donne la raison complète du comportment plastique des argiles, suffisament imbibées d'eau. La structure elle-même, rend compte, en premier lieu, des facteurs qui, depuis longtemps, étaient reconnus comme étant nécessaires pour la plasticité, entre autres: la forme feuillettée, la flexibilité des lamelles, leur petite dimension etc. Il faut relier la capacité des argiles de donner avec l'eau des mélanges plastiques dans le sens le plus étendu du mot (bien entendu, à condition que la teneur en eau n'aille pas au-delà de certaines limites), à la possibilité, qu'offre le type particulier de structure des minéraux argileux, de développer un lien chimique avec quelques liquides et surtout avec l'eau. Pour être à même de comprendre les variations de toutes ces propriétés et parmi celles-ci en premier lieu de la plasticité par rapport à la teneur en eau, à la qualité et à la quantité des électrolytes dissous dans celle-ci, il faut avoir recours à la théorie électrostatique des suspensions en général, avec les adaptations nécessaires au cas des suspensions des minéraux argileux du type kaolinique, montmorillonitique et micacé (séricitique ou illitique).

26. S. M. SHUAIB. *A laboratory study of the minerals in the sediment of the Tyrrhenian sea, taken from a depth of 1990 metres in the Gulf of Naples.*

27. G. KULBICKI. *Phénomènes de diagénèse dans les sédiments argileux.*

L'étude microscopique des roches argileuses en plaques minces permet de mettre en évidence des minéraux argileux authigènes formés après la consolidation des sédiments. On a pu, dans beaucoup de cas, retracer les conditions de ces néoformations.

On décrit des néogenèses de kaolinite, halloysite et dickite au sein de sédiments kaoliniques. Des passages de minéraux à trois couches à des minéraux à deux couches et réciproquement sont également étudiés.

28. E. J. WEISS & R. A. ROWLAND. *X-ray diffractometer thermal studies of dehydroxylation.*

29. V. T. ALLEN. *Formation of diaspore clays (U.S.) by secondary processes.*

In Missouri and Pennsylvania diaspore clays occur in flint clays composed chiefly of kaolinite. Diaspore replaces colliform and nodular structures in flint clays and fills cracks and pipes cutting early diaspore. Porosity provided by nodules, carbonaceous materials, and cracks allowed ground water to leach silica from flint clay and form diaspore.

30. W. A. MITCHELL. *An occurrence of saponite in vesicular lava.*

A soft green mineral occurs in vesicular cavities in andesitic lava of Old Red Sandstone age in Kincardineshire, Scotland. It is associated with calcite and quartz and is a product of late stage pneumalolytic processes. In addition to the occurrence in the vesicles, some of which are completely filled with the mineral, it also occurs in very small irregular patches in the ground mass of the rock, causing rapid disintegration of the rock on exposure when used for building and road-making. Pure material selected from the vesicles was examined by X-ray diffraction and was found to be a trioctahedral mineral of the montmorillonite group. Differential thermal analysis curves supported this identification and the cation exchange capacity was found to be 99 m. eq. per 100 g. Chemical analysis identified the mineral as saponite with the approximate formula

$$(Si_{6.7}Al_{1.3})(Al_{0.6}Mg_{4.9}Fe_{0.5})O_{20}(OH)_4.$$

After heating to 600° C. X-ray analysis showed the pattern of talc, but only if precautions were taken to prevent rehydration. On heating to 900° C. enstatite was formed.

The basal spacing of the mineral after drying at 110° C. was found to vary with the nature of the cation in the exchange positions.

31. D. CARROLL. *Clay mineral investigations in the United States Geological Survey.*

The U.S. Geological Survey is conducting research into several aspects of clay mineralogy: chemical composition of various hydrous micas and montmorillonites; ion-exchange capacity of soils, of unconsolidated sediments, and of the clay fraction (< 2-micron grain diameter); X-ray identification using a wide-angle goniometer with Geiger–Müller tube and automatic recording, as well as powder photographs; differential thermal analysis; and electron microscopy. Special features of the equipment and of the analytical methods are described.

Clay-containing materials from a wide variety of sources and geological environments are being investigated. The relationship between the kind of clay mineral and the environment is studied wherever possible. Outlines of several research projects will be discussed.

32. A. M. BYSTRÖM. *'Mixed layer' minerals from the Ordovician bentonites at Kinnekulle, Sweden.*

An investigation of the Ordovician bentonites at Kinnekulle, Sweden, has shown, that the main part of the bentonite beds consists of clay minerals belonging to the type, described as mixed layers of illite and montmorillonite in random interstratification. Two characteristic combinations of layers have been found; one type, attached to the two-meter-thick main bed, has an illite-montmorillonite proportion of 1:4, as determined from X-ray data, and the other type found in the thin beds, with a thickness of about 15 cm. each, has the proportion 3:2. Except in X-ray diffraction, the most pronounced properties in which the two types differ are the cation exchange capacity and the K_2O content, the respective values being for the first type 65 mekV./100 g. and ~ 2·5 %, and for the second type 45 mekV./100 g. and ~ 5 %. The following structure formulas have been found:

Type I: $$(Si_{7.57}Al_{0.43})(Al_{2.95}Ti_{0.02}Fe^{3+}_{0.23}Fe^{3+}_{0.08}Mg_{0.75})K_{0.43}O_{20}(OH)_4 \quad M^+_{0.58}$$

Type II: $$(Si_{7.34}Al_{0.66})(Al_{3.11}Ti_{0.04}Fe^{3+}_{0.17}Fe^{2+}_{0.06}Mg_{0.60})K_{0.86}O_{20}(OH)_4 \quad M^+_{0.36}$$

M^+ denotes an exchangeable ion and is chiefly calcium and magnesium in the proportion 4:1.

From the coarser fractions (0·06–1 mm.) of the thick bed, phenocrysts of quartz, biotite, an alkali feldspar (which is found to be a sanidine) and grains of kaolinized plagioclase have been isolated, showing that the original lava was of a rhyolitic type. The thin beds, however, seem to be genetically somewhat different and mineral fragments, except biotite, occur very sparingly. There is no sign of fresh or altered plagioclase grains, and accordingly no kaolin mineral is found in the material from these beds. It might be concluded, that the original volcanic glasses have differed, in the latter case being more rich in potassium, thus giving rise to the mixed-layer mineral with the higher content of illite layers.

33. H. HAMDI. *Mineralogical study of the alluvial suspended matter of the Nile.*

X-ray diffraction patterns, electron micrograph, and DTA classify the suspended matter of the Nile to the illitic clay mineral group. The DT curves indicate the presence of an amorphous part besides the clay mineral. Moreover, the interruptions which occur at about 710° C. in the different curves point to the formation of an intermediate stage between illite and montmorillonite.

34. C. W. CORRENS: *Conférence de clôture.*

§ 18. Données cristallographiques

1. W. PARRISH. *Recommended practice for the powder-diffraction technique.*
2. I. FANKUCHEN. *The status and aims of the A.S.T.M. Index.*
3. G. DONNAY. *Determinative tables based on cell dimensions.*
4. E. G. COX. *Some tests of single-crystal determinative tables for organic compounds.*
5. F. W. MATTHEWS. *Coordination of data-collecting efforts.*

§ 19. L'enseignement de la cristallographie

1. R. W. G. WYCKOFF. *Introductory remarks.*
2. E. G. COX. *Teaching crystallography to chemists.*
3. C. MACGILLAVRY. *Teaching of crystallography in Holland.*
4. J. D. H. DONNAY. *The difference between teaching crystallography and training crystallographers.*
5. R. PEPINSKY. *Who is a crystallographer?*
6. J. WYART. *Nomenclature cristallographique.*

COLLOQUE H. LOCALISATION DE L'ATOME D'HYDROGÈNE ET LIAISON HYDROGÈNE

1. J. D. BERNAL. *The role of hydrogen in crystals.*

Hydrogen is found in crystals in three states; as interstitial atomic hydrogen in transition metals; as non-polar hydrogen in molecular compounds such as the hydrocarbons; and as polar hydrogen in acids, alkalis and neutral polar molecules such as water and alcohols. In the first two groups it has only a small effect on the binding forces of crystals; in the last it may greatly modify them, as in ionic compounds (particularly hydrates), or dominate them, as in acids, in zwitter ions like urea and amino acids or in neutral poly alcohols. In these cases the structure is explicable in terms of hydrogen bonds. The location of hydrogen has led to a quantitative study of this bond. Its strength depends essentially on that of the field in which the hydroxy, amino or hydrofluoric group is exposed. In the free hydroxyl ion the OH distance is only 0·94 Å and this must be close to its condition in the alkaline hydroxides where the weakest hydrogen bond is 3·02 Å. In the strongest acid ion $PO_2(OH)_2$ in which the hydrogen position is accurately known the OH distance is 1·05 Å and the hydrogen bond is 2·50 Å. The strength of the hydrogen bond depends on the effective ionic charge of the hydrogen atom which increases in acids from its value of approximately $\frac{1}{2}e$ in water. Electrostatic interaction accounts for the larger part of the hydrogen-bond energy but quantum conditions serve to determine its direction, the hydrogen bond being always inclined at an angle to the polarizing direction imposed on the atom that contains it. This angle varies from 105° in water to 120° in the recently determined structure of HF. There is evidence that in addition to the concentration of electrons in the neighbourhood of the hydrogen atom other negative regions occur in the oxygen (nitrogen, fluorine) atoms disposed approximately tetrahedrally. Such considerations are beginning to explain not only the structures of hydrogen-containing compounds but also the relative ease of transfer of the hydrogen atom from one place to another in such compounds, on which depend their special electrical properties, notably ferroelectricity and capacity for catalysis.

2. W. COCHRAN. *The use of diffraction methods to study the hydrogen bond.*

Until comparatively recently, physical methods of studying the hydrogen bond were limited to spectroscopic measurements. Deductions from crystal-structure determinations were based on measurements of the distances between hydrogen-bonded atoms. The results obtained in this way are now being supplemented by direct determinations of the distribution of electrons, protons, or the potential in a bond by X-ray, neutron or electron diffraction respectively.

A comparison of the experimental techniques and of the scope and accuracy of the results obtained by these three diffraction methods for the investigation of hydrogen bonding will be made. The possibility of using similar methods to study the chemical bond in general will be discussed.

3. M. MAGAT. *La localisation de l'hydrogène dans les cristaux au moyen des méthodes spectrographiques, infrarouge, hyperfréquence, effet Raman.*

La position de l'atome d'hydrogène dans une liaison-H est liée à la nature même de cette liaison. Toutes les expériences pouvant nous renseigner sur celle-ci nous donneront donc des informations plus ou moins directes sur la position de l'hydrogène par rapport aux autres atomes participant à la liaison.

On examine successivement les renseignements fournis par la cinétique chimique, par la viscosité et l'auto diffusion des liquides, et par la dispersion diélectrique. Tous ces renseignements tendent à prouver que la liaison-H est d'origine essentiellement électrostatique, c'est-à-dire que l'atome d'hydrogène dans une liaison A–H...B se trouve sensiblement plus près de l'atome A que de l'atome B.

Des renseignements plus directs sont fournis par la spectroscopie qui permet d'étudier les modifications apportées par la liaison-H aux vibrations A–H et B–R participant à la liaison A–H...B–R et de tirer des conclusions semi quantitatives sur les distances X–H. Divers cas décrits dans la bibliographie seront discutés.

L'existence des harmoniques supérieurs et l'ensemble des autres données confirment l'interprétation de la liaison-H proposée ci-dessus.

4. J. M. ROBERTSON. *The location of hydrogen atoms by X-ray methods.*

Early work in this field was confined to the observation that structure-factor agreements could in some cases be substantially improved if allowance were made for hydrogen atoms in the positions predicted by the chemical formulae. With the development of more accurate Fourier methods, hydrogen atoms became plainly 'visible', especially in aliphatic structures, and in sections of three-dimensional Fouriers taken through the planes of aromatic molecules like anthracene. Interest now centres on more detailed work regarding charge transfer from hydrogen to carbon in different states of chemical bonding, and particularly from hydrogen to other more electronegative atoms. The method of difference synthesis as developed by Cochran in his study of salicylic acid promises to be of great importance in studying many questions of chemical interest in this connection.

5. J. M. ROBERTSON & H. M. M. SHEARER. *Acetylenic hydrogen.*

We have attempted to prepare the simplest easily crystalline compound containing hydrogen directly attached to triple bonded carbon. This appears to be ethynylacetic acid $H.C{:}C.CH_2.COOH$, m.p. 83·5° C. Unfortunately, the crystal structure is complex, with eight molecules in the monoclinic cell, the asymmetric unit consisting of two chemical molecules. A full analysis has been carried out, however, and the results show that the dimensions of the two molecules are identical within the probable limits of error, bond lengths being close to the expected values. Hydrogen bonds of 2·66 Å link the molecules in pairs, forming dimers.

The acetylenic hydrogen at the end of the linear array of carbon atoms is favourably placed for observation by two-dimensional X-ray methods, and has been located by Fourier and difference syntheses. Electron

counts based on the difference maps indicate a transfer of about 0·25*e* from the acetylenic hydrogen to the adjacent carbon. This result is probably subject to a fairly large experimental error, but may be correlated with the expected increase of the *s*-component of the carbon orbitals.

6. R. PEPINSKY. *Neutron and X-ray diffraction studies of hydrogen bonding in crystals.*

Joint neutron and X-ray single-crystal diffraction studies of hydrogen-bonded crystals at Brookhaven National Laboratory and Pennsylvania State University are discussed, with particular emphasis on ferroelectric Rochelle salt. Applications of H–D replacement in neutron diffraction are indicated.

7. H. A. LEVY. *Location of hydrogen atoms in crystals by neutron diffraction.*

Neutron diffraction is the only method of general applicability for the precise location of hydrogen atoms in crystals. Use of single-crystal methods and Fourier analysis has marked recent progress. Some recent results to be cited include confirmation of the disordered structure of ice, ordering of hydrogen atoms in low-temperature KH_2PO_4, and the hydrogen location and thermal motion in urea, oxalic acid dihydrate, and iodic acid. Some observations relative to the thermal motion of hydrogen atoms will be described, and a correlation between O–H distance and the length of O–H · · · O hydrogen bonds will be presented.

8. J. P. MATHIEU. *Étude sur l'orientation des liaisons* OH, NH, CH, *dans les cristaux au moyen des spectres Raman.*

La légèreté de l'atome d'hydrogène fait que le concept de fréquence caractéristique est correct pour les radicaux NH, CH, OH. On peut mettre à profit cette remarque pour localiser ces liaisons dans les cristaux par l'étude du spectre Raman de monocristaux dans des orientations diverses, en polarisant la radiation excitatrice et en analysant le rayonnement diffusé.

(1) Dans le chlorure et le bromure d'ammonium (type NaCl), les ions tétraédriques NH_4 ont leurs axes ternaires parallèles à ceux de la maille. Dans l'iodure d'ammonium (type CsCl) un axe ternaire du tétraèdre est parallèle à un axe quaternaire de la maille et la structure cubique n'est réalisée que de façon statistique.

(2) L'orientation des liaisons C–H dans les cristaux d'acide tartrique a pu être déterminée et s'accorde avec la structure de Beevers & Stern.

(3) De la même façon, on a pu distinguer dans l'acide tartrique les atomes d'oxygène des groupes C–OH et ceux des groupes C=O. On a pu déterminé l'orientation des molécules d'eau dans des cristaux hydratés où elles ne sont pas trop perturbées par le champ cristallin local: perchlorate de lithium, acide oxalique, chlorure cuivrique, mercurichlorure de potassium.

9. A. N. LOBATCHIOV. *Détermination par diffraction électronique de la position des atomes d'hydrogène dans les cristaux d'urotropine.*

10. W. A. WOOSTER. *Evidence on the position of hydrogen atoms from the physical properties of crystals.*

The amount of hydrogen present in crystals is usually rather small and the physical properties do not depend on the hydrogen atoms alone. It is, therefore, necessary to infer from a number of hydrogen-containing crystals the nature of the specific contribution of the hydrogen atoms. A hydrogen atom placed in a structure between two oxygen atoms frequently gives rise to abnormal properties which can be partially explained in terms of the movement of the hydrogen atoms along the line joining the two oxygen atoms. This applies to infra-red absorption spectra, and in a less direct way to the dielectric, piezoelectric and elastic properties of a number of hydrogen-containing crystals. This paper consists of illustrations of this relation between the positions of hydrogen and oxygen atoms and the various physical properties of a number of substances.

11. V. VAND. *Contribution to the wave-mechanical treatment of hydrogen bonding.*

If it is assumed that in hydrogen bonding the π electron orbital is excited on the hydrogen, the hydrogen bond can be treated by the method of the molecular orbital approximation, and some degree of 'resonance' is then found to extend across the bond. The difficulties are the assignment of the correct Coulomb and overlap integrals for the hydrogen.

However, the excitation of the π electrons on free hydrogen requires quite a high energy, so that in practice this orbital can be considered empty at room temperature. The presence of neighboring atoms, such as oxygens, when the hydrogen bond is formed, would lower this energy considerably. The energy would be a function of distance; but the question arises whether in the normal hydrogen bonds this is enough for the excitation.

This point can be examined by considering the electrical conductivity of a substance in which hydrogen bonds, if resonating, would form continuous resonating paths.

12. D. HYNDMAN. *The location of the hydrogen atoms in urea by the nuclear magnetic resonance method.*

The nuclear magnetic resonance spectrum from the protons in a single crystal of urea, $OC(NH_2)_2$, has been studied at room temperature for a series of orientations of the crystal with respect to the applied magnetic field. The width and shape of the spectrum are mainly determined by the magnetic dipolar interaction between the protons, which depends strongly on their separation and their angular disposition in the applied field. From an analysis of the mean square width and the shape of the observed spectra it has therefore been possible to derive information concerning the positions of the protons in the unit cell. In particular, the results obtained support an entirely planar structure for the molecule.

13. L. E. DRAIN. *Nuclear magnetic resonance in the ammonium halides.*

The magnetic resonances of the hydrogen and fluorine nuclei in polycrystalline ammonium fluoride have been investigated as a function of temperature in the range, 100–350° K. Both resonances show line-width transitions at about 300° K., a temperature much higher than those

of the corresponding transitions in the other ammonium halides. Below the transitions, the mean square widths of the H and F resonances are about 58 gauss^2 and 33 gauss^2 respectively. The width of the fluorine resonance is particularly dependent on the H–F distance in the crystal. The results are consistent with the supposition that the protons lie along the N–F bonds. The line widths above the transition indicate that the ammonium ion can change its orientation between its possible equivalent positions. The potential barrier to this motion (about 10,000 cal./mole.) gives an indication of the strength of the N–H–F bonds.

14. G. E. Bacon. *Some considerations in single-crystal neutron diffraction measurements.*

As a preliminary to the construction of a two-dimensional projection of sodium sesquicarbonate from neutron-diffraction data, a study has been made of the information regarding the hydrogen atoms that can be obtained from a line synthesis. The substance may be considered as an example of a less symmetrical structure in which X-rays have located all atoms other than hydrogen and where significant information regarding the latter is given by quite simple neutron measurements. Line syntheses using sixteen orders of reflexion by the $h00$ planes establish the hydrogen atom at the centre of symmetry and suggest the positions of the hydrogen atoms in the water molecules. Although the coherent scattering amplitude of hydrogen atoms is not inferior to that of Na, K (and many other atoms), large thermal vibrations may limit the accuracy with which they may be positioned in this and other structures.

15. T. R. R. McDonald. *The electron-density distribution in ammonium hydrogen fluoride.*

An account is given of an accurate three-dimensional analysis of ammonium hydrogen fluoride NH_4HF_2. The diffraction data were obtained with an X-ray Geiger-counter spectrometer and supplemented with photographic intensity measurements. The absolute scale was established experimentally by comparison with a standard crystal.

The object of the investigation was to determine the fine structure of the HF_2 ion and, in particular, to locate the hydrogen atoms. The results indicate that they are situated centrally between the fluorine atoms, no departure from spherical symmetry being detectable in their electron-density distributions. This result has also been established elsewhere by neutron diffraction and infra-red spectroscopic investigations. The additional evidence which the X-ray method affords about the electron distribution is discussed in the light of present views on the resonance state of the HF_2 ion.

There is also evidence for a very marked anisotropy in the thermal vibration of the fluorine atoms, the direction of maximum vibration being, in each case, perpendicular to the mean plane of the hydrogen bonds.

16. W. C. von Dohlen & G. B. Carpenter. *The crystal structure of the high temperature form of isocyanic acid.*

The structure of the HNCO molecule in the vapor is well known: N–C–O linear and H–N–C angle about 128°. The crystal structure was determined in order to discover the manner of packing and the function of the hydrogen atoms.

Single crystals were grown in capillaries, and powder, rotation, and oscillation photographs were prepared at about −125° C. The crystals are orthorhombic with $a = 10{\cdot}82$, $b = 5{\cdot}23$, $c = 3{\cdot}57$ Å. The space group is $Pnma$ or $Pn2_1a$ with 4 molecules per unit cell.

The structure was solved by Patterson projections and was refined by Fourier and three-dimensional least-squares methods. The final discrepancy factor, for observed reflections only, is 9·3 %; H contributions decrease this figure slightly.

Although it was not possible to obtain reliable direct evidence for the positions of the H atoms, indirect evidence, including infra-red spectra, indicated the following conclusions. The expected N–H · · · O hydrogen bond fails to form, but instead N–H · · · N bonds are present. The positions of the heavier atoms are consistent with space group $Pnma$; this is correct if the H atoms are disordered, but $Pn2_1a$ cannot be definitely excluded.

Powder photographs and infra-red spectra show the existence of a second modification, stable below about −100° C. (but the high-temperature form supercools very readily). The structure is unknown but the spectrum indicates the presence of a much stronger hydrogen bond than in the high-temperature form.

17. V. Luzzati. *Le rôle des atomes d'hydrogène dans la structure des acides nitriques anhydre et hydratés.*

Les dimensions du groupement NO_3 des trois espèces cristallines HNO_3, $HNO_3.H_2O$ et $HNO_3.3H_2O$ sont intermédiaires entre celles de la molécule HNO_3 à l'état gazeux et celles de l'ion NO_3^-: ces dimensions tendent vers celles de l'ion avec l'augmentation du taux d'hydratation. On trouve dans ces cristaux trois espèces d'atomes d'oxygène de l'eau: une est caractérisée par une disposition tétraédrique des liaisons hydrogène, avec deux atomes d'hydrogène attachés à l'oxygène, dans la deuxième l'atome d'oxygène échange trois liaisons hydrogène, qui forment une pyramide aplatie, deux atomes d'hydrogène étant attachés à l'oxygène, tandis que dans la troisième trois atomes d'hydrogène se trouvent à courte distance de l'oxygène, les trois liaisons hydrogène formant une pyramide aplatie. Ces observations indiquent que des interactions profondes s'échangent entre les molécules d'acide et d'eau, par l'intermédiaire des liaisons hydrogène.

18. J. A. A. Ketelaar. *Le spectre infra-rouge de* KH_2PO_4 *et* KD_2PO_4.

Le spectre infra-rouge étudié en absorption et en réflexion à la température ambiante et au dessous du point de Curie ne montre pas de changements essentiels dans les bandes dues aux vibrations de valence et de déformation du groupement OH.

La vibration de valence trouvée en absorption à 2750 cm.$^{-1}$ (KD_2PO_4: 2060 cm.$^{-1}$) à 20° C. a la même fréquence dans l'état ferro-électrique.

Alors la liaison O–H · · · O isolée aussi ne change pas et les distances O–H · · · O doivent rester les mêmes. Il n'est pas question d'un changement d'une liaison symmétrique en liaison asymmétrique ou de l'arrêt d'une rotation. Ce résultat est tout à fait en accord avec les résultats les plus récents sur la diffraction des neutrons

par Pease & Bacon (*Proc. Roy. Soc.* A, (1953), **220**, 397; *Nature, Lond.* (1954), **173**, 443) pour la distance OH et avec les résultats de Frazer & Pepinsky (*Acta Cryst.* (1953), **6**, 273) sur la distance O–O et avec la discussion de Megaw (*Acta Cryst.* (1954), **7**, 187). L'absence du premier harmonique est un phénomène caractéristique pour les fortes liaisons hydrogène, dû au caractère quasi-symmétrique de l'énergie potentielle pour les niveaux supérieurs. La vibration de déformation OH située à 1575 cm.$^{-1}$ ne se déplace à basse température qu'à 1540 cm.$^{-1}$.

À de plus grandes longueurs d'onde nous trouvons pour KH_2PO_4 à 20° C. trois bandes: 1290, 1092 et 885 cm.$^{-1}$ (réflexion (vecteur électrique $\perp z$)); 1299, 1098 et 913 cm.$^{-1}$ (absorption) (C. La Lan, (1947), thèse, Amsterdam; J. J. Oberley & G. Weiner, *J. Chem. Phys.* (1952), **20**, 740).

Avec la polarisation perpendiculaire à l'axe z il n'y a pas d'autres changements avec le refroidissement qu'une augmentation de l'intensité. Pour l'autre direction de polarisation à basse température il n'y a que des traces très petites de bandes de réflexion qui probablement ont leur origine dans la polarisation incomplète. À la température ambiante il y a une réflexion intense à 867 cm.$^{-1}$ avec une faible bande secondaire à 1025 cm.$^{-1}$.

La bande centrale doit être la vibration triplement dégénérée ν_4 du tétraèdre PO_4. Les deux autres bandes ne peuvent pas être considérées comme dues à l'abolition de la dégénérescence par le champ cristallin, parce qu'elles se trouvent dans la même direction de polarisation.

Dans le KD_2PO_4 La Lau a déjà remarqué qu'on trouve la bande centrale à la même place exactement que dans KH_2PO_4, mais que les deux autres se sont déplacées symmétriquement vers la bande centrale dans un rapport approximativement $\sqrt{2}:1$.

Maintenant nous avons trouvé en plus un dédoublement.

L'origine de ces bandes à côté de la bande centrale est un problème intéressant parce qu'une explication qui la rapporte à la somme et la différence de la fréquence ν_4 avec une fréquence liée avec l'hydrogène n'est pas en accord avec le comportement à basse température.

19. K. FAJANS. *Quantum states and functions of hydrogen in molecules and crystals.*

The functions of hydrogen in determining the polarity and other properties of molecules and crystals depend on the type of quantization of the electrons which bind the proton to other nuclei or atomic cores.

1. An electron pair is quantized with respect to a single nucleus H^+, i.e. forms an atomic orbital; then $H^- = (H^+)1^2$ is the negative pole of the M^+H^- dipole and the degree of polarity $p = \mu(er)^{-1}$ in the $M \rightarrow H$ direction depends on the strength of the polarizing field of M^+.

2. A group of electrons forms a molecular orbital, i.e. is quantized with respect to a proton *and* one or more nuclei or cores, as in $H_2O = (2H^+, O^{6+})2^8$. Considering, for example, H_2O as the result of interpenetration of H^+ into $(HO)^- = (H^+, O^{6+})2^8$, one sees that the field of H^+ is less effectively screened the smaller the electronic polarizability of the system which it penetrates.

Such an incompletely screened proton attracts negative regions of adjacent groups and can act as an intermolecular bridge. Since the polarizability increases in the series $F^- < (RO)^- < (R_2N)^-$, the proton field is screened least in HF which in fact forms the strongest proton bridge. The asymmetry of the proton position in a bridge $X^- - H - - - - X^-$ can be expected to increase with the polarizability of X^- and is undetectable only in the case of $F^- - H^+ - F^-$.

20. A. R. UBBELOHDE: *Localisation of the hydrogen atom in the hydrogen bond in crystals.*

COLLOQUE P. MÉCANISME DES CHANGEMENTS DE PHASES DANS LES CRISTAUX

1. A. GUINIER. *Généralités sur les changements de phase dans les cristaux.*

La *thermodynamique* definit les conditions générales des changements de phase, indépendamment de toute considération structurelle.

Buerger a classé les types de transformations subies par la *structure cristalline*: (1) disposition des seconds voisins, par deformation ou reconstruction, (2) désordre entre les motifs, par rotation ou substitution, (3) motif des premiers voisins par dilatation anisotrope ou reconstruction, (4) type de liaison.

Les mouvements des atomes pendant la transition se font par *diffusion* et propagation de *dislocations*. Les deux types extrêmes de mécanisme sont la transformation brusque par glissement et le processus de formation et croissance des germes.

2. A. GUINIER. *Processus de la précipitation dans une solution solide sursaturée.*

La ségrégation des atomes dissous en excès résulte d'une diffusion de ces atomes et de la formation du germe d'une nouvelle phase dans les domaines enrichis. A basse température, le germe du précipité d'équilibre ne peut pas se former. D'où l'apparition de un ou plusieurs processus intermédiaires, de degré de cohérence avec la matrice décroissant: *zones* et *précipités orientés* en structure de Widmanstätten. La complexité des propriétes des alliages durcissants est due à la superposition des differents mecanismes de décomposition. On passe de l'un à l'autre par l'action du temps, de la température, et aussi par écrouissage ou addition d'impuretés.

3. B. E. WARREN. *X-ray studies of order–disorder in alloys.*

Long-range order produces superstructure reflections, and the long-range-order parameter S is obtained from their integrated intensities. Short-range order produces modulations in the Laue monotonic scattering. The modulated scattering is periodic in reciprocal space, and when represented as a Fourier series, the coefficients give the short-range-order parameters α_1. Measurements of the long-range-order S, as a function of temperature, are available for representative alloys such as CuZn, Cu_3Au, CuAu, and CuPt. Short-range order above T_c has been measured for Cu_3Au and less completely for AuAg, CuAu and CuPt. No satisfactory measurements are as yet available for short-range order in a β-brass type

structure. Short-range-order measurements in both CuAu and CuPt indicate a layer type of short-range order which is related to the long-range order. Most of the short-range- and long-range-order measurements have been made close to the simple stoichiometric compositions. Recent measurements in various laboratories, at other than the stoichiometric compositions, clearly indicate the existence of two-phase regions containing ordered and disordered material in equilibrium.

Three origins of the driving force for ordering are usually discussed: (*a*) a reduced interaction energy for unlike nearest neighbors (*A* loves *B*), (*b*) a reduction of the strain energy resulting from atoms of different size, (*c*) a reduction in the electronic energy by changes in the Brillouin zones. The 'size effect' diffuse scattering demonstrates the difference in size postulated in (*b*). In the ordering of CuPt there is no increase in the number of unlike nearest neighbors, (*b*) and (*c*) can apply but not (*a*) for nearest neighbors. The ordering of the complex orthorhombic CuAu II may be an example of (*c*). Most of the theories are based on assumption (*a*), and their success may be due to the fact that the constants involved partially include effects of (*b*) and (*c*).

For obvious reasons, the X-ray studies have concentrated on the measurement of order in samples in equilibrium. There are but few examples of the X-ray study of the kinetics of ordering, the earliest is perhaps the observation of broad superstructure reflections due to antiphase domains. The kinetics of order is still largely unexplored, and it deserves serious efforts in the next few years.

Mécanisme de transition du type martensitique

1. M. Cohen. *The nature of martensitic transitions.*

2. T. A. Read. *Recent theories of martensite crystallography.*

The various theories recently proposed to account for the observed habit planes, orientation relationships and macroscopic distortions in terms of crystal lattice properties will be summarized. A common feature of all these treatments is the provision for inhomogeneity of the distortions accompanying transformation; various methods which have been used for describing this inhomogeneity will be contrasted. Experimental studies have established that for certain martensite reactions the inhomogeneity can be represented as a shear on a unique plane and in a unique direction of either the parent or product lattice. In the cases where the plane and direction are known, corresponding to either slip or twinning, the method of analysis of Wechsler, Lieberman & Read provides a definite and unique method of calculating habit plane, orientation relation and macroscopic distortion. A new graphical method of carrying out this analysis will be described.

In conclusion, the present status of our knowledge of the type of inhomogeneity involved in the martensite reactions of iron-base alloys will be summarized.

3. B. A. Bilby. *The rôle of dislocations in transition processes.*

Groups of dislocations, such as exist at the end of stopped slip bands, may on occasion nucleate deformation twinning and martensitic transformations. The habit phenomena in the latter are, however, apparently controlled by other factors. Cracks under shear, deformation twins, kink bands and martensite plates all have stress fields similar to these dislocation groups, and any one of them may initiate any of the others. It is possible in this way to explain twinning near a cleavage crack, and to interpret 'burst' phenomena.

The interface separating the transformed and untransformed regions in a transition process is an array of dislocations. Some subtleties are involved, however, in defining the dislocations in such an interface. A general topological property ensures that suitable generating nodes will always exist between any two lattices. Such a description of the motion of the interface is clearly most appropriate when it approximates to a rational plane of low index, and there are some indications that such interfaces are relatively immobile. This topological property may enable transition products to grow from stacking faults or imperfect dislocations of the parent structure. When the interface is not a plane of low index, its motion is more appropriately described in terms of an array of dislocations moving on planes intersecting it. Such a description focuses attention on the type of coherency of the interface and provides a model for calculating some of its properties. Applied to martensitic transformations it permits a discussion of habit plane phenomena which is complementary to the phenomenological treatments using matrix algebra.

4. M. A. Jaswon. *The nucleation problem in the austenite–martensite transformation.*

Nucleation theory requires the existence of metastable martensitic embryos in austenite, which nucleate into martensite plates on quenching. These embryos are identified with 'half-twinning' dislocations of Burgers vector $a/12\langle 112\rangle_\gamma$, and have the effect of producing a body-centred tetragonal structure (α') when they become active for slip. Dislocation movements are readily initiated and propagated, involve little activation energy, and (owing to the reduced damping effect of lattice vibrations) are completely uninhibited by lowering of temperature. We thus understand at once many of the characteristic features of the transformation, including the significant fact that martensite forms preferentially to more stable phases separating out by the usual diffusion processes.

The intermediate structure α' is unstable relative to the final b.-c.c. structure (α), but may be transformed into the lattice by the movement of 'half-twinning' dislocations of the form $b/12\langle 111\rangle_\alpha$. These are most probably created at the interface between α' and untransformed γ by stress concentrations arising from the disregistery of the atoms and the volume and shape misfit of the transformed region. The appearance of irrational habit planes, and the existence of isothermal martensite, is discussed and it is concluded that martensite transformation is a mode of plastic deformation akin to slip and twinning, and taking place by essentially the same kind of mechanism.

5. E. Scheil. *Messung der Umklappzeit bei der Martensit-Bildung.*

6. C. Crussard & O. Krisement. *Étude dynamique de la transformation martensitique.*

Dans les aciers et quelques alliages, la 'martensite' apparaît sous forme de petites plaquettes dont la croissance est extrêmement rapide, comme l'ont montré Scheil et, plus récemment, Bunshah & Mehl.

A cause de cette rapidité, négligée jusqu'ici par les théoriciens de la transformation martensitique, la formation des plaquettes de martensite produit un échauffement local et temporaire. Partant de ces considérations l'un de nous a construit une *théorie adiabatique de la transformation martensitique.*

On peut perfectionner cette théorie en tenant compte de l'énergie cinétique des atomes lors de la transformation; la transformation martensitique apparaît alors comme une onde explosive ou *onde de choc et réaction.*

Le front de cette onde se propage plus vite que le son, ce qui peut expliquer la forme des courbes enregistrées par Bunshah & Mehl.

De même qu'il existe pour les ondes explosives un régime suprasonique et un régime de déflagration plus lent, bien distincts, de même on est amené à distinguer les *transformations martensitiques véritables*, à vitesse de croissance de l'ordre de la vitesse du son, des *transformations pseudo-martensitiques*, beaucoup plus lentes.

Du point de vue cristallographique, dans les premières le mécanisme exact n'a pas d'importance, car l'énergie au front de l'onde est telle qu'elle est toujours capable de transporter les atomes dans une nouvelle position d'équilibre, en *créant* des dislocations au besoin, pour l'adaptation plastique des tensions internes. C'est dans la transformation pseudo-martensitique par contre qu'entrent en jeu les mécanismes compliqués imaginés à l'heure actuelle (double glissement, macles répétées, etc.).

7. H. Knapp. *About the temperature hysteresis and nucleation of austenite–martensite transformation.*

A driving force, i.e. a difference in free energy, of 290 cal./mol. in Fe–C and 200 cal./mol. in Fe–Ni, respectively, is necessary to start the transformation. As the displacement of the atoms in a martensitic reaction is exactly defined by the mechanism of the transformation, and as coherency exists between the new phase and the matrix, the distortional energy can be calculated by solving a boundary problem of theory of elasticity.

The martensite plates were considered as ellipsoids; elliptic functions could be used. At the moment of their first appearance the plates are small; that means that only elastic strains will occur and that the fields of tension will not interact.

The energy of distortion in austenite depends on the ratio of the thickness to the diameter of the martensite plates. The shape of small plates was determined by estimating the most favourable shape that forms, corresponding to a surface energy produced by an interface of parallel screw dislocations. The resulting strain energy of 200 cal./mol. and more explains the great hysteresis of the transformation.

There is some evidence that martensite nuclei must already be present in austenite, and it was proposed that stresses caused by dislocations may initiate the transformation. It can now be shown that the strains of two dislocations will transfer a small volume of austenite directly into the structure of martensite, thus producing a nucleus above the transition temperature similar to the nuclei in Co.

By a dislocation in the (111) austenite plane the close-packed $[1\bar{1}0]$ rows will be arranged like the close-packed rows in martensite. If a second dislocation in a (110) plane crosses this area the shear-like distortion near the dislocation line will produce the final martensite structure and transformation can begin from this nucleus as soon as the driving force can do the deformation work.

8. L. S. Birks. *Prediction of phase transformation in steel during cooling.*

An especially constructed X-ray diffraction instrument was developed for studying the phase transformation in polycrystalline metals under variable conditions of temperature and stress. It was found that neither the standard isothermal transformation diagrams nor ordinary cooling-curve diagrams could be used to predict the bainite transformation in steel. A new method for predicting the transformation was developed based on relating the phase change to the *rate of cooling* through a critical temperature region rather than the total time required to reach a given temperature. This relation may be expressed as

$$\frac{1}{v_T}\frac{dv_T}{dt} = f\left(\frac{dT}{dt}, T\right),$$

where

T = temperature, t = time, v_T = relative amount of the high-temperature phase present at temperature T.

Values for substitution in this relation are obtained from the X-ray instrument from a few linear cooling rates, and the relation is then used to predict the transformation under practical conditions. Close agreement is obtained between predicted and observed results. The effect of stress on the transformation is separated from the effect of temperature change and the relative importance of the two is evaluated.

9. Z. Nishiyama. *Recent work on martensitic crystallographic transitions in Japan.*

Takeuchi, Suzuki & Homma (Tohoku) have observed two types of the martensitic transformations in Fe–Ni alloys by means of the resistance measurement and the moving-picture microscope. One of them has a slow propagation speed of the order of 2×10^{-3} cm.sec.$^{-1}$ and the other a fast one of more than $5\sim10$ m.sec.$^{-1}$. Therefore they considered them to correspond to *Schiebung* and *Umklapp* transformations, respectively (Förster & Scheil). On account of these facts, Suzuki proposed two mechanisms for the development of martensite transformation.

Nishiyama and his co-workers (Osaka) have found by electron microscopy that the martensite crystal appearing on the etched surface of quenched white pig iron, has a sub-structure consisting of parallel bands, having a spacing of $0{\cdot}2\sim0{\cdot}3\ \mu$ and sometimes $2\sim3\ \mu$. They are

very similar to those formerly found in the tempered martensite. In some crystals the mid-rib itself is broken into steps with a similar spacing as that of the parallel bands. In Fe–30% Ni alloys electrolytically polished and then quenched in liquid air, the surface shows the relief effect of the martensite crystal consisting of parallel needles. These needles look like twins. The needles, sometimes, have small steps through which parallel markings pass, as if slipping has occurred crossing the needle. The sub-structures have also been found in Co–Ni alloys by Homma (Tohoku). The rôle of these sub-structures on the mechanism of martensitic transformation will be given.

Transformations dans les alliages; phénomènes de précipitation

1. K. W. Andrews. *The transformation $\gamma \rightarrow \alpha$ in certain iron alloys.*

There is evidence from published work that the transformation austenite to ferrite (martensite) may occur in different ways under different conditions. The mode of transformation by cold working of polycrystalline materials is difficult to establish (unless examination of chosen individual crystals is possible).

An examination has been made of the preferred orientation effects in stainless steel wire (18% Cr, 8% Ni). The predominant γ-austenite phase orientation is [111]. The orientation of the α-ferrite phase, which is produced by the cold work during wire drawing, depends upon that of the parent γ-phase lattice. There is a mutual relationship of the two lattices resulting from the transformation mechanism. Four possible lattice relationships were considered: (i) Kurdjumov & Sachs, (ii) Nishiyama & Wassermann, (iii) Neerfeld & Mathieu, (iv) Greninger & Troiano. The best agreement between the calculated diffraction pattern and that actually obtained was found for the second of these relationships. The orientation is not perfect and the appearance of the intensity distribution round a diffraction ring can be affected by the degree of departure from ideal orientation. The direction for the ferrite phase parallel to [111] is not generally given by integral indices.

2. H. Wilman. *Electron-diffraction evidence on the mechanism of the $\alpha \rightarrow \gamma$ transformation in iron.*

Unidirectional abrasion of an electropolished, nearly (110), face of an α-iron crystal of low carbon content led to a surface layer of randomly disposed α-iron fragments, but after about 45 sec. etching in 1% picric acid in alcohol, randomly disposed γ iron crystals were exposed. Further etching removed this and exposed the usual layer of rotationally disturbed α iron, the rotation decreasing with progressive etching until when this was all removed, the electron diffraction spot patterns showed γ iron strongly orientated relative to the main α-iron crystal which was also partly exposed.

The main orientations of this γ-iron (apart from {111} twinning), which were independent of the direction of the abrasion, were such that a $\{111\}\gamma$ plane was inclined at 5° to $(110)\alpha$, with a $\{110\}\gamma$ plane normal to $(110)\alpha$ and to a cube diagonal in this plane. More simply, this is of the type: $(001)\gamma$ parallel to $(01\bar{1})\alpha$, and in this common plane $[\bar{1}10]\gamma$ is parallel to $[\bar{1}11]\alpha$. This differs from the Kurdjumov–Sachs and Nishiyama relations for the $\gamma \rightarrow \alpha$ transformation on quenching austenite and 30:70% Ni–Fe, respectively. The presence of {110} facets on the underlying α iron indicate, together with these orientations, that the γ–α interface was $\{110\}\alpha$, i.e. $\{001\}\gamma$. This suggests that in the transformation the centred $\sqrt{2}$-rectangular atomic array in this plane becomes a centred square array in the γ iron, as a result of a homogeneous shear of $\{211\}\alpha$ planes along $[\bar{1}11]\alpha$, combined with a homogeneous 6·0% extension along $[211]\alpha$; a subsequent homogeneous contraction of 13·4% along the normal to this plane, i.e. $[01\bar{1}]\alpha$ or $[001]\gamma$, converting the f.-c. tetragonal lattice ($c/a = 2/\sqrt{3} = 1{\cdot}155$) to f.-c. cubic. The net atomic movements in this process are along $\langle 111\rangle\alpha$, i.e. $\langle 110\rangle\gamma$, as in normal slip.

3. A. Klug. *The kinematics of the austenite–pearlite transition under continuous heating and cooling.*

4. S. Miyake & K. Suzuki. *On precipitation of metastable centres in solid solutions* NaCl–$CaCl_2$.

We found that stationary X-ray diffraction patterns from transparent single crystals of solid solutions of NaCl dissolved with a few per cent of $CaCl_2$, which were made by cooling the melt of the mixed salts, contain a number of diffuse spots. When the specimen was reheated to 400° C. and then quenched to room temperature, the diffuse spots disappeared, but they reappeared gradually within a month. Recovery to similar extent occurred when the quenched specimen was kept at 100° C. for 1 hr. The displacements of the diffuse spots with the change of the direction of incident X-rays revealed the existence of rods in the reciprocal space, passing through certain matrix lattice points along $\langle 111\rangle$ and $\langle 310\rangle$ directions.

The origin of the rods seems to be explained in the manner analogous to the case of alloys. Namely, the homogeneous structure is not stable, and a number of thin plate-like metastable centres, or *plates*, may be formed in the interior of the matrix, whereto Ca^{++} ions replacing Na^{+} sites and vacancies of Na^{+} sites compensating the extra positive charge are locally concentrated.

We were able to explain qualitatively the main features of the pattern by assuming a suitable structure of the plate-like centres. Each of them cannot be regarded as a simple inclusion, but is supposed to be an assemblage of many smaller units of several kinds.

5. B. Dreyfus-Alain & R. Viallard. *Transformations allotropiques progressives des métaux de transition et insertion d'hydrogène.*

6. A. Boettcher & H. Treupel. *Einige Beispiele kontinuierlicher Gittertransformationen.*

Mit einer für die Untersuchung des Ablaufs von Gittertransformationen besonders geeigneten Elektronenbeu-

gungsanordnung wurden die thermischen Umwandlungen der Kupfer- und Silber-Selenide und -Sulfide untersucht. Dabei wurde einerseits gefunden, dass bei einigen dieser Stoffe mehr Modifikationen bestehen, als bisher aus Röntgenuntersuchungen bekannt war, andererseits einige Umwandlungen durch die kontinuierliche Änderung von Gitterparametern gekennzeichnet sind. Umwandlungen dieser Art werden gezeigt bei Silber- und Kupfer-Selenid sowie beim Silbersulfid.

Es wird der Versuch einer Deutung solcher kontinuierlicher Gitteränderungen gemacht. Die Strukturen dieser Stoffe sind nach älteren Untersuchungen dadurch gekennzeichnet, dass für die Metallionen eine grössere Zahl von möglichen Gitterplätzen angegeben werden, als aufgrund der stöchiometrischen Verhältnisse besetzt werden können. Nimmt man an, dass die Gitterparameter einiger Modifikationen innerhalb gewisser Grenzen von der Verteilung der Metallionen abhängig sind, lassen sich die beobachteten Gitteränderungen so deuten, dass während einer Temperaturbehandlung ein langsamer Übergang der Metallionen von einer Gruppe von Plätzen auf eine andere erfolgt, der zu einer kontinuierlichen Änderung der Gitterparameter führt in ähnlichem Sinne wie bei einem Mischkristall, bei dem die Konzentration der gelösten Komponenten laufend geändert wird.

Transitions ferroélectriques et magnétiques

1. R. Pepinsky. *Ferroelectric and antiferroelectric phase transitions.*

2. H. D. Megaw. *Crystallography of ferroelectric materials.*

As a basis for any theoretical treatment of ferroelectricity or evaluation of experimental results, a knowledge of the geometry of the substances is necessary. Most of the evidence about this has come hitherto from X-ray diffraction or optical studies; neutron diffraction and other techniques may be expected to contribute in the future.

Ferroelectricity can occur only in crystals belonging to polar symmetry classes, i.e. classes in which the symmetry allows a resultant vector to exist. The known ferroelectrics differ only slightly in cell dimensions and atomic parameters from structures of higher symmetry—which are in fact the structures of the 'para-electric' polymorphs—where the atoms lie in special positions on symmetry elements.

Antiferroelectrics, which must be defined from their electrical properties, have structures in which the atomic displacements from special positions in a high-symmetry polymorph are compatible with a non-polar symmetry class.

Determination of exact atomic parameters is difficult and often comes at a very late stage in the investigation of a crystal structure. It is important to consider how much can be learned about the geometry from more easily obtained evidence and to distinguish clearly between what is definitely known, what may plausibly be assumed, and what is certainly ruled out. The existing work relating to crystal structures of ferroelectrics and certain non-ferroelectrics will be surveyed from this point of view.

3. G. H. Jonker & J. Volger. *Influence of crystal dimensions on the transitions of* $BaTiO_3$.

It has been found by several investigators that the crystallographic transitions in ferroelectric materials depend on the method of preparation. Especially of $BaTiO_3$ it is known that the c/a ratio of the tetragonal form is variable.

A new series of ceramic samples has been prepared at different temperatures. The influence of the different crystal dimensions obtained in this way has been studied by the measurement of the cell dimensions, the specific heat and the dielectric constant.

4. H. P. Rooksby & B. T. M. Willis. *Changes in magnetic materials.*

An account is given of some X-ray studies of structural changes associated with various types of magnetic transition. The investigations have involved powder photography over the temperature range −195° C. to 1000° C.

Two types of second-order change are considered, namely transitions from antiferromagnetism and ferromagnetism respectively to paramagnetism; each type is described in terms of the behaviour of typical cubic and non-cubic substances. An anomalous lattice dilatation occurs in the neighbourhood of the transition temperature, and this may or may not give rise to a change of lattice symmetry.

Unlike other magnetic materials of NiAs type structure, MnSb shows no anomalous dilatation in the c direction at the transition temperature. This is interpreted to mean that at this spacing of the (0001) sheets of Mn ions the Heisenberg exchange energy is stationary.

First-order changes are briefly considered with reference to MnAs and MnBi.

It is suggested that the effect of magnetostriction may be to lower the symmetry of cubic materials to monoclinic (MnO), rhombohedral (FeO) or tetragonal (α-Fe). These symmetry changes, although extremely small, should be detectable by high-resolution counter diffractometer methods.

5. E. F. Bertaut. *Structures cristallines et transitions magnétiques dans le système* Fe–S.

Le système FeS_{1+x} contient une phase antiferromagnétique ($0 < x < 0{\cdot}08$) et une phase ferromagnétique ($0{\cdot}08 < x < 0{\cdot}14$). FeS stoechiométrique et la pyrrhotine Fe_7S_8 forment les termes initiaux et finaux de cette série.

La susceptibilité magnétique de FeS subit une discontinuité à 120° C. qui correspond au passage d'une surstructure à une structure désordonnée du type NiAs. Cette surstructure est décrite.

FeS est une structure à lacunes ordonnées et ferrimagnétique (Néel) par suite de la non-compensation des moments magnétiques sur des plans (001) successifs.

La courbe de susceptibilité magnétique, déterminée par Benoit, a l'allure caractéristique hyperbolique des ferrimagnétiques jusqu'à 540° C. Elle montre une grande discontinuité vers 560° C., liée au passage à l'antiferromagnétisme habituel et à la disparition de la surstructure des lacunes.

Transitions dans des minéraux et dans des cristaux inorganiques et organiques

1. M. J. Buerger. *Network and interstitial-disorder transformations in minerals.*

For present purposes, network structures can be defined as linked coordination groups in which the linkage is not rigid. The coordination groups may be squares (as in tenorite and braggite), tetrahedra (as in quartz, tridymite, cristobalite) or octahedral (as in WO_3). Both (approximately) octahedral and tetrahedral groups linked into a network occur in bandylite.

In structures which are not networks there is a monotonous change of the structure and its thermodynamic properties with increasing temperature. On the other hand unstuffed networks show phase transformations. From one point of view these are 'displacive' transformations, from another they constitute disorder of the network. The transformation occurs because with each increment of disorder, further increments involve smaller energies.

Many mineral structures are based upon stuffed networks, i.e. networks with interstitial atoms. These include nepheline, kaliophyllite, kalsitite, eucryptite, the feldspars, leucite, analcite and perovskite. The effect of interstitial atoms may be to suppress a transformation. For example, the interstitial lithium suppresses the high–low quartz transformation. On the other hand the transformation of the network may so open the structure that easy flow of interstitial atoms occurs. This can promote a substitutional disorder among the interstitial atoms, as in feldspar.

2. J. P. Mathieu. *Étude sur la rotation éventuelle des ions dans les cristaux au moyen des spectres Raman.*

D'après la théorie de l'effet Raman dans les cristaux cubiques, la mesure du facteur de dépolarisation des raies caractéristiques des vibrations internes d'une molécule ou d'un ion complexe permet de savoir si leur orientation moyenne est entièrement désordonnée ou si, étant bien déterminée par rapport aux éléments de symétrie de la maille, elle a une distribution régulière ou statistique. On a pu montrer ainsi que, lors de la transformation du chlorure d'ammonium à −30° C., les axes ternaires des ions NH_4^+ demeurent parallèles à ceux de la maille cubique et que dans la phase cubique du cyanure de potassium, une partie des ions CN^- a une orientation désordonnée.

3. A. Smekal. *On the α–β transformation of quartz.*

4. J. Whetstone. *A study of the initiation of transition between ammonium nitrate modifications* III *and* IV.

The occurrence of a 'metastable' transition at 50° C. between modifications IV ⇌ II is associated with special drying of the sample or its immersion in a non-solvent; prompt occurrence of the transition IV ⇌ III at 32° C. would thus appear to depend on the presence of an aqueous phase and it is reasonable to suppose that recrystallization in a surface film of saturated solution carried by the hygroscopic salt is responsible for its ready transition.

Janëcke, Hamacher & Rahlfs have found that potassium nitrate in solid solution in the ammonium nitrate modifications alters their temperature ranges of stability. At −16° C., a 30% addition renders the modification III completely stable, while modification IV becomes unstable with more than 8% of the added salt. Between these limits, equilibrium mixtures of III and IV exist. However, with 10% or less of potassium salt in suitable preparations stabilization of ammonium nitrate III between −20° C. and 60° C. may be obtained, and claims have been made that as little as 1% is effective in phase stabilization. Such preparations have been made by mechanically mixing, co-crystallizing or fusing a finely divided potassium salt with ammonium nitrate. It is suggested that their inhomogeneity is responsible for their immunity from transition, since surface solid solutions rich in potassium nitrate would prevent surface nucleation with modification IV. Some experimental observations in support are quoted.

5. S. Takagi & K. Suzuki. *The phase transition in n-paraffin.*

The orthorhombic–hexagonal phase transition in solid normal paraffin has been studied by electron diffraction. Thin-film specimen suitable for transmission experiment was prepared by dropping the benzene solution on a clean surface of water. The crystals were orientated with their *c* axes perpendicular to the plane of the film. Good single-crystal patterns were obtained by placing a small slit before the specimen.

At room temperature (18° C.), the pattern obtained consists of ordinary square nets, the ratio (K) of the spacing of (110) to that of (200) being about 1·10. The $hk0$ spots for which $h+k$ = odd, are clearly seen. At the transition temperature, the above spots disappear, while K remains almost equal to the initial value. At the same time, however, the diffuse satellites appear near (200) spots, at the position corresponding to $K = 1{\cdot}05$. At higher temperatures the satellites become more intense, K approaches 1, and finally the whole pattern becomes hexagonal nets.

These results show clearly that the paraffin molecules become free to rotate or become disordered at the transition temperature at which the new lattice is formed which is not exactly hexagonal and which gradually transforms into the completely hexagonal form at higher temperatures.

6. V. Vand. *Classification of phases in crystals of long-chain compounds, and some mechanisms of their phase transitions.*

Long-chain compounds exist in a bewildering number of polymorphic forms. These arise from the fact that the regular chains of *n*-aliphatic compounds pack side by side in layers, which in turn pack on top of each other to form the crystal. The side packing gives rise to a subcell, a 'crystal within a crystal'. Several types of subcells are possible. The molecular layer boundary can be interpreted as a crystal face of the subcell crystal with its appropriate Miller index. This gives a basis for classifica-

tion of long-chain polymorphic forms. Apart from this, there are possibilities of different types of stacking of the layers themselves.

The different forms often differ only inappreciably in their energies; so although they may be considered metastable, the rate of phase transitions is often zero. Different polymorphic forms may be found side by side in the same batch of crystals. Some of the transitions can be induced by vigorous mechanical working in an apparatus called a 'phase converter'. Several types of microconverters have been developed and transitions studied as a function of temperature.